# Surface and internal tides above sea-floor topography

**Vijayantee Teeluck**

Submitted in accordance with the requirements for the degree of
Doctor of Philosophy

The University of Leeds
Department of Applied Mathematics

September 2013

The candidate confirms that the work submitted is her own and that appropriate credit has been given where reference has been made to the work of others. This copy has been supplied on the understanding that it is copyright material and that no quotation from the thesis may be published without proper acknowledgement.

## Acknowledgements

Dr Stephen Griffiths and Professor Chris A. Jones, my supervisors, deserve many thanks for all their tireless help and advice throughout my PhD. In particular, I would like to thank Dr Griffiths for his lucid explanations and guidance in navigating the complex world of mathematics and oceanography. I am deeply grateful to Professor Jones who has enriched my understanding of fluid dynamics, and provided much positive and encouraging support in what at times has been a difficult journey.

I would like to thank all those people who made it possible for me to complete my studies at Leeds, specifically I would like to mention Professors Alastair Rucklidge and Carmen Molina-Paris, and Dr Thomas Wagenknecht.

My peers of the Satellite room have been a refreshing source of comfort and happiness, and their friendships have been a great help as together we tackled similar frustrations in the world of research. Lucrezia Morticelli has also walked this path with me and her support has been invaluable.

Liz Meenan, Penny Aspinall and Vijay Bundhoo of the Mauritius Institute of Education warrant a special thank you for encouraging me to reach such dizzy heights. I have also very much appreciated the kind support of my good friend Barbara Hockwart.

I have been graced with the presence of two exceptional friends at Leeds. I thank Veiko Palge for his wise words, and for always making time to help me. Tomek Bethell has made me smile and kept me inspired through our mutual love of music.

To my partner and companion Stephen Murray, I am grateful to you for being there.

Finally, I would like to thank my brothers Kishore and Ashok who provided a much needed stability in my childhood. Their unwavering open-mindedness has allowed me to academically flourish and for this I am deeply indebted.

The funding for my PhD was provided by the ESPRC, to whom I am very grateful for the opportunity to study at Leeds.

## Abstract

Waves of long spatial scale (meaning wavelengths of hundreds or thousands of kilometres) and long time scale (meaning periods of hours or days) are important in a range of dynamical phenomena in the ocean. For example, these waves are fundamental to the dynamics of ocean tides, which are the focus of this study. Here we are concerned with both barotropic waves and internal waves, and the forcing of internal waves of tidal frequency (internal tides) by barotropic tides.

After an introduction to the background and physical significance of this subject, the governing equations for long barotropic linear waves are set out and the underlying assumptions are discussed. We then turn to the issue of coastally-trapped barotropic waves, and review some simple solutions for the three main classes of such waves (the Kelvin wave, edge waves, and topographic Rossby waves). Detailed solutions are derived for these waves above a simple step topography, based upon an analytically derived dispersion relation, and these solutions are compared with numerical solutions above a smooth topography. A detailed solution is also derived for a family of topographic Rossby waves above a smooth slope in an unbounded domain, and the frequencies of these waves are shown to be in good agreement with the frequencies determined by numerical solutions with a coastline. Throughout, there is a focus on waves of tidal period.

A simple solution of internal tide generation is also presented, in a two-layer fluid with a step topography (and no background rotation or coastline). Explicit analytical expressions are derived for the outgoing internal wave energy fluxes in this model, and are compared with estimates of energy fluxes in the real ocean.

# Contents

# List of Figures

# List of Tables

# Chapter 1

# Introduction

Waves are ubiquitous in the ocean. They occur on a range of spatial and temporal scales, from a few metres to planetary scale, and from a few seconds to seasonal timescales. This thesis is concerned with long waves, meaning those with a horizontal length scale much larger than the fluid depth – perhaps hundreds or thousands of kilometres. We are also thinking of waves with large time scales, meaning periods of hours or days. The prototypical examples of such waves are ocean tides.

## 1.1 Waves in a homogeneous ocean

The mathematical modelling of such waves dates back to **?**, who derived the so-called shallow-water equations for a homogeneous ocean (i.e., one of constant density). The derivation takes advantage of the separation of length scales between the fluid motions and the fluid depth. The outcome is a system of three partial differential equations for three unknowns with no explicit dependence upon depth. This is a considerable simplification over the full three dimensional system of equations.

Waves can be analysed by considering small amplitude perturbations about a state of rest. The simplest such analyses also assume an ocean of constant depth. In the absence

of rotation, this leads to so-called gravity waves, which owe their restoring mechanism to free-surface perturbations and the action of gravity. In the presence of rotation, this leads to so-called inertia-gravity waves, which are sometimes called Poincaré waves in the presence of boundaries. Of special interest to us will be the Kelvin wave (**?**), which propagates along and is trapped against a coastline. When variations in background rotation are taken into account, one may also identify Rossby waves, which were first diagnosed by Hough in spherical geometry (**??**).

### 1.1.1 Waves and topography

A serious limitation of many simple wave models is the restriction of uniform depth. However, the real ocean is far from this idealisation. Even within the deep oceans, which typically have depths of about 4000m, there are many non-trivial topographic features. For example, the Mid-Atlantic Ridge is mainly an underwater mountain range approximately 1km below the sea surface, and 16000km long. The Mariana Trench is approximately 70km in width and 2500km long, and has a maximum depth of 11km. There also exists thousands of sea mounts and submarine canyons which add to the changing seafloor topography.

However, there are arguably more significant topographic changes near the continents. These are typically surrounded by a shallow continental shelf where ocean depths are 100–300m, and then by a steep continental slope transitioning to the deep ocean. Together, the continental shelf and the continental slope are often referred to as the continental margin, since the combined features are found at the margins of all continents. It is worth noting that the continental shelves are the regions of the oceans best known and the most exploited commercially. They are also an oasis in the ocean for plants and animals due to the abundance of sunlight, shallow waters, and nutrient packed sediment that washes in from rivers, wave action, and in some areas, upwelling.

It should be clear that theoretical models of ocean waves based upon a uniform depth ocean are insufficient to understand motions that may occur around such topography. An

early solution for waves above sloping topography (bounded on one side by a coastline) was given by **?**, describing so-called edge waves. A more recent solution (**?**) describes waves trapped above a slope in an unbounded domain (without a coastline), describing so-called topographic Rossby waves. These are distinct from gravity waves, in that they owe their existence to potential vorticity dynamics, rather than gravity. Where the topographic slope is confined between a coastal wall and a flat-bottom deep ocean, such as for a continental slope, the topographically-guided waves are often called continental shelf waves; further details of these waves can be found in **??**.

### 1.1.2 Tides

All of these waves, which are often called barotropic waves, play a role in ocean tides. Tides owe their origin to the astronomical forcing of the Sun and Moon, which predominantly forces motions with semi-diurnal (i.e., twice daily) and diurnal (i.e., daily) frequencies. By far the largest tide is the principal lunar tide, denoted by $M_2$ and with a period 12.42 hours. The next most energetic are the principal solar tide, denoted by $S_2$ with a period of 12.00 hours, and the $K_1$ tide, with a period of 23.93 hours (**?**).

More precisely, the total energies of the M2, S2 and K1 tides are $312.26\times10^{15}$ J, $49.87\times10^{15}$ J and $49.92\times10^{15}$ J respectively (**?**). Typical surface displacements for the tides are 50cm in the deep ocean and 1–2m on continental shelves, with currents of about 0.02–0.03m/s in the deep ocean and about 0.2m/s on the shelf.

Exactly which types of barotropic waves are excited by tidal forcing depends upon the ocean depth and coastal geometry. Typically, free waves with a frequency close to that of the tidal forcing are strongly excited, i.e., there is a near-resonant excitation with amplitudes limited by weak friction at the sea-floor. Often Kelvin waves are strongly excited, which is partially because they can exist at all frequencies, unlike topographic Rossby waves (which are sub-inertial) and Poincaré waves (which are super-inertial). For example, **?** have determined which of these waves are dynamically dominant off the Californian coast. Their estimates for the relative perturbed sea surface heights of a free Kelvin

wave and a free inertia-gravity (Poincaré-like) non-coastally trapped wave are 54:16 cm for the M2 tide, and 21:24 cm for the K1 tide.

## 1.2 Waves in a stratified ocean

So far we have ignored stratification in the ocean but in reality the density and temperature of seawater varies from the surface to the seabed. The surface of the sea is an area where there is an exchange of heat between the atmosphere and the ocean. Several factors which contribute to this exchange are turbulence generated by the wind, waves and current shear. Over time, this results in an upper layer (to a depth of approximately 200m) of strong mixing leading to approximately uniform temperature and density. Oceanographers refer to this layer as the surface mixed layer. During spring and summer this layer absorbs heat, thus the deeper layers are covered by a shallow layer which is warmer and lighter. In winter when cooling at the sea surface produces convective overturning of water, this action leads to heat stored in the ocean being released to the atmosphere. Therefore, the depth of this upper layer changes according to the season, however, as an approximation we can view the ocean as having layers.

The typical distributions with depth of temperature, density and the buoyancy frequency in the ocean are shown in Figure 1.1. In panel (a), we observe that down to depths of approximately 200m the temperature of the ocean is approximately constant. Below this depth we then start to see a gradual decrease in temperature from approximately $28°$C to $3°$C. These are only typical values and we would expect them to differ according to the spatial location. The region of large temperature gradients at the base of the mixed layer is known as the thermocline. At this same depth range we also observe a large gradient of density called the pycnocline (**?**). Since the depth of the upper layer is seasonal, we also have different thermoclines. The layer where temperature changes most rapidly with depth (during summer or autumn) is known as the seasonal thermocline, and the depth range where temperature changes rapidly with depth throughout the year is known as

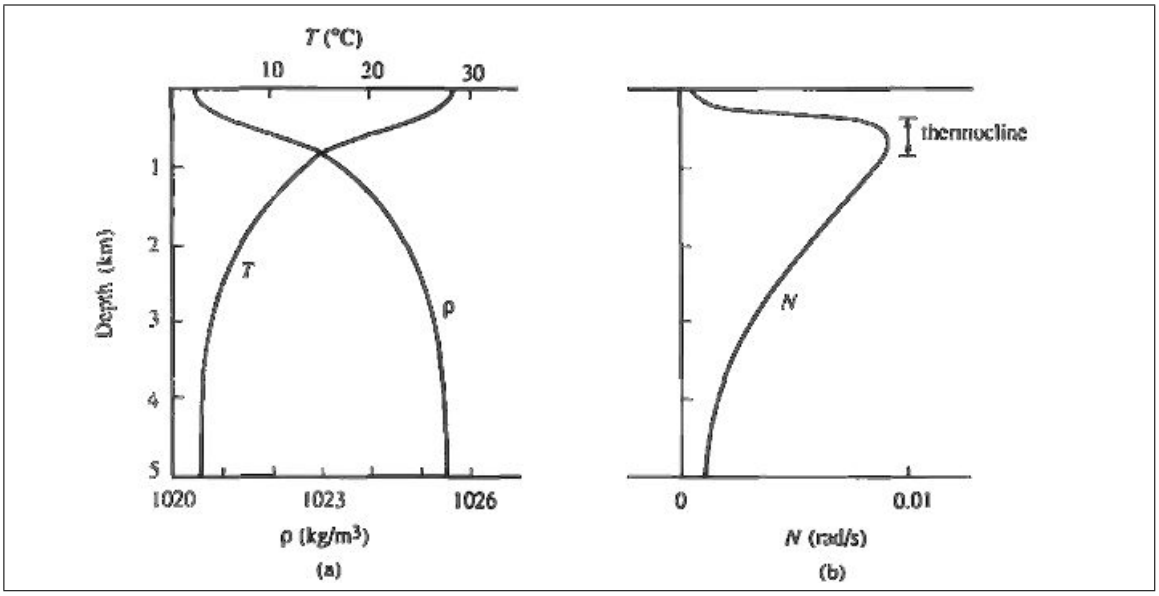


**Figure 1.1:** Typical vertical distributions of: (a) temperature and density; and (b) buoyancy frequency in the ocean. (**?**)

the permanent or oceanic thermocline.

Beneath the thermocline, the ocean is continuously stratified, i.e, the change in density is continuous and we should not think of fixed layers. Panel (b) shows the buoyancy frequency (also known as the Brunt-Väisälä frequency) $N$ which has a fundamental role in the study of stratified flows. It is a measure of the frequency of vibration of a fluid parcel in a purely vertical motion. The general expression for the buoyancy frequency is

$$N^2 = -\frac{g}{\bar{\rho}}\frac{\partial \bar{\rho}}{\partial z}$$

where $\bar{\rho}$ is the fluid density. Consider a fluid parcel which has the same density as its environment at $z$. If this fluid parcel is adiabatically displaced a small distance $\delta z$ upwards, then if it is lighter than its environment it will accelerate upwards because the downward gravitational force is smaller then the upward pressure gradient. Thus, the fluid parcel is regarded as unstable if $\partial\bar{\rho}/\partial z > 0$. However, if the fluid parcel is heavier than its environment it will sink back to its original position, and it will have oscillatory motion. Therefore, the fluid is regarded as stable if $\partial\rho/\partial z > 0$. Typical values of $N$ are $0.01\text{s}^{-1}$ in the pycnocline, this value falls to $0.001\text{s}^{-1}$ in the deep ocean. These frequencies

correspond to periods of approximately 10 and 100 minutes respectively. (**?**).

### 1.2.1 Internal waves

Within such a stratified fluid – either a layered fluid or a continuously stratified fluid – one can then think of gravity waves within the fluid layer due to the buoyancy restoring mechanism described above. As such, internal gravity waves are common in the oceans, and in particular, they are readily generated by the interaction of barotropic tides with variable bottom topography (**?**).

If one is interested in long internal waves (i.e., long in the horizontal scale compared with ocean depth, or long in time compared with the buoyancy frequency), then one can again employ the shallow-water (hydrostatic) approximation. We can pursue with the idea of vertical modes in a continuously stratified ocean, or we can consider a layered ocean, leading to so-called multi-layer shallow-water equations. The solutions thus obtained are known as internal waves. Either way, in an ocean of constant depth, one can identify the same kinds of waves as above – gravity, inertia-gravity, Kelvin, topographic – but internal in nature.

Internal waves have a small surface signature (**?**) but cause more dramatic effects in the interior of the ocean where they cause vertical displacements of isopycnals (layers of constant density). They have heights exceeding 100 metres, one such example in shown Figure 1.2 where measurements of temperature and depth were taken by mooring on the Hawaiian Ridge in water with a depth of 1453m during spring tide at the semi-diurnal period. We remark the peak-to-peak displacements are 300m which are much greater than typical sea surface heights. These internal gravity waves travel much slower than surface waves, about 2-3m/s in the open ocean. They also have smaller wavelengths of about 250m, although this will vary due to location (**?**). It has been observed that surface currents flow over the top of a seamount at 0.1 m/s, however, the same flow for an internal wave is 0.02 m/s (**?**), this gives an indication of how much slower the internal gravity waves are compared with the surface waves, and less energetic.

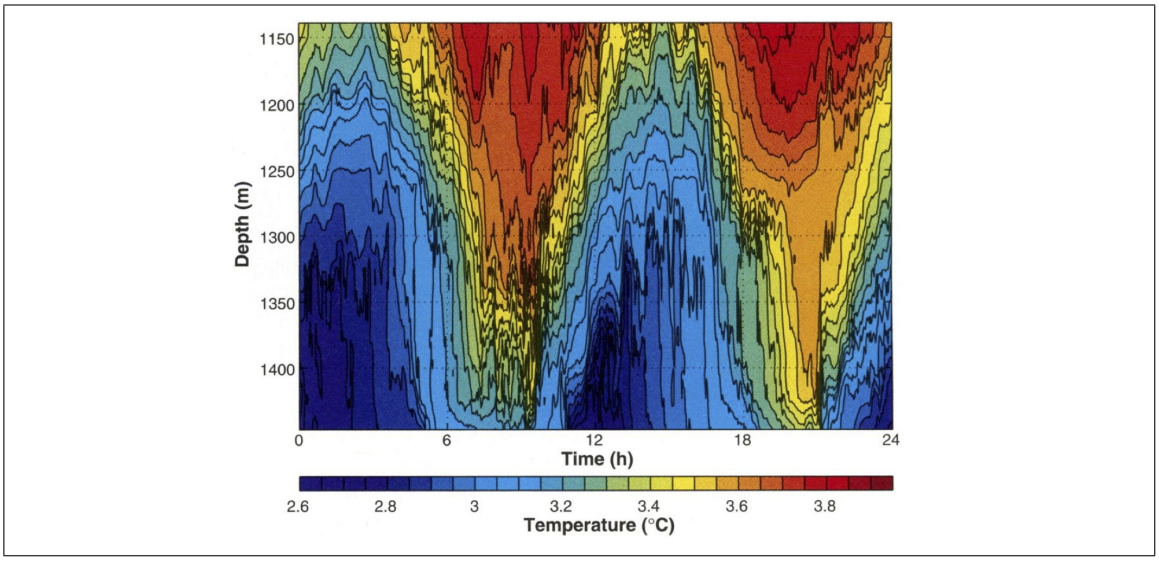


**Figure 1.2:** Moored observations on the Hawaiian Ridge reveal internal waves with peak-to-peak amplitudes as large as 300m at the semi-diurnal period. Temperature as a function of depth and time. (**?**)

### 1.2.2 Internal tides

Internal tides are simply internal waves with tidal frequencies. When a surface tide encounters a change in topography, the water is forced up or down and over the topography which gives rise to internal gravity waves. We clarify this with a simple example. If we assume we have stratified columns of water in the ocean with barotropic flow over a ridge then the water is being pushed up on one side of the ridge and so elevates the isopycnals in the interior of the ocean. On the other side of the ridge the isopycnals are made to depress as they have a flow of water descending on them. Thus the isopycnals near this ridge are made to oscillate with tidal frequency. This leads to disturbances in the isopycnals that propagate away from the ridge as internal tides.

The basic theory for internal tide generation was considered at length several decades ago (**?????**), going as far back as the early 60s. There has been a renewed interest in the study of internal tide generation at mid-oceanic topographic features as it is now believed to be significant factor in mixing in the abyssal ocean, which is known to play an important role

in controlling the large-scale ocean circulation. It is estimated that the Earth's Meridional Overturning Circulation (MOC) requires of order 2 TW of power to fuel the upwelling of abyssal waters and that this process is substantially fuelled by the breaking of internal gravity waves. Most importantly, research is being done on estimating the rate at which energy is extracted from the barotropic tide and radiated into internal gravity waves at topographic features. Such estimates of internal wave energy flux have been considered by **???** (and many others) who have compared numerical simulations with data from sources such as historical moorings and satellite altimetry.

Global simulations suggest that $75\%$ of the open ocean generation of internal tides occur at 20 locations of rough topography (which accounts for approximately $10\%$ of the ocean floor) (**?**), for example, the Pacific trench or Hawaiian ridge. The assimilation of altimeter data into numerical models of barotropic tides show that they lose more energy in the open ocean than can be ascribed to bottom friction (**?**). Research has shown that the semi-diurnal $M_2$ tide is believed to account for approximately $78\%$ of all tidal dissipation (**?**). In particular, **?** show that dissipation in the shallow seas are important with the $M_2$ tide dissipating 1.649 TW in the shallow seas and 0.782 TW in deep seas.

## 1.3 Aims of thesis

To understand the coastal generation of internal tides, a thorough understanding of the structure of barotropic tides (which force the internal tides) is required. We derive and explore the solutions to simple models of barotropic waves, with rotation and topography, that are excited as surface tides. These solutions are analysed numerically, however, with the use of linearised models we are also able to construct analytical expressions which can be compared with the numerics. To understand further how these waves are connected to each other we first analyse them in isolation, and review previous background work.

In Chapter 2, we begin with the complete set of equations governing the motion of a

geophysical fluid, these having been derived from the laws of conservation on mass, momentum and energy. We then discuss the fundamental approximations that reduce this set to the linear shallow water equations (SWEs) for a single-layer flow on the $f$-plane. This system of equations shall form the basis of the work in the proceeding chapters.

In Chapter 3, we develop some theoretical models of barotropic coastal waves, and focus on the case of trapped waves, meaning those that decay away from the coast, and are trapped by the coast, on a shelf or at a step. At tidal frequencies, these coastal barotropic waves are influenced by several factors: the coastline, the (shallow) continental shelf, the (steep) continental slope, and planetary rotation (through $f$). With a combination of all four of these additional effects taken into account, an understanding of the waves becomes rather complex; this discussion is deferred to Chapter 4. In this chapter, we instead consider one or more of these factors in isolation, to develop a basic understanding of the kind of solutions that may be expected.

In Chapter 4, we treat the full problem of coastally trapped waves in the presence of a coastline and topography. However, here we make the assumption that the topography is a step. This allows us to examine a full range of waves, including a Kelvin wave (KW), a topographic Rossby wave (TRW) (or continental shelf wave), and edge waves (EWs). We make comparison of analytical solutions and numerical results for each type of wave.

In Chapter 5, we modify this topography and seek solutions to coastally trapped barotropic waves on a continuous and smoothly varying depth profile which is more representative of the real ocean. The step topography is the simplest possible representation of a continental margin, and in this chapter we examine whether the step solutions are useful as models of waves over continuous topography. We compare the numerical solutions to waves on a continuous profile with the numerical and analytical solutions to waves on a step profile.

In Chapter 6, we introduce stratification and examine a simple model of internal generation at step topography. We do not include a coastline or planetary rotation, and force this system with an incoming barotropic wave. We examine the scattering problem and

derive analytical results for the uncoupled barotropic and internal waves systems. We proceed to make a comparison of these approximate results with numerical calculations. An important aspect of this chapter is to calculate time averaged energy fluxes for the step model and compare this with real life data.

# Chapter 2

# Governing equations and approximations for single-layer shallow-water flows

A complete set of equations governing the motion of a geophysical fluid can be derived from the laws of conservation of mass, momentum and energy. Although not definitive, this set would include variables such as velocity, temperature, pressure, density, and salinity. Our focus is simply to derive a set of governing equations which describes the motion of a constant density fluid in a rotating environment. We then reduce this set to the linear shallow water equations (SWEs).

The theory of tides is founded on Newton's theory of gravitation, and on the equations of fluid motion formulated by Euler. In his original work on differential calculus, Laplace was the first to bring together the work of these two mathematicians, and establish on firm mathematical grounds the theory of long waves and ocean tides (**?**). Here we present Laplace's Tidal Equations (LTEs) (**?**) which encapsulate the motion of a homogeneous,

hydrostatic and incompressible fluid :

$$\frac{\partial u}{\partial t} - (2|\underline{\Omega}|\sin\theta)v = -\frac{g}{r_e\cos\theta}\,\frac{\partial(h-\bar{h})}{\partial\phi}, \tag{2.1a}$$

$$\frac{\partial v}{\partial t} + (2|\underline{\Omega}|\sin\theta)u = -\frac{g}{r_e}\,\frac{\partial(h-\bar{h})}{\partial\theta}, \tag{2.1b}$$

$$\frac{\partial h}{\partial t} + \frac{1}{r_e\cos\theta}\left(\frac{\partial(uH)}{\partial\phi} + \frac{\partial(vH\cos\theta)}{\partial\theta}\right) = 0. \tag{2.1c}$$

In these, $(\phi,\theta)$ are the longitude and latitude, $(u,v)$ are the corresponding eastward and northward components of fluid velocity, $H(\phi,\theta)$ is the undisturbed depth of the ocean, $r_e$ the Earth's mean spherical radius, $|\underline{\Omega}|$ the angular rotation of the Earth, and $h$ the deviation of the sea surface from its undisturbed level. The potential $U$ of all the tide generating forces is introduced in terms of the fictitious equilibrium tide $\bar{h} = U/g$, where $g$ is gravity .

Equations (2.1a,b) are derived from the conservation of momentum, however, we remark that they do not include dissipative or nonlinear terms. To complete his study of long waves and ocean tides, Laplace includes an interpretation of the conservation of mass, i.e., (2.1c) which is found by integrating the incompressible form of the conservation of mass from the seafloor to the free surface.

Laplace's tidal equations (2.1a-c) are a form of the linearised shallow water equations in spherical coordinates, for our purposes we derive the latter by beginning with what are known as the Navier-Stokes and continuity equations:

$$\frac{D\underline{u}}{Dt} + 2\underline{\Omega}\times\underline{u} = -\frac{1}{\rho}\nabla p + \underline{g} + \nu\nabla^2\underline{u}, \tag{2.2a}$$

$$\frac{1}{\rho}\frac{D\rho}{Dt} + (\nabla\cdot\underline{u}) = 0. \tag{2.2b}$$

Here $D\bullet/Dt$ is the material derivative $\partial\bullet/\partial t + \underline{u}\cdot\underline{\nabla}\bullet$ which describes the rate of change of a material element subjected to a space-dependent and time-dependent velocity field. The Earth's gravity is given by $g$ which we take to be approximately 10 m/s$^2$, and $\nu$ is the kinematic viscosity. The vector velocity is $\underline{u}$, $\underline{\Omega}$ is the rotation vector and $\rho$ is the fluid density. Note that these are the equations relative to a rotating frame which we take to

be that of the solid Earth, and that the centrifugal term is omitted, because it is small compared with $g$.

There are several assumptions which lead to (2.2a,b), the details of which can be found in standard texts (**??**). We choose to give special attention to several of these assumptions as we gradually reduce this system to the linear shallow water equations so that some further analysis can be made.

We apply five important approximations: homogeneity of the fluid, and the $f$-plane and shallow water approximations. These approximations are inherent in the linear shall water equations for a single-layer. However, in chapter 6 we will modify the homogeneity assumption to allow for internal gravity waves. Furthermore, to simplify our model, we will also linearise the equations and neglect viscosity.

### 2.0.1 Constant density and inviscid flow

Equation (2.2b) is a consequence of the law of conservation of mass which states that the rate of increase of mass within a fixed volume must equal to the rate of inflow through the boundaries. In the context of the ocean, we shall modify (2.2b). The calculated average density for seawater is approximately 1028 kg/m$^3$, and varies by less than 2-3 kg/m$^3$ (**?**). We take as a first approximation for the density of seawater $\rho_0$ which will be a constant. So (2.2b) reduces to

$$\underline{\nabla} \cdot \underline{u} = 0. \tag{2.3}$$

Thus, we will use the incompressible form of the continuity equation. The dynamic viscosity of seawater, $\mu$, is $1.4 \times 10^{-3}$ kg/ms (**?**), dividing this by $\rho_0$(=1028 kg/m$^3$) we have for kinematic viscosity

$$\nu = 1.36 \times 10^{-6}\,\mathrm{m^2 s^{-1}}. \tag{2.4}$$

Typical timescales for tidal flows are measured in hours ($\sim 10^3$ seconds). Typical length scales are at least many kilometres ($\sim 10^3$ metres). So the order of magnitude of $D\underline{u}/Dt$ is $u/10^3$ m/s$^2$ whereas the order of magnitude of $\nu\nabla^2\underline{u}$ is $u\,\nu\ 10^{-6}$ m/s$^2$, i.e., $u/10^{12}$ m/s$^2$,

i.e., much smaller. We therefore neglect viscous terms in our analysis.

### 2.0.2 The $f$-plane approximation

We seek waves that have a length scale much smaller than the radius of the earth ($r_e$ = 6371 km), so we can ignore the curvature of the Earth and long waves can be studied by a three-dimensional, local Cartesian system. This important approximation is known as the $f$-plane approximation and is shown in Figure 2.1 . The positions and velocities of an

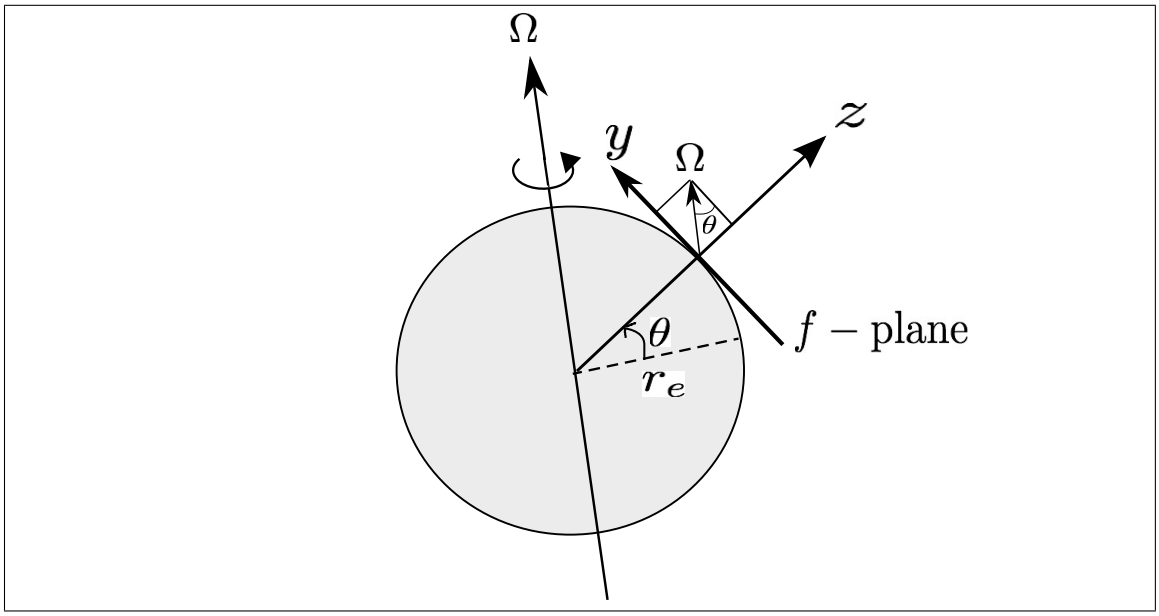


**Figure 2.1:** The $f$-plane at latitude $\theta$. The $x$-axis is into the plane of the paper, $y$ is northwards and $z$ is normal to the surface of the Earth. $r_e$ (6371 km) is the mean radius of the spherical Earth. $\underline{\Omega}$ is the angular velocity ($7.27 \times 10^{-5}$ rad/s) at which the Earth rotates about an axis which intersects the North and South Poles. (**?**)

element of fluid are measured with respect to a frame of reference tangent to the surface of the Earth (the $f$-plane) which rotates with respect to an inertial frame.

Equation (2.2a) is an interpretation of Newton's second law of motion in a rotating frame. This frame is rotating with angular velocity $\underline{\Omega}$ ($7.27 \times 10^{-5}$ rad/s) which gives rise to the Coriolis and centrifugal forces. The ratio of the magnitudes of the centrifugal force to the

gravitational term is less than $3 \times 10^{-3}$ throughout the ocean and so can be neglected (**?**). Consequently, the effects of the rotation of the Earth are manifested in the term $2\underline{\Omega} \times \underline{u}$. This is known as the Coriolis force which is considered a fictitious force since it results from the acceleration of the $f$-plane (reference frame) itself and not from any physical force acting on the body.

The Coriolis force can be evaluated by writing $\underline{\Omega}$ in component form: $\Omega_x = 0, \Omega_y = \Omega\cos\theta, \Omega_z = \Omega\sin\theta$, so that

$$2\boldsymbol{\Omega} \times \underline{u} = \begin{vmatrix} \underline{i} & \underline{j} & \underline{k} \\ 0 & 2\Omega\cos\theta & 2\Omega\sin\theta \\ u & v & w \end{vmatrix} = 2\Omega \begin{pmatrix} w\cos\theta - v\sin\theta \\ u\sin\theta \\ -u\cos\theta \end{pmatrix} = \begin{pmatrix} \gamma w - fv \\ fu \\ -\gamma u \end{pmatrix}, \tag{2.5}$$

here $\gamma = 2\Omega\cos\theta$, and $f = 2\Omega\sin\theta$ is known as the Coriolis parameter. We note that $0 \leq f \leq 1.45 \times 10^{-4}$ rad s$^{-1}$, and since $f$ is dependent on the latitude we are at, we leave the specific calculation of this parameter to chapter 4 where we undertake numerical calculations of the frequencies of waves in our simple models.

We return to our original set of equations (2.2a,b) governing the motion of a fluid and apply the important approximations we have discussed. We linearise (2.2a), neglect kinematic viscosity (2.4) which is negligible and combine this with the $f$-plane approximation (2.5). So expressing the revised form of (2.2a) in component form we have (2.6a-c). The constant density assumption reduces (2.2b) to the incompressible form of the continuity equation (2.6d), so our set of equations is:

$$\frac{\partial u}{\partial t} - fv + \gamma w = -\frac{1}{\rho_0}\frac{\partial p}{\partial x}, \tag{2.6a}$$

$$\frac{\partial v}{\partial t} + fu = -\frac{1}{\rho_0}\frac{\partial p}{\partial y}, \tag{2.6b}$$

$$\frac{\partial w}{\partial t} - \gamma u = -\frac{1}{\rho_0}\frac{\partial p}{\partial z} - g, \tag{2.6c}$$

$$\frac{\partial u}{\partial x} + \frac{\partial v}{\partial y} + \frac{\partial w}{\partial z} = 0. \tag{2.6d}$$

We ignore variations of $\theta$ on the grounds that over a wavelength of these waves $\theta$ is effectively constant, thus we assume $f$ is constant and define $f = 2\Omega\sin\theta_0$.

### 2.0.3 Shallow water assumption

We can consider the ocean as a thin layer where the horizontal length scale is of the order thousands of kilometres, and much greater than the vertical length scale. This is a realistic assumption given that for oceanic surface tides the horizontal scale can be of order 1000km whilst the vertical scale is of order 10km at most.

To determine the consequence of this approximation, we apply a scaling analysis to (2.6a-d). Let $H$ and $L$ be a typical vertical and horizontal length scales, $U$ and $W$ typical horizontal and vertical velocities, $T$ a typical timescale, and $P$ a typical pressure.

Seeking waves of long wavelength we have $H/L \ll 1$. By (2.6d) we can write $U/L \sim W/H$ , so $W \sim UH/L$. Therefore

$$W \ll U \quad \text{since} \quad \frac{H}{L} \ll 1. \tag{2.7}$$

Having made this assumption we compare the magnitude of the terms in each distinct equation in (2.6a-c). In (2.6a) we have

$$\frac{\gamma w}{fv} \sim \frac{H}{L} \ll 1. \tag{2.8}$$

Therefore, we can neglect the $\gamma w$ term. Before applying a scaling analysis to the vertical component of the momentum equation (2.6c) we first find an expression for the pressure $P$ from (2.6a)

$$-\frac{1}{\rho_0}\frac{\partial p}{\partial x} \sim \frac{P}{\rho_0 L}. \tag{2.9}$$

For waves of tidal frequency $f \sim 1/T$, so comparing the scaled pressure gradient with $\partial u/\partial t$ or $fv$ respectively yields the same expression for pressure

$$P \sim \frac{U\rho_0 L}{T}. \tag{2.10}$$

We now compare the vertical acceleration and pressure gradient in (2.6c). Using (2.10) we have

$$\frac{\partial w}{\partial t} \Big/ \frac{1}{\rho_0}\frac{\partial p}{\partial z} \sim \frac{H}{L} \ll 1. \tag{2.11}$$

Therefore, we can neglect the vertical acceleration $\partial w/\partial t$. We now compare $\gamma u$ and the vertical pressure gradient, using (2.10) this reduces to

$$\frac{\gamma u}{\partial p/\rho_0\,\partial z} \sim \frac{H}{L}\,\gamma T. \tag{2.12}$$

We can neglect $\gamma u$ provided $\gamma T \ll L/H$. This is true since $1 \ll L/H$.

The shallow water approximation has now reduced the set of equations (2.6a-d) to the (2.13a-d) where we have linearised and assumed uniform density.

$$\frac{\partial u}{\partial t} - fv = -\frac{1}{\rho_0}\frac{\partial p}{\partial x}, \tag{2.13a}$$

$$\frac{\partial v}{\partial t} + fu = -\frac{1}{\rho_0}\frac{\partial p}{\partial y}, \tag{2.13b}$$

$$0 = -\frac{1}{\rho_0}\frac{\partial p}{\partial z} - g, \tag{2.13c}$$

$$\frac{\partial u}{\partial x} + \frac{\partial v}{\partial y} + \frac{\partial w}{\partial z} = 0. \tag{2.13d}$$

Interestingly, equations (2.13a-c) reveals a number of unexpected properties. Firstly, under the shallow water approximation we have assumed that vertical accelerations are small, thus the fluid behaves as though it is under static equilibrium with regards to vertical motions. This gives an exact balance between the pressure gradient and the gravitational force in the vertical momentum equation (2.13c).

Surprisingly, we can also show that the horizontal velocities are independent of $z$. If we differentiate the right hand side of (2.13a) with respect to $z$ then,

$$-\frac{1}{\rho_0}\frac{\partial}{\partial z}\left(\frac{\partial p}{\partial x}\right) = -\frac{1}{\rho_0}\frac{\partial}{\partial x}\left(\frac{\partial p}{\partial z}\right) = 0. \tag{2.14}$$

Similarly differentiating the left hand side of (2.13b) with respect to $z$ gives

$$-\frac{1}{\rho_0}\frac{\partial}{\partial z}\left(\frac{\partial p}{\partial y}\right) = -\frac{1}{\rho_0}\frac{\partial}{\partial y}\left(\frac{\partial p}{\partial z}\right) = 0. \tag{2.15}$$

So the right hand side of (2.13a,b) is independent of $z$ and we have columns of water not of fixed radius, which make up the ocean. Thus if $u$ and $v$ are independent of $z$ at some time, then they remain independent of $z$. So we can seek $z$ independent solutions.

The above assumptions allows one to develop a simplified model of the ocean which has a single density layer, $\rho_0$ and is of undisturbed depth $H$. The model has an irregular seabed, the ocean has pressure $p$, and $h$ represents displacement of the free surface above the equilibrium level $z = 0$, as shown in Figure 2.2.

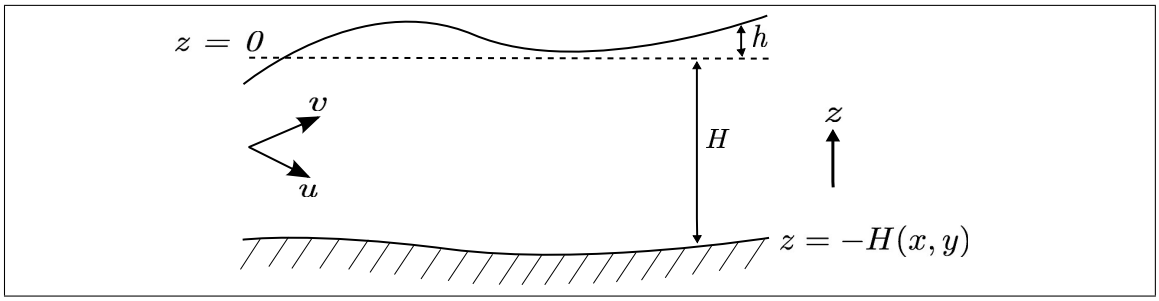


**Figure 2.2:** Simplified model of the ocean as a thin shell. $H(x, y)$ represents the undisturbed depth, $h$ the perturbed sea surface height above the equilibrium, $z = 0$. The horizontal velocities are given by $u$ and $v$.

Separating variables and integrating equation (2.13c) over the depth range we have the following relationship between the $p$, $h$ and $z$,

$$p = p_{atm} + \rho_0 g(z - h), \tag{2.16}$$

where $p_{atm}$ is the atmospheric pressure at $z = 0$. Since density is constant, the pressure gradient terms can be written in terms of $h$ by substituting (2.16) into (2.13a,b). Therefore

$$\frac{\partial u}{\partial t} - fv = -g\frac{\partial h}{\partial x}, \tag{2.17a}$$

$$\frac{\partial v}{\partial t} + fu = -g\frac{\partial h}{\partial y}. \tag{2.17b}$$

Since $(u, v)$ are functions of $x, y, t$ and continuous, it follows by (2.17a,b) that $h$ is also continuous and a function of $x, y, t$.

We now turn our attention to the incompressible form of the continuity equation, (2.13d). The vertical velocity, $w$, is a function of $z$, so we can integrate over the water column from $z = -H$ to $z = h$, where $H = H(x, y)$ and $h(x, y, t)$. Hence

$$\int_{-H}^{h} \frac{\partial w}{\partial z}\, dz = \int_{-H}^{h} -\left(\frac{\partial u}{\partial x} + \frac{\partial v}{\partial y}\right) dz,$$

which gives

$$w(h) - w(-H) = -(h+H)\left(\frac{\partial u}{\partial x} + \frac{\partial v}{\partial y}\right). \tag{2.18}$$

At $z = -H(x, y)$, the normal $\underline{n}$ at any point to the irregular-shaped seabed is

$$\underline{n} = \left(\frac{\partial H}{\partial x}, \frac{\partial H}{\partial y}, 1\right), \tag{2.19}$$

where $|\underline{\nabla} H| \ll 1$. We can calculate an expression for $w(-H)$ using $\underline{u} \cdot \underline{n} = 0$, thus

$$w(-H) = -\left(u\frac{\partial H}{\partial x} + v\frac{\partial H}{\partial y}\right), \tag{2.20}$$

and combining this with (2.18) we have an expression for the vertical velocity at the surface

$$w(h) = -\left(u\frac{\partial H}{\partial x} + v\frac{\partial H}{\partial y}\right) - (h+H)\left(\frac{\partial u}{\partial x} + \frac{\partial v}{\partial y}\right). \tag{2.21}$$

The parcels of fluid remain on the surface, so $z - h$ is materially conserved at $z = h$, giving

$$\frac{D}{Dt}(z-h) = 0 \quad \text{at} \quad z = h(x, y, t). \tag{2.22}$$

But $Dz/Dt = w$, so $w = Dh/Dt$ at $z = h$ and since $\partial h/\partial z = 0$ we have

$$w(h) = \frac{\partial h}{\partial t} + u\frac{\partial h}{\partial x} + v\frac{\partial h}{\partial y}. \tag{2.23}$$

Equating (2.21) and (2.23) yields

$$\frac{\partial h}{\partial t} + u\frac{\partial}{\partial x}(h+H) + v\frac{\partial}{\partial y}(h+H) + (h+H)\left(\frac{\partial u}{\partial x} + \frac{\partial v}{\partial y}\right) = 0,$$

and rearranging gives

$$\frac{\partial h}{\partial t} + \frac{\partial}{\partial x}\left[u(h+H)\right] + \frac{\partial}{\partial y}\left[v(h+H)\right] = 0.$$

Recall that we have long waves of small amplitude, i.e., $h \ll H$, thus

$$\frac{\partial h}{\partial t} + \frac{\partial}{\partial x}(uH) + \frac{\partial}{\partial y}(vH) = 0. \tag{2.24}$$

This states that the divergence of the horizontal (mass) transport depresses the free surface. Hence we obtain the standard linear shallow water equations for the $f$-plane:

$$\frac{\partial u}{\partial t} - fv = -g\frac{\partial h}{\partial x}, \tag{2.25a}$$

$$\frac{\partial v}{\partial t} + fu = -g\frac{\partial h}{\partial y}, \tag{2.25b}$$

$$\frac{\partial h}{\partial t} + \frac{\partial}{\partial x}(uH) + \frac{\partial}{\partial y}(vH) = 0. \tag{2.25c}$$

## 2.1 Boundary conditions

The ocean is of finite dimensions and we have a time-dependent set of equations (2.25a-c), hence we are solving linear PDEs in $x, y, t$.

The ocean tides are strongly influenced by the physical characteristics of the continents (e.g. coastlines, continental shelves/slopes), the sea-floor topography and the sea surface. We begin by discussing two boundary conditions used in deriving the shallow water equations (2.25a-c). We then modify Laplace's simple model of the ocean as a thin shell (Figure 2.2), and in particular focus on two fixed boundaries encountered by the ocean: the coastline and the continental step which always remain below the sea surface.

### 2.1.1 Boundary conditions used in deriving the shallow water equations

The topography of the sea-floor is irregular, and a function of horizontal spatial coordinates, so we can write $H(x, y)$ where $H$ is the depth. At a rigid boundary, the normal component of velocity must vanish, thus in deriving (2.25c) we used

$$\underline{u} \cdot \underline{n} = 0 \quad \text{at} \quad z = -H(x, y). \tag{2.26}$$

On the perturbed sea surface, $h(x, y, t)$, we require continuity of stress (**?**). Therefore, if $p_{atm}$ is the atmospheric pressure on the sea surface, then

$$p = p_{atm} \quad \text{at} \quad z = h(x, y, t). \tag{2.27}$$

This was used in deriving (2.25a,b).

### 2.1.2 Boundary conditions at the coastline

We now consider a lateral boundary in the form of a smooth vertical coastline. Taking our model of the ocean, we introduce a coastline which extends along $x = 0$. Assuming this boundary is rigid, the cross-shore velocity is unable to penetrate it, thus

$$v = 0 \quad \text{at} \quad x = 0. \tag{2.28}$$

### 2.1.3 The internal boundary conditions in the step model

In this section we consider the boundary conditions we shall introduce into our simple model of the ocean by separately considering a continental margin, and then a coastline. Here we do not enter into a discussion of how realistic our interpretation of these features are. Our sole aim is develop a simple model and describe the boundary conditions, we delay an exploration and more detailed discussion of these features until chapters 4, 5 and 6.

As discussed in chapter 1, the continental margin is a combination of a continental shelf and a continental slope which is separated by a shelf-break. As shown in Figure 2.3 we have a shelf-break at $x = 0$, the continental shelf is of depth $H_r$ and to the right of the shelf-break, and the deep ocean has a depth of $H_l$, to the left of the shelf-break.

We require $h$, the perturbed sea surface height to be continuous everywhere since we have continuity of pressure on the surface, including where we have an abrupt change in the sea-floor topography. Thus we impose

$$h_l = h_r \quad \text{at} \quad x = 0. \tag{2.29}$$

Similarly, we require the continuity of mass about the step shelf-break, thus

$$H_l v_l = H_r v_r \quad \text{at} \quad x = 0. \tag{2.30}$$

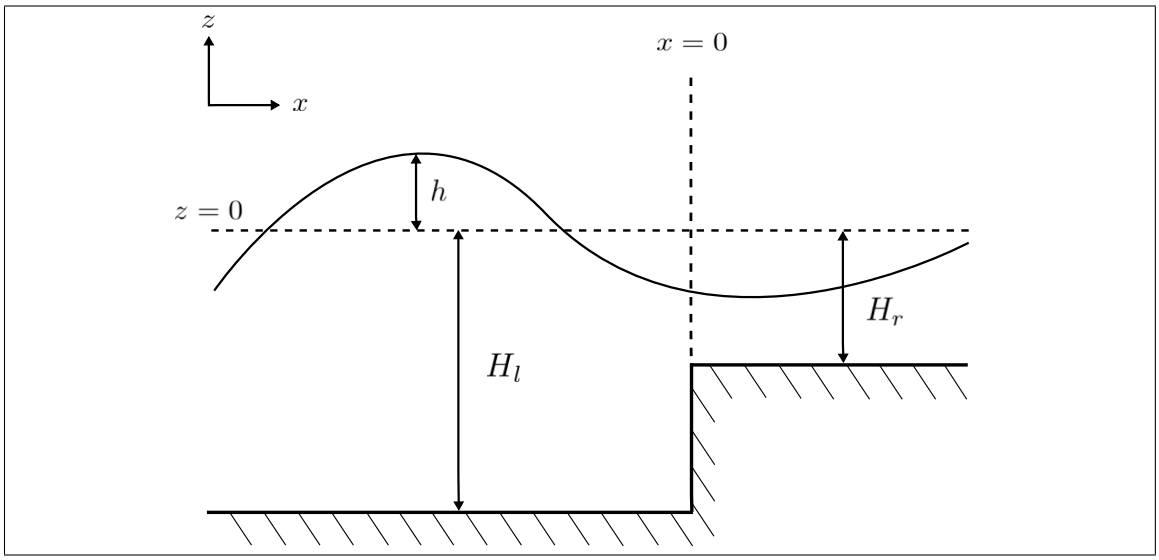


**Figure 2.3:** Schematic of the single layer model with a step. Here $H_l$ is the depth of the deep ocean, $H_2$ the depth on-shelf, and $h$ the perturbed sea surface height.

We have now considered all boundary conditions in our simple model. Furthermore, we have considered adding topographic features to the thin shell model originally considered by **?**.

Does shallow water theory break down in the presence of a step? **?** have shown that the use of shallow water does in fact capture many of the real-life dynamics of water waves. This theory is presented through understanding how tides are scattered at the continental shelf break in a two-layer fluid. When a shallow-water barotropic wave is incident upon a step bottom in a two-layer fluid some of the energy is transmitted, and another part reflected. The scattered waves can be decomposed into barotropic and internal waves and an edge-layer is present in the localised region of the step. This layer can be explained in terms of evanescent modes (linear wave theory) which are considered a perturbation of the main flow. **?** apply a WKBJ technique to compute and prove that these evanescent modes smooth out any discontinuities that may exist. Thus shallow water theory can suitably be applied to the generation of internal waves at real-life continental slopes.

### 2.1.4 The Rossby radius of deformation, $L_R$

$$L_R = \frac{\sqrt{gH}}{|f|} \tag{2.31}$$

This is an important length scale which determines the behaviour of certain waves. We can consider it as a measure of the degree to which Kelvin waves are trapped. For rotation effects to be small the distance of the displaced sea surface height from the coast must be small compared with the Rossby radius. With the effect of rotation, the solution to the classic Kelvin wave shows that $h$, the perturbed sea surface height, scales as $e^{-1/\sqrt{H}}$.

Hence $L_R$ is the distance that a Kelvin wave with speed $\sqrt{gH}$ can travel in time $1/f$, before being significantly affected by the Coriolis force. Note that this force is felt more strongly at the poles and is zero at the Equator as $f = 2\Omega \sin\theta_0$, where $\theta_0$ is a fixed latitude in the $f$-plane. Therefore, the Rossby radius decreases from infinity at the Equator to a minimum at the poles.

## 2.2 Conclusions

In this chapter, we introduced Laplace's Tidal Equations (LTEs) which were the original fundamental dynamic equations governing tides and long waves, and which had remain unchanged until 1940 (**?**). In deriving the shallow water equations (SWEs) (2.25a-c) we have made a number of assumptions, namely we have assumed constant density and inviscid flow, and that atmospheric pressure is constant on the surface of the sea. We have also explained and applied the shallow water and $f$-plane approximations, and linearised. These approximations either on their own, or in combination have been applied to reduce the Navier-Stokes equation (2.2a) and the continuity equation (2.2b) to what are universally known as the linear shallow water equations. It is worth mentioning that although Laplace's Tidal Equations and the linear shallow water equations have many similarities, the former is a forced system, while the latter gives rise to free wave solutions.

# Chapter 3

# Models of simple trapped barotropic waves

## 3.1 Introduction

To understand the coastal generation of internal tides, a thorough understanding of the structure of barotropic tides (which force the internal tides) is required. These barotropic tides can be viewed as various kinds of barotropic waves; for example, coastal tides can often be clearly identified as Kelvin waves. In this chapter, we review and develop some theoretical models of barotropic waves, and focus on the case of trapped waves, meaning those that decay away from the coast or from a submarine slope.

At tidal frequencies, these coastal barotropic waves are influenced by several factors: the coastline, the (shallow) continental shelf, the (steep) continental slope, and background rotation (through $f$). Each of these factors in itself modifies the simplest types of gravity waves. With a combination of all four of these additional effects taken into account, an understanding of the waves becomes rather complex; this discussion is deferred to Chapter 4. In this chapter, we instead consider one or more of these factors in isolation, to develop a basic understanding of the kind of solutions that may be expected.

We start with a brief discussion of the form of typical coastal topography in the real ocean, and set out the equations of motion to be used for the remainder of the chapter. Then, in section 3.2, we consider the effects of a coastline and background rotation in an ocean of uniform depth; this leads to the famous Kelvin wave. In section 3.3, we turn our attention to the effects of a coastline and sloping topography, with no background rotation; this leads to edge waves. In section 3.4, we explore the effects of a region of localised topography with background rotation but no coastline; this leads to topographic Rossby waves. Finally, in section 3.5, we derive in some detail a new solution for topographic Rossby waves over a particular smooth model topography, and demonstrate how these solutions are surprisingly accurate over a wide parameter regime.

Of course, many types of barotropic waves appear in the tidal signal, and as previously mentioned, there also exists a variety of tidal constituents. These are either forced by the gravitational pull of the sun or moon, or a combination of these. **?** have determined which of these waves are dynamically dominant off the Californian coast. Their estimates for the relative amplitudes of a free Kelvin wave, a free inertia-gravity (Poincaré-like) non-coastally trapped wave are 54:16 cm for the $M_2$ (semi-diurnal) tide, and 21:24 cm for the $K_1$ (diurnal) tides. Thus we see the important role played by the Kelvin wave (**?**).

### 3.1.1 Coastal topography in the real ocean

We first look in more detail at the type of coastal topography encountered. We focus on the continental margin which is a combination of a submerged shelf, a shelf-break and a slope which extends from the coastline.

Continental shelves lie under the ocean up to the point of the shelf-break, to give an indication of their size, approximately 7.4% of the world's ocean surface sits above continental shelves, which have a global average width of around 80 km and a depth of 30-600 m. Remarkably, the widest continental shelf in the world extends approximately 1000 km off the coast of Siberia into the Arctic Ocean.

The shelf-break is the boundary which marks the change in inclination between the continental shelf and slope, see Figure 3.1b. Thus, in contrast to the shelves, the continental

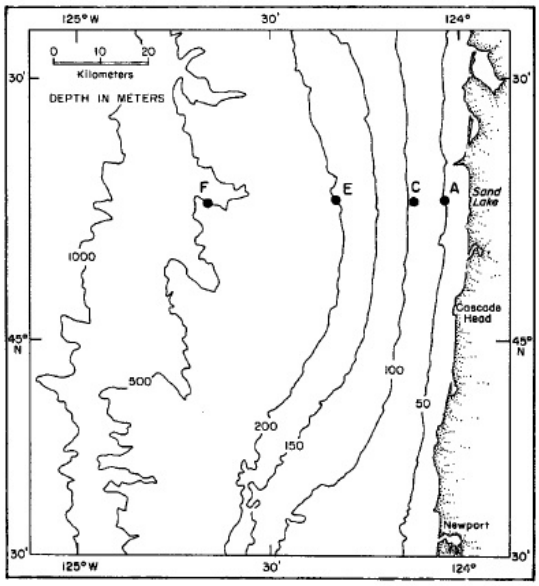


FIG. 2. Bottom topography and location of current meter moorings during CUE II.

(a)

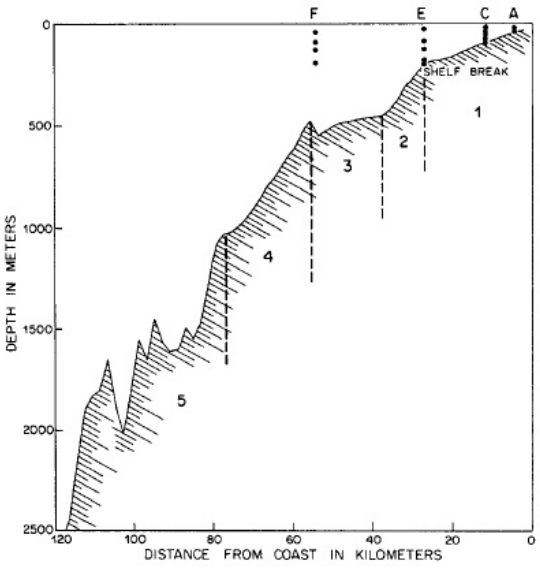


FIG. 3. Bottom topography along 45°16.2'N showing location of current meters during CUE II. The numbers 1, 2, 3, 4 and 5 are used to identify different topographic regions.

(b)

**Figure 3.1:** Oregon continental slope (**?**).

slopes characterise some of the steepest topographies in the ocean.

Figure 3.2 demonstrates the variability in steepness of slopes, and shelf lengths at several coastal regions across the United States. Obviously, the geological make-up of the coast contributes to its character, for example, the steepest continental slope is in West Florida (B) due to its resistant carbonate lithology. It is steepest below 1800m (along the Florida escarpment) with a mean incline of approximately 31% over an area of 470 $m^2$. The next steepest is the New Jersey-Maryland slope (A) which is steeper and less rugged than the tectonically active Louisiana (C), California (D) and Oregon slopes (E). It is suggested that the greater steepness of (A) may be due to the region's relative stability with the steepest slopes being less than 1500m in depth (**?**).

The Oregon slope (E) is shown in more detail in Figure 3.1b. The figure clearly indicates

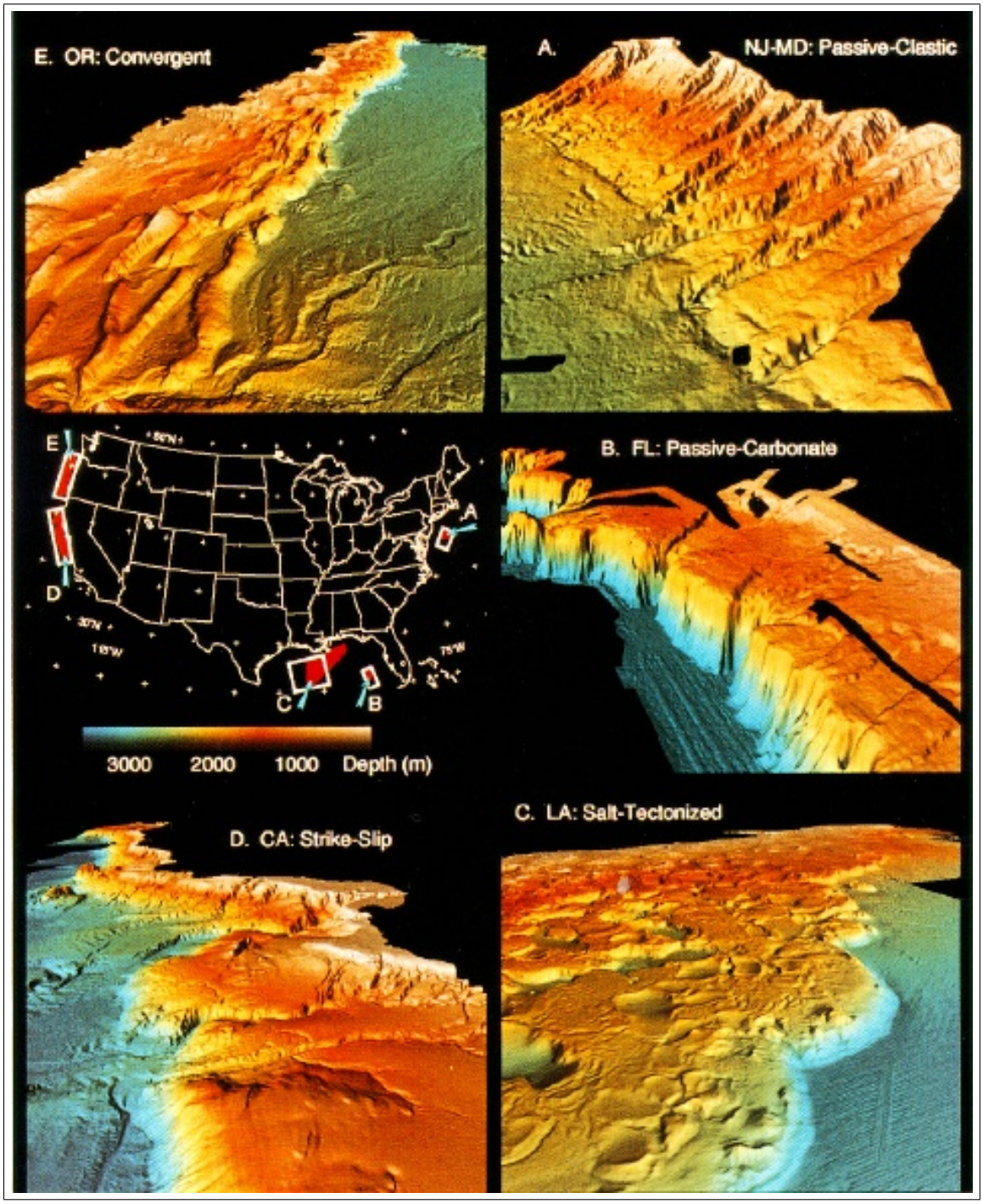


**Figure 3.2:** Continental slopes of the US (**?**).

the steepness of the slope compared to the shelf. The deep ocean depth is $2500$ m ($H_1$), the on-shelf depth is approximately 200 m ($H_2$), and the slope half-width, ($L_s$) about 60 km. Thus the average gradient of the slope is approximately 0.02.

We have made the shallow water assumption in developing our theoretical model, that is, that the horizontal length scale is much greater than the vertical length scale. In real-life several continental margins are consistent with this assumption; for example, the average gradient of the West Florida slope is 0.08 over an area of $1520\text{km}^2$. Thus, for every $100$m in the horizontal direction, there is a vertical drop of $8$m. In general, the majority of continental slopes have a gradient in the range 0.03-0.18 which allows us to use the shallow water equations. In more extreme cases one may expect the underlying assumptions to break down.

### 3.1.2 Equations of motion

Since we are considering barotropic waves, we use the single-layer shallow water equations (2.25a-c). However, now we consider variations in the undisturbed ocean depth $H$. Even though coastal topographies are three-dimensional, the dominant character is two-dimensional. Here, we make the simplifying assumption that there are no topographic variations in the alongshore direction, $x$. Taking the cross-shore direction to be $y$, we thus assume $H = H(y)$. We seek wave-like solutions of the form

$$(h, u, v) = \mathrm{Re}\Big[(\hat{h}(y), \hat{u}(y), \hat{v}(y))e^{i(kx-\omega t)}\Big]. \tag{3.1}$$

Here $\omega$ is the frequency, $k$ is the wavenumber along the topography which we take as $k > 0$ without loss of generality. $\hat{h}(y)$, $\hat{u}(y)$ and $\hat{v}(y)$ give the cross-shore structure of the perturbed sea surface height, and the alongshore and cross-shore velocities. We can now

write equations (2.25a-c) as

$$-i\omega\hat{u} - f\hat{v} = -igk\hat{h}, \tag{3.2a}$$

$$-i\omega\hat{v} + f\hat{u} = -g\frac{d\hat{h}}{dy}, \tag{3.2b}$$

$$-i\omega\hat{h} + ikH\hat{u} + \frac{d(H\hat{v})}{dy} = 0. \tag{3.2c}$$

## 3.2 The Kelvin wave (KW)

We start by considering the influence of a coastline in isolation, that is, with no other topographic variations. As first noted by Lord Kelvin, (**?**), the coastline can act to trap a wave in a semi-infinite domain. The solution, known as a the Kelvin wave, has the special property that the cross-shore velocity is identically zero. Despite the simplicity of the setting, the classic Kelvin wave solution remains a widely used paradigm in geophysical fluid dynamics. For example, the speed with which the equilibrium tide moves around the Earth happens to be similar in magnitude to the speed of long gravity waves, **?** uses the Kelvin wave speed as a scaling parameter. The behaviour of the Kelvin wave at a channel end has been used to describe seiches and tides in the North Sea (**?**).

The cross-shore structure $\hat{h}(y)$ of the Kelvin wave can be found by considering the linear shallow water equations (3.2 a-c), and setting $\hat{v} = 0$ everywhere. Making $\hat{u}$ the subject in (3.2a), and substituting this into (3.2c) implies

$$\omega = \pm k\sqrt{gH}. \tag{3.3}$$

Now (3.2a) gives the alongshore velocity as

$$\hat{u} = \frac{gk}{\omega}\,\hat{h}, \tag{3.4}$$

and substituting this into (3.2b) yields

$$\hat{h}(\hat{y}) = \hat{h}(0)e^{-fky/\omega}. \tag{3.5}$$

Since we require the perturbed sea surface height to decay exponentially away from the coast, then $fk/\omega$ must be positive. This is the only physically acceptable solution if the

coast is at $y = 0$, and we have the deep ocean at $y > 0$. Since we have taken $k > 0$, then $\omega > 0$ if $f > 0$ so that Kelvin waves propagate in the positive $x$-direction in the northern hemisphere, or with the coast on their right. Given $f < 0$, in the southern hemisphere, we must have $\omega < 0$, so Kelvin waves propagate in the negative $x$-direction in the southern hemisphere, that is, with the coast on their left. We are therefore able to resolve the $\pm$ in (3.3) and obtain

$$\omega = k\sqrt{gH}\,\mathrm{sgn}(f). \tag{3.6}$$

Thus the Kelvin wave is non-dispersive, and although trapped by the rotation of the Earth, surprisingly, its frequency and phase-speed are only influenced by the sign of $f$.

In addition to coastally trapped Kelvin waves, there also exist equatorial Kelvin waves which travel eastwards and are trapped by the equator (**?**). At $f = 0$, these special waves become trapped between what are known as inertial latitudes (**?**). However, these waves are not the focus of our work in considering generation of internal gravity waves at the coast.

By (3.6), we can now rewrite (3.5) as

$$\hat{h} = \hat{h}(0)e^{-y/L_R}, \tag{3.7}$$

where $L_R$ is the Rossby radius of deformation.

## 3.3 Edge waves (EWs)

We now turn our attention to waves that are very different to Kelvin waves. Although coastally trapped edge waves do not need background rotation to exist, they need some kind of varying topography. These high frequency gravity waves, are able to travel in both directions along the coastline, and tend to 'live' on the continental shelf. It was originally thought that edge waves were a mathematical curiosity; however, it is now recognised that they play an important role in near-shore hydrodynamics, such as beach erosion and the forming of sand bars (**?**). For example, edge wave run-up patterns on

beaches have been observed, demonstrating the existence of these waves (**?**).

These waves of super-inertial frequencies are uniquely trapped by critical internal reflection at the shelf edge/slope. Initially let us consider a flat shelf model so we have a discontinuity in depth. Snell's Law describes the relationship between an incident (I) and transmitted (T) wave as

$$\frac{\sin \alpha_{2_I}}{\sin \alpha_{1_T}} = \frac{c_{2_I}}{c_{1_T}}$$

where $c_1$ and $c_2$ represent the speeds in each respective region, and the depths in each region are such that $H_1 > H_2$. Now let us consider a wave moving from the shallow towards the discontinuity as shown in Figure 3.3. Then

$$\frac{\sin \alpha_{2_I}}{\sin \alpha_{1_T}} = \frac{(gH_2)^{1/2}}{(gH_1)^{1/2}},$$

since $c = \sqrt{gH}$ for non-rotating gravity waves. Therefore

$$\sin \alpha_{2_I} < \sin \alpha_{1_T}, \tag{3.8}$$

since $H_2 < H_1$. Thus the angle of incidence is less than the transmitted angle. As $\alpha_{2_I}$ increases it reaches a critical value at which the transmitted angle, $\alpha_{1_T} = \pi/2$. Thus for any incident angle greater than this critical angle all waves are reflected back towards the coastline, which is known as total internal reflection. Since it is possible that we have an infinite number of waves 'arriving' at the discontinuity at different angles greater than the critical angle, we can therefore have an infinite number of edge wave modes existing.

### 3.3.1 Stokes' mode

Without making the shallow water assumption, the classical solution for the fundamental edge wave mode was discovered by **?**. Originally **?** considered the problem of wave propagation in a canal. Stokes' simplified this problem by exploring wave propagation in a one-sided canal, with water increasing in depth away from the inclined wall at an angle of $\pi/4$, (which we generalise to an arbritary angle $\alpha$). In setting up this problem we

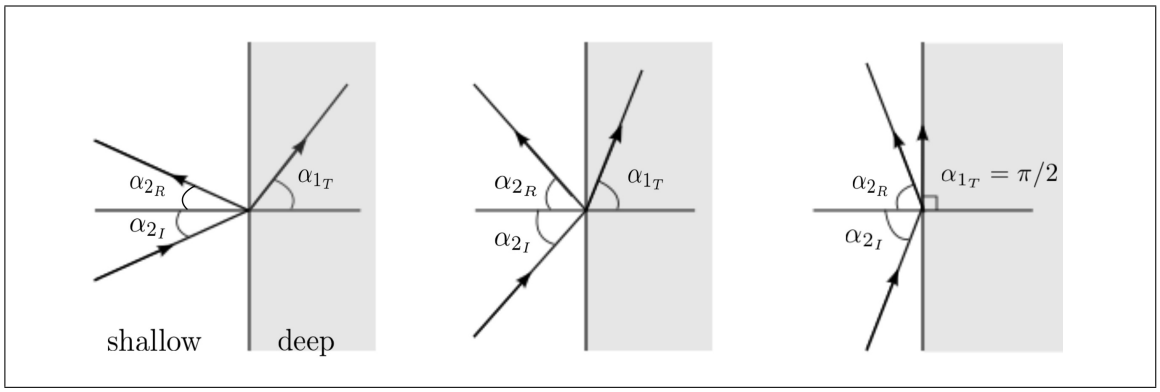


**Figure 3.3:** Total internal reflection: the trapping mechanism for edge waves

consider an inviscid, incompressible flow bounded by a free surface above, with $x$ along the canal and $y$ normal to the canal wall. Here $z = h(x, y, t)$, and we can write the fixed, impermeable surface of the canal wall as

$$z = -y \tan \alpha \tag{3.9}$$

where $\alpha$ represents the angle below the horizontal.

The basic state of pressure is given by (2.16) $p_0 = p_{atm} - \rho g z$, where $p_{atm}$ is the atmospheric pressure. If we have a small perturbation $p'$ in pressure to the basic state then

$$\implies p'(z = h) = \rho g h$$

Within linear theory, $p'(z = h) = p'(z = 0)$, so

$$p'(z = 0) = \rho g h.$$

Linearising (2.2a), and by the continuity of mass, we have to leading order

$$\frac{\partial \underline{u}}{\partial t} = -\frac{1}{\rho} \underline{\nabla} p' \qquad \text{and} \quad \underline{\nabla} \cdot \underline{u} = 0 \tag{3.10a}$$

where $\underline{\nabla} = (\partial/\partial x, \partial/\partial y, \partial/\partial z)$ and $\underline{u} = (u, v, w)$. At the free surface $z = h$ we have an expression for $w(h)$ (2.23)

$$w = \frac{\partial h}{\partial t} + \underline{u} \cdot \underline{\nabla} h \quad \text{on} \quad z = h. \tag{3.11}$$

Thus in the linear approximation we have

$$w(z=0) = \frac{\partial h}{\partial t}. \tag{3.12}$$

We can now derive an expression for $w$ as we have no normal flow on the surface of the canal, thus

$$w + v\tan\alpha = 0. \tag{3.13}$$

Summarising we have

$$\underline{\nabla}\cdot\underline{u} = 0, \tag{3.14a}$$

$$\frac{\partial \underline{u}}{\partial t} = -\frac{1}{\rho}\underline{\nabla} p', \tag{3.14b}$$

$$p'(0) = \rho g h, \tag{3.14c}$$

$$w = \frac{\partial h}{\partial t} \quad \text{on} \quad z = 0, \tag{3.14d}$$

$$w + v\tan\alpha = 0 \quad \text{on} \quad z = -y\tan\alpha, \tag{3.14e}$$

and since we are seeking trapped waves

$$|\underline{u}| \longrightarrow 0 \quad \text{as} \quad y \longrightarrow \infty. \tag{3.15}$$

**Deriving dispersion relation**

We seek irrotational solutions by writing $\underline{u} = \underline{\nabla}\varphi$, where $\varphi$ is the velocity potential. (Note that vorticity perturbations associated with planetary vorticity may be ignored for waves on a sufficiently small scale.) Thus (3.14a) implies $\nabla^2\varphi = 0$, and assuming $\varphi = \mathrm{Re}\left(Ae^{i(kx-\omega t)+lz-my}\right)$ where we require $\mathrm{Re}(m) > 0$ for trapping, we have

$$k^2 = l^2 + m^2. \tag{3.16}$$

By (3.14b) we have $\varphi_t = -p'/\rho + c(t)$. Setting $c(t) = 0$, gives $\varphi_t = -p'/\rho$ so that

$$p' = \mathrm{Re}\left(i\omega\rho A e^{i(kx-\omega t)+lz-my}\right). \tag{3.17}$$

Now, $p'(z=0) = \rho g h$, thus by (3.14c)

$$h = \mathrm{Re}\left(\frac{iA\omega}{g} e^{i(kx-\omega t)-my}\right). \tag{3.18}$$

At $z = 0$, we have $w = \partial\varphi/\partial z = \partial h/\partial t$, therefore

$$\omega^2 = gl, \tag{3.19}$$

and by (3.14e),

$$l = m\tan\alpha. \tag{3.20}$$

By (3.16) and (3.20) we arrive at

$$m = \frac{|k|}{\sec\alpha}. \tag{3.21}$$

Combining (3.20), (3.19), (3.21) and the boundary condition of exponential decay, we are able to derive the simple dispersion relation

$$\omega^2 = g|k|\sin\alpha. \tag{3.22}$$

Although this relation is only for the leading mode in Stokes' model, it highlights that for an edge wave to exist we need a sloping beach (i.e., $\alpha = 0 \implies \omega = 0$).

Non-linear corrections have been added to Stokes' linear solution **?**, for the shallow water and full equations. Again irrotationality was assumed, leading to

$$\omega^2 \sim gk(1+\gamma\delta^2k^2)\sin\alpha, \quad 0 < \alpha < \frac{\pi}{2} \tag{3.23}$$

where $\gamma$ is a constant independent of $\delta$. Here $(\underline{u}, p, h) \to \delta(\underline{u}, p, h)$, and when $\delta \longrightarrow 0$, we again recover Stokes' mode.

### 3.3.2 Continuous and discrete spectra

**?** showed that (3.22) was the first in a finite number of trapped edge wave modes that satisfies the linear problem. An irrotational flow field is also assumed; however, Ursell does not impose that the edge wave is sinusoidal cross-shore

$$\phi(x,y,z,t) = A(y,z)e^{i(kx-\omega t)}.$$

Essentially Ursell derives the following dispersion relation and condition which determines the $n+1$ modes

$$\omega^2 = g|k|\sin[(1+2n)\alpha] \quad \text{where} \quad (1+2n)\alpha \leq \frac{\pi}{2} \quad \text{and} \quad n = 0, 1, 2, \cdots . \tag{3.24}$$

The number of modes depends on the angle of the slope, and additionally there is a continuous spectrum of modes for

$$g|k| \leq \omega^2 \leq \infty, \tag{3.25}$$

hence the generation of edge waves will consist of a mixture of continuous and discrete modes.

### 3.3.3 Shallow water assumption

**?** makes the shallow water approximation but unlike Stokes and Ursell includes background rotation, and derives

$$\omega^2 = g(1+2n)|k|\,\tan\alpha \quad \text{given} \quad 0 < \alpha < \frac{\pi}{2}. \tag{3.26}$$

This gives the same result as Ursell as $\alpha \longrightarrow 0$, however there is no continuous spectrum of modes.

Therefore, it has been proved that there exists a spectrum of edge waves which live on the slope, and are trapped by critical internal reflection caused by the changes in depth along the slope.

## 3.4 Topographic Rossby waves (TRWs)

Having considered the presence of a coastline and rotation, and a slope and no rotation, we now turn our attention to rotation combined with the a slope acting as a waveguide for propagating waves. Note, in this section, there will be no coastline; that more complex scenario will be investigated in Chapter 4. This single-slope configuration was initially

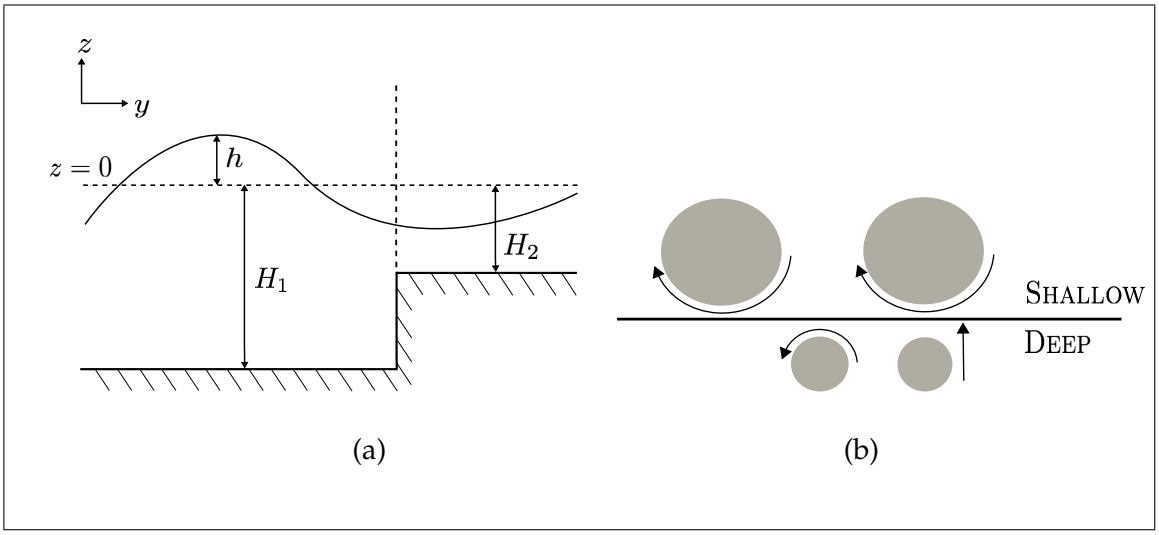


**Figure 3.4:** (a) Single density layer model with a step (b) Behaviour of TRWs in order to conserve Potential Vorticity (PV) (shown in more detail in Figure 3.5).

considered by **?** for a discontinuous topography in a doubly-infinite domain. We develop this solution by considering the type of waves generated on a smooth, continuous slope.

### 3.4.1 Restoring mechanism of topographic Rossby waves (TRWs)

The topographic Rossby wave (TRWs) relies on background rotation, and we take the simplest representation of this: the $f$-plane. We can understand the nature of these long waves through the conservation of shallow water potential vorticity, $Q$. It can be shown from (2.25 a-c) that $Q$ is materially conserved (**?**). Here

$$Q = \frac{f + \zeta}{H + h},$$

the absolute vorticity (sum of the background vorticity and the vertical component of the relative vorticity) divided by the height of the column, where $\zeta = \partial v/\partial x - \partial u/\partial y$.

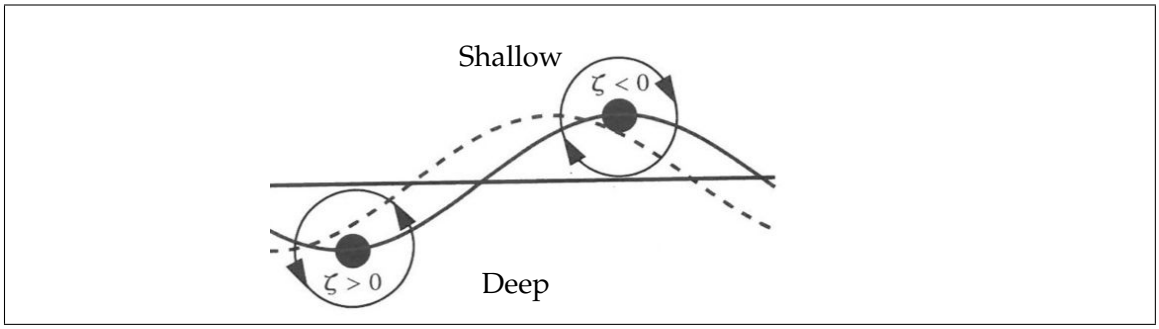


**Figure 3.5:** Conservation of PV of a column of water. (**?**)

Let us consider a column of water that moves across a discontinuous topography in the Northern hemisphere. If the column moves from deep to shallow water (as shown in Figure 3.4 and Figure 3.5), the column becomes shorter (bounded above by the sea-surface) with a larger radius. Thus $H + h$ is reduced, so to conserve potential vorticity we require the absolute vorticity to decrease. Thus $\zeta$ takes the opposite sign to $f$ ($\zeta < 0$), and so we have anticyclonic motion (i.e., clockwise in the Northern hemisphere). If the column of water were now to move from the shallow to deep water, then $H + h$ would increase and to conserve potential vorticity $\zeta$ would need to increase ($\zeta > 0$), thus we would have cyclonic motion. These vorticity perturbations can also be understood in terms of conservation of angular momentum; i.e., changes in moment of inertia.

As shown in Figure 3.5 the solid line is a material line of stationary columns of water. If displaced the columns wish to conserve potential vorticity and as explained in the previous paragraph, if moving from deep to shallow waters the column of water spins anti-clockwise i.e., we have negative relative vorticity. When the column of water moves from shallow to deep water we have positive relative vorticity. The associated velocity field advects the columns of water, the solid line evolves into the dashed line. Thus the columns of water propagate to the left with the shallow water to the right of the motion. Thus, we have what is known as a topographic Rossby wave which is completely analogous to the Rossby wave with planetary vorticity. .

### 3.4.2 Non-dimensional equations for $L_R \gg L$

Although the linear shallow water equations (2.25a-c) may be used to analyse topographic Rossby waves, an important simplification may be made that simplifies the analysis. To do this, we determine which are the important terms in (2.25 a-c) which lead to the topographic Rossby wave. In this section, we thus temporarily work in non-dimensional coordinates and variables.

Let us scale the lengths by $L$, a typical length-scale of the wave, and velocities by a typical velocity $U$ such that

$$\tilde{x} = \frac{x}{L}, \quad \tilde{y} = \frac{y}{L}, \quad \tilde{u} = \frac{u}{U}, \quad \tilde{v} = \frac{v}{U}.$$

We also scale the depth by $H_0$, and time by $f$:

$$\tilde{H} = \frac{H}{H_0}, \quad \tilde{t} = ft.$$

For flows that are close to geostrophic balance,

$$fU \sim \frac{gh}{L} \quad \Longrightarrow \; h \sim \frac{fUL}{g}.$$

We can thus scale the perturbed sea surface height

$$\tilde{h} = \frac{g}{fUL}h.$$

The derivatives transform as

$$\frac{\partial}{\partial t} = f\frac{\partial}{\partial \tilde{t}}, \quad \frac{\partial}{\partial x} = \frac{1}{L}\frac{\partial}{\partial \tilde{x}} \quad \text{and} \quad \frac{\partial}{\partial y} = \frac{1}{L}\frac{\partial}{\partial \tilde{y}}.$$

We can now write the linearised shallow water equations (2.25 a-c) in non-dimensional form.

$$\frac{\partial \tilde{u}}{\partial \tilde{t}} - \tilde{v} = -\frac{\partial \tilde{h}}{\partial \tilde{x}}, \tag{3.27}$$

$$\frac{\partial \tilde{v}}{\partial \tilde{t}} + \tilde{u} = -\frac{\partial \tilde{h}}{\partial \tilde{y}}. \tag{3.28}$$

$$\left(\frac{L}{L_R}\right)^2 \frac{\partial \tilde{h}}{\partial \tilde{t}} + \left(\frac{d(\tilde{H}\tilde{u})}{d\tilde{x}} + \frac{d(\tilde{H}\tilde{v})}{d\tilde{y}}\right) = 0, \tag{3.29}$$

where $L_R = \sqrt{gH_0}/|f|$ is the Rossby radius of deformation. Note, we are implicitly assuming that $d\tilde{H}/d\tilde{y}$ is of order unity, so that the lengthscale of the topography should be of the same order of magnitude as that of the waves. Thus, when

$$L \ll L_R,$$

i.e., when the length scale of the wave is much smaller than $L_R$, (3.29) is approximated by

$$\frac{d(\tilde{H}\tilde{u})}{d\tilde{x}} + \frac{d(\tilde{H}\tilde{v})}{d\tilde{y}} = 0.$$

This approximation is sometimes known as the rigid-lid approximation. This name is misleading because free surface displacements are needed to give pressure gradients in (3.27) and (3.28). However, if we were to impose a rigid lid at $z = 0$, then the same pressure gradients would still be achieved because the rigid lid would provide the necessary pressure (**?**). Converting back to dimensional variables we have

$$\frac{\partial u}{\partial t} - fv = -g\frac{\partial h}{\partial x} \tag{3.30a}$$

$$\frac{\partial v}{\partial t} + fu = -g\frac{\partial h}{\partial y} \tag{3.30b}$$

$$\frac{\partial (Hu)}{\partial x} + \frac{\partial (Hv)}{\partial y} = 0. \tag{3.30c}$$

where $H = H(y)$.

### 3.4.3 The wave equation for the rigid lid approximation

Further analysis is most easily performed in terms of a streamfunction. To eliminate $h$, differentiate (3.30b) with respect to $x$ and subtract this from (3.30a) which has been differentiated with respect to $y$, to obtain

$$(u_y - v_x)_t - f(u_x + v_y) = 0. \tag{3.31}$$

We now introduce a streamfunction $\psi(x, y, t)$ which satisfies (3.30c). So we can write the velocities as

$$u = -\frac{\psi_y}{H}, \quad v = \frac{\psi_x}{H} \tag{3.32}$$

where $H \neq 0$. If we consider that a change in the topography only occurs in the cross-shore direction while in the alongshore direction the topography remains constant then $H = H(y)$. We substitute (3.32) into (3.31) to give

$$H\psi_{yyt} - \psi_{yt}H_y + H\psi_{xxt} + f\psi_x H_y = 0. \tag{3.33}$$

Assuming wave-like solutions of the form

$$\psi(x, y, t) = \mathrm{Re}\left(\Phi(\hat{y})e^{i(kx-\omega t)}\right) \tag{3.34}$$

(3.33) becomes

$$H\Phi'' - H'\Phi' - \left[\frac{fkH'}{\omega} + Hk^2\right]\Phi = 0, \tag{3.35}$$

where prime denotes differentiation with respect to $y$. We choose to eliminate the $\Phi'(y)$ term; writing

$$\Phi(y) = \phi(y)H^n, \tag{3.36}$$

substituting into (3.35) and taking $n = 1/2$, gives

$$\phi'' + \left[\frac{1}{2}H''H^{-1} - \frac{3}{4}H^{-2}(H')^2 + \frac{fk}{\omega}H'H^{-1} - k^2\right]\phi = 0. \tag{3.37}$$

This is the general equation governing waves (**?**) where we have made the rigid lid approximation, for an arbitrary depth profile $H(y)$. For trapped waves we have the boundary condition $\phi \to 0$ as $|y| \to \infty$. Now $\psi_x \sim ik\phi$, so if we have a coastline then $\phi = 0$ at $y = 0$ and hence $v = 0$ by (3.32). However, we still have an alongshore velocity since $\psi_y \sim \phi'$.

### 3.4.4 A step solution derived by ?

Let us consider a topographic profile in which there exists only a step at $y = 0$, separating two regions of constant depth, and no coastline. This leads to the solution of **?**, which we derive from (3.35). The profile is given by

$$H = H_0 - \Delta H(1 - 2\Theta(y)) \tag{3.38}$$

where $H_0 = 1/2(H_1 + H_2)$, $\Delta H = 1/2(H_1 - H_2)$ and $H_1$ and $H_2$ are shown in Figure 3.4. We define $\Theta$ which represents the Heaviside function

$$\Theta(y) = \begin{cases} 0 & y < 0, \\ 1 & y > 0. \end{cases}$$

**On either side of the step**

Since $H(y)$ is constant on either side of the step (3.35) becomes $\Phi'' - k^2\Phi = 0$. We require exponentially decaying solutions as $y \longrightarrow \pm\infty$, thus

$$\Phi(y) = \begin{cases} A_- e^{+|k|y} & y < 0, \\ A_+ e^{-|k|y} & y > 0. \end{cases} \tag{3.39}$$

**Continuity of mass at** $y = 0$

By the continuity of mass (2.30), $\psi_x$ is continuous at $y = 0$ by (3.33). This implies $ik\,\Phi$ is continuous by (3.34), and hence $\Phi$ is continuous. This gives the result $A_- = A_+$, therefore (3.39) becomes

$$\Phi(y) = \begin{cases} Ae^{+|k|y} & y < 0, \\ Ae^{-|k|y} & y > 0. \end{cases} \tag{3.40}$$

**Integrating across** $y = 0$

The dispersion relation can be determined by evaluating $h$ on either side of the step and then applying the condition of continuity of $h$ at the step (2.29). However, the same result can be obtained directly from (3.35). Integrating across the step, we find

$$\int_{0_-}^{0_+} \left( H\Phi'' - H'\Phi' - \left[ \frac{fkH'}{\omega} + Hk^2 \right] \Phi \right) \mathrm{d}y = 0.$$

Now

$$\int_{0_-}^{0_+} Hk^2\Phi \,\mathrm{d}y = 0,$$

since $H$ and $\phi$ are finite but the other terms may involve $\delta$ functions; thus we are left with

$$\int_{0_-}^{0_+} H\Phi'' \,\mathrm{d}y - \int_{0_-}^{0_+} H'\Phi' \,\mathrm{d}y - \int_{0_-}^{0_+} \frac{fkH'}{\omega}\Phi \,\mathrm{d}y = 0$$

Integrating the first term by parts, and substituting for $H'$ from (3.38) leads to

$$\left[H\Phi'\right]_{0_-}^{0_+} - 2\int_{0_-}^{0_+} H'\Phi' \,\mathrm{d}y - \frac{2fk\Delta H}{\omega} \int_{0_-}^{0_+} \delta(y)\Phi \,\mathrm{d}y = 0. \tag{3.41}$$

By the properties of the delta function, $\delta(y)$, (**?**)

$$\int_{-\infty}^{\infty} \delta(y)F(y) \,\mathrm{d}y = F(0) \tag{3.42}$$

where $F$ is continuous at zero. Thus by (3.40),

$$\int_{0_-}^{0_+} \delta(y)\Phi \,\mathrm{d}y = A, \tag{3.43}$$

applying this to the last term in (3.41) results in

$$-2|k|AH_0 - 2\int_{0_-}^{0_+} H'\Phi' \,\mathrm{d}y - \frac{2fkA\Delta H}{\omega} = 0. \tag{3.44}$$

The second term is evaluated by another property of the $\delta(y)$ function (**?**) .

$$\int_{0_-}^{0_+} H'\Phi' \,\mathrm{d}y = 0.$$

Therefore

$$-2|k|AH_0 - \frac{2fkA\Delta H}{\omega} = 0.$$

Thus we have the solution for a topographic Rossby wave trapped along a discontinuity (**?**).

$$\omega = -\frac{f\Delta H\mathrm{sgn(k)}}{H_0}. \tag{3.45}$$

We have taken the positive cross-shore component in the opposite direction as **?**, making this amendment we have

$$\omega = \frac{f\Delta H\mathrm{sgn(k)}}{H_0}. \tag{3.46}$$

The topographic Rossby wave in previous studies has confusingly been referred to as double Kelvin waves (**????**). However, as discussed in section 3.4, the topographic Rossby wave only travels in one direction, with the shallow water to the right.

## 3.5 Topographic Rossby waves (TRWs) on a continuous topography

In section 3.4.1, we established the nature of the topographic Rossby wave is to conserve potential vorticity. We have derived the dispersion for a topographic Rossbby wave in which the step acts as a waveguide (3.46) (**?**). However what happens if we have a continuous topography?

### 3.5.1 New solution for a hyperbolic tangent profile

We now consider a more realistic profile that has a smooth, continuous slope

$$H = H_0 + \Delta H \tanh\left(\frac{y}{L_s}\right) \tag{3.47}$$

where $L_s$ is half the slope-width, $H_0 = 1/2(H_1 + H_2)$ and $\Delta H = 1/2(H_1 - H_2)$. Hence as $|y| \longrightarrow \pm\infty$, we have $H \longrightarrow H_1$ and $H_2$ respectively. We solve for waves in an unbounded ocean, i.e. with no coastline. The essence of the waves depends on the change in the topography, and of course a coastline will affect the details of the frequency but we shall later show that this has a small effect. Substituting (3.47) into (3.37), and writing

$$\hat{y} = \frac{y}{L_s} \implies \frac{d}{dy} = \frac{1}{L_s}\frac{d}{d\hat{y}}$$

we find

$$\frac{d^2\phi}{d\hat{y}^2} + \left[ -k^2L_s^2 - \left(\frac{\Delta H}{H}\tanh\hat{y} + \frac{3}{4}\left(\frac{\Delta H}{H}\right)^2 \operatorname{sech}^2\hat{y} - \frac{fk\Delta H L_s}{\omega H}\right)\operatorname{sech}^2\hat{y}\right]\phi = 0. \tag{3.48}$$

We can make analytical progress by making a small topography assumption, $\Delta H \ll H_0$. To leading order, we thus neglect the second and third terms in the square bracket provided

$$\frac{\Delta H}{H} \ll k^2L_s^2. \tag{3.49}$$

Note that, as mentioned in section 3.4.2, our scaling analysis formally requires $kL_s \sim 1$; equivalently we are taking $\Delta H/H \ll 1$. The final term of (3.48) must be retained for

wave-like solutions; indeed we know from (3.46) that $\omega$ scales like $f|\Delta H|/H_0$, from the result given by (3.46). Thus $fk\Delta HL_s/\omega H_0$ is an O(1) term. Thus to leading order, we consider

$$\frac{d^2\phi}{d\hat{y}^2} + \left( -k^2L_s^2 + \frac{fk\Delta HL_s}{\omega H_0}\,\mathrm{sech}^2\,\hat{y}\right)\phi = 0, \tag{3.50}$$

where in the denominator we have replaced $H$ by $H_0$ because $\Delta H \ll H_0$. We solve this such that $|\phi| \to 0$ as $|y| \to \infty$ resulting in an eigenvalue problem for $\omega$.

### 3.5.2 Dispersion relation

We write this in general form as

$$\phi_{yy} + (E + \nu\,\mathrm{sech}^2\,y)\phi = 0 \tag{3.51}$$

where $E$ and $\nu$ are constants. **?** have solved (3.51) which is the Schrödinger equation. However, we proceed to derive the same results which will prove the existence of multiple topographic Rossby waves for this topography and why these solutions have either an odd or even number of zeros.

This is an eigenvalue problem, with $|\phi| \to 0$ as $|y| \to \infty$, and, in general, either $\nu$ is given and we solve for $E$ or, $E$ is given and we solve for $\nu$. We want to find a relationship for $\omega$ in terms of $k$, so we seek $\nu$ in terms of $E$. (Of course, we take $E = -k^2L_s^2$ and $\nu = fk\Delta HL_s/\omega H_0$ as in (3.50)).

Without performing any detailed calculations, some things may be said about $E$ and $\nu$. In the limit of large $|y|$, $\mathrm{sech}^2\,y$ vanishes, thus we are left with

$$\phi_{yy} + E\,\phi = 0.$$

The solutions are oscillatory if $E > 0$, and may be exponentially decaying solutions if $E < 0$. So, we require $E < 0$. To determine the sign of $\nu$, we multiply (3.51) by $\phi$ then

integrate

$$\int_{-\infty}^{\infty} \left( \phi\phi'' + E\phi^2 + \nu \operatorname{sech}^2 y \, \phi^2 \right) \mathrm{d}y = 0,$$

$$[\phi\phi']_{-\infty}^{\infty} - \int_{-\infty}^{\infty} (\phi')^2 \, \mathrm{d}y + E \int_{-\infty}^{\infty} \phi^2 \, \mathrm{d}y + \nu \int_{-\infty}^{\infty} \operatorname{sech}^2 y \, \phi^2 \, \mathrm{d}y = 0,$$

$$- \int_{-\infty}^{\infty} (\phi')^2 \, \mathrm{d}y + E \int_{-\infty}^{\infty} \phi^2 \, \mathrm{d}y + \nu \int_{-\infty}^{\infty} \operatorname{sech}^2 y \, \phi^2 \, \mathrm{d}y = 0,$$

$$\text{since} \quad |\phi| \to 0 \quad \text{as} \quad |y| \to 0.$$

Here the first term is negative, and so is the second term since we have established $E < 0$. Therefore, to balance we require the last term to be positive. Since $\operatorname{sech}^2 y$ and $\phi^2$ are positive, it follows that $\nu$ is positive. Thus we can only obtain decaying solutions when

$$E < 0, \, \nu > 0. \tag{3.52}$$

We have $E = -k^2 L_s^2$ and $\nu = fkL_s \Delta H / \omega H_0$, and we shall assume we are looking for solutions with positive $k$. If we look for negative $k$, then $\omega$ reverses sign and leaves us with the same sign for $\nu$, and $E$. So we can assume without loss of generality $\sqrt{-E} > 0$, and $k > 0$.

To determine the eigenvalue relation, we make two transformations. Firstly

$$z = \tanh\left(\frac{y}{a}\right), \tag{3.53}$$

where $a$ is an arbitrary constant. Thus

$$\phi_{yy} = \frac{1}{a^2}(1 - z^2)^2 \phi_{zz} - \frac{2}{a^2} z(1 - z^2)\phi_z. \tag{3.54}$$

Substituting (3.53) and (3.54) into (3.51) we have

$$\frac{1}{a^2}(1 - z^2)^2 \phi_{zz} - \frac{2}{a^2} z(1 - z^2)\phi_z + [E + \nu(1 - z)^2]\phi = 0. \tag{3.55}$$

Secondly, we use the transformation

$$\phi(z) = (1 - z^2)^\alpha \, \gamma(z). \tag{3.56}$$

Thus

$$\phi_z = \gamma_z (1 - z^2)^\alpha - 2\alpha z (1 - z^2)^{\alpha - 1} \gamma, \tag{3.57}$$

and

$$\phi_{zz} = (1-z^2)^{\alpha}\gamma_{zz} - 4\alpha z(1-z^2)^{\alpha-1}\gamma_z - 2\alpha\Big[(1-z^2)^{\alpha-1} - 2(\alpha-1)z^2(1-z^2)^{\alpha-2}\Big]\gamma. \quad (3.58)$$

Substituting (3.56), (3.57) and (3.58) into (3.55) gives

$$(1-z^2)^2\gamma_{zz} - (4\alpha+2)z(1-z^2)\gamma_z + \Big[4\alpha^2z^2 + Ea^2 + \Big(\nu a^2 - 2\alpha\Big)(1-z^2)\Big]\gamma = 0. \quad (3.59)$$

To write this in standard form, we require the last term to be proportional to $(1-z^2)$, which can be achieved by choosing

$$\alpha^2 = -\frac{Ea^2}{4}, \quad \alpha > 0. \quad (3.60)$$

Note as $|z| \to 1$ (i.e. as $|y| \to \infty$) then $\phi(z) \to 0$, by (3.56) and the boundary conditions are satisfied. Without loss of generality we allow $a = 1$, thus (3.59) becomes

$$(1-z^2)\gamma_{zz} - (4\alpha+2)z\gamma_z + (E+\nu-2\alpha)\,\gamma = 0. \quad (3.61)$$

### 3.5.3 The eigenvalue condition

**$\nu$ in terms of $E$**

We seek a power series solution of (3.61):

$$\gamma_n = \sum_{j=0}^{n} C_j z^j, \quad (3.62)$$

$$(\gamma_n)_z = \sum_{j=0}^{n} (j+1)\,C_{j+1}\,z^j, \quad (3.63)$$

$$(\gamma_n)_{zz} = \sum_{j=0}^{n} (j+1)(j+2)\,C_{j+2}\,z^j. \quad (3.64)$$

Substituting into (3.61) yields

$$(1-z^2)\sum_{j=0}^{n}(j+1)(j+2)\,C_{j+2}\,z^j - (4\alpha+2)z\sum_{j=0}^{n}(j+1)\,C_{j+1}\,z^j + (E+\nu-2\alpha)\sum_{j=0}^{n} C_j z^j = 0.$$

By the method of index shifting we transform the above into a more useful expression

$$\sum_{j=0}^{n}(j+1)(j+2)\,C_{j+2}\,z^j - \sum_{j=2}^{n} j(j-1)\,C_j\,z^j - (4\alpha+2)\sum_{j=1}^{n} j\,C_j\,z^j + (E+\nu-2\alpha)\sum_{j=0}^{n} C_j z^j = 0.$$

Collecting $z^j$ terms we have

$$(j+1)(j+2)\,C_{j+2} = \Big[j(j-1) + (4\alpha+2)j - (E+\nu-2\alpha)\Big]C_j, \tag{3.65}$$

where the formula also works for $j = 0, 1$. Thus

$$C_{j+2} = \frac{1}{(j+1)(j+2)}\Big[j(j+1+4\alpha) - (E+\nu-2\alpha)\Big]C_j, \qquad j \geq 0. \tag{3.66}$$

This series terminates when $j = n$, if

$$n(n+1+4\alpha) - (E+\nu-2\alpha) = 0. \tag{3.67}$$

This leads to a polynomial solution for $\gamma_n$, and hence $|\phi| \to 0$ as $|y| \to \infty$ as required because of (3.56) and (3.62). We therefore obtain a sequence of polynomial solutions for any integer $n$. If $n = 0$, then $\gamma_0 = C_0$, if $n = 1$, then $\gamma_1 = C_0 + C_1 z$. We can see that even $n$ leads to solutions symmetric about $y = z = 0$, and odd $n$ leads to antisymmetric solutions.

Since $\alpha$ is given in terms of $E$ from (3.61), (3.67) is a relationship between $E$ and $\nu$ i.e, the desired eigenvalue condition.

We can find an expression for $\nu$ which leads to a surprising result. Substituting $\alpha = \sqrt{-E}/2$ from (3.60) into (3.67), and rearranging for $\nu$ we have

$$\nu = \frac{(2n+1+2\sqrt{-E})^2 - 1}{4}, \qquad n \in \mathbb{N}_0. \tag{3.68}$$

This is the eigenvalue condition when $\nu$ is regarded as the eigenvalue and $E$ as the parameter, as we do here. With this understanding, at fixed $E$ there are infinitely many eigenvalues $\nu$.

This significant result is shown in Figure 3.6. We take, without loss of generalisation, $E = -1$, where $k = 1 \times 10^{-5}\text{m}^{-1}$ and $L$=100km. Clearly we can see intersections of $-E$ for different $\nu$, where I have only gone so far as $n = 6$. If one were to take the alternative view of requiring $E$ as a function of $\nu$, we rearrange (3.68):

$$2n+1+2\sqrt{-E} = \pm\sqrt{1+4\nu}.$$

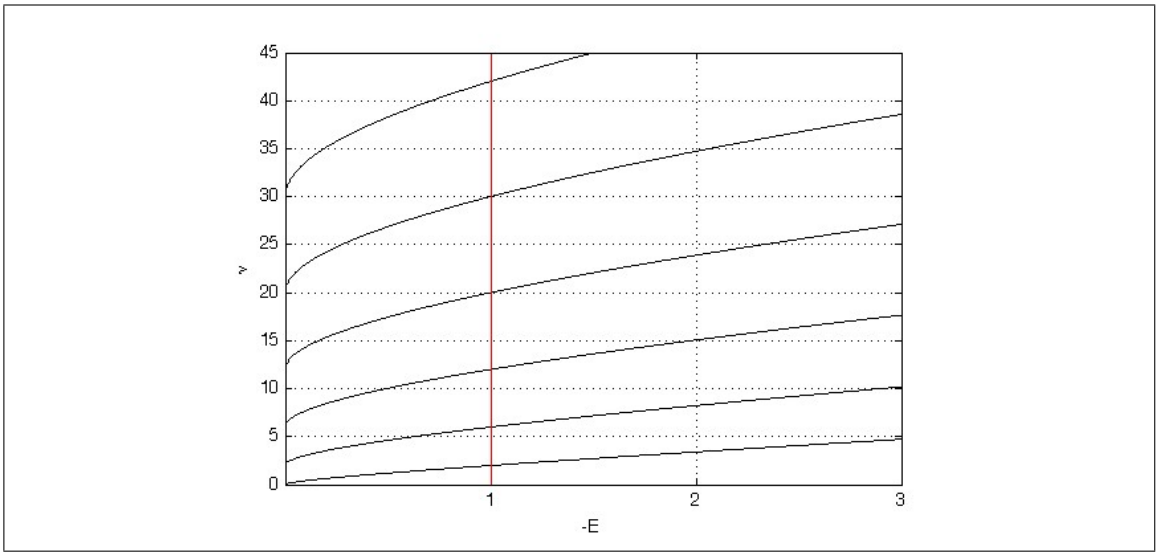


**Figure 3.6:** $E$ as a function of $\nu$ ($j = 0, 1, 2, 3, 4, 5$)

Since $n$ and $(\sqrt{-E})$ are positive, we take the positive square root and

$$2n + 1 + 2\sqrt{-E} = \sqrt{1 + 4\nu}. \tag{3.69}$$

We can also determine the conditions that $n$ must satisfy. Since $\sqrt{-E} > 0$, thus

$$n < \frac{1}{2}[\sqrt{1 + 4\nu} - 1]. \tag{3.70}$$

Thus we have the standard condition, as given in **?**. Note, in this form we only have a finite number of eigenvalues.

$$E = -\frac{1}{4}(2n + 1 - \sqrt{1 + 4\nu})^2 \quad \text{where} \quad 0 \leq n \leq \frac{\sqrt{1 + 4\nu} - 1}{2}. \tag{3.71}$$

**Determining coefficients of $\gamma_n$**

We have to take into account that $C_j$ (in each expansion of $\phi_n$) will not be the same for different $n$. For example, $C_2$ when $n = 2$ (in $\phi_2$), will not be the same as the $C_2$ when $n = 4$ (in $\phi_4$). We define

$$\phi_n = \gamma_n \operatorname{sech}^{|kL_s|} \hat{y} \quad \text{and} \quad \hat{y} = \frac{y}{L_s}. \tag{3.72}$$

Thus we arrive at a more helpful expression for (3.66) by using (3.68) to eliminate $\nu$

$$C_{j+2} = \frac{1}{(j+1)(j+2)}\Big[(j-n)(2|kL_s| + j + n + 1)\Big]C_j \quad \text{where} \quad j = 0, 1, \cdots, n \tag{3.73}$$

where $j$ is chosen depending upon which coefficient we wish to find for $\phi_n$. Here we choose $C_0$ and $C_1$ to be one.

**Dispersion relation**

We arrive at a dispersion relation by substituting $E = -k^2L_s^2$ and $\nu = fkL_s\Delta H/\omega H_0$ into (3.68), this leads to the simple expression

$$\omega = \frac{4fkL_s\Delta H}{H_0\left[\left(2n + 1 + |2kL_s|\right)^2 - 1\right]} \quad \text{where} \quad n \in \mathbb{N}_0. \tag{3.74}$$

This is a leading order analytical solution (in $\Delta H/H_0$). It quite clearly shows that there are an infinite number of topographic Rossby waves in the continuous model.

The frequencies of these topographic Rossby waves (3.74) scale with $f$ and have an upper bound when $n = 0$

$$\omega = \frac{f\Delta H\ \mathrm{sgn(k)}}{H_0(1 + |kL_s|)}. \tag{3.75}$$

This upper bound is $\sim f\Delta H/H_0$ which is less than 1, thus the frequency of these waves are sub-inertial.

As $n$ increases in (3.74), $\omega$ tends to zero; however, the ratio of $\Delta H$ to $H_0$ is a considerably influential factor. For the same $n$, it follows that the frequencies for a large step are much greater than that for a small step. Therefore, for a large step these dispersive waves have shorter periods.

As $L_s \to 0$ in (3.75), the hyperbolic tangent profile turns into a step profile and we obtain

$$\omega \to \frac{f\Delta H\ \mathrm{sgn(k)}}{H_0}. \tag{3.76}$$

Interestingly have recovered (3.46), the **?** solution for the frequency of a topographic Rossby wave where we have a step profile and no coastline.

### 3.5.4 Dispersion relation derived by Saint-Guily (1976)

**?** derived a dispersion relation which proved the existence of several topographic Rossby waves. From the linearised shallow water equations, he non-dimensionalised time and the wavenumber

$$\hat{t} = 2ft \quad \hat{k} = kL$$

where $L$ represents a typical length scale, and $f$ the Coriolis parameter. He works in terms of a transformed cross-shore co-ordinate $\hat{z}$, defined by

$$\hat{z} = \int \frac{d\hat{y}}{q}. \tag{3.77}$$

Here $q = H/H_0$ is the non-dimensional depth, where $H_0$ is the average depth, which is defined in terms of $\hat{z}$ via $q = 1 + \lambda \tanh \hat{z}$ where $\lambda$ is a fractional change in height. Thus the non-dimensional height profile is defined implicitly, since $\hat{z}$ is defined in terms of $q$. Differentiating (3.77) with respect to $\hat{y}$ we have $d\hat{z}/d\hat{y} = 1/q$. Substituting $q = 1+\lambda \tanh \hat{z}$ into this and integrating we have

$$\hat{y} = \hat{z} + \lambda \ln|\cosh(\hat{z})| + k$$

where $k$ is a constant. This equation must satisfy the boundary conditions, i.e., at $\hat{y} = 0$ we have $\hat{z} = 0$, and when $\lambda \ll 1$ then $\hat{y} \approx \hat{z}$. Therefore

$$\hat{y} = \hat{z} + \lambda \ln|\cosh(\hat{z})|. \tag{3.78}$$

So for large $\hat{z}$ and $\lambda \ll 1$,

$$\hat{y} \sim \hat{z}$$

this is true even as $z \to \infty$ as the second term is always smaller than the first term when $\lambda \ll 1$. This is now equivalent to

$$q = 1 + \lambda \tanh(\hat{y}), \quad \lambda \ll 1. \tag{3.79}$$

We can write (3.79) in dimensional variables

$$H = H_0 + (\lambda H_0) \tanh\left(\frac{\hat{y}}{L}\right), \quad \lambda \ll 1, \tag{3.80}$$

this is equivalent to (3.47) with $\lambda H_0 = \Delta H$ and $L = L_s$.

Saint-Guily makes a rigid-lid approximation by choosing suitable parameter values such that

$$\epsilon = \frac{4L^2}{L_R^2} = 10^{-2}. \tag{3.81}$$

Here $L$ represents a typical lengthscale of 100km, $H_0$ is a typical depth of 1km, $\omega$ the Coriolis parameter is approximately $10^{-4}\mathrm{s}^{-1}$, and $g$ is taken to be $10\,\mathrm{ms}^{-2}$. Since $L_R^2 \gg L^2$ we have a rigid lid which eliminates waves in which surface displacement is a necessary characteristic required to exist. To leading order he solves the full set of equations to obtain

$$\hat{\omega}_0 = -\frac{\hat{k}\lambda}{\hat{k}^2(1-\lambda^2) - \hat{k}(2s+1) + s(s+1)}, \quad \epsilon \ll 1. \tag{3.82}$$

Note that $k$, the wavenumber is negative, and $s$ is a positive integer which gives us the different modes for the topographic Rossby wave. Rewriting (3.82) back into dimensional variables we have

$$\omega_0 = -\frac{fkL\Delta H}{H_0[(kL)^2(1-(\Delta H/H_0)^2) - kL(2s+1) + s(s+1)]}. \tag{3.83}$$

Assuming $\Delta H/H_0 \ll 1$ we now have

$$\omega_0 = -\frac{fkL\Delta H}{H_0\left[(kL)^2 - kL(2s+1) + s(s+1)\right]} \tag{3.84}$$

We can make an explicit link between (3.74) and (3.84) by comparing them in the same parameter regime. Both models have assumed $L \ll L_R$ (3.81) however, to obtain (3.74) we assume $\Delta H \ll H_0$, i.e. $\lambda \ll 1$. So, we consider the reduction of (3.84) in this limit.

Let $L \to L_s$, $s \to n$ (where $n \in \mathbb{N}_0$) and $k \to |-k|$. Thus

$$\omega_0 = \frac{f|-kL_s|\Delta H}{H_0\left[|kL_s|^2 + |-kL_s|(2n+1) + n(n+1)\right]}$$

reduces to

$$\omega_0 = \frac{4f|kL_s|\Delta H}{H_0\left[(2n+1+|2kL_s|)^2 - 1\right]}, \tag{3.85}$$

i.e., (3.74). This is equivalent to Saint-Guily's result in the limit of $\Delta H/H_0 \ll 1$. However, the simplicity of the derivation leading to (3.74) is convenient. Furthermore, we will show that (3.74) gives excellent prediction for $\omega$ over a wide parameter range with remarkable agreement between the analytical and numerical results for the first few modes.

### 3.5.5 The analytical and numerical solutions of the TRWs

We now return to making a comparison of the analytical and numerical solutions of the cross-shore velocities $v$ and frequencies $\omega$ of these waves. For the cross-shore velocity $v$ we can just as easily use solutions of the stream function, $\psi$, where $v = \psi_x/H$ (3.32). By (3.34) we have

$$i\psi_x = -\phi\, k\, H^{1/2} = V. \tag{3.86}$$

We can also write $V = ivH$, thus we will compare the analytical and numerical solutions for $V$.

Without loss of generality, let $a = 1$, then $\alpha = |kL_s|/2$ by (3.60). Combining (3.53), (3.56) and (3.62), we have

$$\phi_n = \gamma_n \operatorname{sech}^{|kL_s|}\left(\frac{y}{L_s}\right). \tag{3.87}$$

Writing

$$\gamma_n = \sum\nolimits_{j=0}^{n} C_j\, z^j \quad (j, n \in \mathbb{N}_0) \tag{3.88}$$

we have

$$V = -H^{1/2}\, k\, \operatorname{sech}^{|kL_s|}\left(\frac{y}{L_s}\right) \sum\nolimits_{j=0}^{n} C_j\, z^j \quad (j, n \in \mathbb{N}_0). \tag{3.89}$$

We expand (3.88), where $z = \tanh(y/L_s)$. If $n$ is even we have

$$\gamma_n = C_0 + C_2\, \tanh^2\left(\frac{y}{L_s}\right) + \cdots + C_n\, \tanh^n\left(\frac{y}{L_s}\right) \tag{3.90}$$

which is even in $y$. If $n$ is odd then

$$\gamma_n = \left[C_1 + C_3\, \tanh^2\left(\frac{y}{L_s}\right) + \cdots + C_{n-1}\, \tanh^{n-1}\left(\frac{y}{L_s}\right)\right] \tanh\left(\frac{y}{L_s}\right) \tag{3.91}$$

which is odd in $y$.

**Accuracy of prediction for various waves**

Equation (3.48) is a two point boundary value problem which we solve to determine $\phi$, the cross-shore structure of the topographic Rossby wave. We use a standard shooting algorithm combined with a Newton–Raphson iteration method to achieve this. The shooting method entails choosing values for all of the dependent variables (which depend on free arbitrary parameters) at one boundary, the choice of these variables must be consistent with the boundary conditions at that particular starting point. We then integrate the ODEs by initial value methods, arriving at the other boundary point we check whether the boundary conditions are again satisfied. This method depends on choosing free parameter values (randomly chosen) that zeros the discrepancy at the other boundary point (**?**).

The Newton-Raphson method is a root-finding routine which requires the evaluation of a function and its derivative at arbitrary points. We supply this method with an initial guess for the root, if we are far from the root this can result in meaningless solutions. However, if we are close to the root then the advantage of the Newton–Raphson method is that it will converge quickly to this root (**?**).

We plot and compare the different solutions for $V(y)$ given by the numerical solutions obtained from (3.48), the leading order correction (n=0) (3.75) and the analytical solution (3.89). These are shown in Figure 3.7 in blue, green and red respectively.

In Figure 3.7 we choose $y < |1250|$km, $k = 1 \times 10^{-5}$ m$^{-1}$, and $2L_s$, the length of slope to be $200$ km. We fix $H_0$ at 4km, and although $L_s$ is longer than a typical length scale, as discussed in section 3.1.1 it does not violate the condition $kL_s \geq 1$.

We characterise each solution by the number of zeros $n$ in the solution for $V$, and we start by examining solutions with $\Delta H$=0.5km, so that $\Delta H/H_0$=1/7. The first column of Figure 3.7 illustrates a very close fit between the numerical solutions and analytical predictions for $n = 0, 1, 2$. As expected we have the correct number of zeros for each $n$, and demonstrated quite clearly is the asymmetry of the odd solutions. The solutions

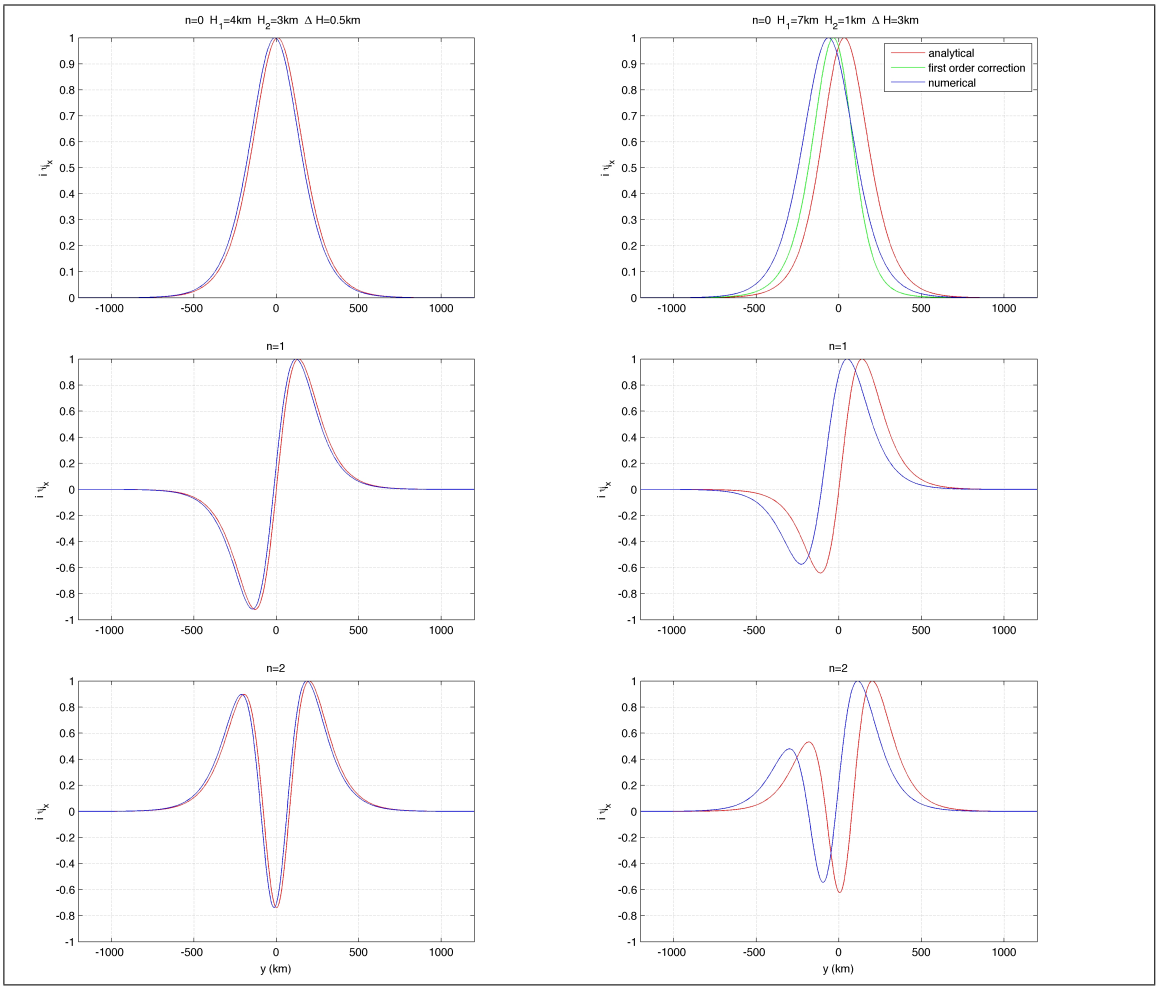


**Figure 3.7:** Comparison of analytical and numerical solutions of $V$. Plots of the leading order correction (n=0) (3.75) (–), numerical solutions (–) obtained from (3.48), analytical solution (3.89) (–). First column: $H_1$=4km, $H_0$=3.5km and $\Delta H$=0.5km. Second column: $H_1$=7km, $H_0$=4km and $\Delta H$=3km.

with even $n$ are not symmetric about $y = 0$. This can be explained by noting that for $y < 0$ we are on the shelf. Thus the combination of (3.47) which is smaller for $y < 0$, and (3.86) leads to an asymmetric effect.

We now examine solutions with $\Delta H$=3km, so that $\Delta H/H_0$ =3/4. Thus the small topography assumption should be violated and we would expect a noticeable discrepancy between the analytical predictions and numerical solutions. However, surprisingly the

results including the leading order correction shown (for $n = 0$ only) (3.75) are in very good agreement. For $n = 0, 1, 2$ we consistently see the same amplitude shift between the analytical predictions and numerical solutions. We can account for this by comparing (3.48) and (3.50). In determining the latter we neglected two terms.

### 3.5.6 Why the predicted and actual frequencies are so close

We now turn to comparing the numerical and analytical solutions for the frequencies $\omega$. Figure 3.8 clearly illustrates for increasing $\Delta H$ how closely the numerical and analytical solutions for $\omega$ match. Here we have used different parameter values, that is, $k = 2 \times 10^{-5}\text{m}^{-1}$, and a more realistic slope length of 50km ($2L_s$).

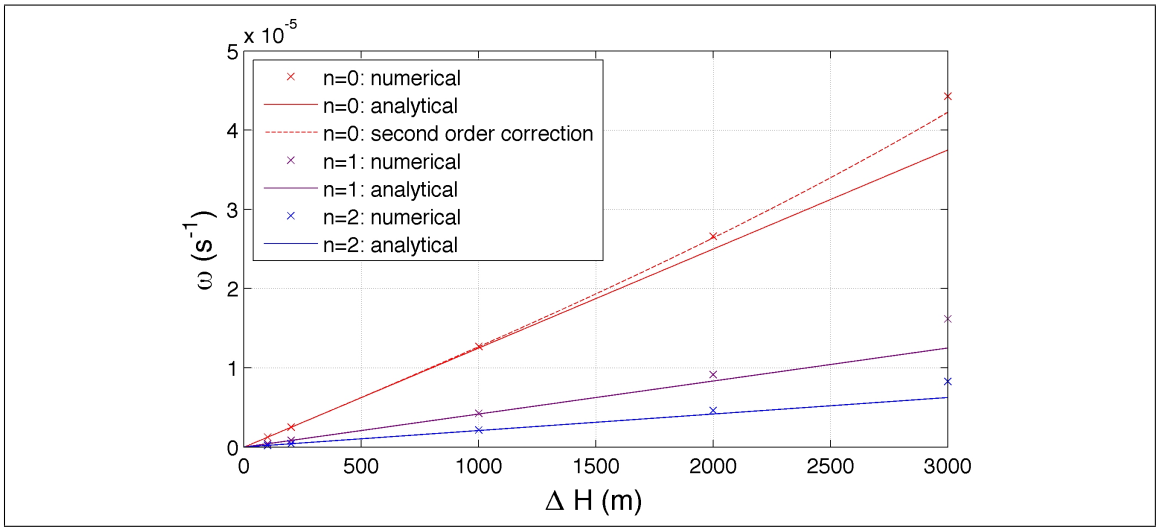


**Figure 3.8:** $\Delta H$ as a function of $\omega$ where $n = 0, 1, 2$. Here $k = 2 \times 10^{-5}\text{m}^{-1}$, $L_s$=25km, slope length=50km and $H_1$=4km.

In order to examine the robustness of this unexpected result we consider the first and second order corrections to $\phi$. Rearranging (3.48) so that we have the leading order terms on the left gives

$$\frac{d^2\phi}{d\hat{y}^2} + \left[ -k^2 L_s^2 + \frac{fk\Delta H L_s}{\omega H} \operatorname{sech}^2 \hat{y} \right] \phi = \phi \left( \frac{\Delta H}{H} \tanh \hat{y} + \frac{3(\Delta H)^2}{4H^2} \operatorname{sech}^2 \hat{y} \right) \operatorname{sech}^2 \hat{y}. \quad (3.92)$$

Using the profile (3.47), let $\epsilon = \Delta H/H_0$ and $T = \tanh \hat{y}$, thus

$$\frac{1}{H} = \frac{1}{H_0}(1 - \epsilon T + \epsilon^2 T^2 + \cdots). \tag{3.93}$$

Similarly expanding $\omega$ in terms of $\epsilon$ we have

$$\omega = \omega_0 + \epsilon\omega_1 + \epsilon^2\omega_2 + \cdots . \tag{3.94}$$

So

$$\frac{1}{\omega} = 1 - \frac{\omega_1}{\omega_0}\epsilon + \left(\frac{\omega_1^2}{\omega_0^2} - \frac{\omega_2}{\omega_0}\right)\epsilon^2 + \cdots \tag{3.95}$$

We define $S = \operatorname{sech} \hat{y}$, and substituting (3.93) and (3.95) into (3.92) gives to $O(\epsilon^2)$

$$\begin{aligned} L\phi = &\left[\frac{fk\Delta HL_s}{\omega_0 H_0}\frac{\omega_1}{\omega_0}S^2 + \left(\frac{fk\Delta HL_s}{\omega_0 H_0} + 1\right)S^2T\right]\phi\,\epsilon + \\ &\left[\frac{fk\Delta HL_s}{\omega_0 H_0}\left(\frac{\omega_2}{\omega_0} - \frac{\omega_1^2}{\omega_0^2} - \frac{\omega_1 T}{\omega_0}\right)S^2 - \left(\frac{fk\Delta HL_s}{\omega_0 H_0} + 1\right)S^2T + \frac{3}{4}S^4\right]\phi\,\epsilon^2 \end{aligned} \tag{3.96}$$

where

$$L = \frac{d^2}{d\hat{y}^2} - k^2L_s^2 + \frac{fk\Delta HL_s}{\omega_0 H_0}\,S^2. \tag{3.97}$$

Let $\phi = \phi_0 + \phi_1\epsilon + \phi_2\epsilon^2\cdots$, and collecting orders of $\epsilon$ from (3.96) we have

$$\epsilon^0 : L\phi_0 = 0 \tag{3.98a}$$

$$\epsilon^1 : L\phi_1 = \left[\frac{fk\Delta HL_s}{\omega_0 H_0}\frac{\omega_1}{\omega_0}S^2 + \left(\frac{fk\Delta HL_s}{\omega_0 H_0} + 1\right)S^2T\right]\phi_0. \tag{3.98b}$$

Thus (3.98a) is the leading order solution given by the left hand side of (3.92). It leads to the dispersion relation (3.74) for $\omega_0$ in terms of $k$. In the special case $n = 0$, which we pursue here, we obtain

$$\omega_0 = \frac{f\Delta H\,\operatorname{sgn}(\mathrm{k})}{H_0(1 + |kL_s|)}\,. \tag{3.99}$$

By (3.87) and setting $C_0 = 1$, we have

$$\phi_0 = S^{|kL_s|}. \tag{3.100}$$

An expression for $\omega_1$ can be derived by multiplying (3.98b) by (3.100) and integrating over $(-\infty, \infty)$. Since

$$\int_{-\infty}^{\infty}\phi_0\,L\,\phi_1\,\mathrm{d}\hat{y} = \int_{-\infty}^{\infty}\phi_1\,L\,\phi_0\,\mathrm{d}\hat{y} = 0$$

we obtain

$$\int_{-\infty}^{\infty}\left[\frac{fk\Delta HL_s}{\omega_0 H_0}\frac{\omega_1}{\omega_0}S^2+\left(\frac{fk\Delta HL_s}{\omega_0 H_0}+1\right)S^2T\right]\phi_0^2\,\mathrm{d}\hat{y}=0.$$

Since $S^2T\phi_0^2$ is an odd function and thus integrates to zero we obtain

$$\frac{fk\Delta HL_s}{\omega_0 H_0}\frac{\omega_1}{\omega_0}\int_{-\infty}^{\infty}S^2\mathrm{d}\hat{y}=0\implies\omega_1=0.$$

We now proceed to determine $\phi_1$. Assume

$$\phi_1=g(\hat{y})\,\phi_0=g(\hat{y})\,S^{|kL_s|}, \tag{3.101}$$

substituting this into (3.98b) we have

$$g''\,\phi_0+2g'\,\phi_0'+g\,\phi_0''+\left[-k^2L_s^2+\frac{fk\Delta HL_s}{\omega H}S^2\right]g\,\phi_0=\left(\frac{fk\Delta HL_s}{\omega_0 H_0}+1\right)S^2T\,\phi_0$$

where the prime represents differentiation with respect to $\hat{y}$. Using (3.98a) we have

$$g''\,\phi_0+2g'\,\phi_0'=\left(\frac{fk\Delta HL_s}{\omega_0 H_0}+1\right)S^2T\,\phi_0.$$

Substituting (3.99) and (3.100) into this, and with the cancellation of common terms this reduces the expression to

$$g''-2|kL_s|g'T=[1+|kL_s|(1+|kL_s|)]\,S^2T. \tag{3.102}$$

If we let $g=C\tanh\hat{y}$ where $C$ is a constant, then by substituting this expression into (3.102) we are able to determine $C$,

$$C=-\frac{[1+|kL_s|(1+|kL_s|)]}{2(1+|kL_s|)}.$$

Hence

$$\phi_1=-\frac{[1+|kL_s|(1+|kL_s|)]}{2(1+|kL_s|)}\,S^{|kL_s|}T \tag{3.103}$$

where we had already defined $S=\mathrm{sech}(\hat{y})$ and $T=\tanh\hat{y}$. Thus to $O(\epsilon)$

$$\phi=\mathrm{sech}^{|kL_s|}\left[1-\frac{([1+|kL_s|(1+|kL_s|)]}{2(1+|kL_s|)}\tanh(\hat{y})\,\epsilon+\cdots\right] \tag{3.104}$$

We now consider the $O(\epsilon^2)$ terms from (3.96)

$$L\phi_2=\left(\frac{fk\Delta HL_s}{\omega_0 H_0}+1\right)S^2T\,\phi_1+\left[\frac{fk\Delta HL_s}{\omega_0 H_0}\,\frac{\omega_2}{\omega_0}\,S^2-\left(\frac{fk\Delta HL_s}{\omega_0 H_0}+1\right)S^2T+\frac{3}{4}S^4\right]\phi_0. \tag{3.105}$$

Using the solvability condition

$$\int_{-\infty}^{\infty} \phi_0 \; L \; \phi_2 \, \mathrm{d}\hat{y} = \int_{-\infty}^{\infty} \phi_2 \; L \; \phi_0 \, \mathrm{d}\hat{y} = 0,$$

(3.105) thus implies

$$\int_{-\infty}^{\infty} \left( \frac{fk\Delta H L_s}{\omega_0 H_0} + 1 \right) S^2 T \; \phi_0 \; \phi_1 \, \mathrm{d}\hat{y} + \int_{-\infty}^{\infty} \left[ \frac{fk\Delta H L_s}{\omega_0 H_0} \; \frac{\omega_2}{\omega_0} \; S^2 - \left( \frac{fk\Delta H L_s}{\omega_0 H_0} + 1 \right) S^2 T + \frac{3}{4} S^4 \right] \phi_0^2 \, \mathrm{d}\hat{y} = 0. \quad (3.106)$$

Having found expressions for $\omega_0$ (3.99), $\phi_0$ (3.100), and $\phi_1$ (3.103), we can now determine $\omega_2$ by solving (3.106) using our new found expression for $\phi_1$. By (3.99) we have

$$\frac{fk\Delta H L_s}{\omega_0 H_0} = |kL_s|(1 + |kL_s|) \quad (3.107)$$

Substituting (3.100), (3.103) and (3.107), into (3.106) we have an expression where $\omega_2$ is the only unknown. Using $1 - S^2 = T^2$ we have

$$- \left[ 1 + |kL_s|(1 + |kL_s|) \right] \left( 1 + \frac{[1 + |kL_s|(1 + |kL_s|)]}{2(1 + |kL_s|)} \right) \int_{-\infty}^{\infty} (S^{2+2|kL_s|} - S^{4+2|kL_s|}) \, \mathrm{d}\hat{y} + \left[ \frac{H_0 |kL_s|(1 + |kL_s|)^2 \mathrm{sgn(k)}}{f\Delta H} \right] \omega_2 \int_{-\infty}^{\infty} S^{2+2|kL_s|} \, \mathrm{d}\hat{y} + \frac{3}{4} \int_{-\infty}^{\infty} S^{4+2|kL_s|} \, \mathrm{d}\hat{y} = 0.$$

Rearranging this gives the desired result for $\omega_2$ in terms of $|kL_s|$

$$\left[ \frac{H_0 |kL_s|(1 + |kL_s|)^2 \mathrm{sgn(k)}}{f\Delta H} \right] \omega_2 \int_{-\infty}^{\infty} S^{2+2|kL_s|} \, \mathrm{d}\hat{y} = \left[ 1 + |kL_s|(1 + |kL_s|) \right] \left( 1 + \frac{[1 + |kL_s|(1 + |kL_s|)]}{2(1 + |kL_s|)} \right) \int_{-\infty}^{\infty} (S^{2+2|kL_s|} - S^{4+2|kL_s|}) \, \mathrm{d}\hat{y} - \frac{3}{4} \int_{-\infty}^{\infty} S^{4+2|kL_s|} \, \mathrm{d}\hat{y}. \quad (3.108)$$

We can write now (3.108) in terms of the Gamma function. We know from Appendix A

$$\int_{-\infty}^{\infty} \mathrm{sech}^n \, \hat{y} \, \mathrm{d}\hat{y} = 2^{n-1} \frac{[\Gamma(n/2)]^2}{\Gamma(\alpha)}$$

Hence, (3.108) can be simplified to

$$\left[\frac{H_0|kL_s|(1+|kL_s|)^2\mathrm{sgn(k)}}{f\Delta H}\right]\left(2^{1+2|kL_s|}\frac{[\Gamma(1+|kL_s|)]^2}{\Gamma(2+2|kL_s|)}\right)\omega_2 =$$

$$[1+|kL_s|(1+|kL_s|)]\left(1+\frac{[1+|kL_s|(1+|kL_s|)]}{2(1+|kL_s|)}\right)\times$$

$$\left(2^{1+2|kL_s|}\frac{[\Gamma(1+|kL_s|)]^2}{\Gamma(2+2|kL_s|)}-2^{3+2|kL_s|}\frac{[\Gamma(2+|kL_s|)]^2}{\Gamma(4+2|kL_s|)}\right)-\frac{3}{4}\left(2^{3+2|kL_s|}\frac{[\Gamma(2+|kL_s|)]^2}{\Gamma(4+2|kL_s|)}\right). \tag{3.109}$$

Now using **?**

$$\Gamma(n+1)=n\Gamma(n)\quad\forall\, n\in R,$$

thus we have

$$\begin{aligned}\Gamma(2+|kL_s|) &= (1+|kL_s|)\Gamma(1+|kL_s|)\\ \Gamma(2+2|kL_s|) &= (1+2|kL_s|)\Gamma(1+2|kL_s|)\\ \Gamma(4+2|kL_s|) &= (1+2|kL_s|)(2+2|kL_s|)(3+2|kL_s|)\Gamma(1+2|kL_s|).\end{aligned}$$

Using the above results of the Gamma function, we can now simplify (3.109) to obtain

$$\omega_2=\frac{f\Delta H\,\mathrm{sgn(k)}}{H_0(1+|kL_s|)}\,\frac{|kL_s|(2+|kL_s|)^2}{2\,(3+2|kL_s|)\,(1+|kL_s|)^2}. \tag{3.110}$$

Hence

$$\omega=\omega_0\left(1+\frac{|kL_s|\,(2+|kL_s|)^2}{2\,(3+2|kL_s|)\,(1+|kL_s|)^2}\,\epsilon^2\,+\cdots\right). \tag{3.111}$$

This is the desired result. Alternatively, since $\epsilon=\Delta H/H_0$, it may be written as

$$\omega=\omega_0(1+a\epsilon^2+\cdots), \tag{3.112}$$

where

$$a=\frac{|kL_s|\,(2+|kL_s|)^2}{2\,(3+2|kL_s|)\,(1+|kL_s|)^2}\,. \tag{3.113}$$

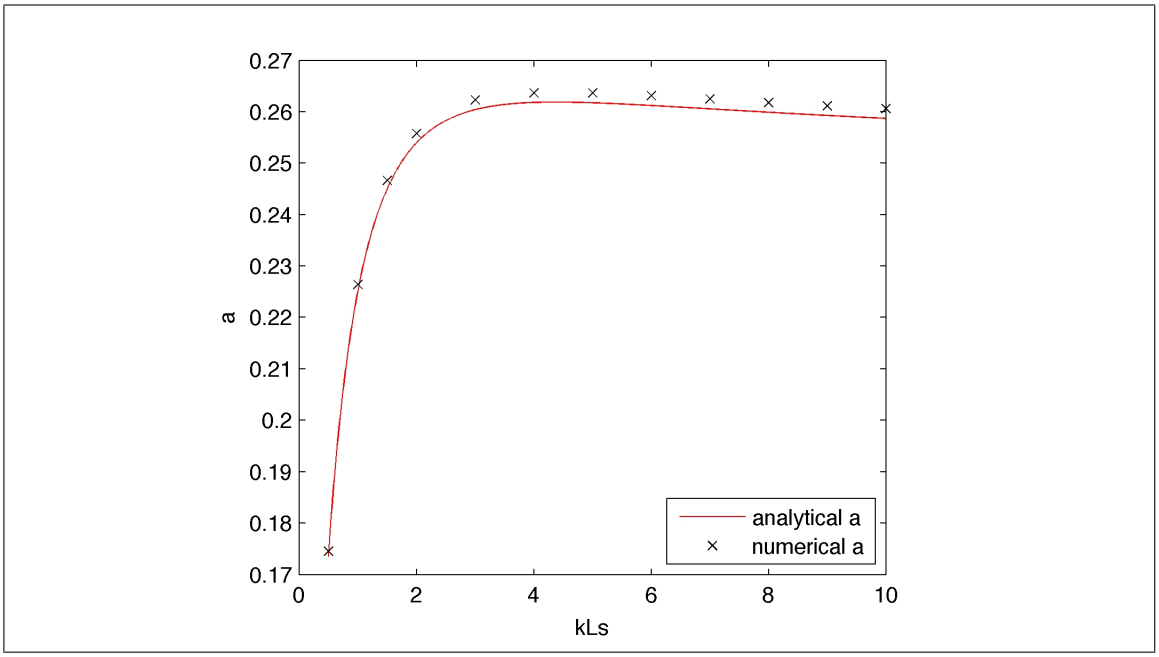


**Figure 3.9:** $a$ for increasing $kL_s$ or small step values (50m to 500m)

### 3.5.7 Comparing numerical and analytical results for $a$

We test this prediction for $a$ by rearranging (3.112) for $\omega_2$. So we have have a numerical value for $a$,

$$a_{num} = \frac{1}{\epsilon^2}\left(\frac{\omega}{\omega_0} - 1\right). \tag{3.114}$$

Substituting $\omega_0$ (3.99) into this we can compare the calculated values with the analytical results given by (3.113). Figure 3.9 demonstrates the good agreement between $a_{num}$ and $a$ up to $kL_s = 2$. There is less than 1% difference between the solutions. This is a result of two outcomes. The O($\epsilon$) correction vanishes, and the values of $a$ are small ($\leq 0.3$). So corrections are small, even when $\epsilon$ is large. This reaffirms why the predicted and actual frequencies are so close.

## 3.6 Conclusions

We have now examined trapped barotropic waves in a range of simple scenarios. In order to understand these waves it was important to consider different combinations of the effects of rotation, a coastline, and topography. We started by reviewing existing theories for

- flat topography and coast (KW),
- uniformly sloping topography and coast (EW),
- step topography and rotation and no coast (TRW).

However, most of this chapter was concerned with deriving a simple solution for topographic Rossby waves over a smooth slope (a hyperbolic tangent profile). This builds upon the classic solution for step topography of **?**, and considerably simplified the analysis of **?**. Although our analysis has been built upon a small topography assumption $\Delta H \ll H_0$, we have shown that the analysis works well for surprisingly large topography; an analytical analysis of (3.92) has provided a convincing argument as to why this is the case.

Although this analysis was performed for an unbounded domain (i.e., one with no coastline), we shall see (in chapter 5) that this solution also has great relevance for bounded domains (i.e., ones with a coastline). Thus, it will have direct relevance as a model of the kind of coastally trapped wave that is excited by tidal forcing in the real ocean. For this reason, our detailed analysis focussed on the $n = 0$ mode, which is the highest frequency, and most likely to be relevant to tides.

# Chapter 4

# Coastally trapped barotropic waves with rotation and step topography

## 4.1 Introduction

In the previous chapter we developed theoretical models of the structure and behaviour of the barotropic waves in various simple settings. Specifically, we examined

- waves trapped against a coast,
  - with background rotation but no topography (Kelvin waves, or KWs);
  - waves trapped against a coast, with a uniformly sloping sea-floor but no rotation (edge waves, or EWs).
- Waves trapped above a smooth localised slope, with background rotation but with no coast (topographic Rossby waves, or TRWs).

However, to model the kind of waves present in tidal flows, we need to include the effects of a coastline, rotation and continental shelf/slope topography simultaneously.

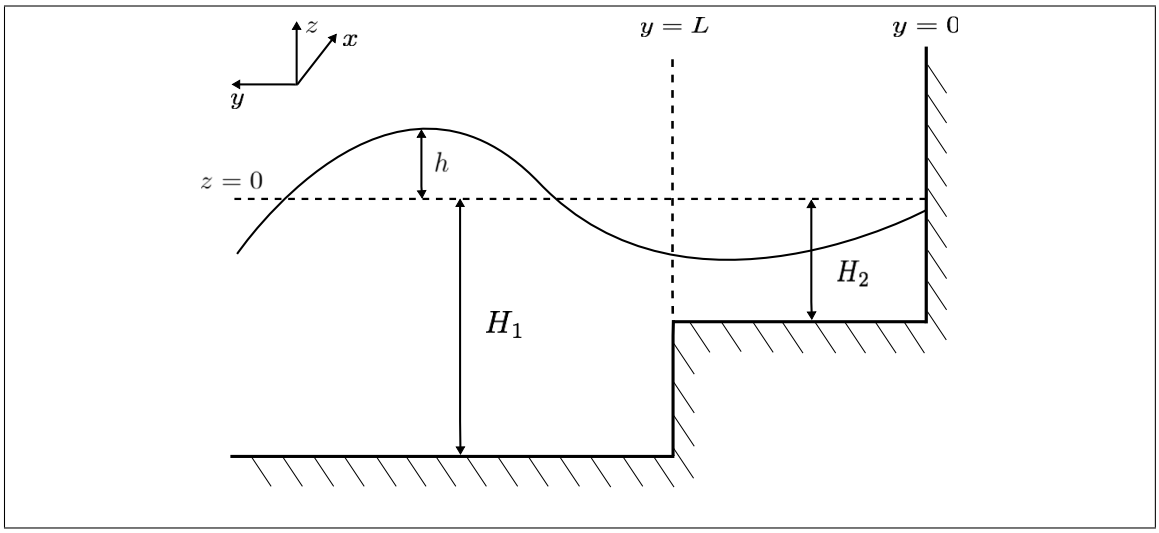


**Figure 4.1:** Schematic of the step model. Single density layer with a coastline with a continental shelf of constant depth, $H_2 \neq 0$ and length $L$. The step at $y = L$ is pronounced by a discontinuity which separates $H_2$ and the deep ocean of depth $H_1$.

We now do this in the simplest possible way, by assuming a step-like topography, as illustrated in Figure 4.1. This profile consists of a coast (at $y = 0$), a flat continental shelf (for $0 < y < L$) of depth $H_2$ and width $L$, and a deep sea (for $y > L$) of depth $H_1$. So, the continental slope is idealised as a discontinuity in the depth profile.

In section 3.5 we considered a more realistic profile (3.47)

$$H = H_0 + \Delta H \tanh\left(\frac{y}{L_s}\right).$$

However, as $L_s \to 0$, this profile reduces to the depth discontinuity as shown in Figure 4.1. We would expect the step model to support the three types of waves as discussed in chapter 3: edge waves, the Kelvin wave, and topographic Rossby waves. However, it is not clear if these kinds of waves will remain separate in parameter space, or indeed if completely new types of waves will occur. Interestingly, we discover that the waves found in the step model are more complicated because the different types of waves are connected to each other. For example, we find that a particular edge wave that evolves into a Kelvin wave, as parameters are smoothly varied.

**?** derived solutions for a step topography (in a similar manner to **?**) with a coastline. The solutions indicate the existence of a Kelvin-like wave, and a topographic Rossby wave that is related to the step. Larsen also refers to 'leaky modes' which exist for high frequencies, although he does not go into great detail. **?** considered two analytical models: a shelf of constant depth and an exponential profile. The solutions for the waves found fall into four four classes these being, a Kelvin wave which has edge-wave-like behaviour, continental shelf waves, Poincaré waves and forced waves. **?** describes the latter as a distortion of the sea bottom by tide producing forces. Our main interest in this work is with the dispersion relations derived by **?** that can account for the main features of observed tidal heights off the coast of California.

We start by deriving a single dispersion relation encapsulating all possible types of waves. Unfortunately, this only defines the frequency implicitly, and is rather difficult to work with. However, it may be solved numerically, and we take advantage of the fundamental characteristics of the barotropic waves to derive simple analytical dispersion relations in various limits. Our emphasis is on deriving various asymptotic limits explicitly, and comparing these with our numerical solutions.

### 4.1.1 Governing equations

We begin with the linear shallow-water equations (2.25a-c) derived in chapter 2

$$\frac{\partial u}{\partial t} - fv = -g\frac{\partial h}{\partial x}, \tag{4.1a}$$

$$\frac{\partial v}{\partial t} + fu = -g\frac{\partial h}{\partial y}, \tag{4.1b}$$

$$\frac{\partial h}{\partial t} + \underline{\nabla} \cdot (H\underline{u}) = 0. \tag{4.1c}$$

As in section 3.1.2, we seek wave-like solutions of the form

$$\{h, u, v\} = \mathrm{Re}\left( \left\{ \hat{h}(y), \hat{u}(y), \hat{v}(y) \right\} e^{i(kx-\omega t)} \right), \quad k > 0. \tag{4.2}$$

Thus, on either side of the depth discontinuity at $y = L$, (2.25a-c) can be written as

$$-i\omega\hat{u} - f\hat{v} = -igk\hat{h}, \tag{4.3a}$$

$$-i\omega\hat{v} + f\hat{u} = -g\frac{d\hat{h}}{dy}, \tag{4.3b}$$

$$-i\omega\hat{h} + H\left(ik\hat{u} + \frac{d\hat{v}}{dy}\right) = 0, \tag{4.3c}$$

where $H$ is the local (constant) depth on either side of the discontinuity.

$$H = \begin{cases} H_1 & y > L, \\ H_2 & 0 < y < L. \end{cases} \tag{4.4}$$

These equations are to be solved subject to two boundary conditions. Firstly

$$\hat{v} = 0 \text{ at } y = 0. \tag{4.5}$$

Secondly, we seek solutions trapped against the shelf and coast and thus need

$$|\hat{u}| \to 0, |\hat{v}| \to 0, |\hat{h}| \to 0 \text{ as } y \to \infty. \tag{4.6}$$

Finally, we need to apply the appropriate matching conditions as stated in section 2.1.3. At $y = L$ we require the continuity of $\hat{h}$ (2.29), and the continuity of mass (2.30).

Combining (3.2a) and (3.2b), we can eliminate $\hat{u}$ to find

$$(\omega^2 - f^2)\hat{v} = -ig\left(fk + \omega\frac{d}{dy}\right)\hat{h}. \tag{4.7}$$

Similarly, we can combine (3.2a) and (3.2b) to eliminate $\hat{v}$, giving

$$(\omega^2 - f^2)\hat{u} = g\left(\omega k + f\frac{d}{dy}\right)\hat{h}. \tag{4.8}$$

If $\omega^2 \neq f^2$, then we can write $\hat{u}$ and $\hat{v}$ in terms of $\hat{h}$ by substituting (4.7) and (4.8) into (4.1a), we then obtain a single ODE for $\hat{h}$:

$$\frac{d^2\hat{h}}{dy^2} - \left(k^2 - \frac{\omega^2 - f^2}{gH}\right)\hat{h} = 0. \tag{4.9}$$

However, this is not possible if $\omega^2 = f^2$. So these two cases shall be examined separately in the next two sections.

## 4.2 Inertial waves

We first investigate waves with $\omega^2 = f^2$, which are known as inertial waves because they take the local 'inertial frequency', $f$. Setting $\omega^2 - f^2 = 0$, then (4.7) and (4.8) each give

$$\frac{d\hat{h}}{dy} = -\frac{\omega k}{f}\hat{h}. \tag{4.10}$$

We now consider two cases: (i) no topography ($H_1$=$H_2$=$H$= constant), (ii) non-trivial topography with $H_1 \neq H_2$.

### 4.2.1 No topography

If $H_1$=$H_2$=$H$, then (4.10) applies for $0 < y < \infty$, so we obtain

$$\hat{h} = \hat{h}_0 e^{-\frac{\omega k}{f} y}, \tag{4.11}$$

where $|\hat{h}_0|$ is the amplitude of the perturbed sea surface height at $y = 0$. If $\omega = f$, then $\hat{h} = \hat{h}_0 e^{-ky}$ and we have exponentially decaying waves which are trapped at the coastline (since $k > 0$). If $\omega = -f$, then $\hat{h} = \hat{h}_0 e^{ky}$ which means that the perturbed sea surface height is unbounded. This violates (4.6), and thus the only possible solution is

$$\hat{h} = \hat{h}_0 e^{-ky}, \quad \text{with} \quad \omega = f. \tag{4.12}$$

We now find an expression for $\hat{v}$. Eliminating $\hat{u}$ from (4.3a) and substituting into (4.3c) we obtain

$$(\omega^2 - gHk^2)\hat{h} - ikHf\hat{v} + i\omega H\frac{d\hat{v}}{dy} = 0. \tag{4.13}$$

Substituting for $\omega$ and $\hat{h}$ from (4.12) into (4.13), and introducing the integrating factor $e^{-ky}$, we can write

$$\frac{d}{dy}(\hat{v}e^{-ky}) = \frac{i\hat{h}_0}{fH}(f^2 - gHk^2)\, e^{-2ky}. \tag{4.14}$$

Integrating between 0 and $y$ and applying $\hat{v} = 0$ at $y = 0$ gives

$$\hat{v} = \frac{-i\hat{h}_0}{2kfH}(f^2 - gHk^2)(e^{-ky} - e^{ky}). \tag{4.15}$$

Since we require $\hat{v} \to 0$ as $y \to \infty$, and since $\hat{h}_0 \neq 0$, we must have $k = |f|/\sqrt{gH}$. Thus, the solution (4.12) is only possible for a single value of the along-shore wavenumber $k$. To complete the solution we must check that $\hat{u} \to 0$ as $y \to \infty$. Given $\hat{v} = 0$, then by (3.2b) and (4.12) we have $\hat{u} = (gk/f)\hat{h}_0\, e^{-y/L_R}$ which does satisfy (4.6). So the complete solution is

$$\hat{h} = \hat{h}_0\, e^{-y/L_R}, \quad \hat{v} = 0, \quad \hat{u} = \frac{gk}{f}\hat{h}_0\, e^{-y/L_R}, \quad \omega = f, \text{ where } L_R = \frac{1}{k} = \frac{\sqrt{gH}}{|f|}, \tag{4.16}$$

provided

$$k = \frac{|f|}{\sqrt{gH}}. \tag{4.17}$$

Substituting (4.17) into the dispersion relation (3.6) for the classic Kelvin wave $\omega = k\sqrt{gH}\,\mathrm{sgn(f)}$ as derived in chapter 3, we recover the same result, $\omega = f$. Thus we have a Kelvin wave which exists for a specific $k$ value whose frequency is equal to the inertial frequency.

Note that the result for the perturbed sea surface height for a Kelvin wave, (3.7), was already derived in chapter 3. However, this was done in a different way by assuming from the outset that $\hat{v} = 0$ everywhere.

### 4.2.2 Non-trivial topography

We now examine the more general case with $H_1 \neq H_2$. On-shelf and in the deep ocean, the structure of $\hat{h}$ is given by (4.10), but appropriate matching conditions must now be applied at $y = L$.

In the deep ocean we need to satisfy (4.6), that is, solutions decay as $y \to \infty$. From (4.10), we require $\omega = f$ (since $k > 0$), so that

$$\hat{h}_1 = A_1 e^{-ky}, \quad y > L. \tag{4.18}$$

Then, on-shelf (4.10) implies

$$\hat{h}_2 = A_2 e^{-ky}, \quad 0 < y < L. \tag{4.19}$$

Since $\hat{h}$ is continuous at $y = L$, it follows that $A_1 = A_2 = \hat{h}_{0_s}$. To establish a solution we need to calculate $\hat{u}$ and $\hat{v}$, apply the coastal and deep ocean boundary conditions, (4.5) and (4.6), and apply matching conditions at $y = L$.

We find an expression for the on-shelf cross-shore velocity, $\hat{v}_2$, by integrating (4.14) between 0 and $y < L$ and applying $\hat{v}_2(0) = 0$, which gives

$$\hat{v}_2(y) = \frac{i\hat{h}_{0_s}}{2fkH_2}(f^2 - gH_2k^2)(e^{ky} - e^{-ky}), \quad 0 < y < L_-. \tag{4.20}$$

So

$$\hat{v}_2(L_-) = \frac{i\hat{h}_{0_s}}{2fkH_2}(f^2 - gH_2k^2)(e^{kL_-} - e^{-kL_-}). \tag{4.21}$$

To determine the cross-shore velocity in the deep ocean, $\hat{v}_1$, we integrate (4.14) from $L$ to $y > L$ which gives

$$\hat{v}_1(y)e^{-ky} - \hat{v}_1(L_+)e^{-kL} = \frac{i\hat{h}_{0_s}}{2kfH_1}(f^2 - gH_1k^2)(e^{-2kL} - e^{-2ky}). \tag{4.22}$$

Since we require $\hat{v}_1(y)e^{-ky} \to 0$ as $y \to \infty$ , we must have

$$\hat{v}_1(L_+) = -\frac{ih_{0_s}}{2fkH_1}(f^2 - gH_1k^2)e^{-kL}. \tag{4.23}$$

Then, applying continuity of mass at the step, that is, $H_1\hat{v}_1 = H_2\hat{v}_2$ at $y = L$, we obtain the dispersion relation

$$1 - e^{-2kL} = \frac{f^2 - gH_1k^2}{f^2 - gH_2k^2}. \tag{4.24}$$

This may be viewed as an equation defining a particular $k$ for which these inertial waves exist; it is analogous to (4.17).

Clearly,

$$1 - e^{-2kL}\Big|_{k=0} = 0, \quad \text{and} \quad \frac{f^2 - gH_1k^2}{f^2 - gH_2k^2}\Big|_{k=0} = 1$$

Since $f^2 - gH_1k^2/f^2 - gH_2k^2 > 0$ when $k^2 < f^2/gH_1$, there can be no root there. And since $f^2 - gH_1k^2/f^2 - gH_2k^2 \to \infty$ as $k^2 \to f^2/gH_1$, the curves must intersect for some $k$ with

$$\frac{f^2}{gH_1} < k^2 < \frac{f^2}{gH_2}. \tag{4.25}$$

The intersection point is unique since both functions are monotonically decreasing. So there are no roots for $k^2 > f^2/gH_2$, and we have a solution when

$$\frac{|f|}{\sqrt{gH_1}} < k < \frac{|f|}{\sqrt{gH_2}}. \tag{4.26}$$

Thus inertial waves in a step topography only exist in a particular range of $k$ determined by $f$, $H_1$ and $H_2$.

In the following example we illustrate that we will have only one solution for $k$ given by (4.26). Let $H_2 = 250$m, $H_1 = 4$km, $L = 200$km and $f = 10^{-4}\,\mathrm{s}^{-1}$. Then $5 \times 10^{-7}\,\mathrm{m}^{-1} < k < 2 \times 10^{-6}$ m$^{-1}$, these bounds are shown in Figure 4.2 by the dashed lines. Here we clearly see we have only one solution for $k$.

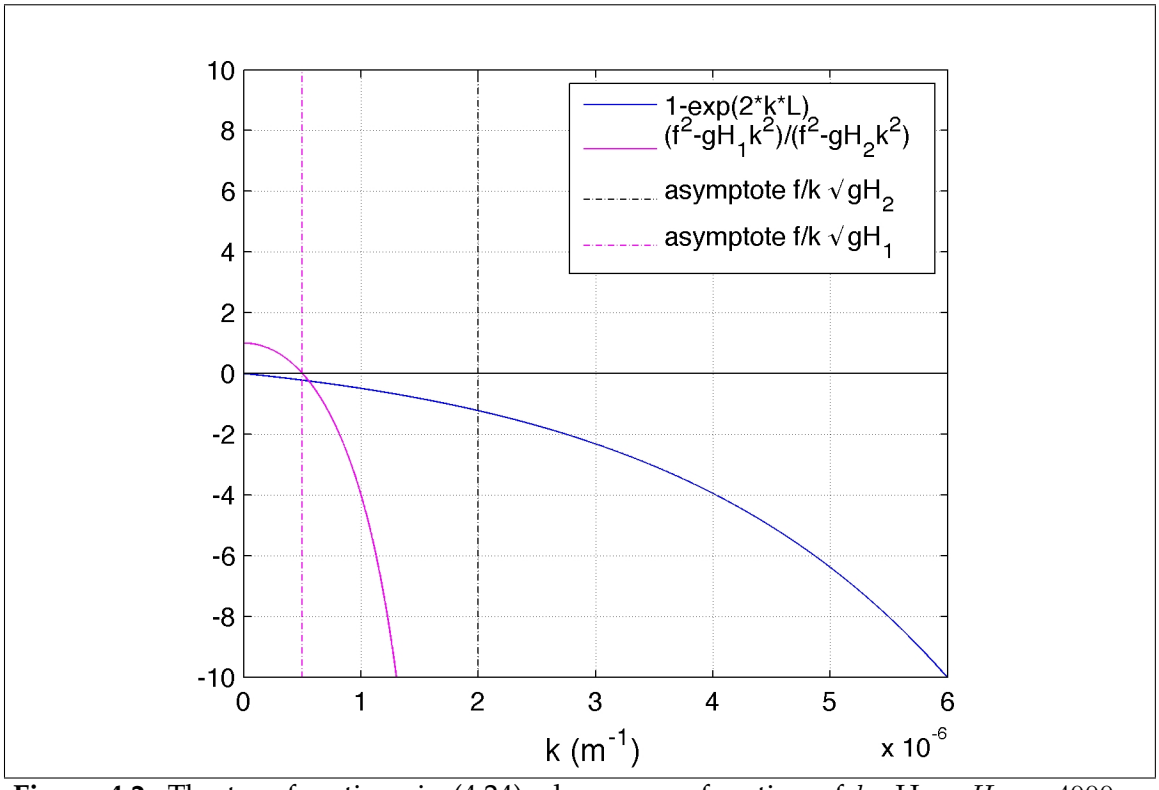


**Figure 4.2:** The two functions in (4.24), shown as a function of $k$. Here $H_1 = 4000$m, $H_2 = 250$m, and $L = 200$km for the step topography. The trapped inertial wave exists for the value of $k$ at which these two curves intersect.

## 4.3 Non-inertial waves

We now consider the case with $\omega^2 \neq f^2$, we return to (4.9):

$$\frac{d^2\hat{h}}{dy^2} - \left(k^2 - \frac{\omega^2 - f^2}{gH}\right)\hat{h} = 0 \quad \text{for} \quad y > L \quad \text{and} \quad 0 < y < L. \tag{4.27}$$

We will derive solutions on either side of $y = L$, subject to the coastal boundary condition (4.5) and trapping condition (4.6), and then match solutions at $y = L$ to determine a dispersion relation.

Writing $\hat{h} = Ae^{ly} \neq 0$ where $A$ is a non-zero constant, we find

$$l = \pm\sqrt{k^2 - \frac{\omega^2 - f^2}{gH}}. \tag{4.28}$$

For $y > L$, we need to satisfy (4.6), so

$$\hat{h} = \hat{h}_1 = B_1 e^{-l_1 y}, \tag{4.29}$$

where

$$l_1 = \sqrt{k^2 - \frac{\omega^2 - f^2}{gH_1}} \quad \text{and} \quad \mathrm{Re}(l_1) > 0, \tag{4.30}$$

when $\omega$ is real, we will have $l_1$ as a positive real number. On the continental shelf, $0 < y < L$, we write

$$\hat{h}_2 = A_2 e^{l_2 y} + B_2 e^{-l_2 y} \tag{4.31}$$

where

$$l_2 = \sqrt{k^2 - \frac{\omega^2 - f^2}{gH_2}} \quad \text{and} \quad -\frac{\pi}{2} < \arg(l_2) \leq \frac{\pi}{2}. \tag{4.32}$$

Again in the case of interest with real $\omega$, we will have $l_2$ either real or imaginary.

With an aim of working towards a dispersion relation, it will be beneficial to reduce the number of unknown constants. Setting $\hat{v}(0) = 0$ in (4.7) gives

$$\left(\frac{d}{dy} + \frac{fk}{\omega}\right)\hat{h} = 0. \tag{4.33}$$

Substituting (4.31) into (4.33) gives

$$A_2 = \left(\frac{\omega l_2 - fk}{\omega l_2 + fk}\right) B_2, \quad \text{at} \quad y = 0.$$

We can now eliminate $A_2$ from $\hat{h}_2$:

$$\hat{h}_2 = B_2\left[\left(\frac{\omega l_2 - fk}{\omega l_2 + fk}\right)e^{l_2 y} + e^{-l_2 y}\right]. \tag{4.34}$$

Note that $l_2$ may be real or imaginary, however, for $l_1$ we impose the condition that $\mathrm{Re}(l_1) > 0$.

**Matching conditions at $y = L$**

The dispersion relation is obtained by applying the matching conditions (2.29) and (2.30). The former implies $\hat{h}_1 = \hat{h}_2$ which from (4.29) and (4.34) gives $B_1$ in terms of $B_2$ :

$$B_1 = B_2 e^{l_1 L}\left[\left(\frac{\omega l_2 - fk}{\omega l_2 + fk}\right)e^{l_2 L} + e^{-l_2 L}\right]. \tag{4.35}$$

To apply (2.30), we need to derive expressions for the cross-shore velocitiy on and off the shelf. We substitute expressions for $\hat{h}_1$ (4.29) and $\hat{h}_2$ (4.34) into (4.7) and (4.8), to give

$$\hat{v}_1 = -\frac{igB_1(fk - \omega l_1)e^{-l_1 y}}{\omega^2 - f^2}, \quad y > L. \tag{4.36}$$

$$\hat{v}_2 = -\frac{igB_2}{\omega^2 - f^2}\left[(\omega l_2 - fk)(e^{l_2 y} - e^{-l_2 y})\right] \quad 0 < y < L. \tag{4.37}$$

Then (2.30), which implies $H_1\hat{v}_1 = H_2\hat{v}_2$ at $y = L$, gives

$$H_1(fk - \omega l_1)e^{-l_1 y}B_1 = H_2(\omega l_2 - fk)(e^{l_2} - e^{-l_2 y})B_2. \tag{4.38}$$

Combining this with (4.35), and demanding that $B_1$ and $B_2$ are not both zero at any time gives

$$\omega l_1 - fk = \frac{H_2}{H_1}\cdot\frac{(\omega l_2 - fk)(\omega l_2 + fk)(e^{-2l_2 L} - 1)}{(\omega l_2 - fk) + (\omega l_2 + fk)e^{-2l_2 L}}, \quad \omega^2 \neq f^2. \tag{4.39}$$

At fixed $k$ this is a dispersion relation defining $\omega$. Pleasingly it potentially contains solutions for all the different types of waves derived in chapter 3: edge waves, the Kelvin wave, and topographic Rossby waves. Here $l_1$ and $l_2$ are given by (4.30) and (4.32) respectively. Unfortunately, since $l_1$ and $l_2$ depend on $\omega$, we are unable to obtain an explicit expression for $\omega$. However, we will show that (4.39) can be solved numerically and that useful analytical predictions in certain limits may be derived.

For completeness, we also give expressions for the along-shore velocity on and off the shelf. Substituting $\hat{h}_1$ (4.29) and $\hat{h}_2$ (4.34) into (4.8) gives

$$\hat{u}_1 = \frac{g(k\omega + fl_1)B_1 e^{-l_1 y}}{\omega^2 - f^2}, \quad y > L. \tag{4.40}$$

$$\hat{u}_2 = \frac{gB_2}{\omega^2 - f^2}\left[(\omega k + fl_2)\left(\frac{\omega l_2 - fk}{\omega l_2 + fk}\right)e^{l_2 y} + (\omega k - fl_2)e^{-l_2 y}\right], \quad 0 < y < L. \tag{4.41}$$

### 4.3.1 Reduction for the classic Kelvin Wave (KW)

To determine how robust (4.39) is, we should definitely be able to recover the classic Kelvin wave dispersion relation (3.6). Thus we consider two limits in which (4.39) should reduce to $\omega = k\sqrt{gH_1}\mathrm{sgn(f)}$.

First we consider the limit of no continental shelf, that is $L = 0$. Then (4.39) reduces to $\omega l_1 = fk$. Squaring this expression and eliminating $l_1$ using (4.30) gives

$$(\omega^2 - f^2)(\omega^2 - gH_1 k^2) = 0. \tag{4.42}$$

The roots with $\omega^2 = f^2$ are spurious, since we have assumed $\omega^2 \neq f^2$ to obtain (4.39). So the only possible roots are $\omega = \pm k\sqrt{gH_1}$. Either way, $l_1 = \sqrt{k^2 - \frac{\omega^2 - f^2}{gH_1}} = \frac{|f|}{\sqrt{gH_1}}$ (since $\mathrm{Re}(l_1) > 0$), and substituting back into $\omega l_1 = fk$ we find that only one root is valid:

$$\omega = k\sqrt{gH_1}\,\mathrm{sgn(f)}. \tag{4.43}$$

Second, we consider the limit of $H_1 = H_2$. Then $l_1 = l_2 = l$ and (4.39) reduces to

$$\omega l = 0 \qquad \text{or} \qquad \omega l = fk. \tag{4.44}$$

The first condition implies either $\omega = 0$ (which is not of interest here, since we are interested in waves of non-zero (tidal) frequency) or $l = 0$ (which violates the condition $\mathrm{Re}(l) > 0$, meaning that we do not have a trapped wave). The second condition implies $\omega l = fk$, which is the case considered above, and again leads to the Kelvin Wave dispersion relation (4.43), as required.

We can now determine $\hat{u}$ and $\hat{v}$ for the classic Kelvin wave in this special limit. We know the cross-shore velocity, $\hat{v}$ should reduce to zero. Substituting (4.43) into the second solution of (4.44) we can write $l = |f|/\sqrt{gH}$. Thus substituting expressions for $h_1$ (4.29), $h_2$ (4.34), $\omega = k\sqrt{gH}\mathrm{sgn(f)}$ and $l$ into (4.7) and (4.8) results in

$$\hat{u} = \sqrt{\frac{g}{H}} B e^{-ly}\,\mathrm{sgn(f)} \qquad \text{and} \qquad \hat{v} = 0 \tag{4.45}$$

which is correct as the classic Kelvin wave has zero cross-shore velocity.

## 4.4 Overview of solutions

In section 2.0.2 we introduced the $f$-plane which is tangential to the earth at a latitude $\theta_0$. In our simple models we take $\theta_0 = 30\,^\circ$ then $f \approx 10^{-4}$ s$^{-1}$. We choose to focus on waves with a semi-diurnal period thus $\omega \approx 1.45 \times 10^{-4}$ s$^{-1}$.

For Kelvin waves, $\omega = k\sqrt{gH}\,\mathrm{sgn}(f)$, using $\omega \approx 1.45 \times 10^{-4}$ s$^{-1}$ and $H$=4km we have $k \approx 10^{-7}$ m$^{-1}$. If $H$=0.1km then $k \approx 5\times10^{-6}$ m$^{-1}$. Therefore the range for the wavelength $\lambda$ is $1290\mathrm{km} \leq \lambda \leq 9000$km. For Topographic Rossby waves, $\omega \sim f\Delta H/H$, so we can consider any value of $k$.

Given the radius of the earth is 6371 km, then $\lambda \approx 9000$ km violates the $f$-plane approximation on two counts

- for small $k$ values we find that our longest waves far exceed $r_e$,
- we fix $\theta$ at $30\,^\circ$ but the size of the larger wavelengths means that the value of $\theta_0$ will vary as we are not at a fixed point, thus $f$ is not constant.

Although these violations compromise our simple models they would become far too complicated if we were to consider using spherical coordinates. The simplicity of our models informs us on the behaviour of coastally trapped waves although there may be compromises to be made.

**?** discusses the effects of the Earth's curvature, reduction in depth over the continental shelf, and bends in the coastline on the classic Kelvin wave. Numerical examples are given for Cape Mendocino on the Californian coastline, he concludes that the Kelvin wave speed is reduced by 8-10% by the Earth's curvature (southwards) and by 2-8% by the continental shelf. Thus observations of disturbances similar to Kelvin waves in the ocean suggests that the changes in topography have secondary effects on the classic Kelvin wave at tidal frequencies.

**The parameters**

We now look for solutions of the dispersion relation (4.39), which requires us to specify $f, g, H_1, H_2, L$ and $k$. To illustrate the wide range of possible solutions we fix

$$f = 10^{-4}\,\mathrm{s}^{-1},\ g = 10\,\mathrm{ms}^{-2}\,\text{and}\,H_1 = 4\,\mathrm{km},$$

and consider variations of $H_2, L,$ and $k$. We will vary $H_2$ from 4km (no step) to 50m (which is a shallow continental shelf), $L$ from zero (no shelf) to 3000km (an exceptionally long shelf) and $k$ from $10^{-6}$ m$^{-1}$ to $10^{-5}$ m$^{-1}$ (so that we can investigate some extra dynamics of short waves with wavelengths of O(100km)).

The classic Kelvin wave exists when $H_1 = H_2$ and we have a coastline, and the topographic Rossby wave where $H_1 \neq H_2$ and we have no coastline, using these conditions we can isolate the solutions for these specific waves. To track the frequency of the Kelvin wave, we can use the classic Kelvin wave frequency (3.6) as our initial guess and gradually introduce a shelf, $L$. Similarly we can track the topographic Rossby wave frequency by using Longuet-Higgin's result (3.46) and gradually reduce the depth of the shelf, $H_2$, from a large starting value.

To track the Kelvin wave we calculate an initial guess $\omega = k\sqrt{gH_1}\,\mathrm{sgn(f)}$ (3.6) with no shelf, that is, $L_0 = 0$. In our Newton-Raphson iteration we input this initial guess along with a new value for $L$ , that is, $L_0 + \delta L$ where $\delta L = 5$km. This generates a frequency which is again used to calculate a new frequency value where $L_0 + 2\delta L$.

Although in my step model I have a coastline, we can use Longuet-Higgin's solution $\omega = f(H_1 - H_2)\mathrm{sgn}(k)/(H_1 + H_2)$, (3.46) to calculate an initial root when $H_2$ is large. As in the method for tracking the Kelvin wave frequency, we calculate an initial guess using (3.46) where $H_2 = 3500$m. The next frequency is calculated by the Newton-Raphson iteration method using $H_{2\,new} = 3500 - \delta H_2$ where $\delta H_2 = 100$m.

We solve (4.39) using simple codes. At the heart of these codes lies the Newton-Raphson iteration method mentioned in chapter 3. The convergence condition is that the difference between consecutive values of $\omega$ is less than $10^{-8}\,\mathrm{s}^{-1}$. One approach we take is to scan across the possible range of $\omega$ for trapped solutions as determined by (4.30), that is $\mathrm{Re}(l_1) > 0$, which gives $|\omega_{max}| < \sqrt{f^2 + gH_1k^2}$. Note that we have chosen $k < 10^{-5}$ m$^{-1}$ so the largest possible frequency is $2 \times 10^{-3}$ s$^{-1}$. The scanning entails increasing each consecutive initial value of $\omega$ by $d\omega = \omega_{max}/10^5$.

### 4.4.1 Solutions to the step model

We begin our discussion of the waves by looking at Figures 4.3-4.11. The numerically determined solutions to (4.39) are plotted as blue crosses. As discussed in chapter 3 there are also analytical predictions, which are secondary; these may or may not be in agreement with the numerical solutions and are shown by dashed lines. To summarise, we have

- - - - classic Kelvin wave (KW) with a coast but no topography, $\omega = k\sqrt{gH_1}\,\mathrm{sgn(f)}$, (3.6) (section 3.2).
- - - - a topographic Rossby wave (TRW) without a coastline, $\omega = \frac{f|H_1 - H_2|}{H_1 + H_2}$ (3.46) (section 3.4).
- - - - $\omega = \pm\omega_{max}$ where $\omega_{max} = \sqrt{f^2 + gH_1k^2}$ from (4.30) (section 4.3).
- $\times$ numerical solutions to (4.39) (section 4.3).

Here we consistently see

- a modified Kelvin wave (MKW) which is an extension of the Kelvin wave where $H_1 \neq H_2$ and approaches the classic Kelvin wave (KW) as $H_2 \to H_1$. In Figure 4.3 we would see this as $L \to 0$. The cross-shore structure of $\hat{h}$ and $\hat{v}$ are shown in Figures 4.9(a,b) and 4.10(a,b) and distinguished by the monotonic decay of $\hat{h}$.

- A topographic Rossby wave (TRW) which approaches the prediction (3.46) as defined by **?** as $H_2 \to H_1$, this is shown in Figure 4.7. More precisely it is a good approximation when $kL \gg 1$. This vorticity wave is distinguished by peaks in $\hat{h}$ and $\hat{v}$ around the step. We see this in Figure 4.11(a-d) where it peaks at $L = 200$km.

- Edge waves (EW) when $L$ is large, or $H_2$ is small. The cross-shore structure of $\hat{h}$ and $\hat{v}$ for these waves are shown in Figures 4.8(a-d) and 4.10(c,d) and are distinguished by wave-like behaviour on the shelf.

- We also see an edge wave which appears to almost be a reflection of the modified Kelvin wave. We refer to this as an 'anti-Kelvin wave' (AKW). The cross-shore structure of $\hat{h}$ for these waves are shown in Figures 4.9(c,d) and 4.10(c,d) and are distinguished by monotonic decay of $\hat{h}$. The cross-shore structure of $\hat{v}$ is distinguished by a peak at the shelf edge. It is almost a reflection of the cross-shore velocity of the modified Kelvin wave, this is clearly seen when comparing panels (b) and (d) of Figures 4.9 and 4.10.

**Fixing $H_2$ and changing the length of the shelf $L$**

We show the type of waves which exist for shallow shelves of depth $H_2$=200m, 500m and 800m for $k = 1 \times 10^{-5}$ m$^{-1}$, see Figure 4.3, and for a shelf depth of $H_2 = 200$m for $k = 1 \times 10^{-6}$ m$^{-1}$ as shown in Figure 4.4.

We note several important points which emerge from these figures

- there are no edge waves for small $L$, however, as $L$ increases from zero, these edge waves begin to emerge. This is more clearly shown on the right hand side of Figures 4.3. For example, in Figure 4.3 when $H_2 = 200$ m and $L = 100$ km, there are four edge waves plus a topographic Rossby wave. At the same depth, if we look at $L$=1000 m we now have six edge waves plus a topographic Rossby wave.

- As we increase the depth of the shelf, $H_2$, the edge waves begin to disappear. This can be seen in Figures 4.3(a,b,c), when $100\text{km} \leq L \leq 300\text{km}$.

- In agreement with the theory of Kelvin waves, when there is no shelf we obtain the classic Kelvin wave (see far left of Figures 4.3(a-c) and Figure 4.4, where the blue crosses intersect with the red line). As a shelf is introduced this wave is modified by the step, and surprisingly we find in the presence of a shelf the Kelvin wave exhibits edge wave-like behaviour (see right hand side of Figures 4.3(a-c) and Figure 4.4).

- For $k = 1 \times 10^{-5}$ m$^{-1}$ we see a topographic Rossby wave whose frequency remains very small as the length of the shelf increases ($H_2$ is fixed, see (3.46)), and is in close agreement with the analytical solution for an unbounded domain, even though there is a coastline. This occurs since $k^{-1} \ll L$, that is , the decay scale for the topographic Rossby wave is less than or equal to the length of the shelf. This is clearly shown in Figure 4.3, although this is not true for smaller values of $L$.

- For $k = 1 \times 10^{-6}$ m$^{-1}$ the numerical and analytical solutions for the topographic Rossby waves are not in agreement (see Figure 4.4). The analytical prediction for the unbounded topographic Rossby wave (3.40) exponentially decays as $-ky$ but this is only an approximate solution since it does not take into account a coastline. So for a very small $k$ the exponential decay is very slow, that is the length of decay is greater than the length of the shelf, thus the theoretical and numerical solutions are not in good agreement.

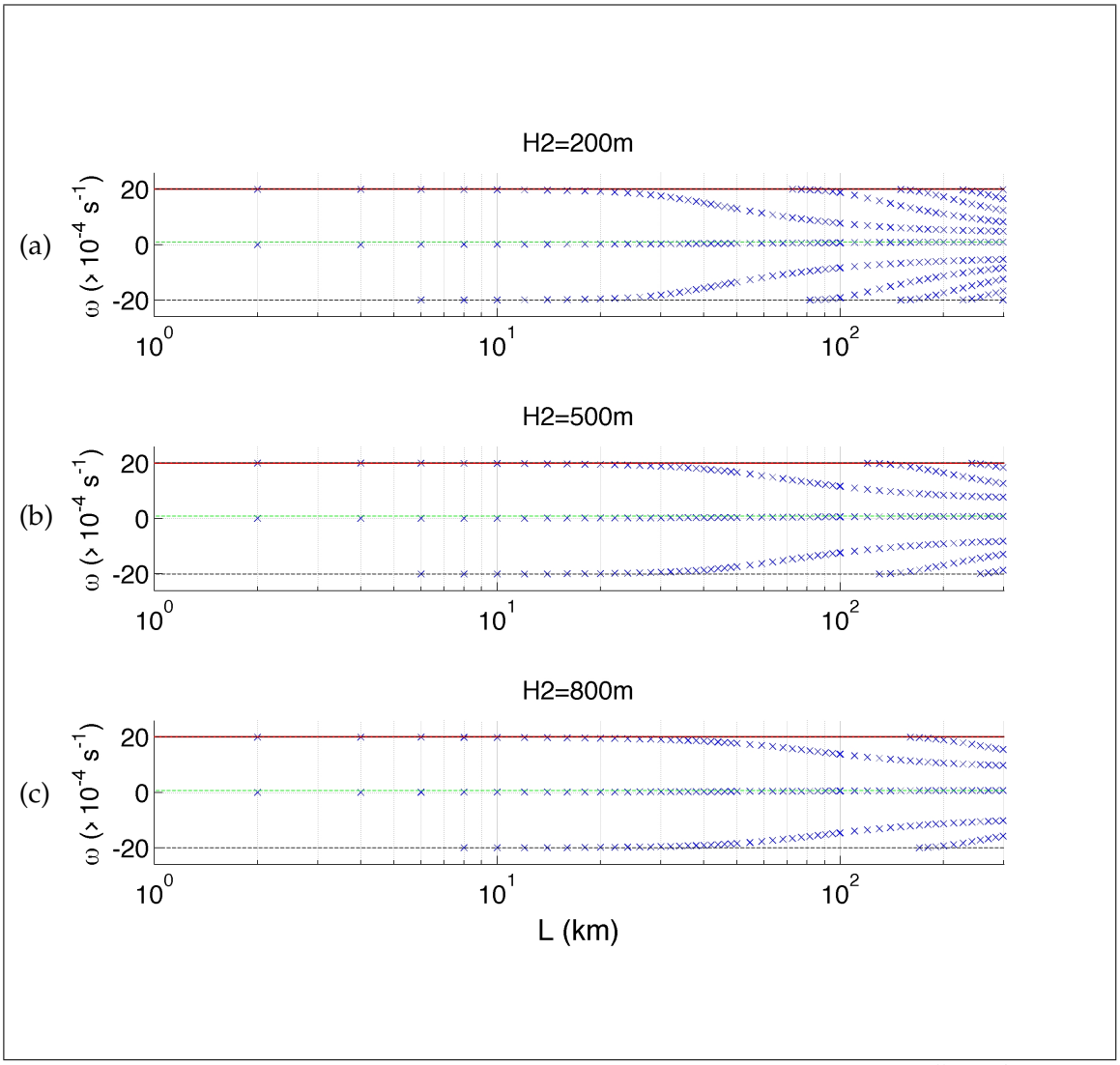


**Figure 4.3:** Frequency $\omega$ as a function of shelf width $L$ for $k = 1 \times 10^{-5}$ m$^{-1}$, where $0 \leq L \leq 300$ km and $H_2$=200, 500 and 800 m. Numerical solutions of dispersion relation (4.39) found using Newton-Raphson iteration method are shown as blue crosses (×). The solid red line (—) is the classic KW (3.6), the green dashed line (- -) the unbounded TRW (3.46), and the black dashed lines (- -) are the maximum possible frequencies for trapped waves $\omega = \omega_{max} = \pm\sqrt{f^2 + gH_1k^2}$.

**Fixing $L$ and changing the depth of the shelf $H_2$**

We now fix the length of the shelf $L$, and vary the shelf properties by increasing $H_2$ from 0 to $H_1$. In Figure 4.6, results are shown at $k = 1 \times 10^{-5}$ m$^{-1}$, with $L$= 100, 200 and 300km.

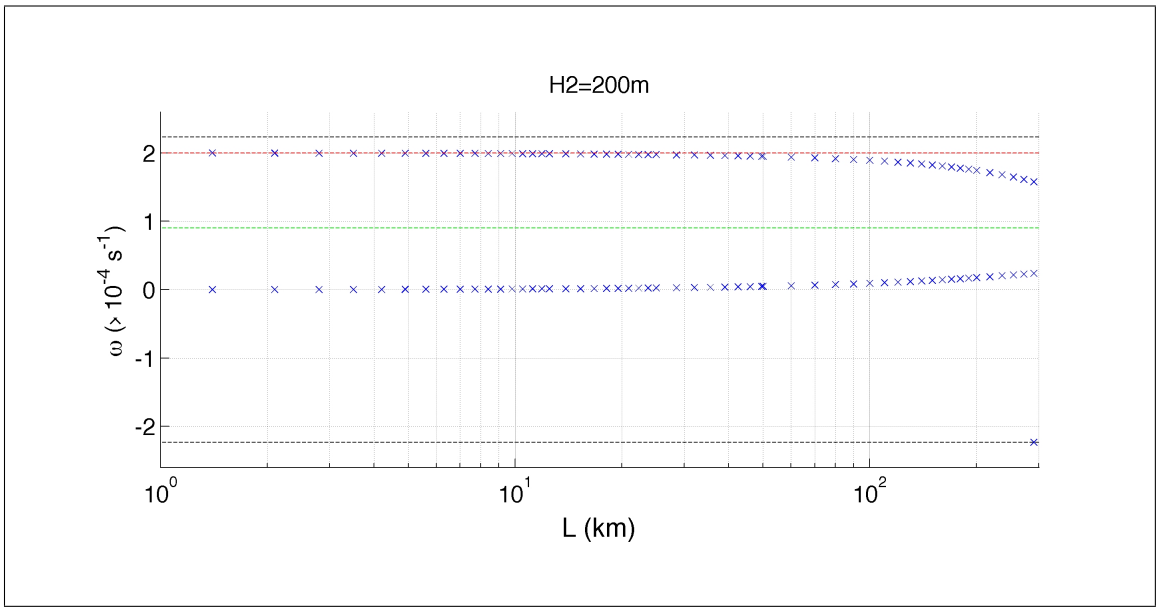


**Figure 4.4:** Frequency $\omega$ as a function of shelf width $L$ at $k = 1 \times 10^{-6}$ m$^{-1}$, where $0 \leq L \leq 300$ km and $H_2 = 200$m . Numerical solutions of dispersion relation (4.39) found using Newton-Raphson iteration method are shown as blue crosses ($\times$). The red dashed line (- -) is the classic KW (3.6), the green dashed line (- -) the unbounded TRW (3.46), and the black dashed lines (- -) are the maximum possible frequencies for trapped waves $\omega = \omega_{max} = \pm\sqrt{f^2 + gH_1k^2}$.

In Figure 4.7, results are shown for $k = 1 \times 10^{-6}$ m$^{-1}$, with $L = 200$ km since the results are almost identical at $L$=100km and 300km. We note the following

- as the depth of the shelf increases we see an edge wave evolve into a modified Kelvin wave, this is clearly seen in Figures 4.5, 4.6 and 4.7(a).

- Beyond a certain value of $H_2$ we no longer have total internal reflection, as discussed in section 3.3, and the edge waves disappear. For example in Figure 4.6(b) the edge waves do not exist when $H_2 \gtrsim 1100$ m.

- It initially appears that edge waves do not exist in Figure 4.7(a) for $k = 1 \times 10^{-6}$ m$^{-1}$. However, when we zoom in on $0 \leq H_2 \leq 100$m, as shown Figure 4.7(b), several edge waves are apparent.

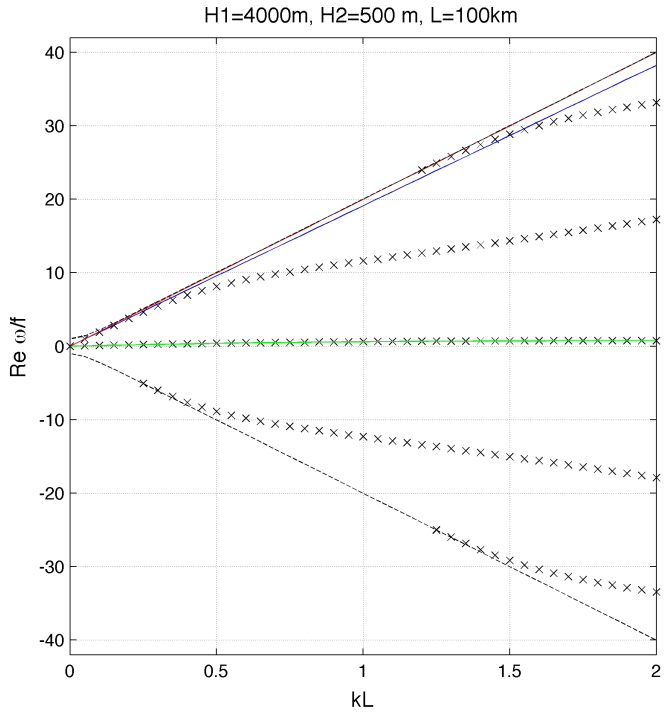


**Figure 4.5:** Frequency $\omega$ as a function of alongshore wavenumber $k$. Here $H_1$=4km, $H_2$=0.5km and $L$=100km. Figure 4.3(b) demonstrates the frequency when $k = 1 \times 10^{-5}\text{m}^{-1}$. Numerical solutions of dispersion relation (4.39) found using Newton-Raphson iteration method and are shown as blue crosses (×). The red dashed line (- -) is the classic KW (3.6), the green dashed line (- -) the unbounded TRW (3.46), and the black dashed lines (- -) are the maximum possible frequencies for trapped waves $\omega = \omega_{max} = \pm\sqrt{f^2 + gH_1k^2}$. Here we see the MKW behaving as an EW.

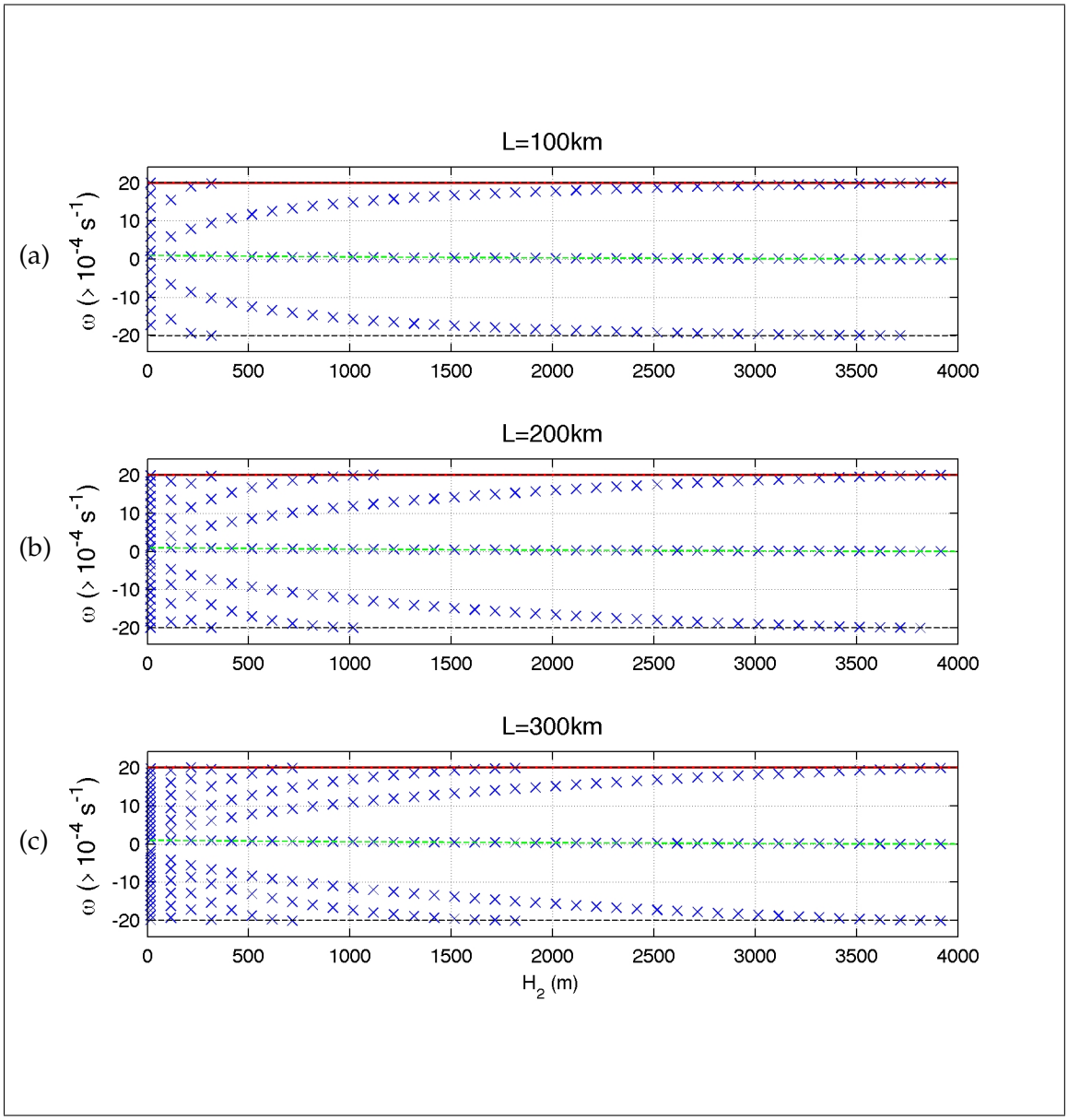


**Figure 4.6:** Frequency $\omega$ as a function of shelf depth $H_2$ for dispersion relation (4.39) at $k = 1 \times 10^{-5}$ m$^{-1}$ where shelf width $L$=100, 200 and 300 km and $H_1 = 4$ km. Numerical solutions of dispersion relation (4.39) found using Newton-Raphson iteration method are shown as blue crosses (×). The solid red line (—) is the classic KW (3.6), the green dashed line (- -) the unbounded TRW (3.46), and the black dashed lines (- -) are the maximum possible frequencies for trapped waves $\omega = \omega_{max} = \pm\sqrt{f^2 + gH_1k^2}$.

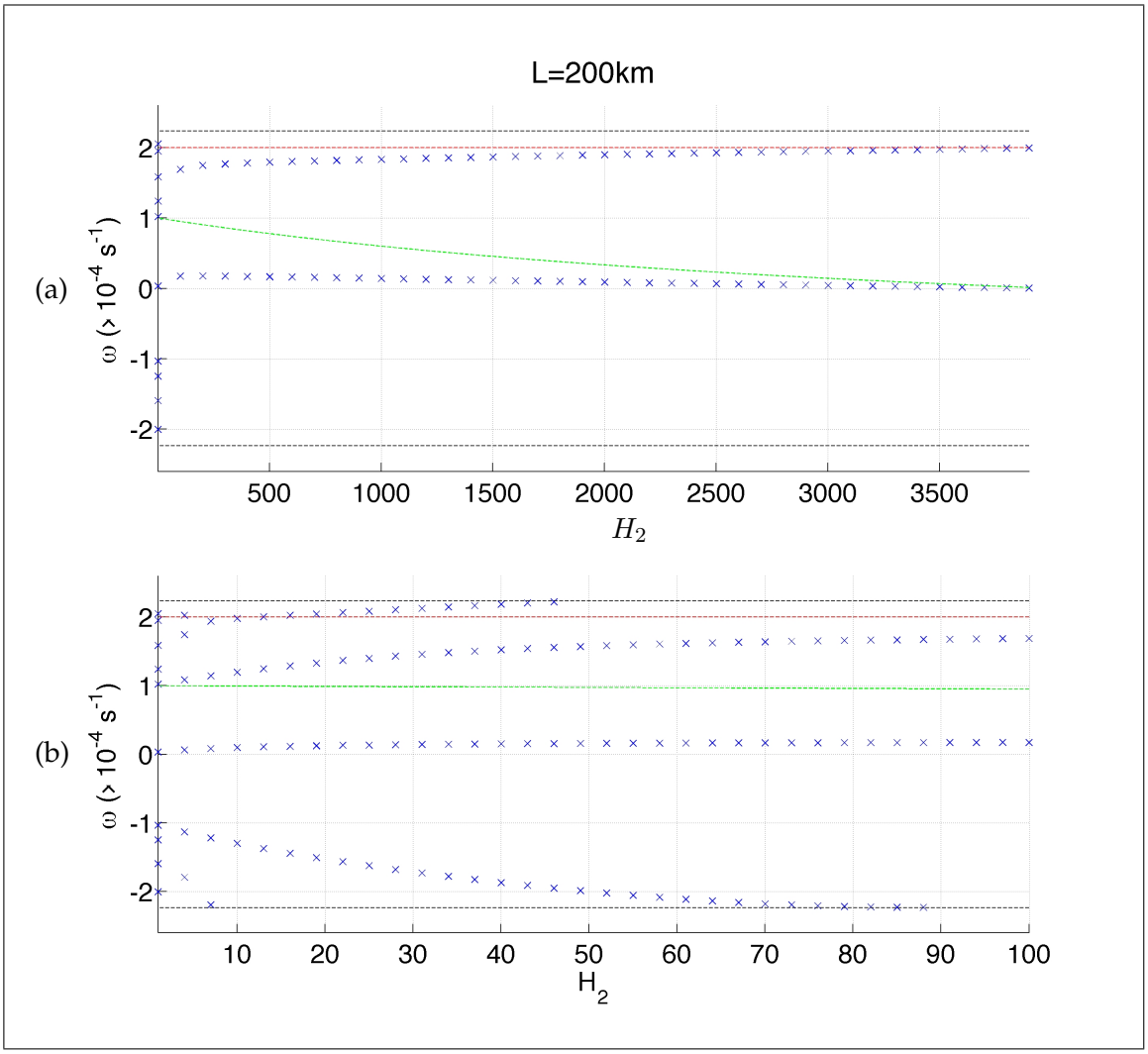


**Figure 4.7:** Frequency $\omega$ as a function of shelf depth $H_2$ for dispersion relation (4.39) at $k = 1\times10^{-6}m^{-1}$ where shelf width $L$=200 km. Numerical solutions of dispersion relation (4.39) found using Newton-Raphson iteration method are shown as blue crosses (×). The red dashed line (- -) is the classic KW (3.6), the green dashed line (- -) the unbounded TRW (3.46), and the black dashed lines (- -) are the maximum possible frequencies for trapped waves $\omega = \omega_{max} = \pm\sqrt{f^2 + gH_1k^2}$.

To determine the nature of these waves, we need to

- improve the predictions for the Kelvin and topographic Rossby waves, allowing for coastal effects. These predictions are found through the method of perturbation

analysis as shown in sections 4.5 and 4.6.

- Understand how an edge wave becomes a Kelvin wave (see Figure 4.5).

- Investigate why we have an edge wave which appears to become a reflection of the Kelvin wave. We refer to this in the chapters as an 'anti-Kelvin wave' (AKW).

### 4.4.2 Profiles of sea surface height, $\hat{h}$, and cross-shore velocity, $\hat{v}$

Before pursuing further mathematical analysis, we examine the cross-shore structure of some waves at $L = 200$km, $k = 1 \times 10^{-5}$ m$^{-1}$ and $H_2 = 500$m and $H_2$=3000m. As can be seen in Figure 4.6(c) at a shelf depth of $H_2 = 500$m there are five waves; we examine the perturbed sea-surface height, $\hat{h}$, (normalised to a maximum amplitude of 1m) and cross-shore velocity $\hat{v}$. The trapped edge waves (EW) are shown in Figure 4.8. Figure 4.11 shows topographic Rossby waves (TRW) at $H_2 = 500$m and $H_2 = 3000$m. Figures 4.9 and 4.10 shows the modified Kelvin wave (MKW) and anti-Kelvin wave (AKW) at $H_2 = 500$m and $H_2 = 3000$m. Of the trapped edge waves, two appear to have a sinusoidal profile on the shelf and display decay off-shelf. The third has a decaying profile on the shelf and off-shelf.

As the size of the step becomes smaller (i.e., $H_2$ increases) from 500m to 3000m (Figure 4.6(c)), the number of waves reduces to three; comprising one edge wave (Figure 4.10(c,d)), a topographic Rossby wave (Figure 4.11(c,d)), and the modified Kelvin wave (Figure 4.10(a,b)).

The edge waves which have short wavelengths (Figure 4.6) and sinusoidal profile (Figure 4.8) no longer exist when we have a small step. In section 3.3 we showed total internal reflection allows edge waves to exist. In this setting $(gH_2)^{1/2}$ is close to $(gH_1)^{1/2}$ so the critical angle is not exceeded, thus waves living on the shelf are not reflected back onto the shelf.

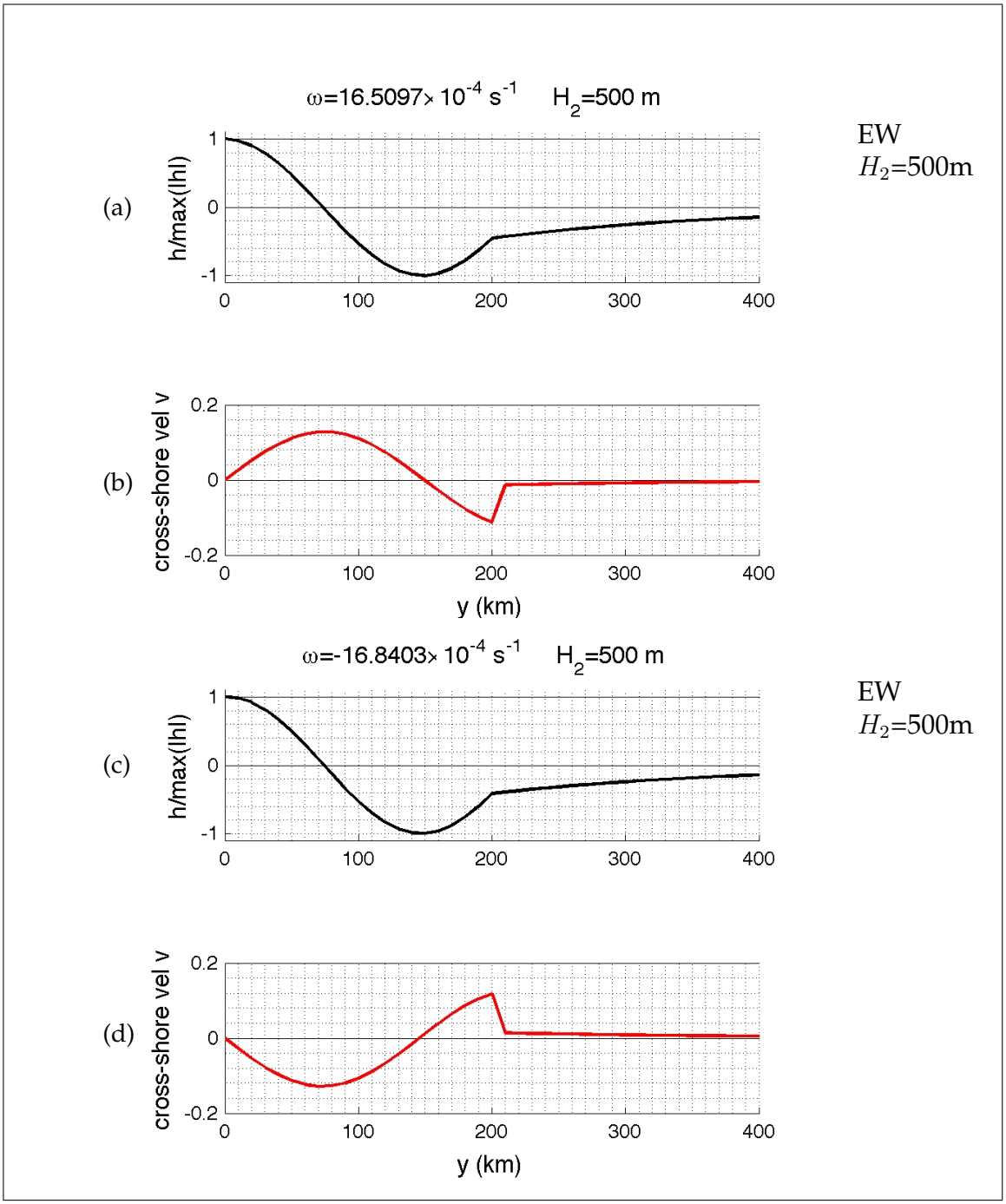


**Figure 4.8:** Profiles of two EW at $H_2 = 500$m, $L = 200$km and $k = 1 \times 10^{-5}$ m$^{-1}$. Normalised perturbed sea surface height $\hat{h}/|\hat{h}_{max}|$(a,c), and cross-shore velocity, $\hat{v}$ (b,d), are shown as a function of $y$. Here we have two EW of similar frequencies but different signs exhibiting sinusoidal behaviour on the shelf with a marked change in behaviour at $y = 200$km. The coastal BC (4.5) and trapped BC (4.6) are satisfied; $\hat{v} = 0$ at $y = 0$, and $(\hat{h}/|\hat{h}_{max}|, \hat{v}) \to 0$ as $y \to \infty$.

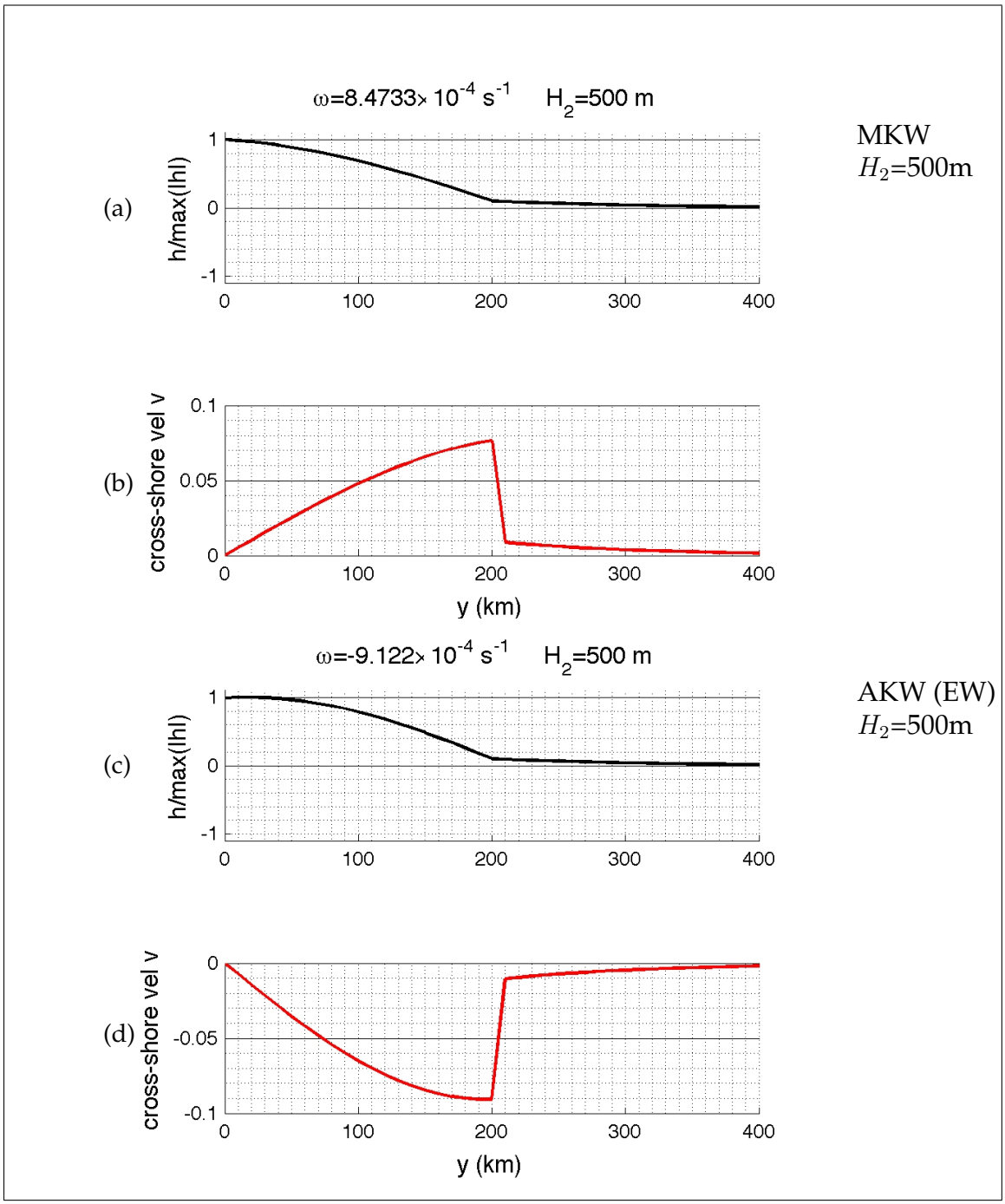


**Figure 4.9:** Normalised perturbed sea surface height $\hat{h}/|\hat{h}_{max}|$(a,c), and cross-shore velocity, $\hat{v}$ (b,d), as a function of $y$ where $L = 200$km, $H_2 = 500$m and $k = 1 \times 10^{-5}$ m$^{-1}$. Here we have a MKW (a,b) and AKW (c,d) with similar frequencies but different signs exhibiting sinusoidal behaviour on the shelf with a marked change in behaviour at $y = 200$km. The coastal BC (4.5) and trapped BC (4.6) are satisfied; $\hat{v} = 0$ at $y = 0$, and ($\hat{h}/|\hat{h}_{max}|$, $\hat{v}$) $\to 0$ as $y \to \infty$.

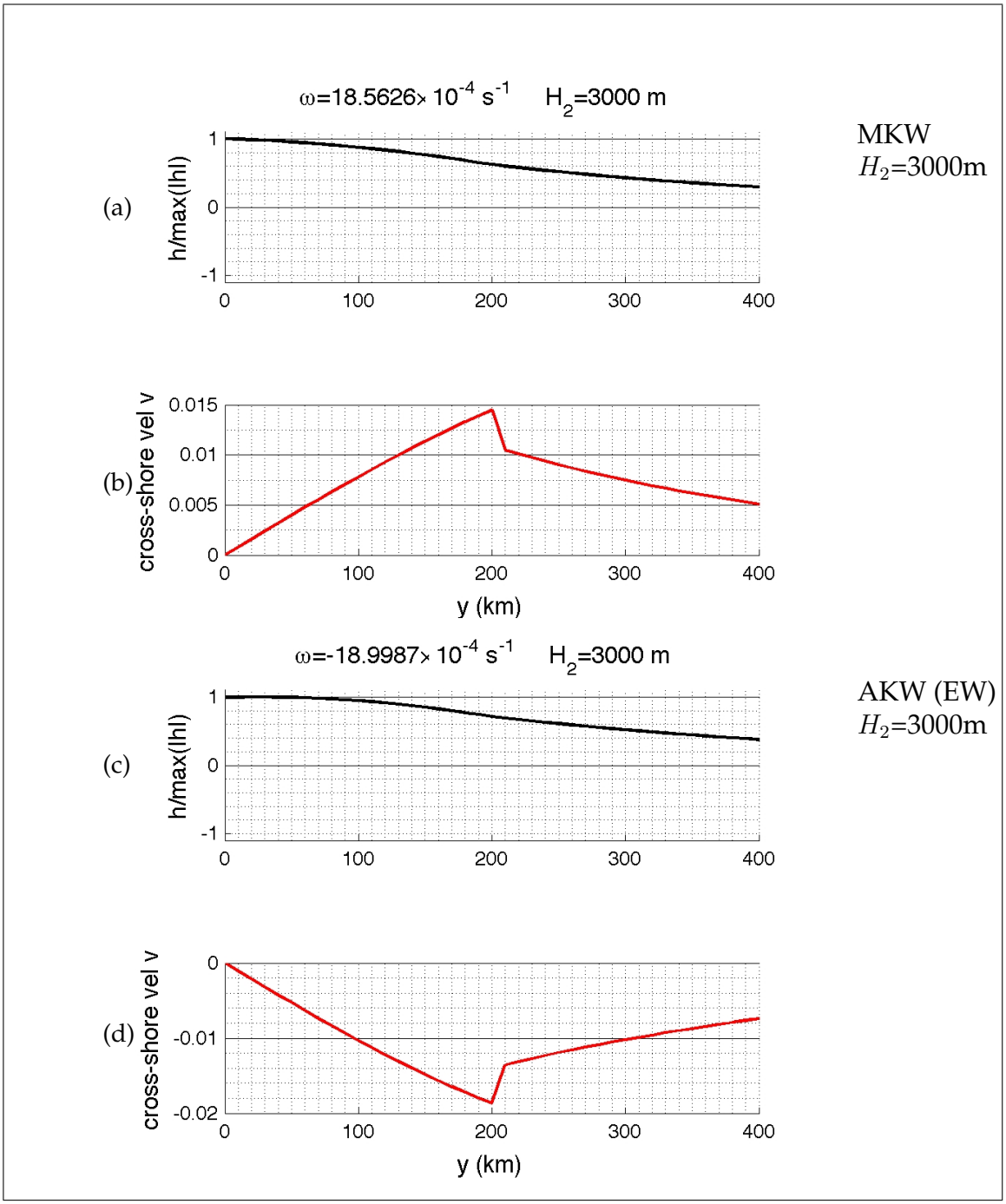


**Figure 4.10:** Normalised perturbed sea surface height $\hat{h}/|\hat{h}_{max}|$(a,c), and cross-shore velocity, $\hat{v}$ (b,d), as a function of $y$ where $L = 200$km, $H_2 = 3000$m and $k = 1 \times 10^{-5}$ m$^{-1}$. Here we have a MKW (a,b) and AKW (c,d) with similar frequencies but of different signs. At $L = 200$km we see a small change in $\hat{h}/|\hat{h}_{max}|$, however, we see a marked change in $\hat{v}$. The coastal BC (4.5) and trapped BC (4.6) are satisfied; $\hat{v} = 0$ at $y = 0$, and ($\hat{h}/|\hat{h}_{max}|$, $\hat{v}$) $\to 0$ as $y \to \infty$.

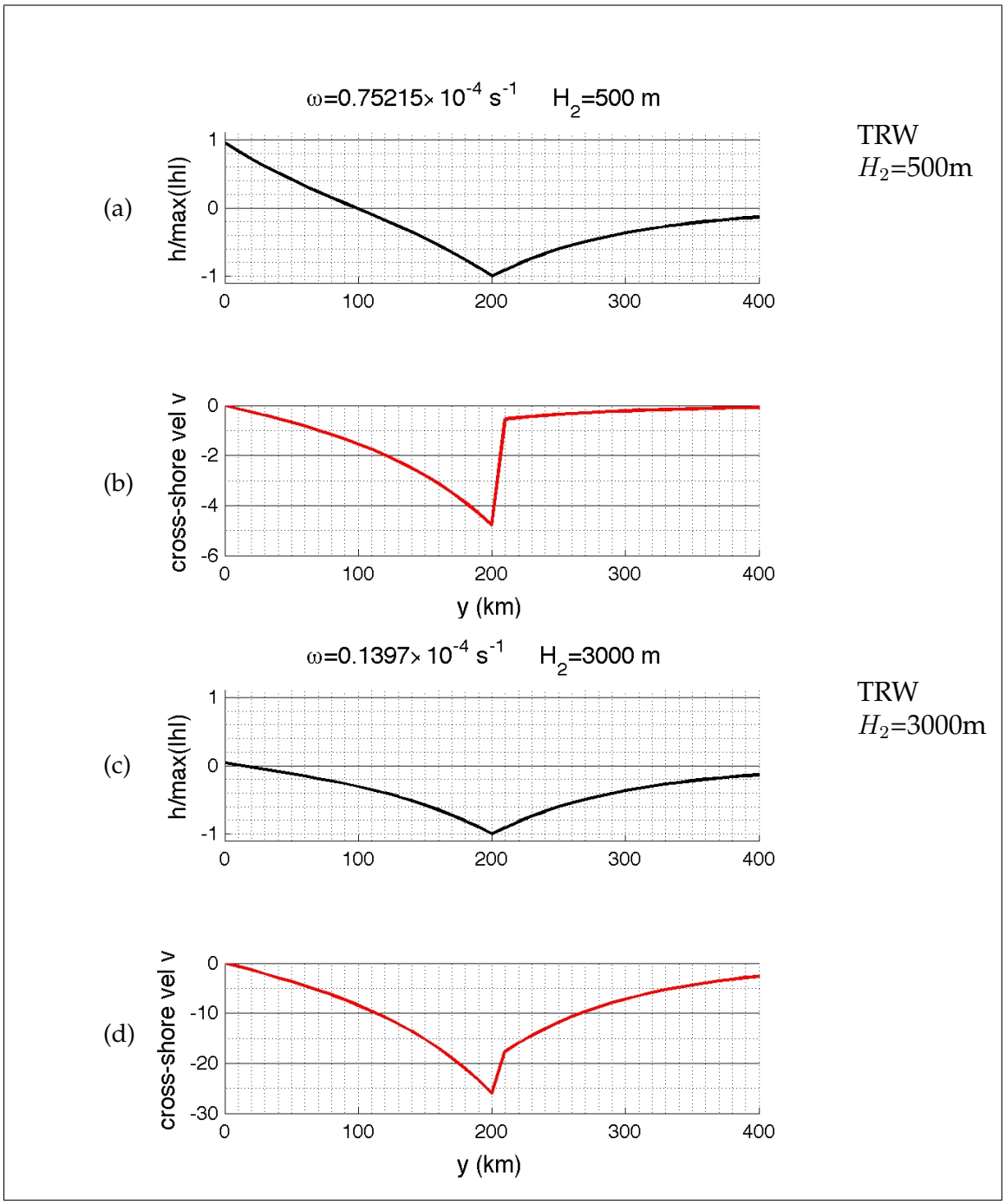


**Figure 4.11:** Normalised perturbed sea surface height $\hat{h}/|\hat{h}_{max}|$(a,c), and cross-shore velocity, $\hat{v}$ (b,d), as a function of $y$ where $L = 200$km, $k = 1 \times 10^{-5}$ m$^{-1}$. Here we have TRW at $H_2 = 500$ m (a,b), and $H_2 = 3000$ m (c,d) with very small frequencies. Note the marked change in $\hat{h}/|\hat{h}_{max}|$ and $\hat{v}$ at the shelf edge ($L = 200$km). The coastal BC (4.5) and trapped BC (4.6) are satisfied; $\hat{v} = 0$ at $y = 0$, and $(\hat{h}/|\hat{h}_{max}|, \hat{v}) \to 0$ as $y \to \infty$.

## 4.5 Perturbation analysis for the modified Kelvin wave (MKW)

In section 4.4.1, we showed how either varying the length of the shelf , $L$, or the depth of the shelf, $H_2$, modified the classic Kelvin wave. Here we perform a perturbation analysis in an attempt to quantify those changes. This could be done by either considering a short shelf or a small step. We choose the former.

We begin with the dispersion relation (4.39) rearranged so that the leading order solution for the Kelvin wave is on the left

$$\omega l_1 - fk = \frac{H_2}{H_1} \cdot \frac{(\omega l_2 - fk)(\omega l_2 + fk)(e^{-2l_2 L} - 1)}{(\omega l_2 - fk) + (\omega l_2 + fk)e^{-2l_2 L}}. \tag{4.46}$$

We assume that the frequency takes the form

$$\omega = \omega_0 + \omega_1 L + \cdots, \tag{4.47}$$

where $\omega_0$ is the leading order solution for the Kelvin wave, (3.6). Substituting (4.47) into the definition for $l_1$ (4.30) we have

$$l_1 = A_1\left(1 - \frac{\omega_0\omega_1 L}{A_1^2 g H_1} - \mathrm{O}(L^2)\right), \tag{4.48}$$

where

$$A_1 = \sqrt{k^2 - \frac{\omega_0^2 - f^2}{gH_1}} = \sqrt{k^2 - \frac{gH_1k^2 - f^2}{gH_1}} = \frac{|f|}{\sqrt{gH_1}} = \frac{1}{L_{R_1}}. \tag{4.49}$$

Similarly for $l_2$, (4.32), we have

$$l_2 = A_2\left[1 - \frac{\omega_0\omega_1 L}{A_2^2 g H_2} + \mathrm{O}(L^2)\right], \tag{4.50}$$

where

$$A_2^2 = k^2 - \frac{\omega_0^2 - f^2}{gH_2} = \frac{k^2 g(H_2 - H_1) + f^2}{gH_2}. \tag{4.51}$$

Finally, the exponential term in (4.46) may be expanded as

$$e^{-2l_2 L} = 1 - 2A_2 L + \mathrm{O}(L^2), \tag{4.52}$$

substituting (4.48), (4.50) and (4.52) into (4.39) gives

$$H_1\left[(\omega_0 A_1 - fk) + \left(\omega_1 A_1 - \frac{\omega_0^2\omega_1}{A_1 g H_1}\right)L + \cdots\right] \times \left[A_2(\omega_0 + \omega_1 L + \cdots)\left(1 - \frac{\omega_0\omega_1 L}{A_2^2 g H_2} + \cdots\right) - (A_2 fk + \omega_0 A_2^2)L + \cdots\right] = -H_2 A_2(\omega_0^2 A_2^2 - f^2k^2)L + \cdots . \quad (4.53)$$

However $\omega_0 = k\sqrt{gH_1}\,\mathrm{sgn}(f)$ and $A_1 = \frac{|f|}{\sqrt{gH_1}}$, so $\omega_0 A_1 - fk = 0$. Then, dividing (4.53) by $L$ and retaining terms of order unity, we obtain

$$H_1\omega_0\left(\omega_1 A_1 - \frac{\omega_0^2\omega_1}{A_1 g H_1}\right) = -H_2(\omega_0^2 A_2^2 - f^2k^2).$$

Using our definition for $\omega_0$ (3.6), $A_1$ (4.49) and $A_2$ (4.51) we have

$$\omega_1 = -\frac{f\ k\ (H_1 - H_2)}{H_1} \quad (4.54)$$

which we can rewrite as

$$\omega_1 = -\frac{|f|\ \mathrm{sgn}(f)\ k\ (H_1 - H_2)}{H_1} \quad (4.55)$$

which is the correction to the classic Kelvin wave due to the step. Substituting (3.6) and (4.55) into (4.47) we have

$$\omega = k\sqrt{gH_1}\,\mathrm{sgn}(f)\left[1 - \frac{|f|}{\sqrt{gH_1}}\left(1 - \frac{H_2}{H_1}\right)\ L\ + \cdots\right]. \quad (4.56)$$

Here we clearly see that the Kelvin wave frequency decreases as the length of the continental shelf, $L$, increases. Furthermore, at fixed $L$, the frequency of the Kelvin wave also decreases as $H_1 - H_2$ increases, i.e., as the height of the step increases.

**Comparison of analytical and numerical results**

Figure 4.12 compares the solutions to the general dispersion relation (4.39), the classic Kelvin wave (3.6) and the perturbation analysis result for the modified Kelvin wave, (4.56). Here we have fixed the depth of the shelves at $H_2 = 200$, 500, 2000 and 3800 m as shown in panels (a)-(d) respectively.

The leading order solution to the modified Kelvin wave (4.56) is the classic Kelvin wave. Clearly we see when comparing panels (a)-(d) of Figure 4.12, the effect of increasing the length of the continental shelf, $L$, is to decrease the frequency of the modified Kelvin wave, and increase the discrepancy between the numerical solution (4.39) and the modified Kelvin wave (4.56). However, a more pronounced effect is seen as we increase the depth of the shelf, $H_2$. If we compare panels (a) and (d), we see the frequency of the modified Kelvin wave becomes closer to that of the classic Kelvin wave over the same range of $L$. We expect this, as increasing $H_2$ means moving towards a flatter topography which is the setting required for the classic Kelvin wave to exist.

When we initially set out to determine an analytical solution for the modified Kelvin wave we assumed $L$ is small. Re-writing (4.56) as

$$\omega = k\sqrt{gH_1}\,\mathrm{sgn}(f)\left[1 - \left(1 - \frac{H_2}{H_1}\right)\frac{L}{L_{R_1}} + \cdots\right], \tag{4.57}$$

we can see as we increase $H_2$, the smaller the discrepancy between the classic Kelvin wave and modified Kelvin wave. We also observe how important the Rossby radius of deformation, $L_{R_1} = \sqrt{gH_1}/|f|$, in the deep ocean is. In section 2.1.4 we discussed the importance of this lengthscale: the closer the wavelength is to $L_{R_1}$, the stronger the effects of the rotation of the earth, $f$, felt by a wave.

In our simple model, we can calculate $L_{R_1}$. We have $f = 1 \times 10^{-4}$ s$^{-1}$, $g = 10$ ms$^{-2}$, and $H_1 = 4$ km, thus $L_{R_1} = 2000$ km. We are unable to display $L_{R_1}$ in Figure 4.12 since the range of $y$ is too small. However, when we consider a greater range, $0 \leq L \leq 3000$ km, see Figure 4.13, we are able to display $L_{R_1}$ as a solid dark pink vertical line (—). Clearly in (4.57) if $L \ll L_{R_1}$ the frequency reduces to that of the classic Kelvin wave, and we observe this in Figures 4.12 and 4.13 too.

We determined the expression for the modified Kelvin wave (4.56) using perturbation theory. Consequently (4.56) should be valid only if

$$L \ll \frac{L_{R_1}}{1 - H_2/H_1}. \tag{4.58}$$

Thus if $H_2 = 200$ m or $H_2 = 3800$, then the theory works if $L \ll 2105$ km or $L \ll 40000$

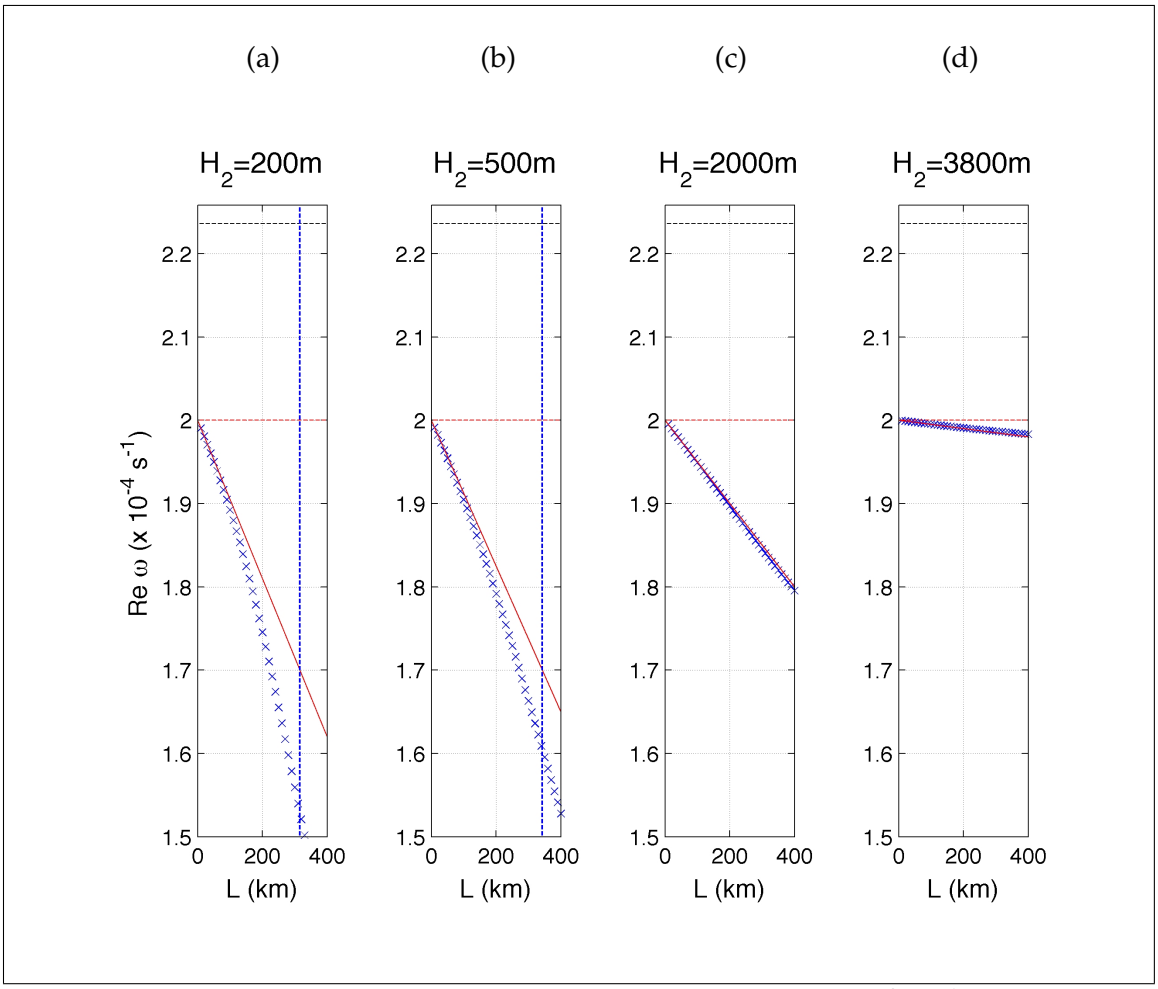


**Figure 4.12:** Frequency $\omega$ as a function of shelf width, $L$ at $k = 1\times10^{-6}$ m$^{-1}$ for $H_2$ =200m (a), 500m (b), 2000m (c) and 3800m (d) where $0 \leq L \leq 400$ km. Numerical solutions of dispersion relation (4.39) found using Newton-Raphson iteration method are shown as blue crosses ($\times$). The solid red line (—) is the MKW (4.56), the red dashed line (- -) is the classic KW (3.6), the black dashed line (- -) is the maximum possible frequency for trapped waves $\omega = \omega_{max} = \pm\sqrt{f^2 + gH_1k^2}$ and the blue dashed line (- -) represents $L_{val}$ (4.59). The deeper the shelf, i.e., as $H_2$ increases we see the error between the MKW and numerical solutions (4.39) decrease.

km respectively. In Figure 4.12 the theory holds as we have only considered a maximum shelf length of 300 km and $L_{R_1} = 2000$ km. If we let

$$\left(1 - \frac{H_2}{H_1}\right)\frac{L}{L_{R_1}} = 0.15,$$

where 0.15 is an arbitrarily chosen value. Then rearranging for the maximum value of $L$ for which the theory holds gives

$$L_{val} = \frac{0.15\, L_{R_1}}{1 - H_2/H_1}. \tag{4.59}$$

So if $H_2 = 200$ m, $L_{val} = 316$ km, and if $H_2 = 3800$ m, $L_{val} = 6000$ km. Thus as long as $L \ll L_{val}$, we have a valid solution to O($L$) for the modified Kelvin wave. We plot $L_{val}$ in Figures 4.12 and 4.13 as a dashed blue vertical line (- -). Note that (4.59) is visible in panels (a,b) but not in panels (c,d) of Figure 4.12 since $L_{val} > 300$ km for these depths.

Considering a greater range, $0 \leq L \leq 3000$ km, see Figure 4.13, we can further test how robust the expression for the modified Kelvin wave is (4.56). We clearly see for any value of $H_2$, the expression (4.56) is definitely not valid beyond $L_{R_1}$, plotted as a solid dark pink line (—). A better approximation for which (4.56) holds is shown by $L_{val}$ (4.59) (plotted as a blue dashed line (- -)).

Since we are looking at a shelf of very long length, we must take into account that the modified Kelvin wave frequency will be strongly influenced by the depth of the shelf, $H_2$. Thus we define the Rossby radius of deformation on-shelf as $L_{R_2} = \sqrt{gH_2}/|f|$, shown in Figure 4.13 as a solid salmon coloured line (—). We also observe that the effect of such a long shelf is to bound the frequency of the modified Kelvin wave by

$$\omega_{kw}(L \to \infty) = k\sqrt{gH_2}\,\mathrm{sgn}(f), \tag{4.60}$$

shown as a solid dark green line (—). With a very long shelf we expect the ratio of the frequencies to be given by

$$\frac{\omega(L \to \infty)}{\omega(L \to 0)} = \sqrt{\frac{H_2}{H_1}}. \tag{4.61}$$

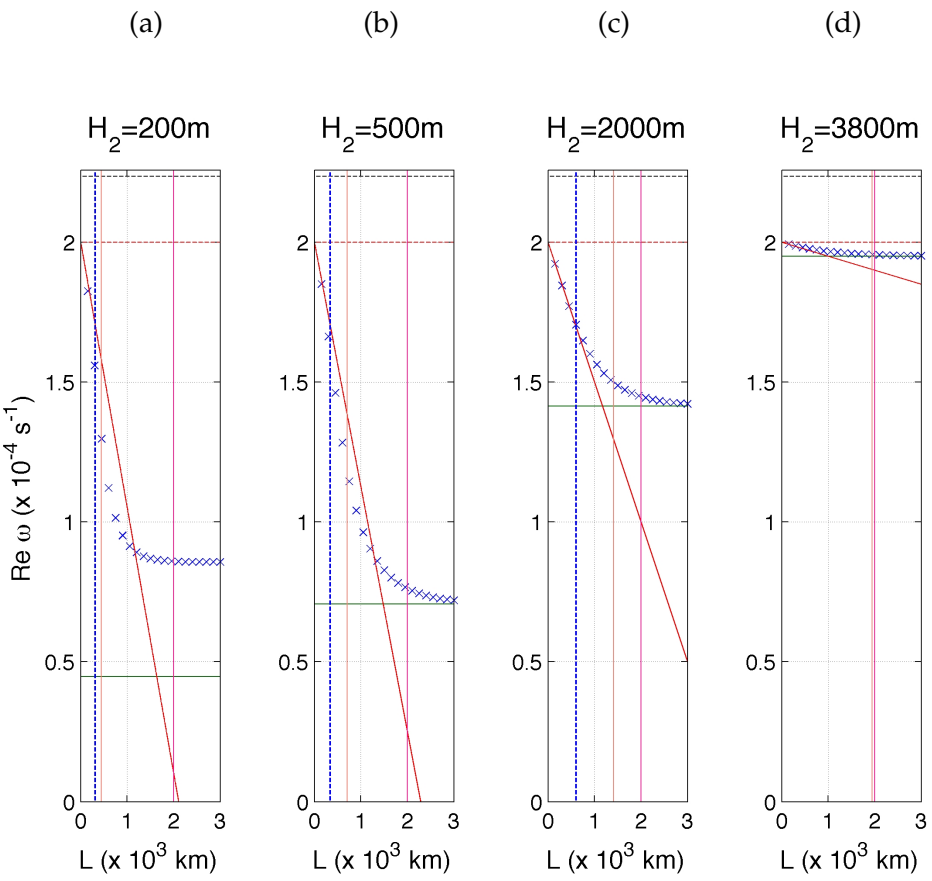


**Figure 4.13:** Frequency $\omega$ as a function of shelf width, $L$ at $k = 1\times10^{-6}$ m$^{-1}$ for $H_2$ =500m (a), 2000m (b), and 3800m (c) where $0 \leq L \leq 3000$ km. Numerical solutions of dispersion relation (4.39) found using Newton-Raphson iteration method are shown as blue crosses ($\times$). The solid red line (—) is the MKW (4.56), the red dashed line (- -) the classic KW (3.6), the black dashed line (- -) the maximum possible frequency for trapped waves, $\omega = \omega_{max} = \pm\sqrt{f^2 + gH_1k^2}$, and the blue dashed line (- -) represents $L_{val}$ (4.59). The solid dark pink line (—) represents $L_{R_1}$, the solid salmon line (—) represents $L_{R_2}$ and the solid dark green line (—) represents the frequency on-shelf, $k\sqrt{gH_2}\,\mathrm{sgn}(f)$.

It is interesting to note that the numerical solutions (4.39) shown in Figure 4.13a does not follow the trend as shown in Figure 4.13 panels (b)-(d) where $\omega \to k\sqrt{gH_2}\,\mathrm{sgn}(f)$ as $L \to 3000$ km. That is, the frequency at $H_2 = 200$ m and $L = 3000$ km is larger than expected. To investigate further we examine the height profiles of these waves.

**Further exploration of the modified Kelvin wave when we have a long and shallow shelf**

If we have a shelf at a depth of $H_2 = 200$ m, of length $L = 3000$ km and $k = 1 \times 10^{-6}$ s$^{-1}$, we expect to see a mixture of edge waves, a modified Kelvin wave and a topographic Rossby wave. The code used to track the modified Kelvin wave modes, shown in Figures 4.12 and 4.13, uses as an initial guess the dispersion relation for the classic Kelvin wave, $\omega = k\sqrt{gH_1}\,\mathrm{sgn}(f)$. To determine further solutions as $L$ increases, we use the Newton-Raphson technique. Therefore, unless the code 'jumps' to another wave, we would expect to see the profiles of a modified Kelvin wave throughout our range of $L$ in Figures 4.12 and 4.13.

We show in Figure 4.14(a)-(d) the normalised perturbed sea surface height of the waves, $\hat{h}/max(\hat{h})$, in Figure 4.13. The numerical solution frequencies when $H_2$=200m, 500m, 2000m, 3800m and $L = 3000$ km are $0.86 \times 10^{-4}$ s$^{-1}$, $0.72 \times 10^{-4}$ s$^{-1}$, $1.42 \times 10^{-4}$ s$^{-1}$, and $2.0 \times 10^{-4}$ s$^{-1}$ respectively. We expect the profile of the modified Kelvin wave to look like a wave that is monotonically decreasing, and exponentially decaying from the coast, as in panels (c) and (d) and Figure 4.9a. However, surprisingly when we have a shallow shelf as in panels (a) ($H_2 = 200$ m) and (b) ($H_2 = 500$ m) we observe the profiles of topographic Rossby waves as previously seen in Figure 4.11. This is puzzling. Are we looking at the modified Kelvin or topographic Rossby wave? It makes sense to return to looking at the frequency curves for this parameter space.

In Figure 4.15 we plot frequency as a function of shelf depth, $H_2$, and fix the length of the shelf at 3000km. We also plot our analytical expressions for the modified Kelvin wave (4.56) (shown in a solid dark green line), and Larsen's result for the bounded topographic

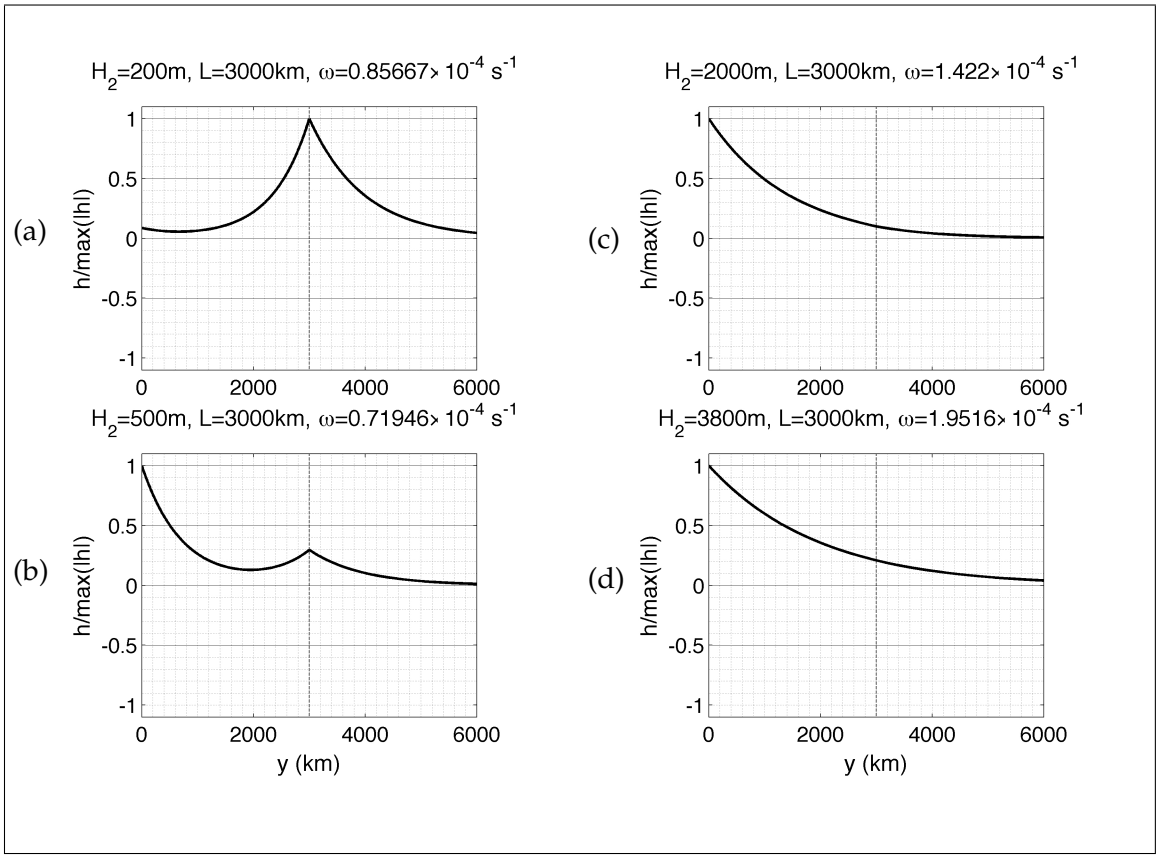


**Figure 4.14:** Normalised perturbed sea surface height, $\hat{h}/max(\hat{h})$, as a function of $y$ where $k = 1 \times 10^{-6}$ m$^{-1}$, $L = 3000$ km. Panels (a)-(d) represent shelf depths $H_2 = 200$m, 500m, 2000m, and 3800m respectively as shown in Figure 4.13.

Rossby wave, (4.74) (shown in a dashed green line). The analytical expressions suggests that the modified Kelvin wave and topographic Rossby wave cross (see Figure 4.16). Thus, if (4.60) is correct then it appears that the modified Kelvin wave exists as an edge wave on the shelf, with a frequency smaller than the topographic Rossby wave, until it reaches a depth of $H_2 = 500$ m. Since these two waves are influenced by different restoring mechanisms, one being gravity, and the other vorticity, and it seems more likely that the waves would 'swap' characteristics as they come close to each other but not cross.

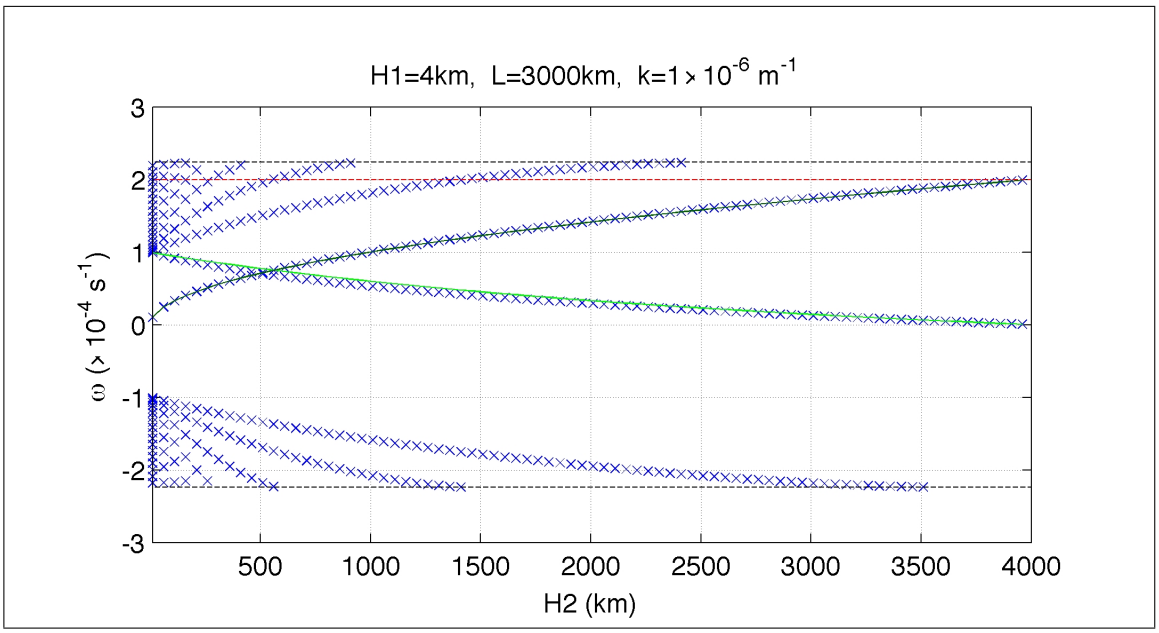


**Figure 4.15:** Frequency $\omega$ as a function of shelf depth, $H_2$ at $k = 1 \times 10^{-6}$ m$^{-1}$ for $L = 3000$ km. Numerical solutions of dispersion relation (4.39) found using Newton-Raphson iteration method are shown as blue crosses (×). The solid red line (—) is the MKW (4.56), the red dashed line (- -) the classic KW (3.6), the black dashed line (- -) the maximum possible frequency for trapped waves, $\omega = \omega_{max} = \pm\sqrt{f^2 + gH_1k^2}$, and the solid dark green line (—) represents the frequency on-shelf, $k\sqrt{gH_2}\,\mathrm{sgn}(f)$.

In Figure 4.17 the perturbed sea surface height of the modified Kelvin wave and topographic Rossby wave for the range $475 \leq H_2 \leq 525$ m are shown. Here we see the cross-shore structure of $h$, and note that the modified Kelvin wave feels the step for a

shallow shelf.

**Avoidance of crossing**

We established that the modified Kelvin wave and topographic Rossby wave on an extremely long shelf interchange characteristsics, this was shown in Figure 4.15. This occurrence known as avoidance crossing (**??**) is shown more clearly in Figure 4.18 for waves of very long wavelength i.e. $k = 1 \times 10^{-6}\text{m}^{-1}$ and $k = 1 \times 10^{-7}\text{m}^{-1}$.

The avoidance of crossings is most easily understood by considering analogous behaviour in a simpler finite-dimensional system: the set of real, symmetric $n \times n$ matrices. Here the occurrence of multiple (degenerate) eigenvalues would be analogous to crossing wave modes. However, it is known (**?**) that the occurrence of multiple eigenvalues in such a system is unlikely.

If we have a set of eigenvalues that are real and distinct, then the eigenvectors are orthogonal. The first eigenvector, corresponding to the largest eigenvalue depends on $n-1$ parameters. The second eigenvector which is orthogonal to the first eigenvector depends on $n-2$ parameters, and so forth, until we reach the $(n-1)$st eigenvector that depends on one parameter. The total number of these parameters sums to $N = n(n+1)/2$, i.e. the dimension of all real, symmetric $n \times n$ matrices.

Now let us consider degenerate matrices which have two equal eigenvalues, with the others being distinct from it and each other. Here the first eigenvector depends on $n-1$ parameters, and so forth, until we reach the last eigenvector which depends on two parameters. The parameters in this instance sum to $N-2$ which equates to a dimensional space of $N-2$ which is much smaller than $N$ dimensional space. Therefore to have eigenvalues intersecting is much more unlikely. A simple example will help to explain avoidance crossing. If we have a line or curve lying in $N$ dimensional space, it will in general avoid intersecting a surface depending on $N-2$ parameters. Our system is infinitely dimensional, therefore, it will be extremely rare for eigenvalues to cross. This

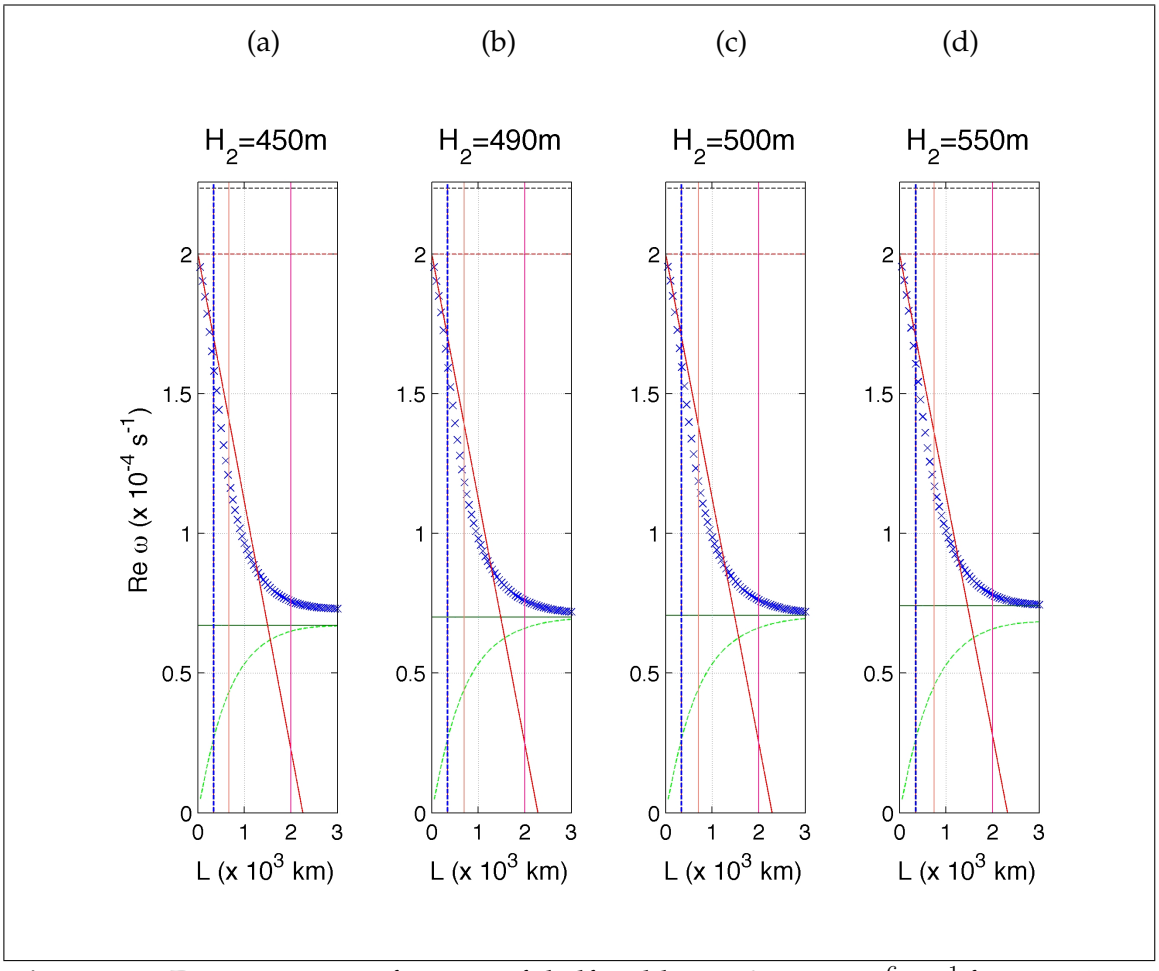


**Figure 4.16:** Frequency $\omega$ as a function of shelf width, $L$ at $k = 1\times10^{-6}$ m$^{-1}$ for $H_2$ =500m (a), 2000m (b), and 3800m (c) where $0 \leq L \leq 3000$ km. Numerical solutions of dispersion relation (4.39) found using Newton-Raphson iteration method are shown as blue crosses (×). The solid red line (—) is the MKW (4.56), the red dashed line (- -) the classic KW (3.6), the black dashed line (- -) the maximum possible frequency for trapped waves, $\omega = \omega_{max} = \pm\sqrt{f^2 + gH_1k^2}$, and the blue dashed line (- -) represents $L_{val}$ (4.59). The solid dark pink line (—) represents $L_{R_1}$, the solid salmon line (—) represents $L_{R_2}$ and the solid dark green line (—) represents the frequency on-shelf, $k\sqrt{gH_2}\,\mathrm{sgn}(f)$. For $H_2 < 500$m, the green dashed line (- -) represents the modified Kelvin wave and the blue crosses (×) represents bounded topographic Rossby wave, (4.74). For $H_2 > 500$m, the green dashed line (- -) represents bounded topographic Rossby wave, (4.74) and the blue crosses (×) represents the modified Kelvin wave.

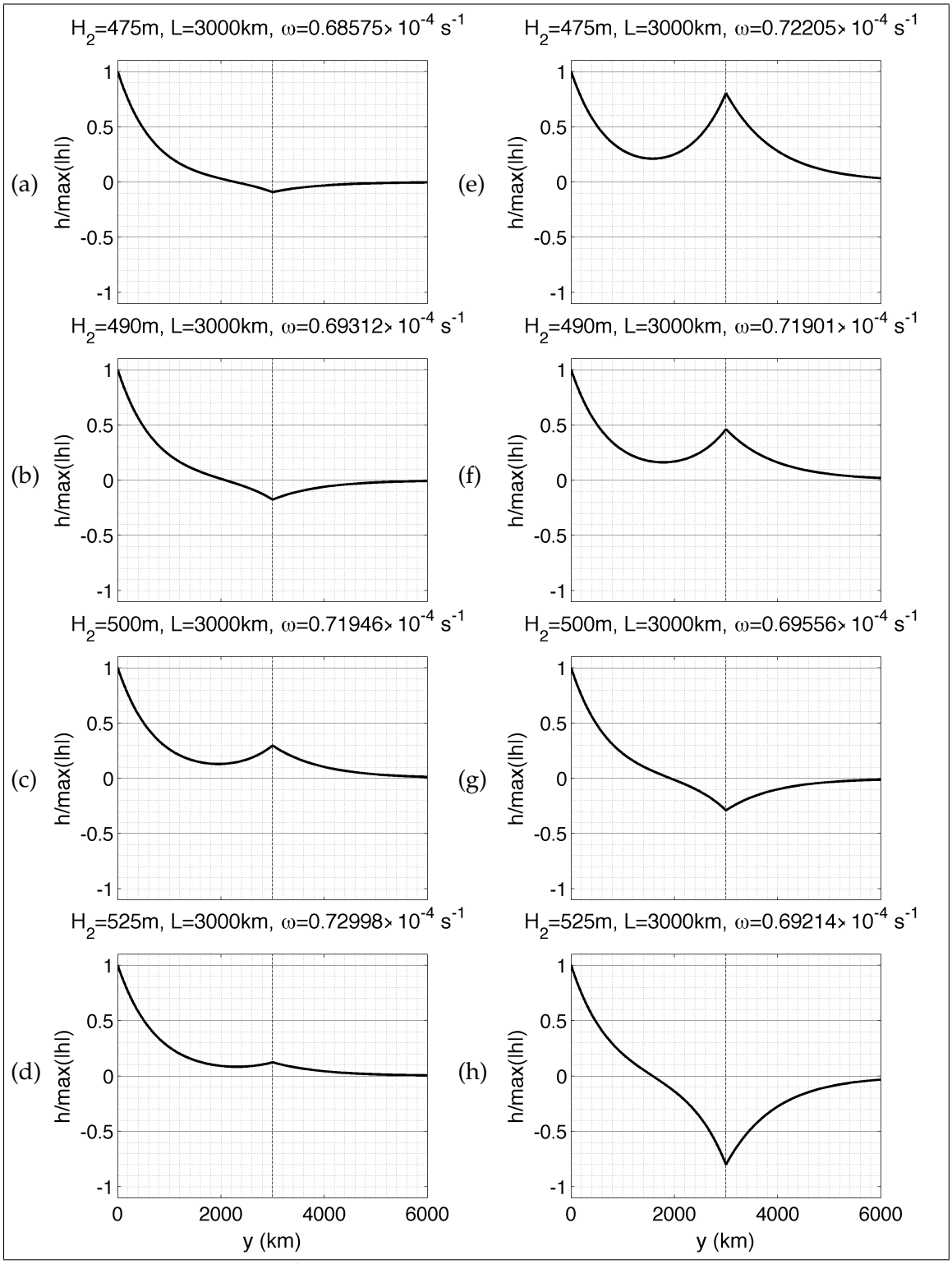


**Figure 4.17:** $k = 1 \times 10^{-6}$ m$^{-1}$, $L = 3000$ km, $475 \leq H_2 \leq 525$ m. The right hand column shows the modified Kelvin wave (MKW), and the left hand column the bounded topographic Rossby wave (TRW).

is shown in Figure 4.18.

## 4.6 Topographic Rossby Wave (TRW) in the presence of a coastline

The topographic Rossby waves seen in Figures 4.3-4.7 (green dashed line) and 4.11 have already been explored in sections 3.4 and 3.5, however, this was without the presence of a coastline, and over a step or smooth topography. We have clearly established that these waves owe their existence to depth variations, nevertheless, the coastline does modify the behaviour of these waves, and they are more commonly known as continental shelf waves (**?**).

In section 3.4.3, we showed that such waves may be analysed with the rigid-lid approximation (**?**), which is valid provided $L \ll L_R$. We return to the linear shallow-water equations (3.2a-c) from section 3.1.2, however now, the topography is quite different. We now have a shelf of constant depth on either side of the step and applying the rigid-lid approximation we can write the governing set of equations as

$$-i\omega\hat{u} - f\hat{v} = -igk\hat{h}, \tag{4.62a}$$

$$-i\omega\hat{v} + f\hat{u} = -g\frac{d\hat{h}}{dy}, \tag{4.62b}$$

$$ik\hat{u} + \frac{d\hat{v}}{dy} = 0. \tag{4.62c}$$

From section 3.4.1 we can write (3.31) as

$$-i\omega\left(\frac{d\hat{u}}{dy} - ik\hat{v}\right) - f\left(ik\hat{u} + \frac{d\hat{v}}{dy}\right) = 0, \tag{4.63}$$

and (3.32) as

$$\hat{u} = -\frac{d\hat{\psi}}{dy}, \qquad \hat{v} = ik\hat{\psi} \tag{4.64}$$

that satisfy (4.62c). We can reduce (4.63) using (4.62c), so

$$\frac{d\hat{u}}{dy} - ik\hat{v} = 0. \tag{4.65}$$

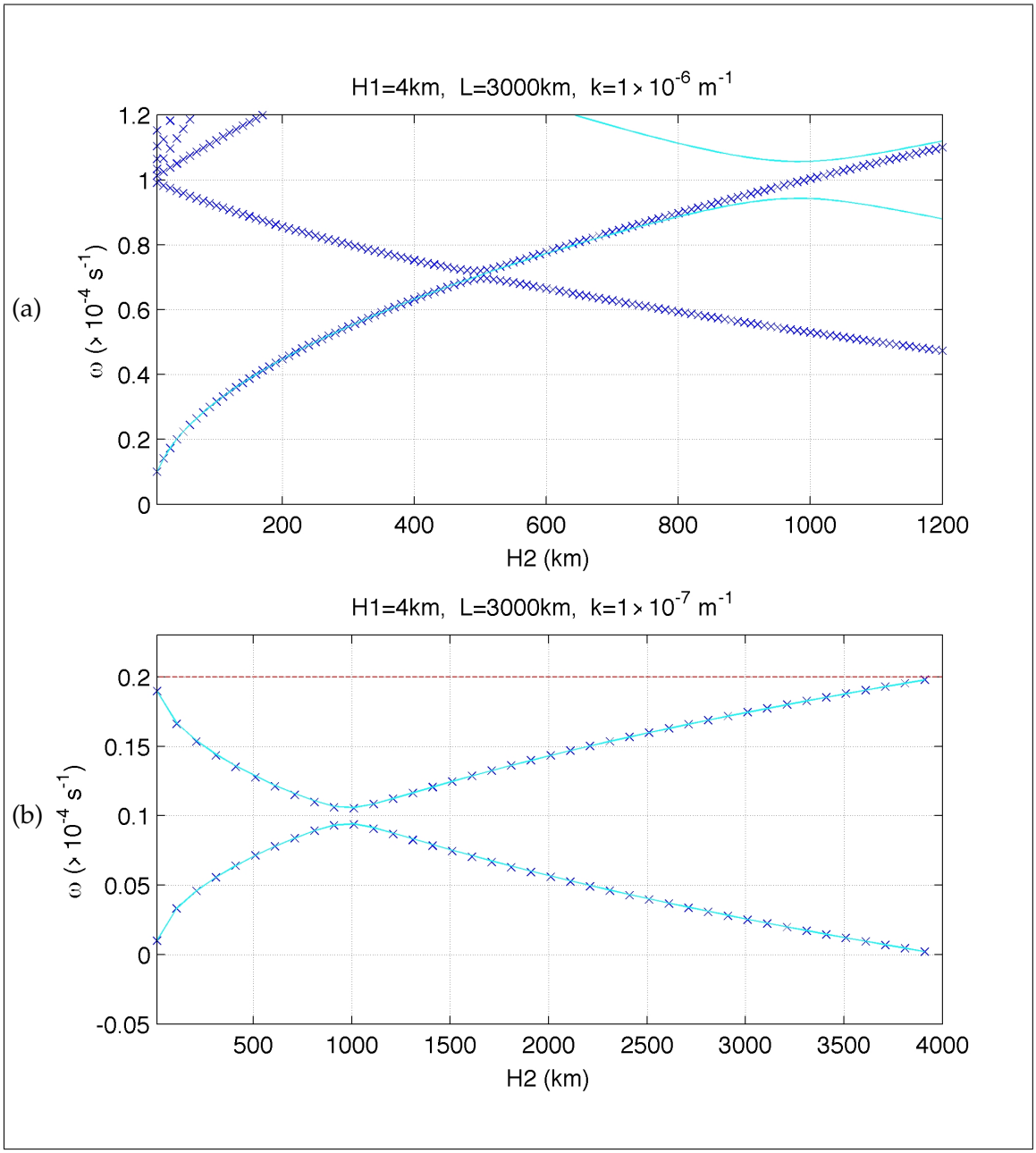


**Figure 4.18:** Avoidance of crossing eigenvalues. Frequency $\omega$ as a function of shelf depth, $H_2$ at $k = 1 \times 10^{-6}$ m$^{-1}$ for where $L = 3000$ km. Numerical solutions of dispersion relation (4.39) found using Newton-Raphson iteration method are shown as blue crosses ($\times$). The red dashed line (- -) is the classic KW (3.6). The cyan line (4.99) represents the LW theory which for very long waves ($k = 1 \times 10^{-7}$m$^{-1}$) which shows an excellent match with the numerics. Here we see the MKW and TRW interchange behaviour at (a) $H_2 = 500$m and (b) $H_2 = 1000$m rather than cross.

By (4.64) we can write (4.65) as

$$\frac{d^2\hat{\psi}}{dy^2} - k^2\hat{\psi} = 0. \tag{4.66}$$

On the shelf, we write $\hat{\psi}$ in the form

$$\hat{\psi}_2 = A_2 \sinh(ky) + B_2 \cosh(ky), \quad 0 \leq y \leq L.$$

Now, at $y = 0$, we require $\hat{v} = 0$, by (4.64) this implies that $|\hat{\psi}_2|$=0 and therefore $B_2 = 0$. Thus

$$\hat{\psi}_2 = A_2 \sinh(ky), \quad 0 \leq y \leq L. \tag{4.67}$$

In the open ocean, we require all variables to decay to 0 as $y \to \infty$, so we take $|\hat{\psi}_1| \to 0$. We can therefore write the solution as

$$\hat{\psi}_1 = A_1 e^{-ky}, \quad y \geq L. \tag{4.68}$$

To determine the surface displacements we substitute our expression for $\hat{\psi}_1$, (4.68), and $\hat{\psi}_2$, (4.67), into (4.62a), and rearrange for $\hat{h}$:

$$\hat{h}_1 = \frac{A_1}{g}\Big[f + \omega \,\mathrm{sgn}(k)\Big]e^{-ky}, \tag{4.69}$$

$$\hat{h}_2 = \frac{A_2}{g}\Big[f \sinh(ky) - \omega \cosh(ky)\Big]. \tag{4.70}$$

Using the continuity condition (2.29) at $y = L$, (4.62a) gives

$$-i\omega\hat{u}_1 - f\hat{v}_1 = -i\omega\hat{u}_2 - f\hat{v}_2 \tag{4.71}$$

which leads to

$$-2\frac{A_1}{A_2}(\omega + f)e^{-kL} = (\omega - f)e^{kL} + (\omega + f)e^{-kL}. \tag{4.72}$$

By the continuity of mass (2.30) at $y = L$ we have

$$2\frac{A_1}{A_2} = \frac{H_2}{H_1}(e^{2kL} - 1). \tag{4.73}$$

Substituting (4.73) into (4.72) we obtain

$$\omega = \frac{f|(H_2 - H_1)(1 - e^{-2kL})|}{H_2(1 - e^{-2kL}) + H_1(1 + e^{-2kL})}. \tag{4.74}$$

This result was obtained by **?**.

Note when $L \to \infty$, i.e., when the coast is removed and there an isolated step in the open ocean, then (4.74) reduces to

$$\omega = \frac{|f(H_2 - H_1)|}{H_2 + H_1}. \tag{4.75}$$

We previously derived this result in section 3.4.4 equation (3.46) where we had a step topography without a coastline. We also arrived at this same result in section 3.5.3 equation (3.76) where we considered a smooth, continuous slope in the limit of the slope width tending to zero, i.e., $L_s \to 0$.

For completeness, we give expressions for the cross-shore structure on and off the shelf:

$$h_1 = \frac{A_1 f}{g}\left[1 + \frac{|(H_2 - H_1)(1 - e^{-2|k|L})|\mathrm{sgn}(k)}{H_2(1 - e^{-2|k|L}) + H_1(1 + e^{-2|k|L})}\right]e^{-|k|y} \tag{4.76}$$

$$h_2 = \frac{A_2 f}{g}\left[\sinh(ky) - \frac{|(H_2 - H_1)(1 - e^{-2|k|L})|\mathrm{sgn}(k)}{H_2(1 - e^{-2|k|L}) + H_1(1 + e^{-2|k|L})}\cosh(ky)\right]e^{-|k|y} \tag{4.77}$$

$$u_1 = |k|A_1 e^{-|k|y} \tag{4.78}$$

$$u_2 = -\frac{kA_2}{4}(e^{2ky} - e^{-2ky}) \tag{4.79}$$

$$v_1 = ikA_1 e^{-|k|y} \tag{4.80}$$

$$v_2 = ikA_2 \sinh(ky) \tag{4.81}$$

**Recovery from general dispersion relation**

It is interesting to note that we can recover Larsen's solution (4.74) from the general dispersion relation (4.39). When $k$ is sufficiently large, or more precisely when $k^2 \gg (\omega^2 - f^2)/gH$. So, we have from (4.30) and (4.32), $l_1 = k$ and $l_2 = k$ . So our general dispersion relation, (4.39), becomes

$$H_1(f - \omega)\left[\left(\frac{\omega - f}{\omega + f}\right) + e^{-2kL}\right] = H_2[(\omega - f) + (f - \omega)e^{-2kL}]. \tag{4.82}$$

This implies

$$\omega = f \qquad \text{or} \qquad H_1\left[\left(\frac{\omega - f}{\omega + f}\right) + e^{-2kL}\right] = H_2[1 - e^{-2kL}].$$

The solution with $\omega = f$ is spurious, since we took $\omega^2 \neq f^2$ to obtain (4.39). The second solution leads to

$$\omega\left[\frac{-H_1}{H_2}(1+e^{-2kL})-(1-e^{-2kL})\right] = f\left[\frac{-H_1}{H_2}(e^{-2kL}-1)+f(1-e^{-2kL})\right], \qquad (4.83)$$

rearranging this for $\omega$ gives (4.74).

Figure 4.19 illustrates the waves we are able to predict: the modified Kelvin wave (4.56), the topographic Rossby waves (4.74) (Larsen's solution), and Longuet-Higgin's solution (3.46) for a step. Alongside these predictions we plot the numerical solutions of (4.39).

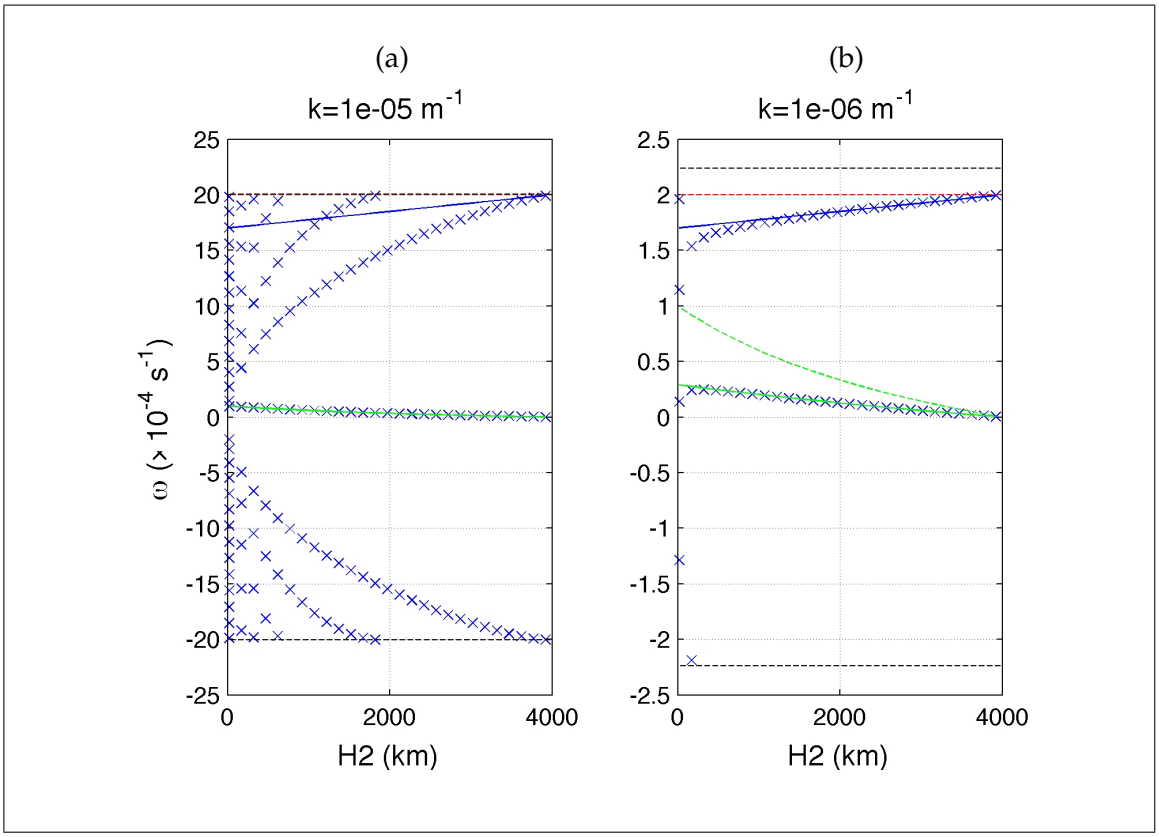


**Figure 4.19:** Frequency $\omega$ as a function of shelf depth, $H_2$ for $k = 1 \times 10^{-5}$ m$^{-1}$ (a) and $k = 1 \times 10^{-6}$ m$^{-1}$ (b) for $L = 300$ km. Numerical solutions of dispersion relation (4.39) are found using Newton-Raphson iteration method are shown as blue crosses (×). The red dashed line (- -) is the classic KW (3.6), the solid black line (—) is the MKW (4.56), the green dashed line (- -) the unbounded TRW (3.46), the green solid line (—) the bounded TRW (4.74), and the black dashed lines (- -) are the maximum possible frequencies for trapped waves $\omega = \omega_{max} = \pm\sqrt{f^2 + gH_1k^2}$.

## 4.7 Long wave theory

If we consider waves of extremely long wavelengths and very low frequency, that is, $k \to 0$ we can choose the following limit $|\omega| \to |k|$. It then follows that certain terms are eliminated from the linear shallow water equations (3.2). We take $\hat{v} \sim ak$ and $\hat{h} \sim 1$ to keep the balance in (4.3a). With this scaling applied to (4.3b) one possibility is $\hat{u} \sim 1$ to get a balance, this results in the first term which is of O$(k^2)$ being negligible. With respect to (4.3c) the terms are all of O$(k)$ and therefore retained. The resulting set of equations in which there is no $k$-dependence is

$$-ic\hat{u} - f\tilde{v} = -ig\hat{h}, \tag{4.84}$$

$$f\hat{u} = -g\frac{d\hat{h}}{dy}, \tag{4.85}$$

$$-ic\hat{h} + iH\hat{u} + \frac{d(H\tilde{v})}{dy} = 0. \tag{4.86}$$

where $c = \omega/k$ and $\tilde{v} = \hat{v}/k$.

To eliminate $\hat{u}$ we substitute $-g/f(d\hat{h}/dy)$ from (4.85) into (4.84) to give

$$\frac{f\tilde{v}}{ig} = \left(\frac{c}{f}\frac{d}{dy} + 1\right)\hat{h}. \tag{4.87}$$

Using the same substitution for $\hat{u}$, (4.86) can be re-written as

$$\left[ic + H\left(\frac{ig}{f}\frac{d}{dy}\right)\right]\hat{h} = H\frac{d\tilde{v}}{dy} \tag{4.88}$$

where $H$ is constant on either side of the step. Applying the the operator $(c/f(d/dy) + 1)$ and rearranging we have

$$\frac{d^2\tilde{v}}{dy^2} - \frac{\tilde{v}}{L_R^2} = 0, \tag{4.89}$$

where $L_R = \sqrt{gH}/|f|$, which applies on either side of the step.

On the shelf, $0 < y < L$, we thus have

$$\tilde{v}_2 = A_2 \sinh\left(\frac{y}{L_{R_2}}\right) + B_2 \cosh\left(\frac{y}{L_{R_2}}\right),$$

where $L_{R_2} = \sqrt{gH_2}/|f|$. At $y = 0$, $\tilde{v} = 0$, therefore $B_2 = 0$, so we have

$$\tilde{v_2} = A_2 \sinh\left(\frac{y}{L_{R_2}}\right). \tag{4.90}$$

In the open ocean, $y > L$, $\tilde{v}$ decays to zeros as $y \to \infty$, and thus

$$\tilde{v_1} = A_1 e^{-y/L_{R_1}} \tag{4.91}$$

where $L_{R_1} = \sqrt{gH_1}/|f|$.

From (4.84) we rearrange for $\hat{u}$ to get $\hat{u} = (ig\hat{h} - f\hat{v})/ic$. Substituting this expression for $\hat{u}$ into (4.86) and rearranging gives a relationship between $\hat{h}$ and $\hat{v}$:

$$(c^2 - gH)\hat{h} = iH\left(f - c\frac{d}{dy}\right)\hat{v}. \tag{4.92}$$

Substituting (4.91) into (4.92) gives

$$(c - \sqrt{gH_1})(c + \sqrt{gH_1})\hat{h}_1 = iA_1H_1\left(f + \frac{c}{L_{R_1}}\right)e^{-y/L_{R_1}}. \tag{4.93}$$

We know that the Kelvin wave is given by $\omega/k = \sqrt{gH_1}\mathrm{sgn}(f)$, then if $c^2 \neq gH_1$

$$h_1 = \frac{iH_1|f|A_1e^{-y/L_{R_1}}}{\sqrt{gH_1}(c - \sqrt{gH_1}\mathrm{sgn(f)})}. \tag{4.94}$$

On the shelf, $y < L$, we have $\hat{v_2} = A_2 \sinh\left(\frac{y}{L_{R_2}}\right)$, therefore by (4.92) we have

$$(c^2 - gH_2)h_2 = iH_2A_2\left(f\sinh\left(\frac{y}{L_{R_2}}\right) - \frac{c|f|}{\sqrt{gH_2}}\cosh\left(\frac{y}{L_{R_2}}\right)\right). \tag{4.95}$$

If $c^2 \neq gH_2$ then

$$h_2 = \frac{iH_2A_2}{c^2 - gH_2}\left[f\sinh\left(\frac{y}{L_{R_2}}\right) - \frac{c|f|}{\sqrt{gH_2}}\cosh\left(\frac{y}{L_{R_2}}\right)\right]. \tag{4.96}$$

Using the continuity condition (2.29) at $y = L$, $\hat{h}_1 = \hat{h}_2$, to derive a dispersion relation:

$$\begin{aligned} iH_1|f|A_1e^{-L/L_{R_1}}(c^2 - gH_2) = iH_2A_2\sqrt{gH_1}(c - \sqrt{gH_1}\mathrm{sgn(f)}) \\ \times\left[f\sinh\left(\frac{L}{L_{R_2}}\right) - \frac{c|f|}{\sqrt{gH_2}}\cosh\left(\frac{L}{L_{R_2}}\right)\right] \end{aligned} \tag{4.97}$$

By continuity of mass (2.30), at $y = L$, we also have

$$H_1 A_1 e^{-L/L_{R_1}} = H_2 A_2 \sinh\left(\frac{L}{L_{R_2}}\right). \tag{4.98}$$

Dividing (4.97) by (4.98), and then dividing through by $\sqrt{gH_1}$ by we have

$$c^2\left[\frac{1}{L_{R_1}} + \frac{1}{L_{R_2}}\coth\left(\frac{L}{L_{R_2}}\right)\right] - c\,\mathrm{sgn}(f)\sqrt{gH_1}\left[\frac{1}{L_{R_1}} + \frac{1}{L_{R_2}}\coth\left(\frac{L}{L_{R_2}}\right)\right] + \frac{g(H_1 - H_2)}{L_{R_1}} = 0.$$

Since $|f| \neq 0$, the dispersion relation for the long-wave theory can be written as

$$c^2\left[\frac{1}{\sqrt{gH_1}} + \frac{1}{\sqrt{gH_2}}\coth\left(\frac{|f|L}{\sqrt{gH_2}}\right)\right] - c\,\mathrm{sgn(f)}\sqrt{\mathrm{gH_1}}\left[\frac{1}{\sqrt{\mathrm{gH_1}}} + \frac{1}{\sqrt{\mathrm{gH_2}}}\coth\left(\frac{\mathrm{|f|L}}{\sqrt{\mathrm{gH_2}}}\right)\right] + \frac{g(H_1 - H_2)}{\sqrt{gH_1}} = 0.$$

We know $c = \omega/k$ thus solving for $\omega$ we have

$$\omega = \frac{1}{2}k\left[\mathrm{sgn}(f)\,\sqrt{gH_1} \pm \sqrt{gH_1 - \frac{4g(H_1 - H_2)}{1 + \sqrt{H_1/H_2}\coth\left(|f|L/\sqrt{gH_2}\right)}}\right]. \tag{4.99}$$

We plot solutions to the LW theory (4.99) in cyan in Figures 4.20 and 4.21. Here we aim to determine how good a fit is the analytical result for the LW theory with the numerical solution, and why the LW theory is an exact solution for the modified Kelvin wave and Larsen's solution.

In Figure 4.20 we initially compare the positive root of the long wave theory (4.99) with the analytical expression for the modified Kelvin wave (4.56).

Here we focus on three fixed depths of the shelf, 500m, 2000m and 3800m. As $L$ increases we see that the difference between the numerical solution and the modified Kelvin wave increases. If we compare the modified Kelvin wave and the positive root of the LW theory we see that the difference in frequency between the modified Kelvin wave and the positive root of the LW theory is relatively small, and there is good agreement between these two analytical results for small $L$.

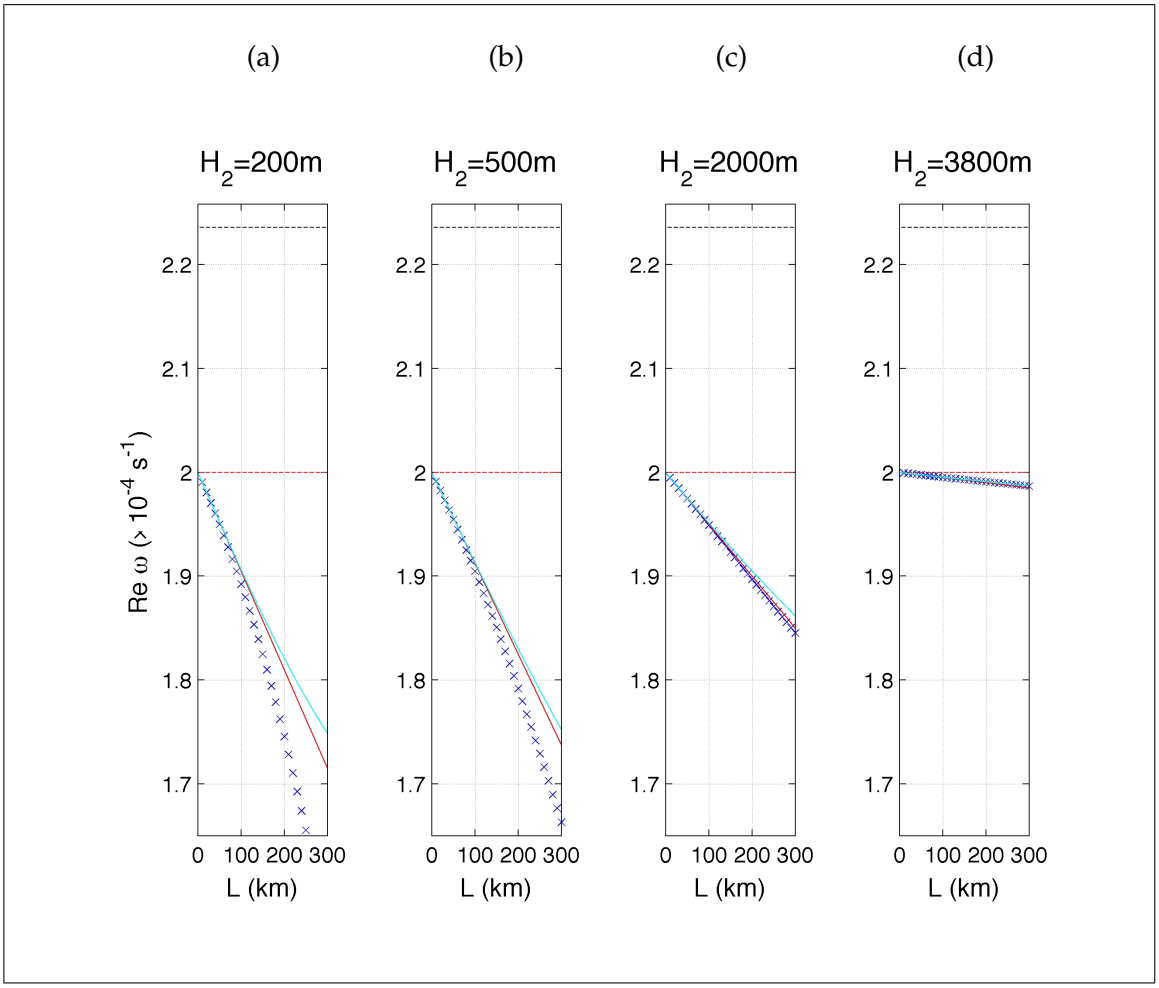


**Figure 4.20:** Comparison of frequencies of LW theory, MKW and numerical solutions. Frequency $\omega$ is plotted as a function of shelf width, $L$ at $k = 1 \times 10^{-6} m^{-1}$ for $H_2$ =500m (a), 2000m (b), and 3800m (c) where $0 \leq L \leq 300$ km. Numerical solutions of dispersion relation (4.39) found using Newton-Raphson iteration method are shown as blue crosses ($\times$). The solid red line (—) is the MKW (4.56), the red dashed line (- -) the classic KW (3.6), the solid cyan line (—) the LW theory (4.99) and the black dashed line (- -) the maximum possible frequency for trapped waves $\omega = \omega_{max} = \pm\sqrt{f^2 + gH_1k^2}$. The deeper the shelf, i.e., as $H_2$ increases we see the error between the classic KW and the numerical solutions decrease, however, as $L$ increases there is greater discrepancy between the classic KW and numerical solutions.

We now consider what happens as $H_2$ increases, this is shown in Figure 4.21 where $L$=300 km and $k = 1 \times 10^{-6}$ m$^{-1}$. We plot in Figure 4.21a the two roots of the LW theory (solid cyan line). In Figure 4.21b we see that the modified Kelvin wave (solid blue line) and Larsen's solution (short wave theory with a coast) (solid green line) replaces the two roots of the LW theory.

A visual comparison of (4.21a) and (4.21b) demonstrates that for any value of $H_2$ there is very good agreement of the modified Kelvin wave (4.56) with the positive root of the LW theory (4.99), and Larsen's solution (4.74) with the negative root of the LW theory (4.99).

**Reduction to the modified Kelvin wave (MKW) and the bounded topographic Rossby wave (TRW)**

To understand why the modified Kelvin wave, short wave theory (with a coastline) and LW theory coincide we need to consider (4.99) in two limits.

Let $|f|L/\sqrt{gH_1} \ll 1$ and $|f|L/\sqrt{gH_2} \ll 1$, and we assume $f$ is positive for simplicity. Now for small $\theta$, $\coth\theta \approx 1/\theta$. Thus we can write (4.99) as

$$\omega = \frac{1}{2}k\sqrt{gH_1}\left[1 \pm \left(1 - \frac{4(1-\frac{H_2}{H_1})}{1+\frac{\sqrt{gH_1}}{fL}}\right)^{1/2}\right],$$

Taking $\sqrt{gH_1}/|f|L \gg 1$ we have

$$\omega = \frac{1}{2}k\sqrt{gH_1}\left[1 \pm \left(1 - \frac{4(1-\frac{H_2}{H_1})|f|L}{\sqrt{gH_1}}\right)^{1/2}\right].$$

We can expand the enclosed bracket using the binomial theorem since $(1-\frac{H_2}{H_1}|f|L)/\sqrt{gH_1} \ll 1$, so we have

$$\omega = \frac{1}{2}k\sqrt{gH_1}\left[1 \pm \left(1 - \frac{2(1-\frac{H_2}{H_1})|f|L}{\sqrt{gH_1}}\right)\right] \tag{4.100}$$

Now taking the positive root, making $\sqrt{gH_1}$ a common factor, and rewriting $(1 - H_2/H_1)$ as $(H_1 - H_2)/H_1$ gives us the analytical result for the modified Kelvin wave (4.56) to O(L),

$$\omega = k\sqrt{gH_1}\left[1 - \frac{|f|(H_1-H_2)L}{H_1\sqrt{gH_1}}\right]. \tag{4.101}$$

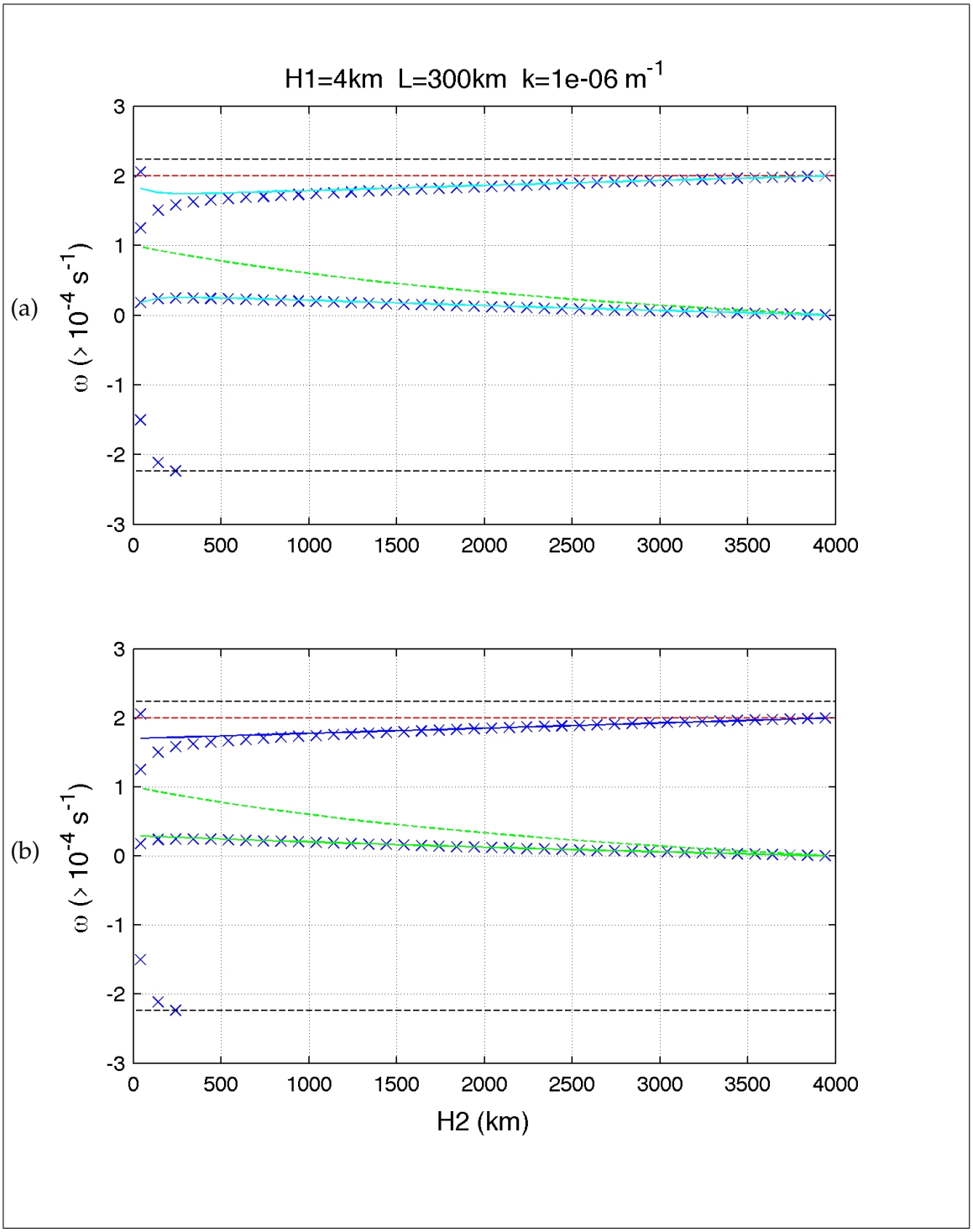


**Figure 4.21:** Frequency $\omega$ as a function of $H_2$ for $k = 1 \times 10^{-6}$ m$^{-1}$ and $L = 300$ km. LW theory (4.99) (—) solutions shown in the panel (a). This is replaced by the MKW (—) (4.56) and Larsen's solution (bounded TRW)(—) (4.74) in panel (b).

To derive Larsen's result (4.74), we return to (4.100) and take the negative sign which gives

$$\omega = |f|kL\left(1 - \frac{H_2}{H_1}\right). \tag{4.102}$$

Larsen's result has exponentials and so in the limit $kL \ll 1$, (4.74) can be written as

$$\omega = \frac{|f|kL(H_2 - H_1)|}{kLH_2 + H_1}.$$

Now $kLH_2 \ll H_1$, thus we have

$$\omega = \frac{|f|kL(H_1 - H_2)}{H_1} \tag{4.103}$$

which matches with (4.102).

Here we have shown that the long wave theory reduces to the modified Kelvin wave in the limit $|f|L/\sqrt{gH_1} \ll 1$ and $|f|L/\sqrt{gH_2} \ll 1$. We have also proved that in the limit $|f|L/\sqrt{gH_2} \ll 1$ and $kL \ll 1$ we can derive the topographic Rossby wave with a coastline from the long wave theory.

## 4.8 Edge Waves (EWs) solutions

Closer inspection of Figures 4.3 and 4.6 shows edge waves (EW) which increase in number as $H_2$ decreases and $L$ increases. As discussed in section 3.3 these edge waves have high frequencies, exhibit sinusoidal behaviour on the shelf (see Figure 4.8) and do not need rotation to exist. In order to define a dispersion relation we begin by assuming $|\omega| \gg |f|$. Consequently, by (4.30) and (4.32) we have

$$l_1^2 = k^2 - \frac{\omega^2}{gH_1} \quad \text{and} \quad l_2^2 = k^2 - \frac{\omega^2}{gH_2}. \tag{4.104}$$

Equation (4.104) implies $k^2 > l_1^2$ and $k^2 > l_2^2$ since $\omega \neq 0$. Combining this with our assumption that $|\omega| \gg |f|$, we have

$$\omega l_1 \gg fk \quad \text{and} \quad \omega l_2 \gg fk. \tag{4.105}$$

To isolate the edge wave solutions in the our general dispersion relation, we substitute (4.105) into (4.39). This gives

$$l_1 = -\frac{H_2}{H_1} l_2 \tanh(l_2 L).$$

Since edge waves have a sinusoidal character on the shelf, we expect $l_2$ to be imaginary. So we write $l_2 = i\hat{l}_2$ and therefore

$$l_1 = \frac{H_2}{H_1}\hat{l}_2 \tan(\hat{l}_2 L) \quad \text{since} \quad \tanh(ix) = i\tan x. \tag{4.106}$$

We can derive a relationship between $l_1$ and $\hat{l}_2$ as follows. To eliminate $k^2$ we add our expressions for $l_1^2$ (4.104) and $\hat{l}_2^2 = (\omega^2/gH_2) - k^2$ to obtain

$$l_1^2 + \hat{l}_2^2 = \omega^2\left(\frac{1}{H_2} - \frac{1}{H_1}\right).$$

We can eliminate $\omega$ by substituting $\omega^2 = gH_2(k^2 - l_2^2)$, thus

$$l_1 = \sqrt{k^2\left(1 - \frac{H_2}{H_1}\right) - \frac{H_2}{H_1}\hat{l}_2^2}. \tag{4.107}$$

Equating (4.106) and (4.107) gives

$$\frac{H_2}{H_1}\hat{l}_2 \tan(\hat{l}_2 L) = +\sqrt{k^2\left(1 - \frac{H_2}{H_1}\right) - \frac{H_2}{H_1}\hat{l}_2^2}. \tag{4.108}$$

Although (4.108) gives a relationship between $l_2$, $k$, $H_2$ and $L$, we still seek a relationship between $\omega$ and $l_2$. To arrive at a dispersion relation we look to find an explicit relationship between $l_2$ and $L$.

**Cycles on the shelf**

The wavenumber on the shelf, $l_2$, is proportional to the number of cycles on the shelf. Figure 4.22 solely displays what we term as edge waves (including the Kelvin wave and anti-Kelvin wave) which exist for the following parameters: $L = 300$ km, $H_2 = 200$ m, and $k = 1 \times 10^{-5}$ m$^{-1}$. Here we see a symmetry in the edge waves for positive and negative frequencies.

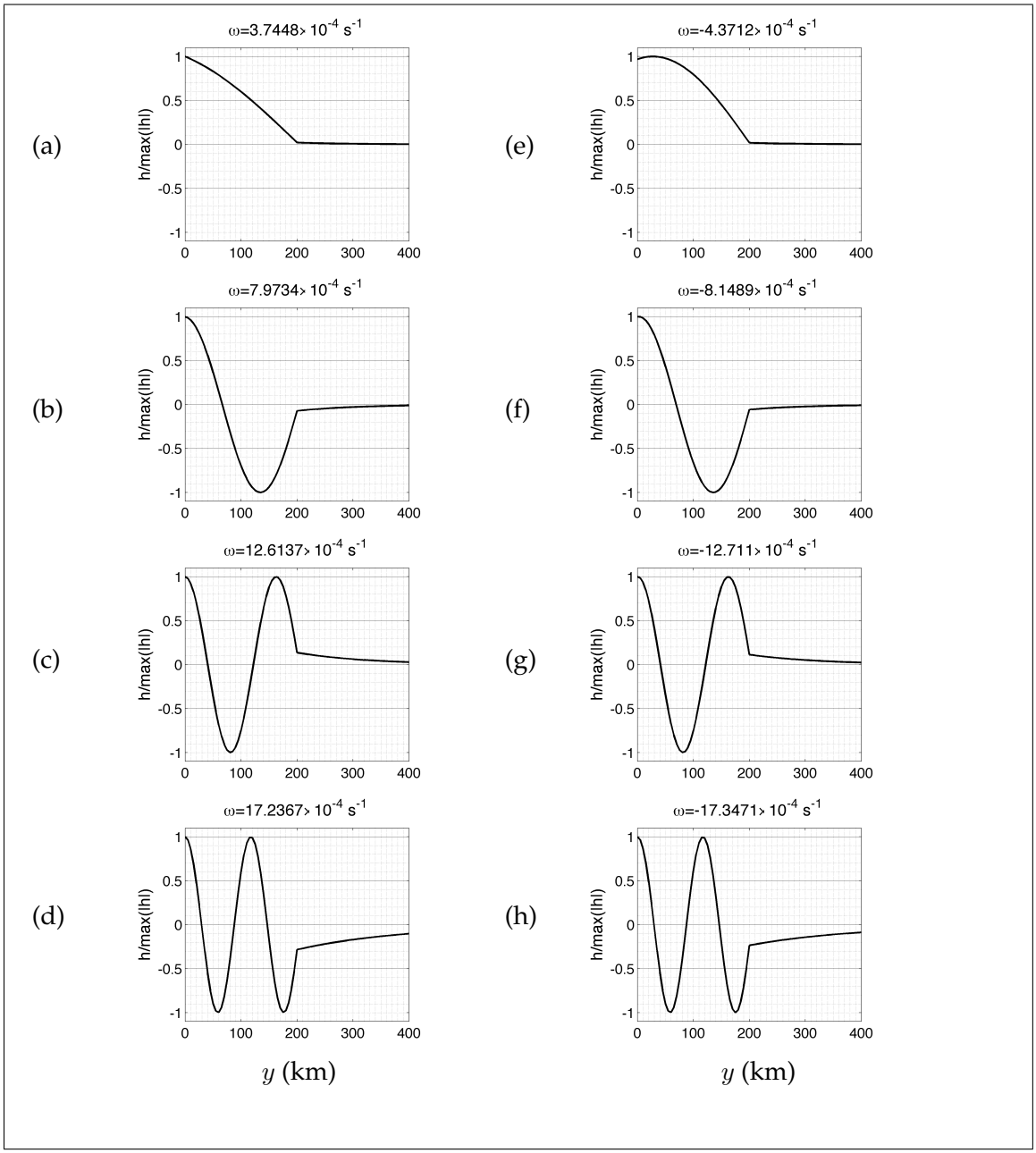


**Figure 4.22:** Normalised perturbed sea surface height, $\hat{h}$, as a function of $y$. Here $k = 1 \times 10^{-5}$ m$^{-1}$, $L = 200$ km, $H_2 = 100$ m. EW on the shelf. The no. of cycles is given by $\frac{1}{4}$ (a), $\frac{3}{4}$ (b), $\frac{5}{4}$ (c), $\frac{7}{4}$ (d). Thus $\lambda = \frac{4L}{2n+1}$, where $n = 0, 1, 2, 3$.

If we focus on Figure 4.22 a-d which in terms of wavelengths is identical to Figure 4.22e-h, then we see that $\lambda$ is given by the length of the shelf divided by the number of cycles

on the shelf ($1/4, 3/4, 5/4, 7/4 \cdots (2n+1)/4$). Thus, we can write $\lambda = 4L/(2n+1)$, where $n = 0, 1, 2, 3, 4$.

We can then write $\lambda = 2\pi/\hat{l}_2 = 4L/(2n+1)$. Equating these expressions gives

$$\hat{l}_2 = \frac{(2n+1)\pi}{2L}. \tag{4.109}$$

Let $\omega^2_{edge} = gH_2(k^2 + \hat{l}_2^2)$, substituting (4.109) into this gives us the following dispersion relation which is written in terms of the alongshore wavenumber, $k$, and is independent of $H_1$

$$\omega_{edge} = \pm\sqrt{gH_2\left(k^2 + \frac{(2n+1)^2\pi^2}{4L^2}\right)} \quad \text{where } n = 0, 1, 2, \cdots \tag{4.110}$$

Note since we have edge waves with positive and negative frequencies the number of edge waves is given by $N = 2(n+1)$.

### 4.8.1 Derivation of edge wave (EW) dispersion relation from shallow water equations

We return to the linear shallow-water equations (2.25a-c). Edge waves live on the shelf and are high frequency waves, thus they are not affected by rotation so $\omega \gg f$, which gives

$$\frac{\partial u}{\partial t} = -g\frac{\partial h}{\partial x}, \tag{4.111a}$$

$$\frac{\partial v}{\partial t} = -g\frac{\partial h}{\partial y}, \tag{4.111b}$$

$$\frac{\partial h}{\partial t} + \underline{\nabla} \cdot (H\underline{u}) = 0. \tag{4.111c}$$

Differentiatiating (4.111c) with respect to $t$ gives

$$\frac{\partial^2 h}{\partial t^2} + \underline{\nabla} \cdot H\left(\frac{\partial u}{\partial t} + \frac{\partial v}{\partial t}\right) = 0. \tag{4.112}$$

Similarly, differentiating (4.111a) with respect to $x$, and (4.111b) with respect to $y$ we have

$$\frac{\partial^2 u}{\partial x \partial t} = -g\frac{\partial^2 h}{\partial x^2}, \qquad \frac{\partial^2 v}{\partial y \partial t} = -g\frac{\partial^2 h}{\partial y^2}. \tag{4.113}$$

We eliminate the mixed partial terms by substituting (4.113) into (4.112) which results in the wave equation

$$\frac{\partial^2 h}{\partial t^2} - gH\underline{\nabla}^2 h = 0. \tag{4.114}$$

Substituting the modal form for $h$ (4.2) into (4.114) we have

$$\omega^2 \hat{h} + gH\left(k^2 - \frac{d^2}{dy^2}\right)\hat{h} = 0. \tag{4.115}$$

If $\hat{h}$ has either a sinusoidal or exponential form then we can write it as $\hat{h} = Ae^{\lambda y} \neq 0$, this gives

$$\lambda^2 - \left(k^2 - \frac{\omega_{edge}^2}{gH}\right) = 0. \tag{4.116}$$

On the shelf the edge waves have a sinusoidal form, therefore $\lambda$ is imaginary i.e. $k^2 - \omega_{edge}^2/gH_2 < 0$. Therefore we can write $\lambda = \pm i\hat{l}_2 = \pm l_2$ to give

$$\hat{h}_2 = A_2 e^{l_2 y} + B_2 e^{-l_2 y}. \tag{4.117}$$

In the open ocean $\hat{h}$ should decay to zero as $y$ tends to infinity, therefore $\lambda$ needs to be real and rewriting $\lambda$ as $l_1$, we have

$$\hat{h}_1 = B_1 e^{-l_1 y} \quad \text{where} \quad \mathrm{Re}(l_1) > 0. \tag{4.118}$$

We now use the matching conditions at $y = L$ given by (2.29), (2.30), and the coastal boundary condition (2.28) ($v = 0$ at $y = 0$) to work towards deriving a dispersion relation.

By (2.29) we equate (4.117) and (4.118), thus

$$B_1 e^{-l_2 L} = A_2 e^{l_2 L} + B_2 e^{-l_2 L}. \tag{4.119}$$

We can write $(u, v) = (\hat{u}(y), \hat{v}(y))e^{-i(kx-\omega t)}$, therefore by (4.111a) and (4.111b) we have $\hat{u} = -gk\hat{h}/\omega$ and $\hat{v} = -(ig/\omega)d\hat{h}/dy$. Substituting these expressions into the second matching condition at $y = L$, (2.30) we have

$$-H_1 l_1 B_1 e^{-l_1 L} = H_2 l_2 (A_2 e^{l_2 L} - B_2 e^{-l_2 L}). \tag{4.120}$$

By the coastal boundary condition, (2.28), $\hat{v} = 0$ at $y = 0$, so our expression for the cross-shore velocity $d\hat{h}/dy = 0$. Therefore (4.117) simplifies to $A_2 = B_2$, and we can write

(4.119) as

$$B_1 e^{-l_1 L} = B_2(e^{l_2 L} + e^{-l_2 L}), \tag{4.121}$$

and (4.120) as

$$-H_1 l_1 B_1 e^{-l_1 L} = H_2 l_2 B_2(e^{l_2 L} - e^{-l_2 L}). \tag{4.122}$$

Dividing (4.122) by (4.121) gives

$$l_1 = -\frac{H_2}{H_1} l_2 \tanh(l_2 L). \tag{4.123}$$

and writing $l_2 = i\hat{l}_2$ we arrive at

$$l_1 = \frac{H_2}{H_1} \hat{l}_2 \tan(\hat{l}_2 L). \tag{4.124}$$

We can now be sure that (4.106) is valid as we have derived it from the shallow water equations. Consequently we have the dispersion relation (4.110)

$$\omega_{edge} = \pm\sqrt{gH_2\left(k^2 + \frac{(2n+1)^2\pi^2}{4L^2}\right)}$$

which we can now try to match with our numerical solutions.

### 4.8.2 Comparison of numerical and analytical edge wave (EW) solutions

Figure 4.23 illustrates how well (4.110) ($n = 6$, pink dashed lines) compares with the numerical solutions to our dispersion relation (4.39).

To explore in more detail the matching between the predicted and numerical solutions Figure 4.24 focuses on $0 < H_2 \leq 1000$ m. The pink dashed lines give a good prediction for the trapped edge waves when $H_2$ is small. We see that when the length of the shelf $L$ is long and $k$ is large (Figure 4.24a) we have better matching for the whole range of $H_2$. However, this is not the case for $k = 1 \times 10^{-6}$ m$^{-1}$ (figure 4.24b) where we only have good agreement between (4.39) and (4.110) for $H_2 < 200$ m.

Figures 4.24 also clearly demonstrates the edge wave-like nature of the modified Kelvin wave and the 'anti-Kelvin' wave. It was certainly not expected that with the introduction of a shelf the modified Kelvin wave would have exhibit sinusoidal behaviour on the shelf.

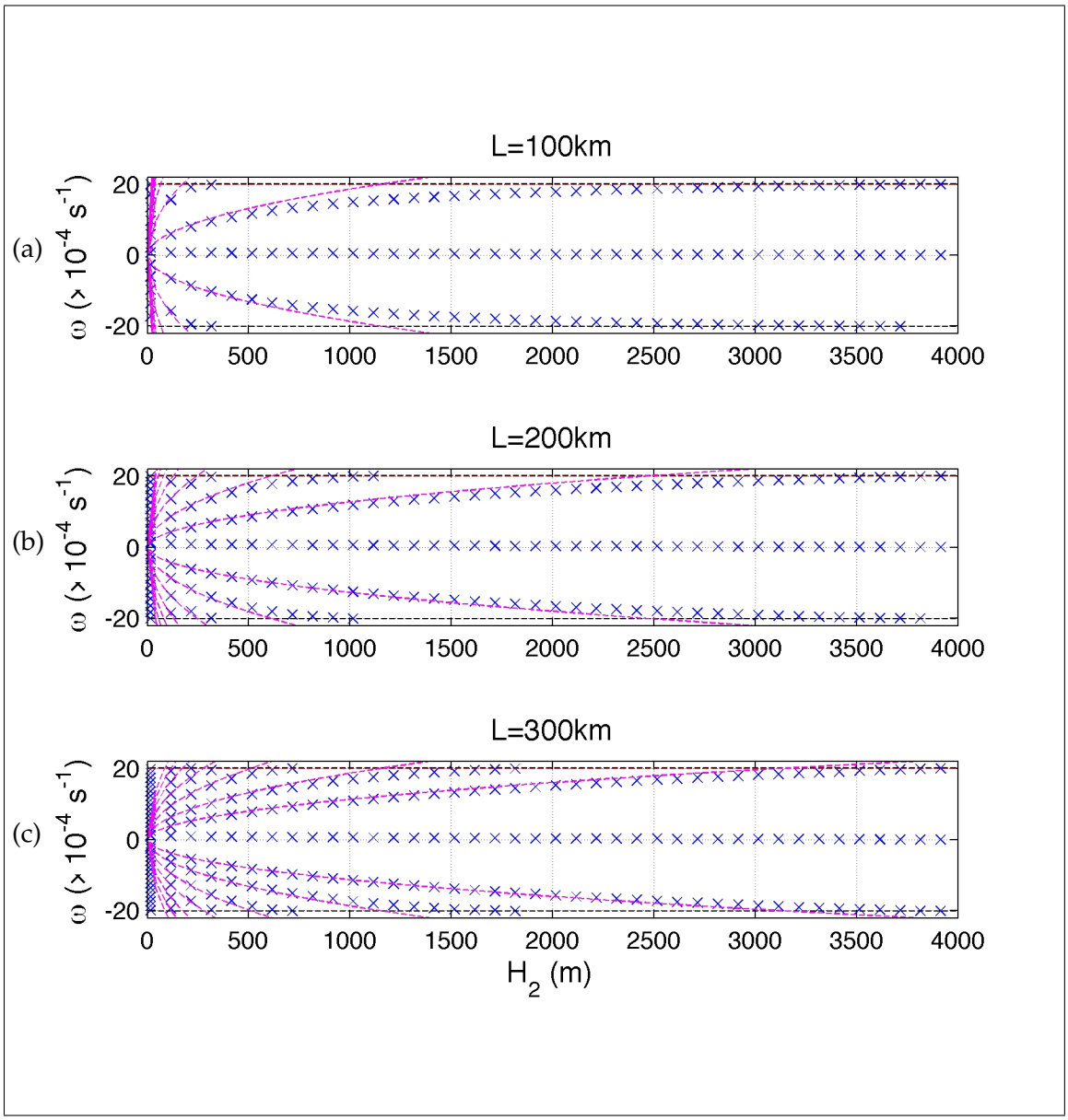


**Figure 4.23:** Frequency $\omega$ as a function of shelf depth, $H_2$, where $k = 1\times10^{-5}\, m^{-1}$, $H_1 = 4$ km and $L$ is 100 km (a), 200 km (b) and 300 km (c). Numerical solutions of dispersion relation (4.39) found using Newton-Raphson iteration method are shown as blue crosses ($\times$). The black dashed lines (- -) are the maximum possible frequencies for trapped waves $\omega_{max} = \pm\sqrt{f^2 + gH_1k^2}$. The pink dashed line (- -) represent the dispersion relation for the predicted EW (4.110). Note that we have less EW for larger $H_2$ and smaller $L$.

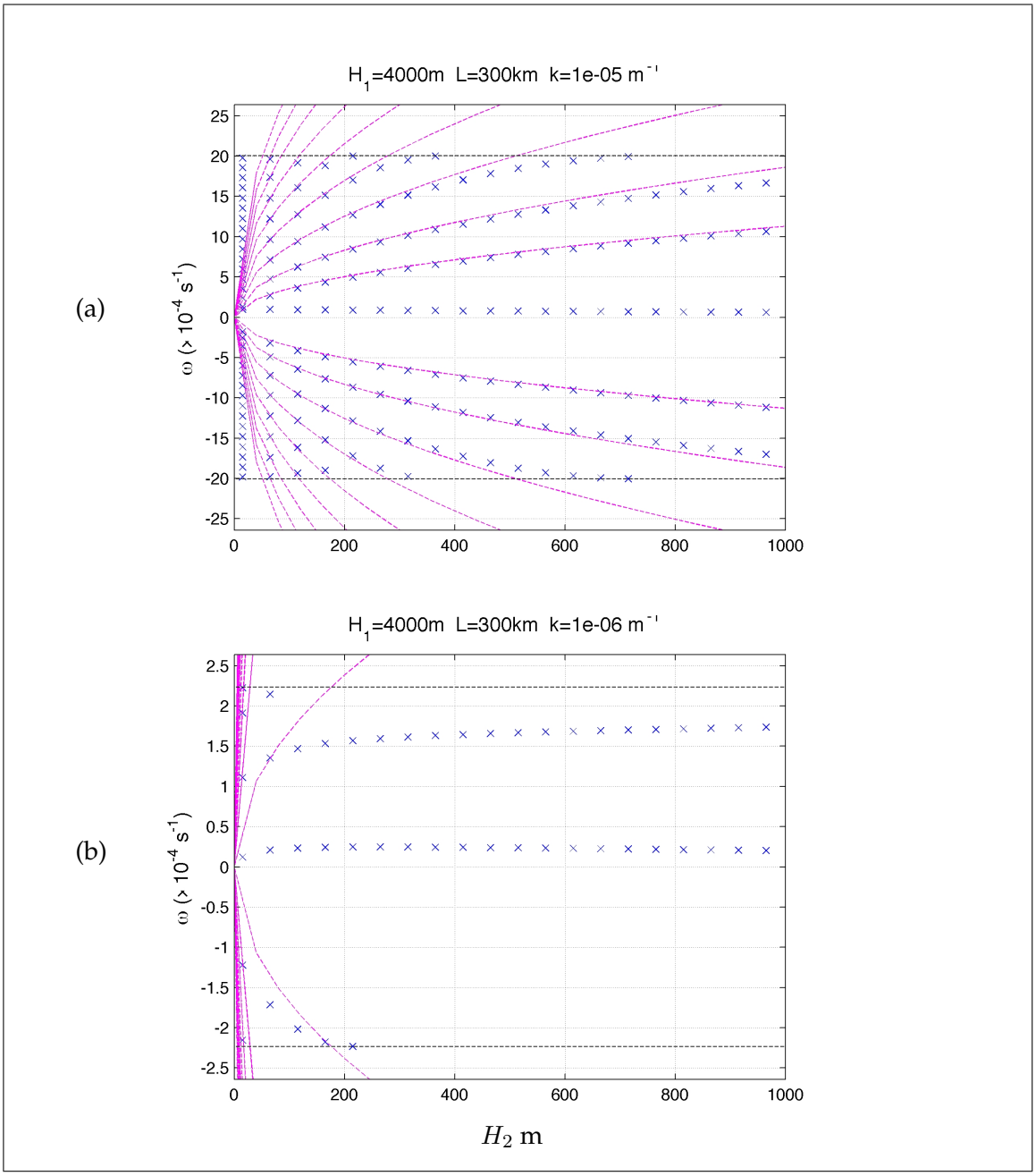


**Figure 4.24:** Frequency $\omega$ as a function of shelf depth, $H_2$, where $L = 300$ km, $H_1 = 4$ km for (a) $k = 1 \times 10^{-5}\ m^{-1}$ and (b) $k = 1 \times 10^{-6}\ m^{-1}$. Numerical solutions of dispersion relation (4.39) shown as blue crosses (×). The black dashed lines (- -) are the maximum possible frequencies for trapped waves $\omega_{max} = \pm\sqrt{f^2 + gH_1k^2}$. The pink dashed lines (- -) shows the dispersion relation for the predicted EW (4.110) where $n = 8$.

### 4.8.3 Predicting the number of edge waves (EWs)

Closer inspection of Figures 4.23 and 4.24 shows that the frequencies of the edge wave are, at some point almost equal to $\pm\omega_{max}$. Therefore, given certain values for the following parameters $k, L, H_1$ and $H_2$, we can predict how many edge waves we should have. Equating $\omega^2_{max} = f^2 + k^2 g H_1$ and $\omega^2_{edge}$ (4.110), and rearranging for $H_2$, we have

$$H_2 = \frac{(2L)^2(f^2 + k^2 g H_1)}{g[(2kL)^2 + \pi^2(2n+1)^2]} \quad \text{where} \quad n = 0, 1, 2, \cdots . \tag{4.125}$$

Therefore, we can calculate the cut-off values of $H_2$ for the predicted edge waves.

Alternatively, we can find a more useful expression which will tell us how many edge waves we should have. We have $\omega^2 = f^2 + k^2 g H_1$, however, since $\omega^2 \gg f^2$, then we have $k^2 g H_1 \gg f^2$. Thus rearranging (4.125) for $n$ we have

$$n = \frac{kL}{\pi}\sqrt{\frac{H_1 - H_2}{H_2}} - \frac{1}{2} \quad \text{where} \quad n = 0, 1, 2, \cdots \tag{4.126}$$

and $N$, the number of edge waves is given by

$$N = 1 + \frac{2kL}{\pi}\sqrt{\frac{H_1 - H_2}{H_2}} \tag{4.127}$$

where $N = 2(n+1)$. If we have a shallow shelf then we can assume $H_2 \ll H_1$, thus

$$N < 1 + \frac{2kL}{\pi}\sqrt{\frac{H_1}{H_2}} \tag{4.128}$$

We can test this by considering Figure 4.25 where $k = 1 \times 10^{-5}$ m$^{-1}$, $L = 300$ km and $H_1 = 4000$ m. By inspection of 4.25 at $H_2 = 500$ m we should have 6 edge waves. Now

$$N < 1 + \frac{6}{\pi}\sqrt{\frac{4000}{500}} = 6.4$$

therefore we have 6 edge waves. If $H_2 = 250$m we have

$$N < 1 + \frac{6}{\pi}\sqrt{\frac{4000}{250}} - \frac{1}{2} = 8.6$$

hence we have 8 edge waves.

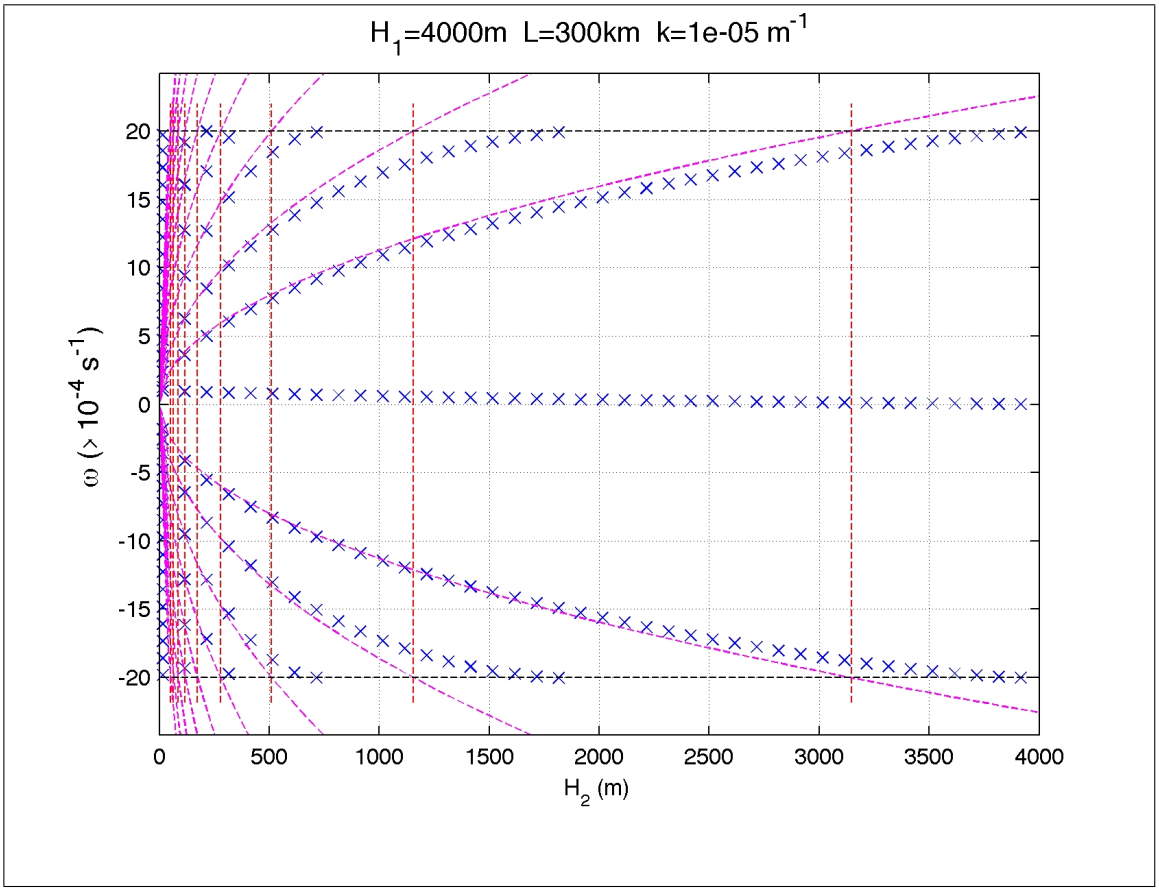


**Figure 4.25:** Frequency $\omega$ as a function of shelf depth, $H_2$, where $k = 1 \times 10^{-5}\ m^{-1}$, $L = 300$km, and $H_1 = 4$km. Numerical solutions of dispersion relation (4.39) found using Newton-Raphson iteration method are shown as blue crosses (×). The pink dashed lines (- -) represent the dispersion relation for the predicted EW (4.110) where $n = 8$. The red dashed vertical lines (- -) (4.125) represent the cut-off values of $H_2$ for the prediction of EWs.

### 4.8.4 Edge wave (EWs) plots

To determine why we have $N$ edge waves we solve (4.108) as a function of $l_2L$. We define functions $f_1$ and $f_2$ as

$$f_1 = \tan(\hat{l}_2 L) \qquad \text{and} \qquad f_2 = \frac{H_1}{H_2}\frac{1}{(\hat{l}_2 L)}\sqrt{(kL)^2\left(1-\frac{H_2}{H_1}\right) - \frac{H_2}{H_1}(\hat{l}_2 L)^2}$$

respectively. If we assume that $H_2 \ll H_1$, $k = O(10^{-5})$, $L = O(10^5)$ then

$$f_1 = \tan(\hat{l}_2 L) \quad \text{and} \quad f_2 = \pm\frac{H_1}{H_2}\frac{(kL)}{(\hat{l}_2 L)}, \tag{4.129}$$

However, we now consider starting with an arbritrary value of $H_2$ and gradually increasing this value. If we do so, then $\frac{H_2}{H_1}$ decreases, $\frac{H_1}{H_2}$ increases and $\left(1-\frac{H_2}{H_1}\right)$ increases. Therefore the steepness of $f_2$ increases and we have fewer intersection points of $f_1$ and $f_2$. We demonstrate this in Figures (4.26 a-d)

### 4.8.5 The effect of the Coriolis force on EWs (?)

In deriving the dispersion relation for the EWs we have assumed $\omega \gg f$, however, it is worthwhile comparing some of these results with those of **?** who included rotation, $f$. He considered solutions with a coast and uniform slope, $h = sy$ where $s \ll 1$. That is $s = \tan\alpha$ where $\alpha$ is the angle between the horizontal and the slope.

Reid finds an infinite set of EWs such that

$$\frac{\omega^2 - f^2}{gs} + \frac{fk}{\omega} = (2n+1)|k| \quad \text{where} \quad n \in \mathbb{N}. \tag{4.130}$$

When $f = 0$, we have

$$\omega^2 = (2n+1)|k|gs \tag{4.131}$$

which is the same as (3.26), the result given by **?**. Thus, when we have no rotation, these solutions essentially behave like Stokes' edge waves (3.22).

We compare this result with (4.110)

$$\omega_{edge} = \pm\sqrt{gH_2\left(k^2 + \frac{(2n+1)^2\pi^2}{4L^2}\right)}.$$

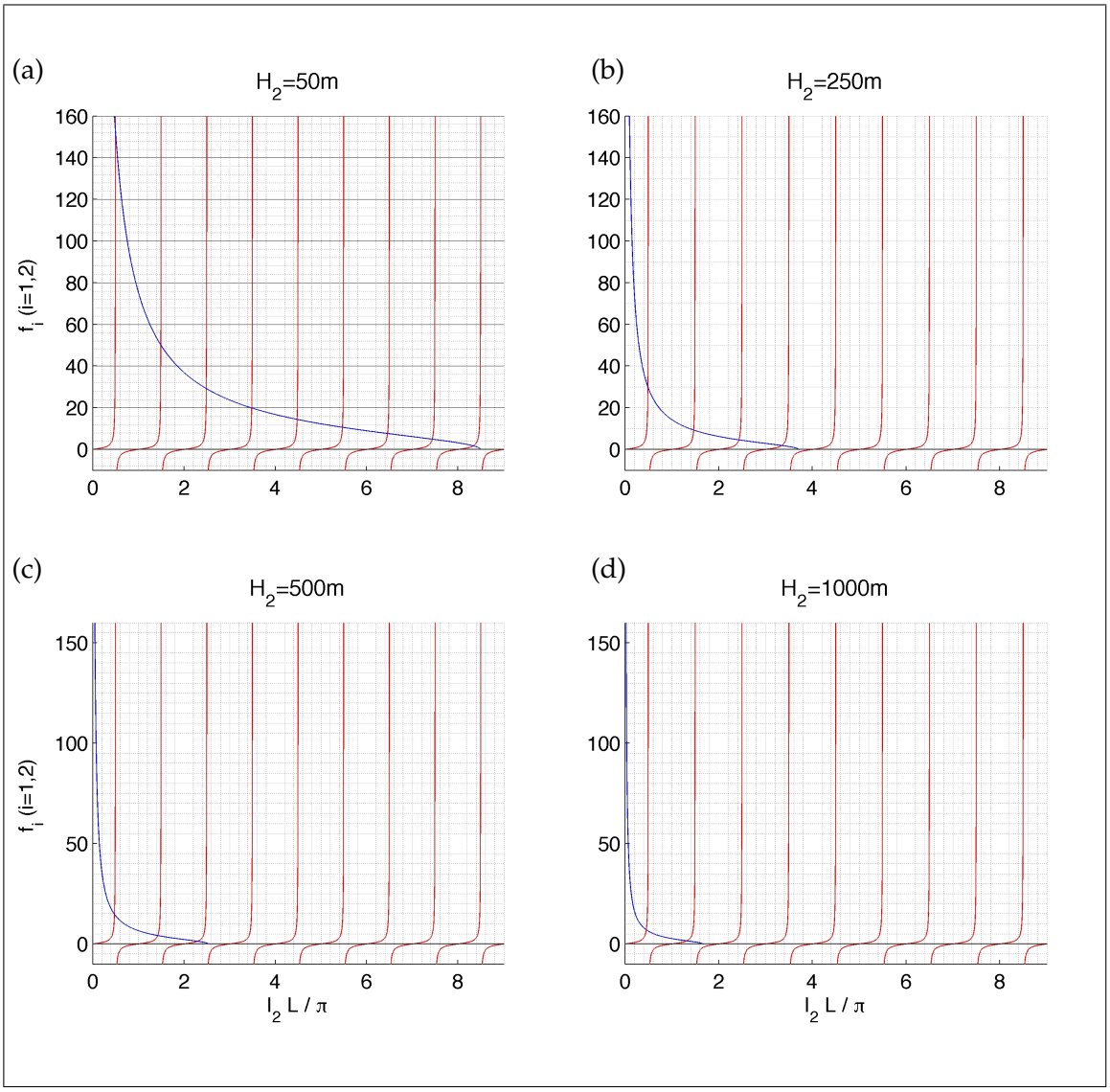


**Figure 4.26:** $(n+1)$ represents the number of intersections of $f_1$ and $f_2$ as shown in these figures, note we plot the value $f_2$ in the first quadrant only and fix $k = 1 \times 10^{-5}$ m$^{-1}$ and $L = 300$ km. The number of edge waves is given by $2(n+1)$. Here $f_1 = \tan(\hat{l}_2 L)$ (—), and $f_2 = \frac{H_1}{H_2}\frac{1}{(\hat{l}_2 L)}\sqrt{(kL)^2\left(1 - \frac{H_2}{H_1}\right) - \frac{H_2}{H_1}(\hat{l}_2 L)^2}$ (—). As $H_2$ increases in value: (a) 50 m, (b) 250m, (c) 500m, and (d) 1000m we see the number of edge waves reduce.

These two results, (4.110) and (4.131), bear many similarities. They both have a minimum frequency but their frequencies are unbounded above. Both results also have $(2n+1)$

edge waves i.e. there are infinitely many modes.

For the fundamental mode $(n = 0)$ **?** has the following solutions

$$\omega_1 = -f/2 - \sqrt{gsk + f^2/4}, \tag{4.132a}$$

$$\omega_2 = -f/2 + \sqrt{gsk + f^2/4}, \tag{4.132b}$$

$$\omega_3 = f. \tag{4.132c}$$

Note, the inertial wave solution $\omega_3$ was discussed in section 4.2.

With no rotation, $\omega = \pm\sqrt{gsk}$. However, with rotation, $\omega_1$ is further reduced, while $\omega_2$ increases. Something resembling this can be seen in Figures 4.3(a,b,c) and 4.7(b) especially for the positive frequency edge wave when we have a long shelf and large step. But this is not the case for the negative edge wave, in contrast to **?**. However, this is not totally unexpected as the topographies are different.

## 4.9 Conclusions

This chapter has been devoted to deriving an understanding of the dynamics of coastally trapped waves with background rotation. The underlying simplification was one of a step topography, i.e., a continental shelf of uniform depth separated from an open ocean of uniform depth by a step (the continental slope). This has allowed us to derive a single dispersion relation that describes all the waves of interest: the Kelvin wave, a topographic Rossby wave, and edge waves. The solutions of this single dispersion relation have also allowed us to explore the structure (velocities and height) of these waves.

The main theme has been to derive simplified explicit analytical approximations for the frequencies of each of these wave modes which had been explored in chapter 3. We were successful in doing this for the modified Kelvin wave, the topographic Rossby wave with a coastline and the edge waves. We also derived an analytical expression for waves in the long wave limit, this compared favourably with the solution to the modified Kelvin wave depending on the depth and length of the shelf.

An interesting feature of the solutions is how the apparently distinct wave modes are connected to each other in parameter space. For example, the modified Kelvin wave turns into an edge wave in the limit of small depth on the shelf. In section 4.7, we have shown an even more surprising result, that the topographic Rossby wave and the modified Kelvin wave exchange identities in certain circumstances. This latter result requires an unrealistically long continental shelf, but it is interesting nonetheless to understand connections between the solutions. In Figure 4.27 we plot the important analytic results with the numerical solutions for the general dispersion relation (4.39). Of course, one

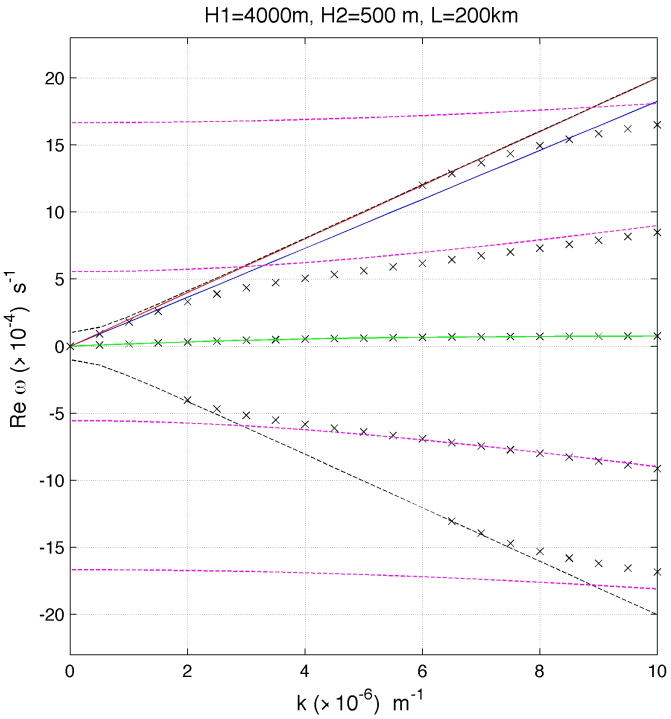


**Figure 4.27:** Plot of $\omega$ against $k$ for $H_1$=4km, $H_2$=0.5km, $L$=200km. Key: classic KW (–) (3.6), MKW (–) (4.56), TRW with coastline (–) (4.74), EWs (- -) (4.110), numerical solutions (x) (4.39), (- -) the maximum frequency for trapped waves $\omega = \omega_{max} = \pm\sqrt{f^2 + gH_1k^2}$.

may wonder as to how relevant all of these solutions are in the real ocean, where the coastal topography does not take the form of a step. In the next chapter, we turn to this question, by replacing the step topography by a continuous topography.

# Chapter 5

# Coastally trapped barotropic waves with rotation and continuous topography

## 5.1 Introduction

In the previous chapter we have explored the behaviour of barotropic Kelvin waves, topographic Rossby waves and edge waves, at the simplest possible representation of the continental margin, with a continental shelf of uniform depth separated from a deep ocean of uniform depth by a step. The main advantage of this simple model is that a dispersion relation may be found analytically, permitting a wide range of solutions to be examined with ease. However, a continuous and smoothly varying depth profile is more representative of the real ocean. One may then ask what properties of waves above a continuous topography are shared by those above a step topography? Do any additional waves arise? Are there significant differences between the frequencies of the waves? The purpose of this chapter is to address these questions, once again in a single-layer (barotropic) model.

There has been much previous study of coastally trapped waves above continuous topography. For example, **?** has shown that provided the ocean depth increases monotonically offshore, then there exists an infinite discrete set of continental shelf waves [1] which have the same general properties, exactly one Kelvin wave which can propagate at sub and super-inertial frequencies, and a discrete set of edge waves all at super-inertial frequencies, which can propagate in either direction. Further, in the limit of small stratification and the rigid-lid approximation, **?** focusses on sub-inertial waves and finds there is only one infinite discrete set of wave modes for any choice of topography and stratification.

For the particular case of an exponential depth profile **?** examined a range of shelf waves. One important result was that they proved these shelf waves travel in the same direction as Kelvin waves. However, their energy can propagate in the opposite direction. The generality of this model also allowed **?** to extend this model to shelf waves that exist on ridges in the deep ocean. In the limiting case of a sharp change in depth, the dispersion relation reduced to that derived by **?** for a topographic Rossby wave.

We anticipate one limitation of the solutions for a step topography. In chapter 4, we found a single topographic Rossby wave above a step. However, **?** has proved the existence of an infinite discrete set of such waves above continuous topography. In this chapter, where we consider a spectrum of depth gradients, it is expected that we find more trapped topographic Rossby waves on the slope. With the inclusion of a coastline we expect these waves to differ in their behaviour from those found in chapter 3.

It is worth noting that these kinds of topographically trapped waves have been observed off the coast of Newfoundland. Figure 5.1 shows the results of a data assimilative tidal model (**?**) showing the sea surface elevation for a diurnal tide. From this figure we note two important features. Firstly, the very close contour lines demonstrate a sharp change in depth from 300m to 3km. Secondly, there is a wave-like motion above the continental slope, with a wavelength between 100-200km.

[1] It is common practice for topographic Rossby waves modified by coast and shelf geometry to be referred to as continental shelf waves.

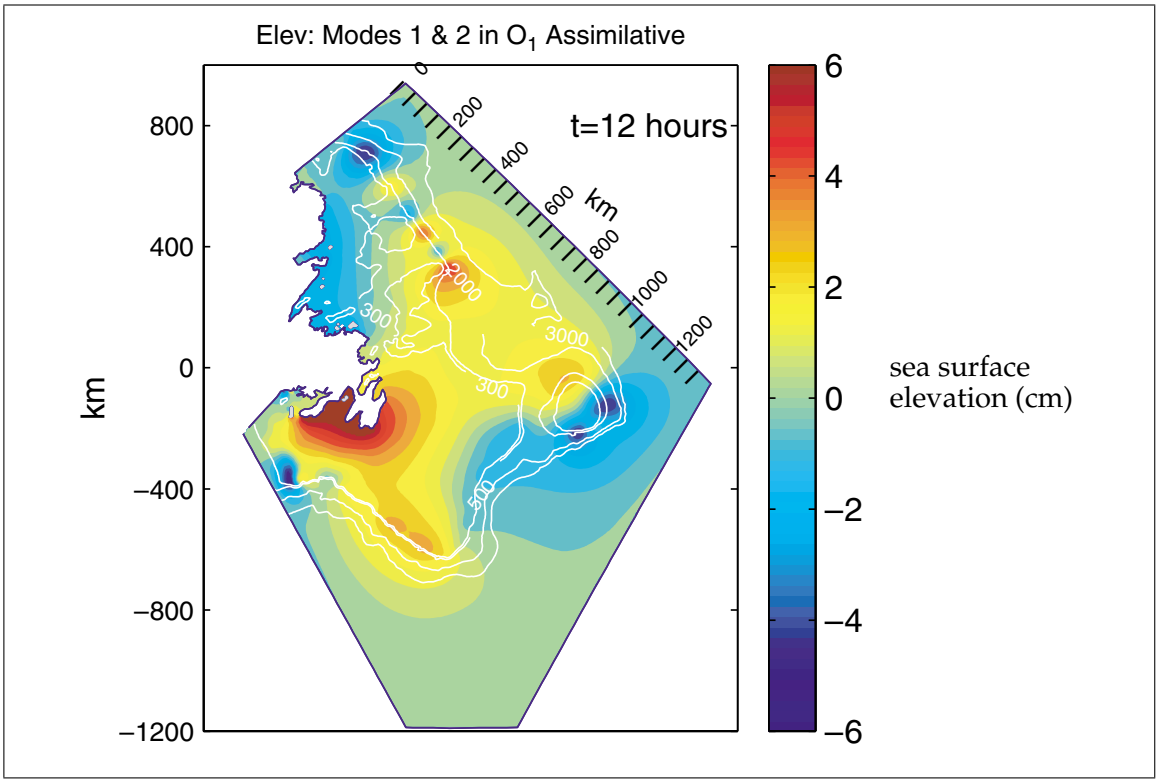


**Figure 5.1:** Sea surface signature of topographic Rossby waves in a data assimilative tidal model over the Newfoundland Shelf-break for the $O_1$ constituent (diurnal period). Here we see a train of eddy-like anomalies located northward of the sudden broadening of the slope region. The scale of the eddies are 50-100km in radius. Their location suggests the possibility that their generation is associated with the abrupt change in topography. (**?**).

As in previous chapters, we ignore stratification and reduce the linear single-layer shallow water equations to an eigenvalue problem for the cross-shore structure of the perturbed sea surface $h$ and the wave frequency $\omega$. Variations in ocean depth follow a hyperbolic tangent profile, giving a smooth continental margin. Solutions are found numerically, sometimes initialised by frequencies from the step model with a coastline.

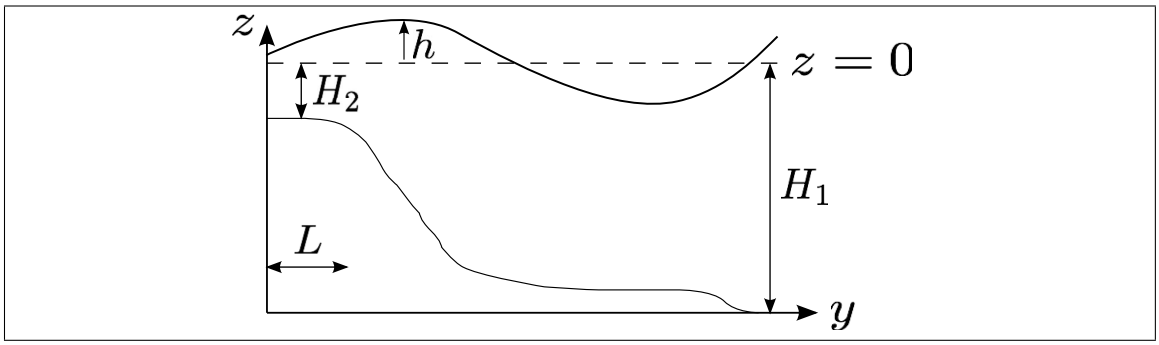


**Figure 5.2:** Schematic of a continental shelf/slope region. Here $h$ represents the perturbed sea surface height, $H_1$ the depth of the deep ocean, $H_2$ the depth of the shelf, and $L$ the length of the shelf.

## 5.2 A simple model of the continental shelf/slope region

As shown in Figure 5.2, we retain $H_1$ as the depth of the deep ocean, and $H_2$ as the depth of the shelf. For detailed calculations we take a smooth, continuous profile given by

$$H(y) = H_0 + \Delta H \tanh\left(\frac{y-L}{\lambda L}\right) \tag{5.1}$$

where $H_0 = (H_1 + H_2)/2$, $\Delta H = (H_1 - H_2)/2$.

Here, if we have no shelf, i.e., $H_2 \to H_1$ then $H(y) \to H_1$. Note also if $y \to \infty$ then $H(y) \to H_1$. The parameter $\lambda$ allows us to change the steepness of the continental slope. The slope-width is approximately $\lambda L$. This is shown in Figure 5.3 for two different values of $\lambda$ and the specific parameters $H_1$=4km and $H_2$=500m, so $H_0$=2250m, $\Delta H$=1750m. The length of the continental shelf $L$ is approximately 200km.

## 5.3 Governing equations for the adjustment of the fluid

To determine $h$, the perturbed sea surface height, along with $u$ and $v$ the cross-shore and alongshore velocities, we initially aim to derive a general equation in $h$ which although complicated we can solve numerically. We begin with the modal form of the linearised

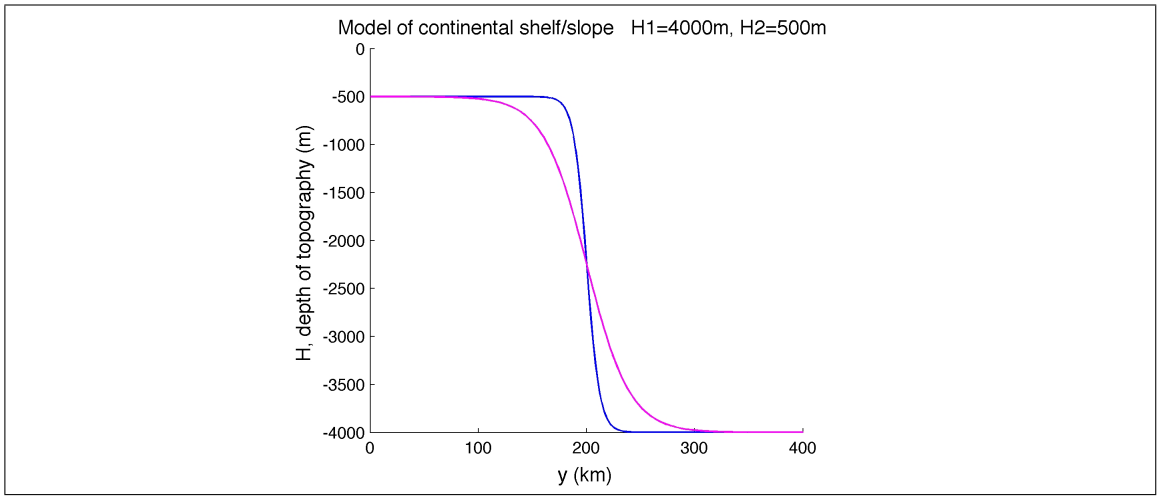


**Figure 5.3:** Hyperbolic tangent profile. Continuous topography modelled by $H(y) = H_0 + \Delta H \tanh(y - L/\lambda L)$ (5.1) where $H_0 = (H_1 + H_2)/2$ and $\Delta H = (H_1 - H_2)/2$. Here $H_1$=4km and $H_2$=500m, so $H_0$=2250m, $\Delta H$=1750m. The length of the continental shelf $L$ is approximately 200km. The topography in magenta has $\lambda = 0.2$ here the slope-width is $2\lambda L \approx 80$ km. The steeper topography in blue has $\lambda = 0.06$ here the slope-width is $2\lambda L \approx$ 24 km.

shallow water equations (3.2a-c):

$$-i\omega\hat{u} - f\hat{v} = -igk\hat{h}, \tag{5.2a}$$

$$-i\omega\hat{v} + f\hat{u} = -g\frac{d\hat{h}}{dy}, \tag{5.2b}$$

$$-i\omega\hat{h} + ikH\hat{u} + \frac{d(H\hat{v})}{dy} = 0, \tag{5.2c}$$

where $H = H(y)$. To eliminate $\hat{v}$ multiply (5.2b) by $f$ and subtract from this (5.2a) multiplied by $i\omega$ to obtain

$$(f^2 - \omega^2)\hat{u} = -fg\frac{d\hat{h}}{dy} - \omega gk\hat{h}. \tag{5.3}$$

Similarly, to eliminate $\hat{u}$, subtract (5.2a) multiplied by $f$ from (5.2b) multiplied by $-i\omega$, thus

$$(f^2 - \omega^2)\hat{v} = i\omega g\frac{d\hat{h}}{dy} + ifkg\hat{h}. \tag{5.4}$$

Now substitute (5.3) and (5.4) into (5.2c) so

$$-i\omega\hat{h}+\frac{ikH}{f^2-\omega^2}\left(-fg\frac{d\hat{h}}{dy}-\omega gk\hat{h}\right)+\frac{1}{f^2-\omega^2}\frac{dH}{dy}\left(i\omega g\frac{dH}{dy}+ifgk\hat{h}\right)$$
$$+\frac{H}{f^2-\omega^2}\left(i\omega g\frac{d^2\hat{h}}{dy^2}+ifg\hat{h}\frac{d\hat{h}}{dy}\right)=0.$$

Multiplying through by $(f^2-\omega^2)/i\omega$ and rearranging gives

$$\frac{d^2\hat{h}}{dy^2}+\left(\frac{1}{H}\frac{dH}{dy}\right)\frac{d\hat{h}}{dy}+\left(\frac{\omega^2-f^2}{gH}-k^2+\frac{fk}{\omega}\frac{1}{H}\frac{dH}{dy}\right)\hat{h}=0. \tag{5.5}$$

We now are able to determine an expression for $\frac{1}{H}\frac{dH}{dy}$, that is

$$\frac{1}{H}\frac{dH}{dy}=\frac{\left(1-\frac{H_2}{H_1}\right)\text{sech}^2\left(\frac{y-L}{\alpha}\right)}{\alpha\left[\left(1+\frac{H_2}{H_1}\right)+\left(1-\frac{H_2}{H_1}\right)\tanh\left(\frac{y-L}{\alpha}\right)\right]} \tag{5.6}$$

where $\alpha=\lambda L_s$ is the slope width. Note that at $y=0$ we have $H=H_2\neq 0$, that is, there exists a wall at the coast. This guarantees that the expression (5.5) is well-behaved at $y=0$.

### 5.3.1 Boundary Conditions

At the coast, we have the boundary condition $\hat{v}=0$ which was discussed in section 2.1.2. Thus (5.4) reduces to

$$\frac{d\hat{h}}{dy}+\frac{fk}{\omega}\hat{h}=0 \quad \text{at} \quad y=0. \tag{5.7}$$

The simple model of our topography (5.1) has $H\to$ constant as $y\to\infty$, so that $\frac{1}{H}\frac{dH}{dy}\to 0$ in the deep ocean. Hence (5.5) becomes

$$\frac{d^2\hat{h}}{dy^2}-l^2\hat{h}=0 \quad \text{where} \quad l=\sqrt{k^2-\frac{\omega^2-f^2}{gH}} \quad \text{and} \quad \text{Re}(l)>0.$$

This has solutions

$$\hat{h}=Ae^{ly}+Be^{-ly},$$

where $A$ and $B$ are constants. Since we seek coastally trapped waves we require $\hat{h} \to 0$ as $y \to \infty$, therefore $A = 0$. Hence, as $y \to \infty$ we have $\hat{h} \to Be^{-ly}$ thus we have

$$\frac{d\hat{h}}{dy} + l\hat{h} = 0. \tag{5.8}$$

This is the boundary condition for large $y$.

## 5.4 Numerical Method

To solve this system (5.5) subject to (5.7) and (5.8) we have used the MATLAB routine bvp4c which is a finite difference code which uses a collocation formula to solve two-point boundary value problems for ordinary differential equations.

To use bvp4c the user needs to supply a definition of the ordinary differential equation, which in our case is (5.5). The boundary condition must also be defined for our second order eigenvalue problem. Here we have three boundary conditions. The first one is (5.7) applied at $y = 0$. The second boundary condition is (5.8), we supply this at $y = y_f$. $y_f$ is a measure of a large distance normal to the coast which is made a function of the wave number in the open ocean. We aim to approximate the $y \to \infty$ behaviour; we found that a convenient definition is $yf = 5L + 10/l_1$, where $l_1 = \sqrt{k^2 - (\omega^2 - f^2)/gH_1}$ and $\mathrm{Re}(l_1) > 0$ (4.30). Sometimes this value of $y_f$ is not sufficiently large enough, if this is so then the new $y_f$ used is stated. Hence, it was possible to eliminate by eye solutions found by bvp4c figures where the exponential decay of $h$ did not occur. The third boundary condition is a normalisation condition which we take to be $h = 1$ at $y = 0$.

We must supply an initial guess for the eigenfunction $h(y)$. Here we used the analytical work in chapter 4 to derive this initial guess, using (4.29) and (4.31). We also need an initial guess for the eigenvalue, and again we used the analytical model frequencies by solving (4.39) using the Newton-Raphson method. These provided the initial estimate.

Finally, we need to choose the tolerance which determines how accurate the solution is. Since computer time was not an issue they were set to very low values of $10^{-12}$.

This tolerance is a measure of the error relative to the size of each solution component. Roughly, it controls the number of correct digits in all solution components, except those smaller than thresholds absolute tolerance which is set at $1 \times 10^{-6}$.

It was also possible to track different modes as the parameters varied. For example, to track the Kelvin wave we know that the modified Kelvin wave frequency (4.56) is a good approximation for the initial guess when there is a shelf. By starting from a large $H_2$ and gradually decreasing this value we can follow how the Kelvin wave evolves. Similarly to track the topographic Rossby wave we start by using as our initial guess a small value for $H_2$ and gradually increasing this value. For the initial frequency guess we use the analytical result for the topographic Rossby wave (4.74). A special MATLAB routine was constructed to facilitate this mode-tracking.

Some solutions were also found using the shooting algorithm described in section 3.5.5.

## 5.5 Overview of numerical solutions

In this section we examine wave-like solutions that are direct extensions of those found above step topography. Throughout we set $k = 1 \times 10^{-5}$ m$^{-1}$, $H_1$=4km, $H_2$=0.5km, $L$=200km and $f = 10^{-4}$s$^{-1}$. For the topographic gradients, we take either $\lambda$=0.06, giving a steep slope of width $\approx$ 24km, or $\lambda$=0.3, giving a shallow slope of width $\approx$ 120km.

In Figures 5.4 and 5.5 we compare solutions for step topography (shown in blue) with those for the continuous topography (5.5) (shown in green). Note that we impose the normalisation condition $h(0) = 1$ for ease of comparison. At these parameters, there are five solutions for the step topography. We have taken the frequencies ($\omega_{step}$) of these five waves from section 4.4.2 (Figure 4.6b) and used these as our initial guesses to determine solutions to (5.5) ($\omega_{cts}$). So we expect five solutions for the continuous model.

Figure 5.4 shows the three edge waves (EWs) in each case ($\lambda = 0.06$ and $\lambda = 0.3$), which have a sinusoidal profile on the shelf. Included is the edge wave referred to as the anti-

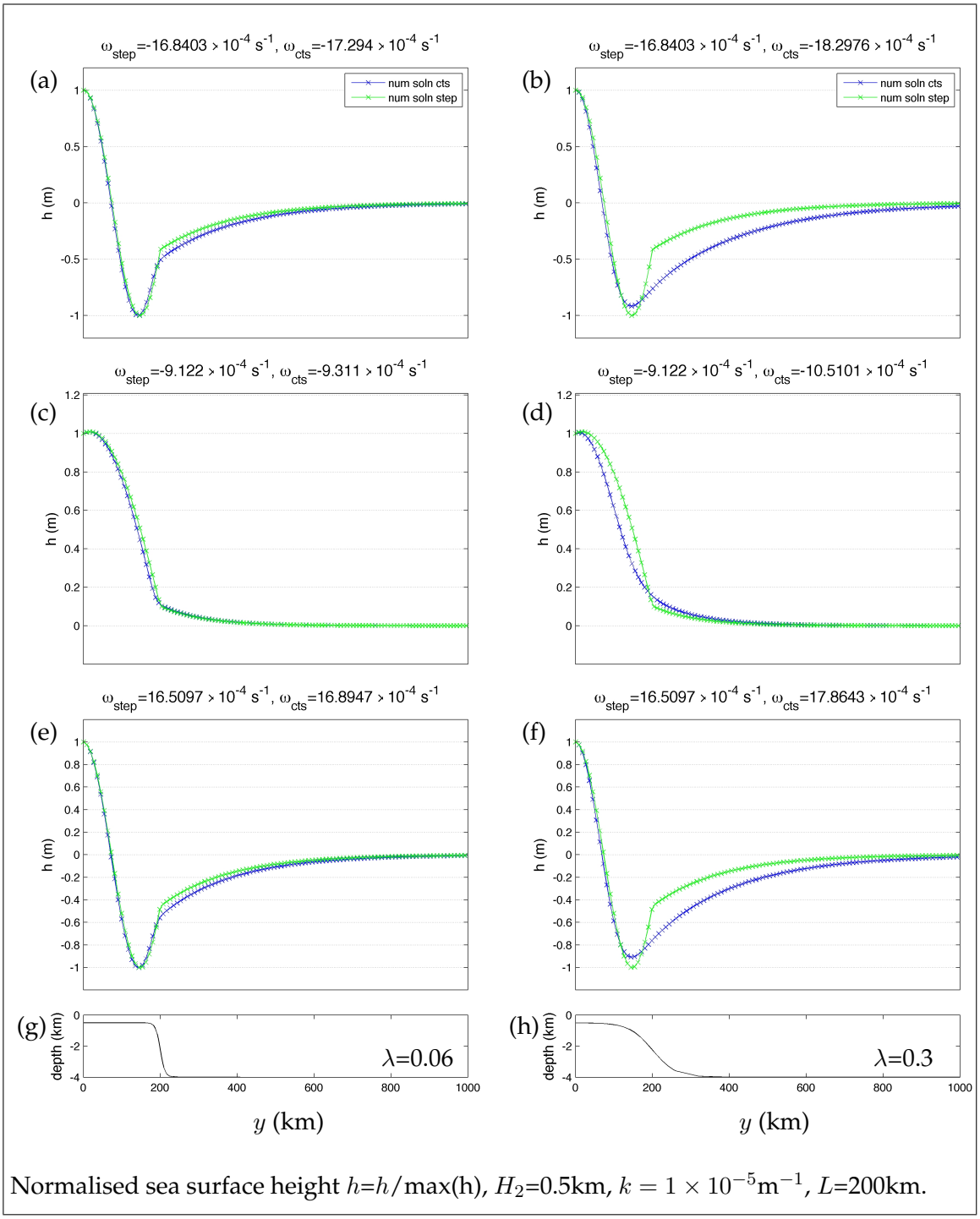


**Figure 5.4:** (g) and (h) are the profiles of steep and shallow continental slopes whose shelf-widths are 24km and 120km respectively. (a), (c) and (e) show the EWs for a steep slope (g). (b), (d) and (f) show the EWs for a shallow slope (f). Numerical solutions for the continuous profile (5.5) are in green, and solutions to the step profile (4.39) are in blue.

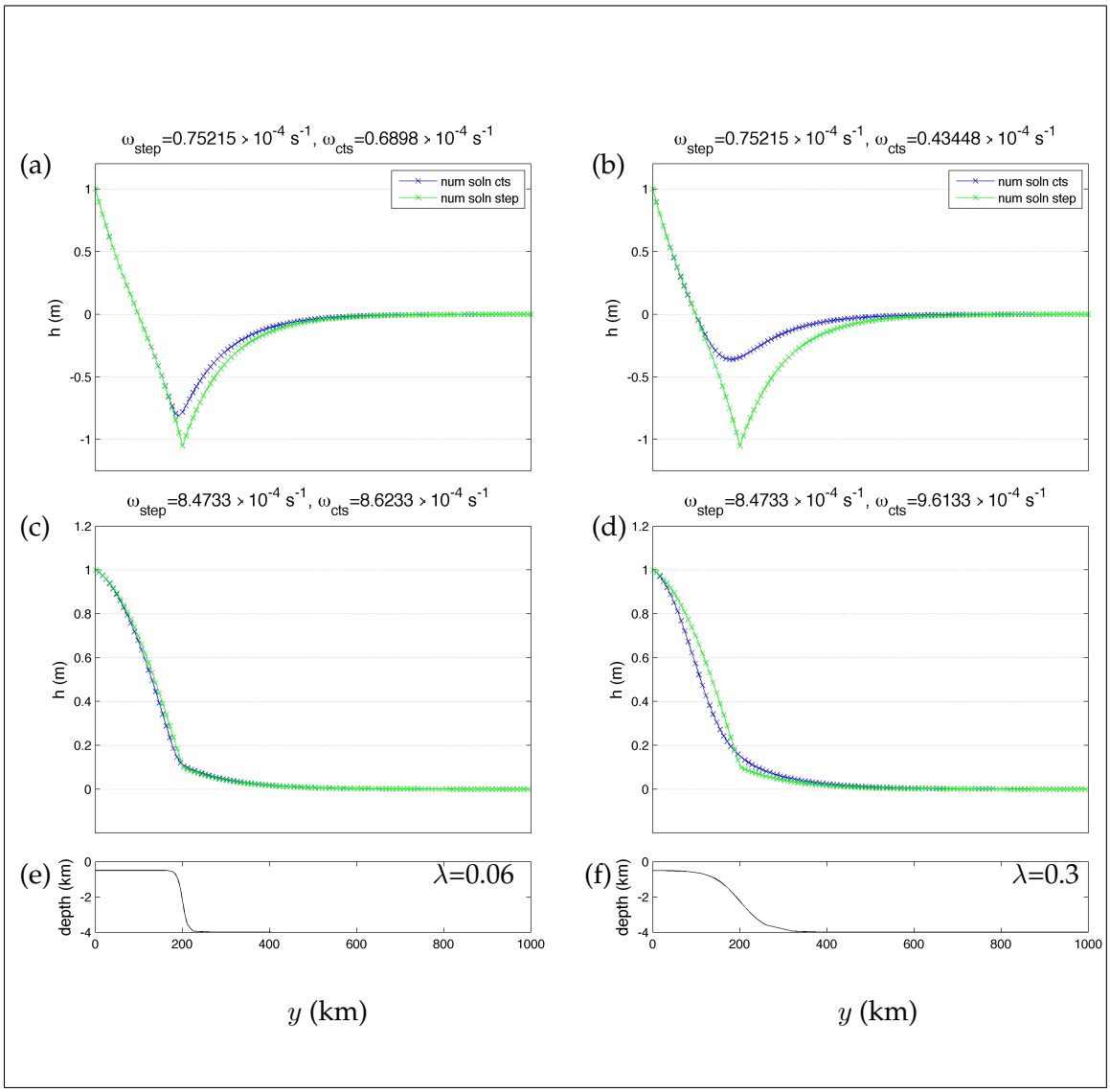


**Figure 5.5:** $H_2$=500m, $k = 1 \times 10^{-5}$ m$^{-1}$, $L$=200km. (e) and (f) show the profiles of the steep and shallow continental slopes where the shelf-widths are 24km and 120km respectively. We have TRW (a) and MKW (c) for a steep continental slope (e), and TRW (b) and MKW (d) for a shallow continental slope (f). The numerical solutions to (5.5) are shown in green, and the solutions to the step profile for the dispersion relation (4.39) are shown in blue. $\omega_{step}$ taken from the step profile are used as the initial guesses in the MATLAB routine bvp4c to generate $\omega_{cts}$.

Kelvin wave (AKW) (Figure 5.4c,d). Figure 5.5 shows the corresponding profiles for the modified Kelvin wave (MKW) and the topographic Rossby wave (TRW). Note that the modified Kelvin wave and anti-Kelvin wave have similar profiles.

With the exception of Figure 5.5b, there is excellent agreement between the profiles from the step model and those from the continuous model. A disparity is most likely for TRWs because they are fundamentally governed by PV dynamics above the slope, in contrast to the other waves which rely upon a shelf or coastline. So the disparity is most prominent in Figure 5.5b, which shows a TRW above a relatively shallow slope.

The frequencies of the waves in the step model and that obtained in the continuous model are clearly see in Figures 5.4a,c,e. Here $\omega_{step}$ and $\omega_{cts}$ are in excellent agreement for the step model and continuous model ($\lambda = 0.06$), with an error of less than 3%. Similarly, when we have shallow slope ($\lambda = 0.3$) as in Figures 5.4b,d,f, the frequencies of the EWs for the step model and continuous model are in very good agreement although not as close when we have a steep slope, the error here being no more than 9%. The frequencies of the TRWs shown in Figure 5.5b show a marked disagreement. This was expected as the topographies which each TRW feels would influence their behaviour. The frequency of the TRW on the slope is smaller than its step model counterpart by $\approx 40\%$, this is quite a difference. The frequencies of the MKWs, shown in Figure 5.5d are remarkably close too, with the difference in frequencies being relatively small.

The good agreement between the step and continuous models extends to other parameter values. In Figure 5.6 we show numerically determined solutions for the MKW in the continuous model along with the analytical expression (4.56) for the frequency of the MKW for the step model. The error is no more than 2.5% for these parameter values, even for small values of $H_2$.

These results strongly suggest that the step profile is a useful limit for the continuous case and that the analytical solutions of chapter 4 are able to describe certain behaviour of waves above continuous topography. The exception are the step solutions for topographic Rossby waves. These will now be examined in more detail.

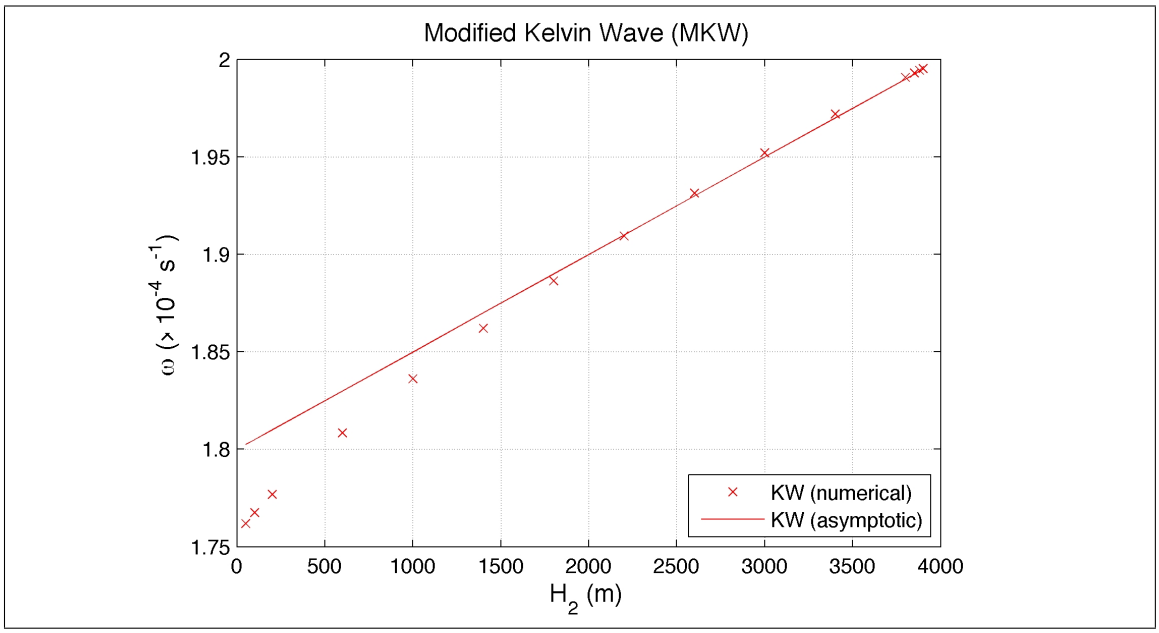


**Figure 5.6:** Comparison of the numerical solutions (5.5) for a continuous slope with coastline and the modified Kelvin wave for the step model with a coastline (4.56). We fix $k = 1 \times 10^{-6}$ s$^{-1}$, $L$=200km, $H_1$=4000m, slope-width=100km ($\lambda = 0.25$).

## 5.6 Topographic Rossby wave-like solutions

As mentioned in the introduction, we expect there to be infinitely many TRWs above a smooth continental slope. In the previous section we found the first such TRW, which is an extension of that found above step topography. We now investigate the remaining lower frequency TRWs.

Unfortunately it is hard to find these low frequency TRWs. However, after much further exploration with initial guesses of very small frequencies, O$(10^{-7})$s$^{-1}$, a few TRW solutions were found. These are shown in Figure 5.7 for a large shelf with either a steep slope or a shallow slope. Figure 5.8 shows solutions for a small step with a shallow slope. We fix $k = 1 \times 10^{-5}$m$^{-1}$ for both these figures. The initial guessed frequencies $\omega_{in}$ and the resulting frequencies $\omega_{out}$ are shown above each panel.

These solutions have a clear signature of TRWs, being localised above the slope and with

an oscillatory structure (as for the TRWs investigated in detail in chapter 3). We characterise each solution by the number of zeros $n$ in the solution for $h$. In Figure 5.7, we thus see TRWs with $n$=0,3,15 and 11 respectively. It is not intentional that $n$ is always odd, this is a random result dependent upon the initial guess and the topography. Note that the numerical domain width differs between the panels.

In Figure 5.8a-d, we see TRWs with $n$=0,1,3,4 for deep shelves (where $L \approx$ 400km) and shallow slopes ($L \approx$ 240km). These solutions have been found by using the same initial guess $\omega_{in}$ of O($10^{-7}\mathrm{s}^{-1}$), however, the shelf depths are different, i.e., (a) $H_2$=3500m, (b) $H_2$=3600m, (c) $H_2$=3700m and (d) $H_2$=3800m. Here the value of $yf$ is $8L$+1/$l_1$.

These waves all have sub-inertial frequencies ($\omega < f$) and display sinusoidal behaviour over the slope. Figure 5.7d additionally displays sinusoidal behaviour on-shelf. We have previously seen this on-shelf behaviour with edge waves (section 4.4.2 Figure 4.8) which have super-inertial frequencies ($\omega > f$). Note the frequency of this wave also has a very small imaginary part of O($10^{-12}\mathrm{s}^{-1}$), which is thought to be a numerical artefact.

## 5.7 Comparison of analytical and numerical solutions for TRWs

These TRW solutions are very reminiscent of those investigated in chapter 3. Although those solutions were obtained in an unbounded domain, the slope acted as a wave-guide and solutions were localised above the slope. It is plausible that they will also be relevant for solutions with a coastline. We now test this.

We use the first order analytical solution (3.74) for the frequency:

$$\omega = \frac{4fkL_s\Delta H}{H_0\left[\left(2n+1+|2kL_s|\right)^2 - 1\right]} \quad (n \in \mathbb{N}_0), \tag{5.9}$$

where $L_s$ is half the slope width and is equivalent to $\lambda L$ in our continuous topography (5.1). This simple expression clearly shows the existence of an infinite number of TRWs in a continuous model.

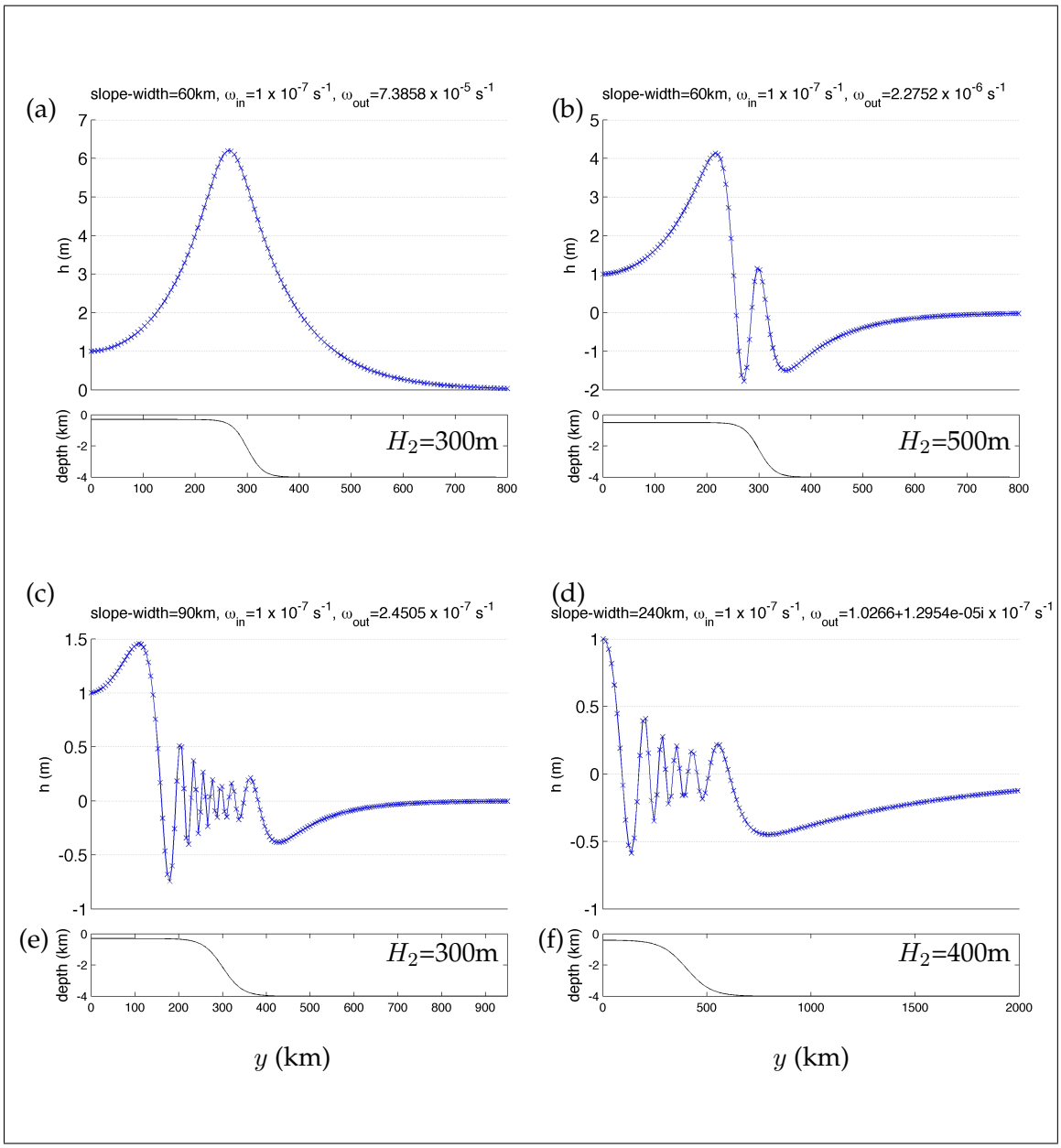


**Figure 5.7:** Topographic Rossby waves: Normalised sea surface amplitude profiles, $h$=$\hat{h}/\max(\hat{h})$. $k = 1 \times 10^{-5}$ m$^{-1}$, $L$=300km and $\lambda = 0.1$ for (a)-(c) and $L$=400km and $\lambda = 0.3$ for (d).

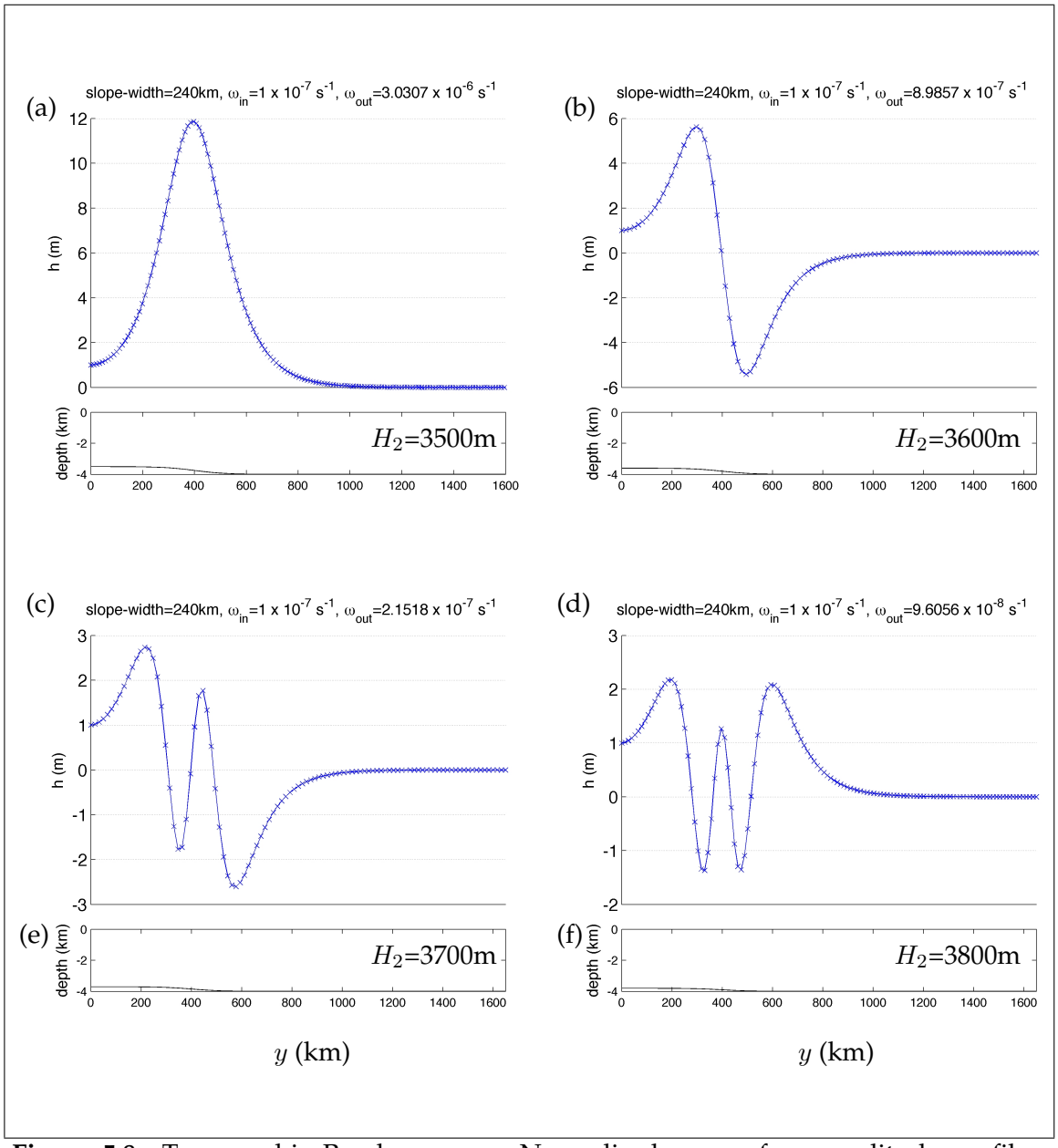


**Figure 5.8:** Topographic Rossby waves: Normalised sea surface amplitude profiles, $h$=$\hat{h}/\max(\hat{h})$. $k = 1 \times 10^{-5}$ m$^{-1}$, $L$=400km and $\lambda = 0.3$ for (a)-(d).

In Figures 5.9 and 5.10, we compare the cross-shore velocities of the analytical and numerical solutions. Note that these numerical solutions (shown in blue) were obtained using the shooting scheme employed in chapter 3 rather than bvp4c, and initiated by the frequency given by (5.9). The analytical solutions, shown in red, were found by combining (3.32), (3.86) and (3.89). In the case with $n = 0$, an additional first order correction (3.75) is shown in green.

Figure 5.9 is for a small shelf of depth $H_2$=3km and slope-width 200km. The cross-shore velocities are O($10^{-4}$) m/s, with very strong agreement between the analytical and numerical solutions over the continuous slope. However, the velocities of the TRWs for the analytical and numerical solutions differ towards the coastline where the boundary condition, $v = 0$ at $y = 0$ is embedded in the numerical solution. The analytical solution is for the unbounded topography and wants to exhibit exponential decay beyond $y = 0$. We see a similar behaviour pattern near the coastline when we have a large shelf of depth $H_2$=0.5km and slope-width 60km in Figures 5.10a-d. In these figures we also see the shift in amplitude as in chapter 3 section 3.5.5 which is a result of neglecting two terms in the numerical solution when making the small topography assumption.

Finally, we compare the predicted frequencies with that obtained from a numerical model which uses a shooting method initialised by (3.74). Figure 5.11 shows the frequencies for $n$=0,1,2. Here we compare the solutions to the first order analytical solution without a coastline (3.74) ($\tanh$ formula), the simple step model with a coastline (4.74) (coastal step formula) and numerical solutions. We see remarkably good agreement between the first order analytical solution without a coastline (3.74) ($\tanh$ formula) and the numerical solutions for all $n$ and shelf depths greater than 300m.

## 5.8 Quantifying the role of shelf width and slope width

Figure 5.11 does not show the influence of the width of the shelf on the solutions because $L$ is fixed. The issue of shelf-width has been discussed by **?** in some detail. With a

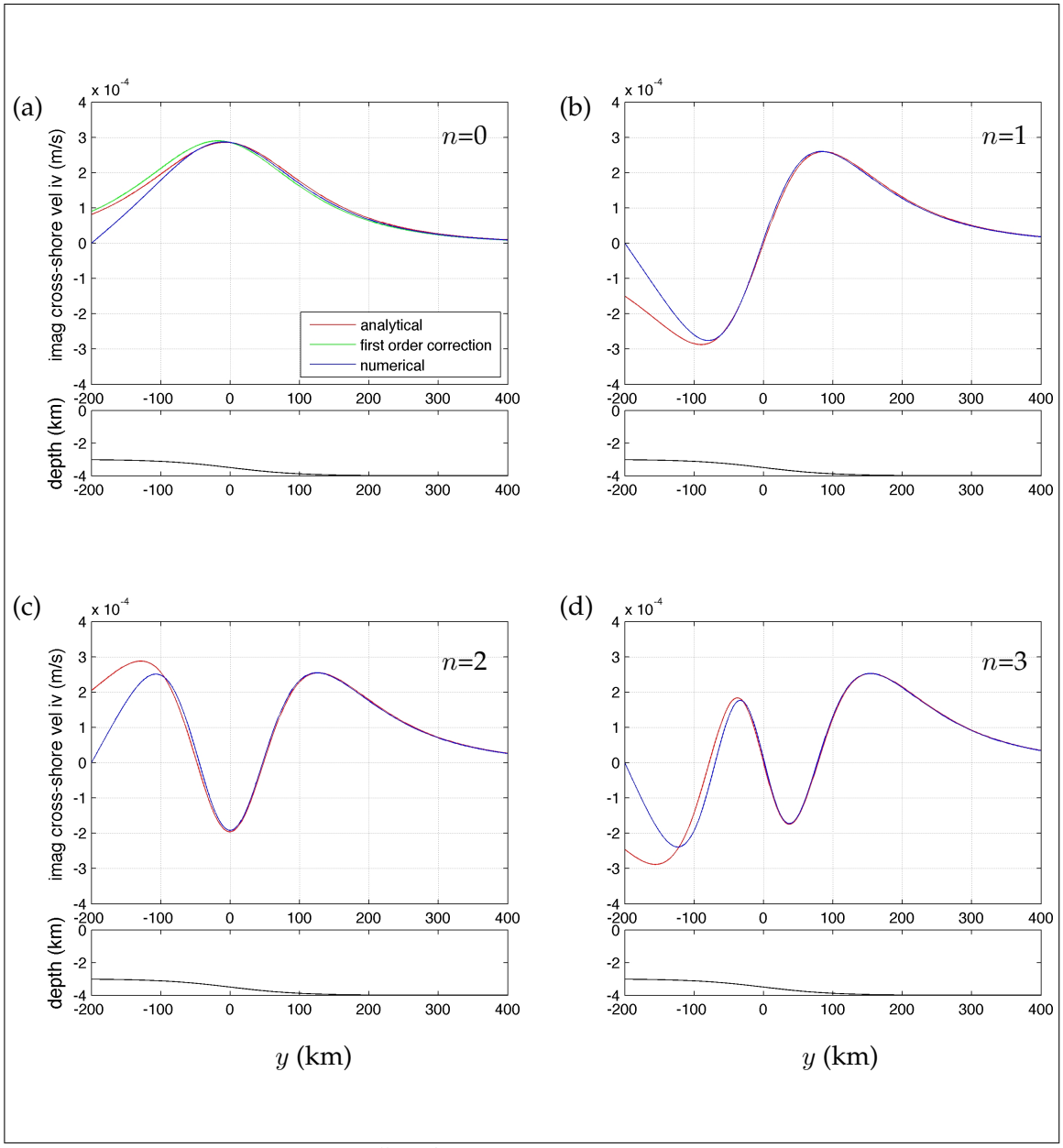


**Figure 5.9:** TRW, $k = 1 \times 10^{-5} m^{-1}$ slope-width=200km, $H_2$=3km, $L$=200km. We plot and compare the cross-shore velocities $v$ obtained from the analytical solution found by combining (3.32), (3.86) and (3.89) (—), the first order correction (n=0) (3.75) (—) and the numerical solutions (—) to (3.48).

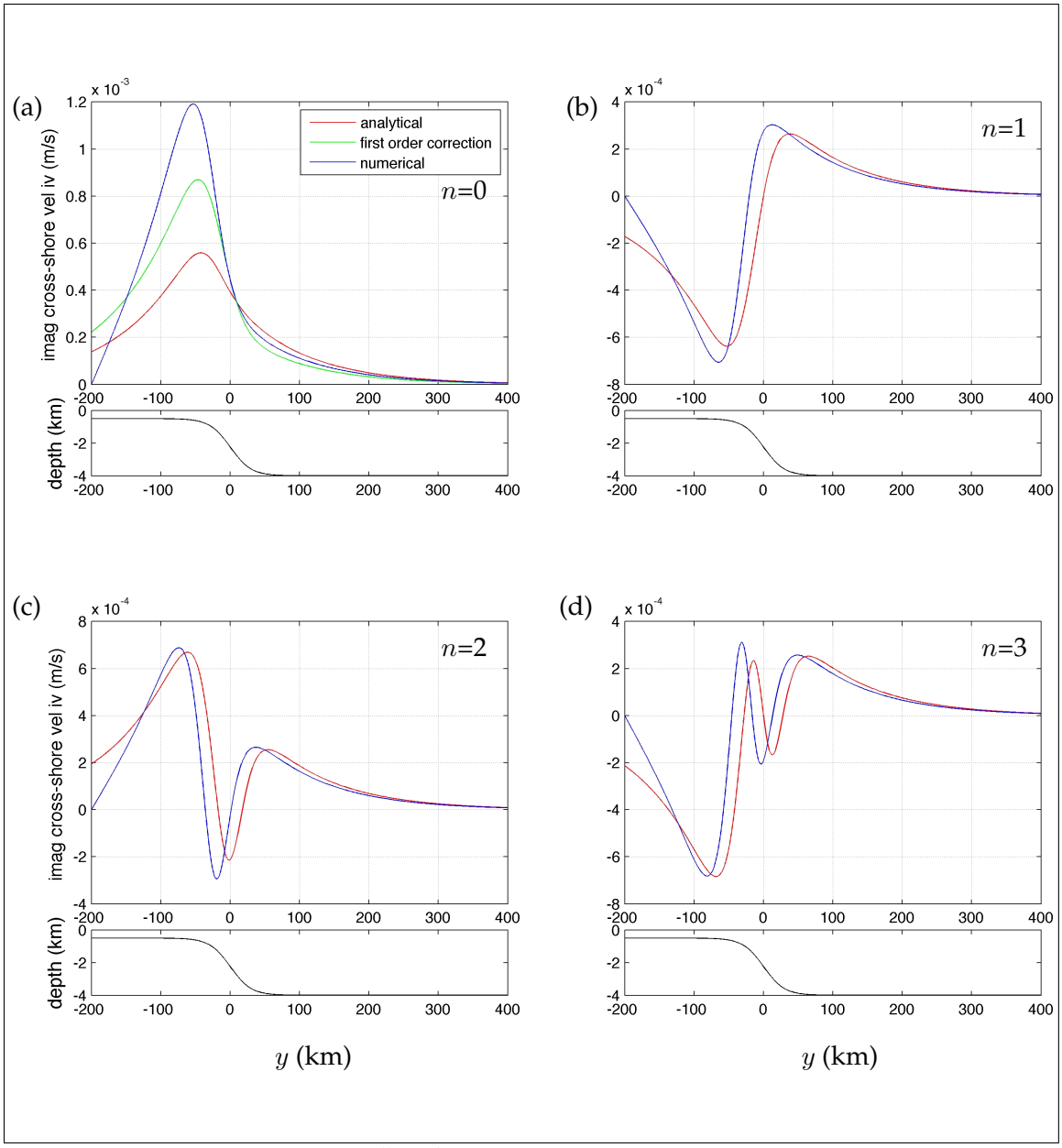


**Figure 5.10:** TRW, $k = 1 \times 10^{-5} m^{-1}$ slope-width=60km, $H_2$=0.5km, $L$=200km. We plot and compare the cross-shore velocities $v$ obtained from the analytical solution found by combining (3.32), (3.86) and (3.89) (—), the first order correction (n=0) (3.75) (—) and the numerical solutions (—) to (3.48).

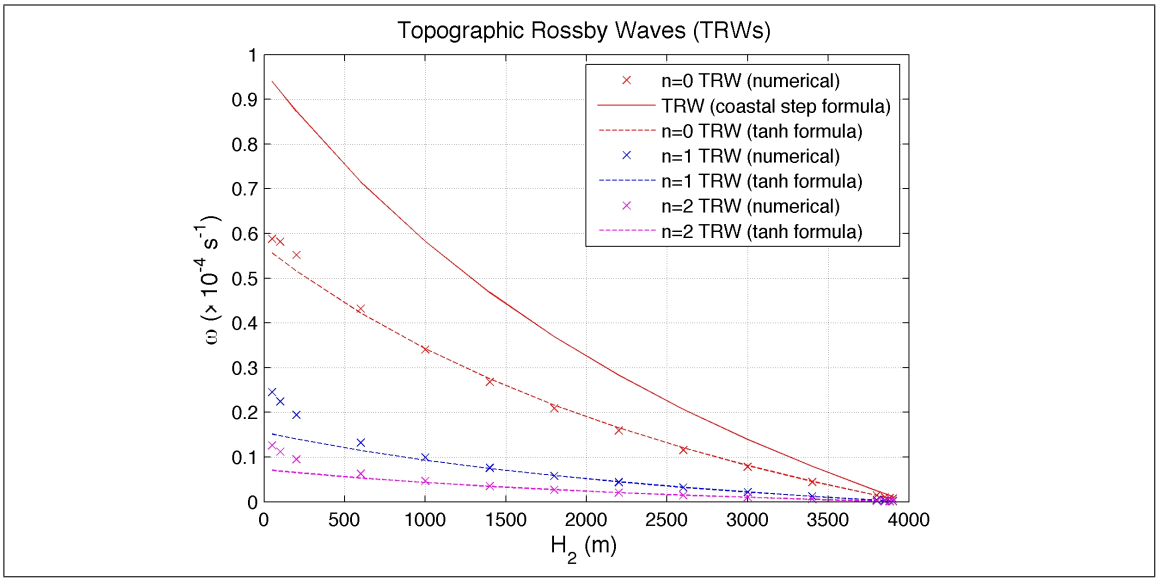


**Figure 5.11:** Comparison of the solutions to the first order analytical solution without a coastline (3.74) ($\tanh$ formula), the simple step model with a coastline (4.74) (coastal step formula) and numerical solutions which are found using a shooting method initialised by (3.74). Here $k = 1 \times 10^{-5}$ m$^{-1}$, $L$=200km, slopewidth=100km ($\lambda = 0.25$), $H_1$=4000m.

similar hyperbolic tangent topography, they showed that the wave frequency is reduced as the length of the continental shelf decreases provided $k_{kj} = kL \lesssim 0.5$ (otherwise, the exponential decay of the TRW renders the shelf meaningless). Here $k_{kj}$ is the non dimensional alongshore wavenumber in **?**.

To see the relationship between the analytical prediction (3.111) and their results we have reproduced their Figure 4(b) (**?**) in Figure 5.12. Also shown in blue is our analytical prediction to the second order (3.111), which in their notation is

$$\omega = \frac{1 - H_0}{(1 + sk_{kj})(1 + H_0)} \left[ 1 + \frac{|sk_{kj}|(2 + |sk_{kj}|)^2}{2(3 + 2|sk_{kj}|)(1 + |sk_{kj}|)^2} \left( \frac{1 - H_0}{1 + H_0} \right)^2 \right]; \tag{5.10}$$

where $s$ measures the steepness of the slope. Figure 5.12 demonstrates this prediction works well for $k_{kj} = kL \gtrsim 0.5$, their $ks \gtrsim 0.5$, as expected. For $|kL| \lesssim 0.5$, the prediction does not capture the shelf effects, since it has no $L$ dependence. Even so, the maximum error is still $\leq$35%.

**?** also discuss the role of the steepness of the continental slope. They show, at fixed $L$, that

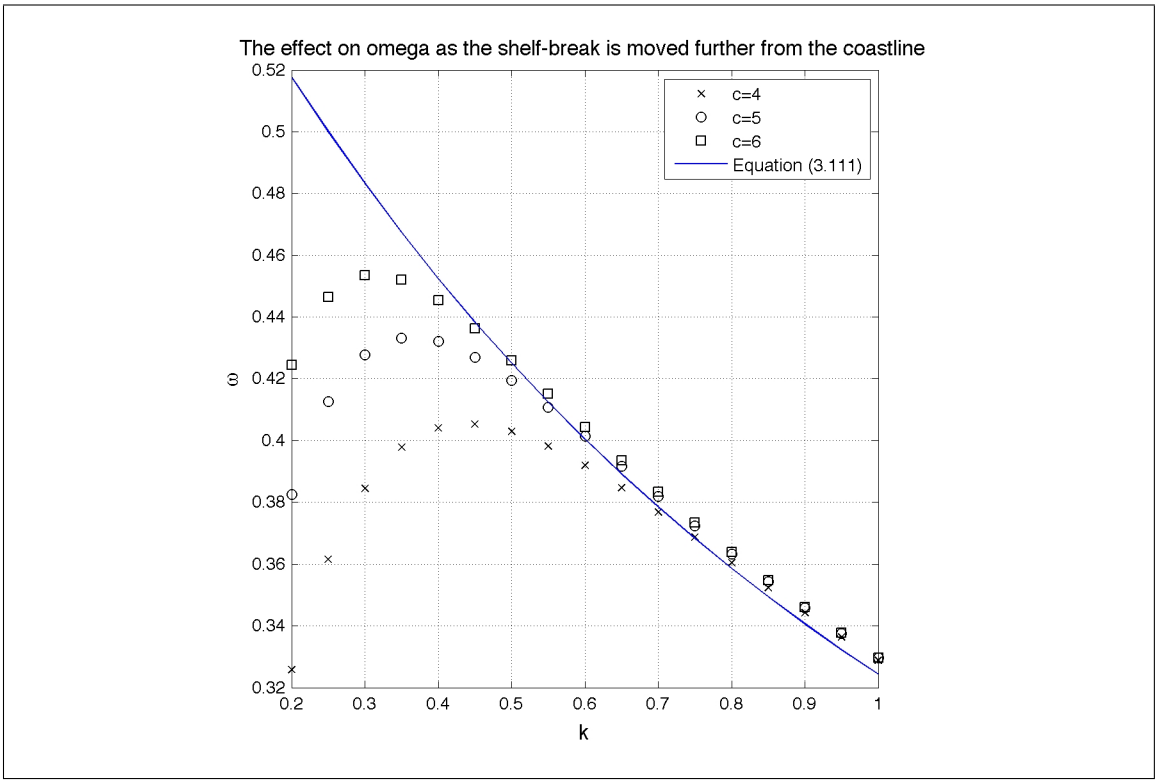


**Figure 5.12:** Comparison of the frequencies for a hyperbolic tangent profile as a function of the alongshore wavenumber $k$. $\omega$ (—) (3.111) is given up to the second order correction. $c$ (**?**) represents the the position of the shelf-break to the coastline, as $c$ increases the distance between the coastline and shelf-break increases. Figure 4(b) (**?**) has been reproduced and compared with (3.111).

all frequencies increase as the slope steepness (or width decreases). We have reproduced their Figure 5(b) (**?**), which shows this effect. Also included is the analytical prediction (3.111), which is accurate for $k_{kj} = kL_s \gtrsim 0.5$ (for the same reasons as above). So, (3.111) does contain the correct dependence on slope width.

To leading order (5.10) is

$$\omega = \frac{1 - H_0}{(1 + sk)(1 + H_0)}. \tag{5.11}$$

Therefore, it is clear that $\omega$ increases as $s$ decreases.

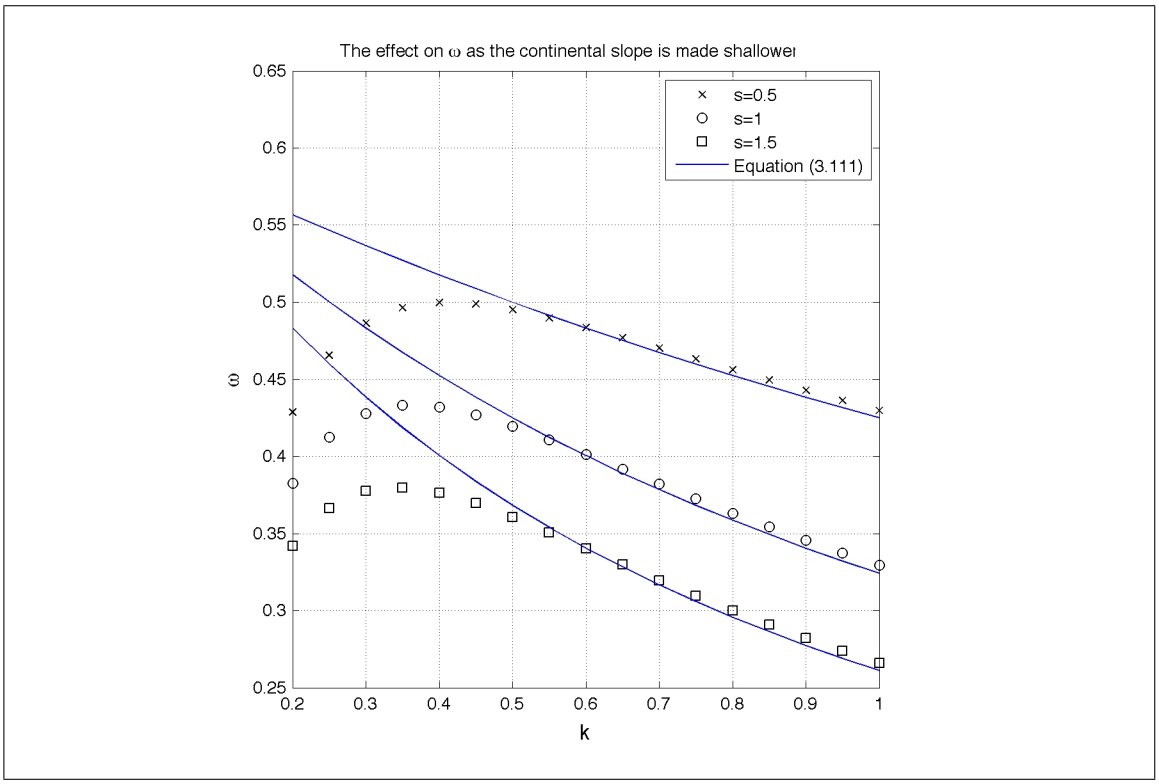


**Figure 5.13:** Comparison of the frequencies for a hyperbolic tangent profile as a function of the alongshore wavenumber $k$. $\omega$ (—) (3.111) is given up to the second order correction. $s$ measures the steepness of the continental slope (**?**), as $s$ increases the slope becomes shallower. Figure 5(b) (**?**) has been reproduced and compared with (3.111).

## 5.9 Discussion

We have investigated the nature of coastally trapped waves that exist due to a combination of rotation and a smooth continuous topography. Using a hyperbolic tangent profile for depth, we know that three types of wave should be found: a single KW modified by the topography, a set of EWs and an infinite set of TRWs (**?**). This is in contrast to the step topography solutions, where only one topographic wave is found.

Having reduced the linear shallow water equations to a second order eigenvalue problem that was solved numerically, we have found results in agreement with these predictions. Furthermore, we have shown that the step topography dispersion relation yields a good approximation (say, to within 5%) for the frequency of the modified Kelvin wave and the edge waves, for the parameter regime examined (and for our particular choice of smooth topography). The cross-shore structure of the solutions is also well predicted by the step topography theory. We conclude that it is safe to use a step topography as a first approximation for wave solutions over a smooth slope, for the Kelvin and edge waves.

However, one cannot make the same assertions for topographic Rossby waves, since there are fundamental differences between solutions above a step and a smooth slope. This is because the TRWs are driven by PV dynamics, and are thus particularly sensitive to the shape and horizontal extent of the slope. Thus, analytical approximations of these waves can only be obtained from some sort of simplified model with continuous topography. These expressions, derived in chapter 3 – which were for a small topography and an unbounded domain – do provide a good approximation for TRWs above large topography bounded by a coastline. Additionally we have shown that the dispersion relation derived by **?** is the upper bound of this infinite set. Thus, we have successfully reproduced the expected results (**?**) for a profile of monotonic depth.

However, these TRWs are all sub-inertial, and we are primarily concerned with waves of tidal frequency, which are generally super-inertial. So we shall use a step topography in the next chapter where we investigate tidally generated internal waves.

# Chapter 6

# Internal tide generation in a two-layer flow

## 6.1 Introduction

Up to now we have we explored waves that are trapped by the coastline or on the continental shelf/slope. In chapter 3 we considered simple trapped barotropic waves in isolation: the Kelvin wave, edge waves, and the topographic Rossby wave. We then proceeded in chapter 4 to consider waves influenced by a combination of planetary rotation and a step-like topography. This model was modified in chapter 5 by assuming the topography is continuous. In these simple models there was no forcing and we assumed that our waves travelled along-shore in a sinusoidal manner. However, in the cross-shore direction we imposed the condition that these waves would exponentially decay away from the coastline, and that the cross-shore motion was perpendicular to the coastline.

In this chapter, we return to the step-like topography, however, we simplify this model by assuming that there is no coastline and planetary rotation, and consider motion in one dimension only. Furthermore, in contrast to previous simple models discussed, we force this system with an incoming barotropic wave which is perpendicular to the step. Previ-

ous models have been developed that treat tides-topography interaction as a scattering problem, **???**. These models have been developed to describe the generation of internal gravity waves over a step topography. Here we discuss some important details and findings of Rattray's and Guizien and Barthélemy's models before developing and solving our own two-layer step problem. We then compare our results with the work of **?**, **?** and **?** and return to compare some details of Guizien and Barthélemy's model and the one explored in this chapter.

In 1960, Rattray wrote 'Although internal tides of tidal period have been observed in various regions of the oceans, their distribution and manner of generation have remained largely unknown'. In particular, Rattray was referring to the coastal generation of internal gravity waves, to illustrate the mechanism of generation he chose two simple topographies which gave rise to analytical solutions; a step with a coastline, and a continental slope with a coastline both systems being forced by a surface wave travelling from the coastline towards the deep sea. Deriving the shallow water equations for a two-layer problem which included planetary rotation and the length of the continental shelf, Rattray concluded that the amplitude of the internal gravity waves are proportional to the amplitude of the barotropic tide; the depth of the upper layer; and the step size (the depth of the deep ocean minus the depth of the shelf). Furthermore, he asserts that the generation of internal tides with large amplitudes compared to the barotropic tide are preferential at greater depths, and the probability for generation is increased the broader the shelf. Rattray (1960) only finds one significant difference between his step and slope model; the standing wave increases in amplitude and decreases in wavelength towards the coast.

Rattray's model has since been modified several times, in particular we refer to **?** who construct an analytical two-layer model using a step-like geometry which they compare with Baines' model (**?**), and the separate UK Land Ocean Interaction Study - Shelf Edge Study program. Guizien *et al*'s model (1999) is forced with an incident oblique barotropic Poincaré wave propagating towards the shelf-break, as opposed to Rattray's model (**?**) in which the barotropic wave was perpendicular to the coastline. Several important as-

sumptions made by **?** are they have a step-like geometry, a two-layer model, and assume the energy of incoming waves are absorbed by the coastline and not radiated away.

Baines' (1982) internal tide generation model is what **?** refer to as a 'composite model' with rotation included. Here the upper layer is well mixed, of fixed density and lies above a shallow thermocline (modelled as an interface) which is above a layer of continuously stratified fluid. His model is forced by a barotropic tide flowing on and off the shelf to which it is perpendicular. The two-layer setting allows Baines to decouple the barotropic motion from the internal gravity wave motion. Guizien *et al* (1999) are able to reproduce the solutions for Baines' (1982) internal tide amplitude provided the angle of incidence of the barotropic tide is the same, i.e. approximately 90°.

The Shelf-Edge-Study (SES) program was a UK Community project designed to observe and collect data of key exchange mechanisms in the continental shelf/slope region in 1996, one area targeted was the Malin Shelf. Figure 6.1a shows the location of this shelf in Western Europe, it is part of a long shelf region which stretches from North Scotland towards the North-West coast of France. In Figure 6.1b we clearly see the sharp change in topography from 150m, the shelf depth, to a deep ocean depth of 2000m. The SES (Shelf-Edge-Study) box shows where the exact location of the Malin Shelf observations were gathered.

Although not exhaustive, the two-layer models discussed here are of significance. **?** developed a simple model which is still used today although with alterations. A major modification by Baines (1982) is the mathematical description of the stratification of the fluid, and Guizien *et al* (1999) has considered the angle of the barotropic tide to be of importance, and made convincing comparisons of their model with real life data. My aim in this chapter is to evaluate the time averaged energy fluxes of the internal gravity waves generated in the two-layer model at the step edge and similarly compare this with observed data. To investigate this we choose to avoid complications to our simple model and so ignore planetary rotation and the coastline. Planetary rotation does play an important part in the motion of a fluid and constrains the adjustment of a wave to

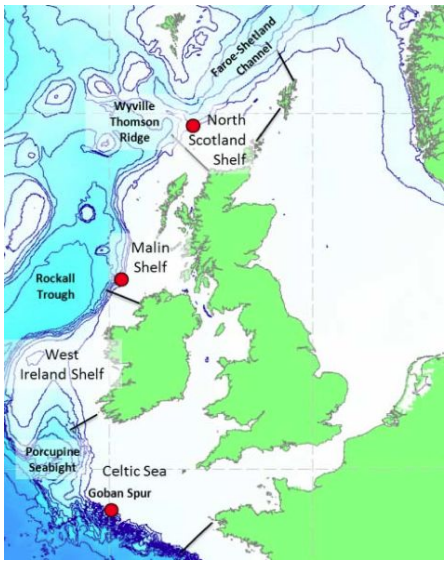


(a)

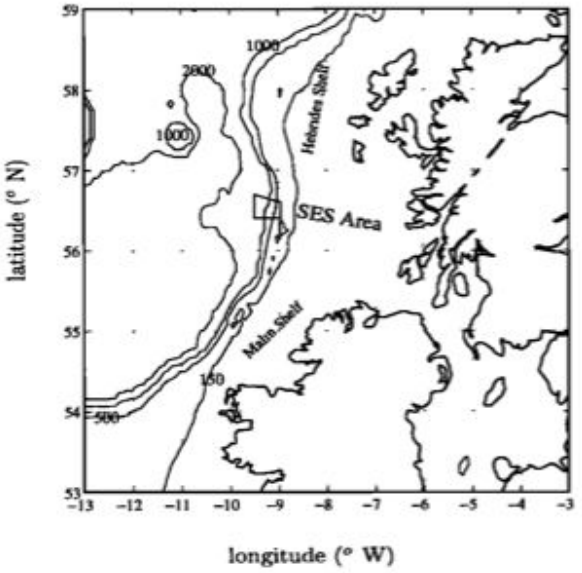


(b)

**Figure 6.1:** Location of the Malin Shelf, North of Ireland, UK. (a) Regional map showing shelves surrounding UK. (b) Exact locate of the Malin Shelf (56°N and 9°W), the SES box area shows where the Shelf-Edge-Study program was undertaken in July 1996. The contours show the Malin Shelf at 150m depth. In 1°-2°latitude, there is a sharp change in the bathymetry, with a deep ocean depth of approximately 2000m. (**?**).

the Rossby radius, however, as we have seen in our shallow water framework (chapter 4), this length scale is thousands of kilometres long. Since we have a two-layer system we are able to decouple the barotropic and internal gravity wave modes so that we may verify our the barotropic analytical and numerical results from the two-layer problem with solutions of the single layer model. Although we do not include a coastline, the advantage of the geometry of our model is it can approximate a barotropic wave travelling parallel to a coastline which flows over a step, or it can be applied to fluid motion over a mid-ocean ridge.

The simplest approach to achieve our goal is to return to the single layer step model and shallow water linear equations of chapter 2. We then explore the two-layer model, this is a modification of the single layer, here a lighter fluid lies above a heavier fluid. A new set of governing equations are derived for this new model, and finally a step is reintroduced so that we may examine in terms of the time averaged energy flux the internal tide generation at the step edge. To understand this effect we study what happens when a barotropic wave, perpendicular to the step edge, travels from the deep ocean over a submerged step by calculating the time averaged energy fluxes, $\langle \underline{J} \rangle$, on either side of the shelf break. To conclude we compare our results with measurements observed in the Hawaiian Archipelago. Here the $M_2$ tide is perpendicular to specific islands of the Hawaiian Rdige, and in particular, I compare my results with the HOME experiment (**?**), a combination of mooring data and satellite altimetry measurements (**?**) and a step model developed by **?**.

## 6.2 Reflection and transmission of barotropic waves in a single layer fluid

Although we are most interested in the case of wave generation in a two-layer fluid, we first lay out the basic mathematical structure involved by considering the corresponding scattering problem for a single layer fluid. We thus consider the geometry shown in

Figure 6.2 which depicts step topography with cross-step coordinate $x$. To the left and right of the step (at $x = 0$) the fluid depths are $H_l$ and $H_r$ respectively. The equilibrium sea level is at $z = 0$, and $h$ denotes the perturbed sea-surface height. The system we shall use to describe the wave motion is the linear shallow water equations (2.25)a-c, however, without rotation.

$$\frac{\partial u}{\partial t} = -g\frac{\partial h}{\partial x} \tag{6.1a}$$

$$\frac{\partial h}{\partial t} + \frac{\partial}{\partial x}(Hu) = 0. \tag{6.1b}$$

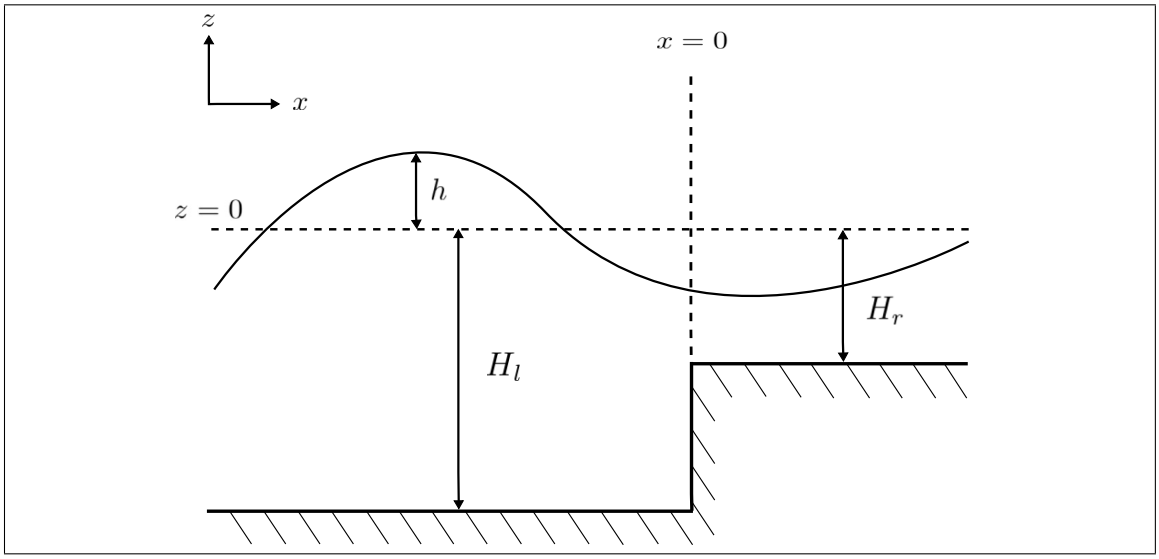


**Figure 6.2:** The shallow water system of constant density with a step. $h$ is the perturbed sea surface above the equilibrium sea level $z = 0$. $H_l$ is the depth of the ocean to the left of the step at $x = 0$. $H_r$ is the depth of the ocean to the right of the step.

We impose an incoming wave of amplitude $h_I$, travelling in the $x$-direction from left to right. This gives a problem of the transmission and reflection of an incident wave passing over step topography. As a consequence, the perturbed sea surface amplitude $h$ and cross-shore velocity $u$ can be described by three separate waves: the incident (I), reflected (R) and transmitted (T) waves.

We choose to write $(h, u)$ in modal form. So $h$ takes the barotropic form

$$h = \begin{cases} \mathrm{Re}\left(h_I e^{i(k_l x - \omega t)} + h_R e^{i(-k_l x - \omega t)}\right) & x < 0, \quad (6.2a) \\ \mathrm{Re}\left(h_T e^{i(k_r x - \omega t)}\right) & x > 0. \quad (6.2b) \end{cases}$$

Here $k_l$ and $k_r$ are both positive, ensuring that the reflected wave is travelling in the negative $x$-direction, and that the transmitted wave is travelling in the positive $x$-direction, as required on physical grounds.

To determine the corresponding form of $u$, we use (6.1a)

$$u_I = \sqrt{\frac{g}{H_l}} h_I, \quad u_R = -\sqrt{\frac{g}{H_l}} h_R, \quad u_T = \sqrt{\frac{g}{H_r}} h_T. \tag{6.3}$$

Substituting (6.3) into (6.2a,b) we have

$$u = \begin{cases} \mathrm{Re}\left[\sqrt{\frac{g}{H_l}}\left(h_I e^{i(k_l x - \omega t)} - h_R e^{i(-k_l x - \omega t)}\right)\right] & x < 0, \quad (6.4a) \\ \mathrm{Re}\left[\sqrt{\frac{g}{H_r}} h_T e^{i(k_r x - \omega t)}\right] & x > 0. \quad (6.4b) \end{cases}$$

**Matching conditions**

In section 2.1.3 we stated the matching conditions at the step: $h$ is continuous at $x = 0$ (2.29), and $H_l u_l = H_r u_r$, at $x = 0$ (2.30) . Equating (6.2a) and (6.2b) at $x = 0$ and using (2.29) yields

$$h_T = h_I + h_R. \tag{6.5}$$

Similarly, substituting (6.4a) and (6.4b) into (2.30) gives

$$H_r u_T = H_l(u_I + u_R). \tag{6.6}$$

We wish to determine relationships for $h_R$ and $h_T$ in terms of $h_I$. Thus we simplify (6.6) by using (6.3) and defining $c_l = \sqrt{gH_l}$ and $c_r = \sqrt{gH_r}$ to obtain

$$h_I = h_R + \frac{c_r}{c_l} h_T \quad \text{where} \quad c_l \neq 0. \tag{6.7}$$

Combining (6.5) and (6.7) gives

$$h_I \begin{bmatrix} 1 \\ 1 \end{bmatrix} = \begin{bmatrix} 1 & \frac{c_r}{c_l} \\ -1 & 1 \end{bmatrix} \begin{bmatrix} h_R \\ h_T \end{bmatrix}. \tag{6.8}$$

leading to

$$h_R = \frac{1 - c_r/c_l}{1 + c_r/c_l}\, h_I, \qquad h_T = \frac{2}{1 + c_r/c_l}\, h_I. \tag{6.9}$$

**Comparing the heights of the perturbed sea surface before and after the step**

How are $h_R$ and $h_T$ affected by the size of the step? To answer this we consider two limits: a small step, and a large step.

First, if we have a small step, then we write $H_r = H_l(1 - \delta)$, where $\delta \ll 1$. Then $c_r/c_r \approx 1 - (\delta/2)$ and

$$h_R = \frac{\delta}{4 - \delta}\, h_I \to \frac{\delta}{4}\, h_I \quad \text{and} \quad h_T = \frac{2}{2 - \delta}\, h_I \to h_I. \tag{6.10}$$

As $\delta \to 0$ decreases the step size decreases, thus we have a decrease in the amplitude of the reflected wave. Furthermore, as the step becomes smaller, the amplitude of the wave transmitted tends to the amplitude of the incident wave which is what we expect.

Finally, if we have a very large step, i.e., $H_r \ll H_l$, then $c_r \ll c_l$. Hence (6.9) reduces to

$$h_R \to h_I \quad \text{and} \quad h_T \to 2h_I. \tag{6.11}$$

Under this assumption, we see that the amplitude of the reflected wave is approximately equal to the incident wave, which seems intuitive. However, surprisingly we also find that the amplitude of the transmitted wave is twice the amplitude of the incident wave. This is quite an unexpected result. We now show how this may be understood by considering the time averaged energy flux across the step.

### 6.2.1 Energy relations for the single layer fluid

Surface gravity waves have kinetic energy due to the motion of the fluid and potential energy due to the deformation of the free surface. In this section we derive expressions

for the kinetic energy, potential energy and time averaged energy flux per unit area for linear disturbances in a single-layer fluid.

With no rotation, the linear shallow water momentum equations (2.25a,b) can be written as

$$\frac{\partial \underline{u}}{\partial t} = -g\underline{\nabla} h \tag{6.12}$$

where $\underline{\nabla} = (\partial/\partial x, \partial/\partial y)$ and $\underline{u} = (u, v)$. Taking the scalar product of (6.12) with $\underline{u}$, we obtain

$$\frac{1}{2}\frac{\partial(\underline{u}\cdot\underline{u})}{\partial t} = -g\underline{u}\cdot\underline{\nabla} h. \tag{6.13}$$

Multiplying (6.13) by $\rho H$ and defining the kinetic energy per unit horizontal area as $E_k = \rho H \underline{u}\cdot\underline{u}/2$ we obtain

$$\frac{\partial E_k}{\partial t} = -g\rho H\underline{u}\cdot\underline{\nabla} h = -g\rho\underline{\nabla}\cdot(hH\underline{u}) + g\rho h\underline{\nabla}\cdot(H\underline{u}). \tag{6.14}$$

By the continuity equation (2.25c) we know $\underline{\nabla}\cdot(H\underline{u}) = -\partial h/\partial t$, so substituting this and $h\,\partial h/\partial t = 1/2\,(\partial h^2/\partial t)$ into (6.14) we obtain

$$\frac{\partial}{\partial t}(E_k + E_p) + \underline{\nabla}\cdot\underline{J} = 0. \tag{6.15}$$

In this, we have defined per unit area the kinetic and potential energies and energy flux

$$E_k = 1/2\,\rho H\underline{u}\cdot\underline{u} \tag{6.16}$$

$$E_p = \frac{1}{2}g\rho h^2 \tag{6.17}$$

$$\underline{J} = g\rho h H\underline{u} \tag{6.18}$$

Since the rate of change of energy inside any volume is $\partial(E_k + E_p)/\partial t$, we may interpret $\underline{J}$ as an energy flux.

### 6.2.2 Time averaged energy flux for transmitted and reflected waves

In this section we proceed to calculate the time averaged energy fluxes for the incident, reflected and transmitted barotropic waves of section 6.2.1. Substituting our expressions

for the modal form of $h$ (6.2) and $u$ (6.4) into our expression for $\underline{J}$ and removing the oscillatory part we are left with the steady part which we refer to as the time averaged energy flux, $\langle \underline{J} \rangle$. Here we state the results to the left ($x < 0$) and right ($x > 0$) of the step-edge respectively

$$\langle \underline{J} \rangle = \begin{cases} \langle \underline{J} \rangle_I + \langle \underline{J} \rangle_R = \dfrac{g\rho c_l}{2} |h_I|^2 - \dfrac{g\rho c_l}{2} |h_R|^2 & x < 0, \quad (6.19a) \\ \langle \underline{J} \rangle_T = \dfrac{g\rho c_r}{2} |h_T|^2 & x > 0. \quad (6.19b) \end{cases}$$

Using the expressions for $h_R$ and $h_T$ (6.9) we are able to express (6.19a,b) solely in terms of $h_I$

$$\langle \underline{J} \rangle = \begin{cases} \langle \underline{J} \rangle_I + \langle \underline{J} \rangle_R = \dfrac{g\rho c_l}{2} |h_I|^2 - \dfrac{g\rho c_l}{2} \left( \dfrac{c_l - c_r}{c_l + c_r} \right)^2 |h_I|^2 & x < 0, \quad (6.20a) \\ \langle \underline{J} \rangle_T = \dfrac{2g\rho c_r}{(1 + c_r/c_l)^2} |h_I|^2 & x > 0. \quad (6.20b) \end{cases}$$

Here $c_l = \sqrt{gH_l}$ and $c_r = \sqrt{gH_r}$ are the speeds of the barotropic waves to the left and right of the step respectively. Using (6.20a,b) it follows that

$$\frac{\langle J \rangle_T}{\langle J \rangle_I} = \frac{4(c_r/c_l)}{(1 + c_r/c_l)^2} \qquad \text{and} \qquad \frac{\langle J \rangle_R}{\langle J \rangle_I} = \frac{(1 - c_r/c_l)}{(1 + c_r/c_l)}. \quad (6.21)$$

If we have a very small step then $H_r/H_l \longrightarrow 0$, so $c_r/c_l \longrightarrow 0$ and we expect most of the time averaged energy to be reflected and very little to be transmitted. Recall $H_r = H_l(1 - \delta)$ where $0 < \delta \leq 1$, so as $\delta \to 1$ i.e., the step size is increasing we have

$$\frac{\langle J \rangle_T}{\langle J \rangle_I} \longrightarrow 0 \qquad \text{and} \qquad \frac{\langle J \rangle_R}{\langle J \rangle_I} \longrightarrow 1. \quad (6.22)$$

To make a link with the 'mystery' of (6.11), note that $\langle J \rangle_T$=0 even though $h_T \to 2h_I$. So looking at the surface alone can be misleading.

We also see that as $\delta \to 0$, i.e., the depth of the shelf increases which is equivalent to the step becoming smaller, we see more of the time averaged incident energy being transmitted and less reflected. So

$$\frac{\langle J \rangle_T}{\langle J \rangle_I} \longrightarrow 1 \qquad \text{and} \qquad \frac{\langle J \rangle_R}{\langle J \rangle_I} \longrightarrow 0. \quad (6.23)$$

## 6.3 Two-layer shallow water equations

The next target is to complete the corresponding calculation in a two-layer fluid, where the incident barotropic wave may also be scattered into internal gravity waves propagating away from the step. However, before performing this calculation, we derive the governing equations and energy fluxes for two-layer flow.

At the outset, it is worth noting that in this two-layer model we explore the effects of stratification in this simple framework through the reduced gravity term $g'$ while keeping the number of equations and variables to a minimum. This two layer model does indeed provide surprisingly good results which are comparable with continuous stratification (**?**). The ocean can be viewed as a fluid of two different densities, the upper layer being of lower density and with more activity, and the lower layer a deep layer of higher density (**?**), so here $\rho_1 < \rho_2$.

Furthermore, we add a step to this simple two-layer model with an aim to comparing our time averaged energy fluxes about the step-edge with observed and calculated data for real-life topography (**???**).

### 6.3.1 Derivation of two-layer Shallow Water Equations

Figure 6.3 illustrates the two-layer model which has upper and lower layers of densities $\rho_1$ and $\rho_2$ respectively. These layers have the associated pressures $p_1$ and $p_2$ respectively. The depths of the upper and lower layer are given by $H_1$ and $H_2 = H - H_1$ respectively. The perturbed interface lies at $z = -H_1 + h(x, y, t)$, and the perturbed sea surface lies at $z = \eta(x, y, t)$. The horizontal velocities of the fluid in the upper and lower layers are $\underline{u}_1$ and $\underline{u}_2$ respectively.

In chapter 2 we derived the momentum, hydrostatic and incompressibility equations (2.13a-d) for a single layer model on the $f$-plane. We now derive the corresponding equations that describe a two-layer system. The starting point are the linear, hydrostatic,

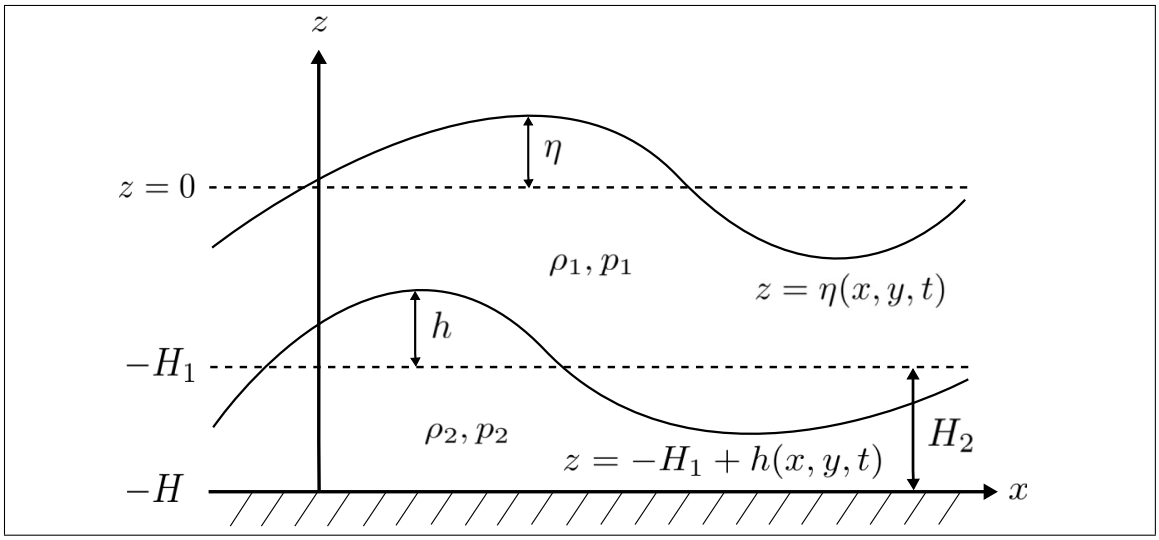


**Figure 6.3:** In this two-layer model we have the upper and lower layers, of densities $\rho_1$ and $\rho_2$, where $\rho_1 < \rho_2$, and pressures $p_1$ and $p_2$. $H_1$ and $H_2$ represent the fixed upper and lower layers, where $H_2 = H - H_1$ and $H$ is the undisturbed ocean depth. Note in this model $\eta(x, y, t)$ is the perturbation of free surface and $h(x, y, t)$ the perturbed interface of the internal gravity wave. The motion of the fluid is described in the upper and lower layers as $\underline{u}_1$ and $\underline{u}_2$ respectively.

incompressible equations of motion:

$$\frac{\partial \underline{u}_i}{\partial t} = -\frac{1}{\rho_i}\underline{\nabla} p_i, \tag{6.24a}$$

$$0 = -\frac{1}{\rho_i}\frac{\partial p_i}{\partial z} - g, \tag{6.24b}$$

$$\frac{\partial u_i}{\partial x} + \frac{\partial v_i}{\partial y} + \frac{\partial w_i}{\partial z} = 0, \tag{6.24c}$$

where $\underline{\nabla} = (\partial/\partial x, \partial/\partial y)$, $\underline{u}_i = (u_i, v_i)$ and $i = 1, 2$ distinguishes between the upper and lower layers respectively.

**Upper layer**

In the upper layer $-H_1 + h < z < \eta$. Hydrostatic balance (6.24b) takes the form

$$\frac{\partial p_1}{\partial z} = -\rho_1 g. \tag{6.25}$$

We integrate this to obtain $p_1 = -\rho_1 g z + k(x, y, t)$. As in section 2.0.3, we assume there is constant atmospheric pressure, $p_{atm}$, on the sea surface. Thus $p_1 = p_{atm}$ at $z = \eta(x, y, t)$, so we have

$$p_1 = \rho_1 g(\eta - z) + p_{atm}. \tag{6.26}$$

It follows $\underline{\nabla} p_1 = \rho_1 g \underline{\nabla}\eta$, so that we can write (6.24a) as

$$\frac{\partial \underline{u}_1}{\partial t} = -g\underline{\nabla}\eta. \tag{6.27}$$

Since $\eta$ is a function of $x, y, t$ we may seek a solution for $\underline{u}_1$, which is also a function of $x, y, t$. Then integrating (6.24d) over the upper layer $-H_1 + h < z < \eta$ gives

$$w_1(\eta) - w_1(-H_1 + h) = -(\eta + H_1 - h)\underline{\nabla} \cdot \underline{u_1}. \tag{6.28}$$

But

$$\frac{D}{Dt}(z - \eta) = 0 \quad \text{at} \quad z = \eta \implies w(z = \eta) = \frac{D\eta}{Dt} \tag{6.29a}$$

$$\text{and} \quad \frac{D}{Dt}(z - (-H_1 + h)) = 0 \quad \text{at} \quad z = -H_1 + h \implies w(z = -H_1 + h) = \frac{Dh}{Dt} \tag{6.29b}$$

Substituting (6.29a,b) into (6.28) we have

$$\frac{D}{Dt}(\eta - h) = -(\eta + H_1 - h)\underline{\nabla} \cdot \underline{u_1}.$$

We will use the linearised form

$$\frac{\partial}{\partial t}(\eta - h) + \underline{\nabla} \cdot (H_1 \underline{u}_1) = 0. \tag{6.30}$$

**Lower layer**

In the lower layer $-H < z < -H_1 + h$, integrating the hydrostatic equation (6.24b) gives $p_2 = -\rho_2 g z + k(x, y, t)$. At the interface $z = -H_1 + h$, pressure is continuous; so

$$p_2(z = -H_1 + h) = p_1(z = -H_1 + h) = p_{atm} + \rho_1 g(\eta - z)$$
$$\implies p_2 = \rho_2 g(-z - H_1 + h) + \rho_1 g(\eta + H_1 - h) + p_{atm}$$
$$\implies \underline{\nabla} p_2 = \rho_2 g \underline{\nabla} h + \rho_1 g \underline{\nabla}(\eta - h),$$

In the setting of the lower layer (6.24a) becomes

$$\frac{\partial \underline{u}_2}{\partial t} = -g\frac{\Delta\rho}{\rho_2}\underline{\nabla} h - g\frac{\rho_1}{\rho_2}\underline{\nabla}\eta,$$

where $\Delta\rho = \rho_2 - \rho_1$. Here we introduce the parameter $g'$ which is commonly known as reduced gravity (**?**):

$$g' = g\frac{\Delta\rho}{\rho_2} > 0. \tag{6.31}$$

To obtain an idea of the magnitude of $g'$, we can roughly replicate the real ocean by taking $\rho_1 = 1025\text{kg/m}^3$ and $\rho_2 = 1028\text{kg/m}^3$, giving $g' \approx 0.03\text{m/s}^2$. Using (6.31) we can write

$$\frac{\partial \underline{u}_2}{\partial t} = -g\frac{\rho_1}{\rho_2}\underline{\nabla}\eta - g'\underline{\nabla} h \tag{6.32}$$

This equation is fine as it stands. However, for oceanic applications, a further approximation is commonly made, which simplifies the analysis somewhat. Since $\rho_1/\rho_2 \approx 1$, to within 0.5% for typical oceanic densities, we replace (6.32) by

$$\frac{\partial \underline{u}_2}{\partial t} = -g\underline{\nabla}\eta - g'\underline{\nabla} h. \tag{6.33}$$

Note: this is not equivalent to setting $\rho_1 = \rho_2$, as for the single layer, since density differences are retained in association with gravity, thus giving a buoyancy force $-g'\underline{\nabla}h$ in (6.38c). This is analogous to making the Boussinesq approximation for a continuously stratified ocean which is the standard treatment for oceanic flows (**??**).

Since $\eta$ and $h$ are independent of $z$, it is consistent to seek a solution with $\underline{u}_2$ independent of $z$. Then integrating the continuity equation (6.24d) over $-H < z < -H_1 + h$ gives

$$w_2(-H_1 + h) - w_2(-H) = -(-H_1 + h + H)\underline{\nabla} \cdot \underline{u_2} \tag{6.34}$$

The kinematic boundary conditions at the top and bottom of the layer give

$$\frac{D}{Dt}(z - (-H_1 + h)) = 0 \quad \text{at} \quad z = -H_1 + h \implies w(z = -H_1 + h) = \frac{D(-H_1 + h)}{Dt} \tag{6.35a}$$

$$\text{and} \quad \frac{D}{Dt}(z - (-H)) = 0 \quad \text{at} \quad z = -H \implies w(z = -H) = \frac{D(-H)}{Dt}. \tag{6.35b}$$

Substituting (6.35a,b) into (6.35) and writing $H_2 = H - H_1$ we have

$$\frac{D}{Dt}(h + H_2) = -(h + H_2)\underline{\nabla} \cdot \underline{u_2}. \tag{6.36}$$

Linearising and assuming we have a flat seabed, i.e., $H_2$=constant, this expression reduces to

$$\frac{\partial h}{\partial t} + \underline{\nabla} \cdot (H_2\, \underline{u}_2) = 0. \tag{6.37}$$

To summarise, we have the set of linear shallow water equations for the non-rotating two-layer model with constant $H_1$ and $H_2$ and a flat sea bed:

$$\text{upper layer} = \begin{cases} \dfrac{\partial \underline{u}_1}{\partial t} = -g\underline{\nabla}\eta, & \text{(6.38a)} \\ \dfrac{\partial}{\partial t}(\eta - h) + \ \underline{\nabla} \cdot (H_1 \underline{u}_1) = 0, \qquad -H_1 + h < z < \eta, & \text{(6.38b)} \end{cases}$$

$$\text{lower layer} = \begin{cases} \dfrac{\partial \underline{u}_2}{\partial t} = -g\underline{\nabla}\eta - g'\underline{\nabla}h, & \text{(6.38c)} \\ \dfrac{\partial h}{\partial t} + \underline{\nabla} \cdot (H_2\, \underline{u}_2) = 0, \qquad -H_1 - H_2 < z < -H_1 + h, & \text{(6.38d)} \end{cases}$$

where $h, \eta$, $u_1$ and $u_2$ are functions of $(x, y, t)$. Note we have six equations with six unknowns.

### 6.3.2 Energy relations for the two layer fluid

In section 6.2.1 we derived the energy relations for a single-layer model. Here we derive the equivalent energy relations for a two-layer model.

We start with the upper layer. The derivation initially follows that leading to (6.14):

$$\frac{\partial K_1}{\partial t} = -g\rho_1 \underline{\nabla} \cdot (H_1 \underline{u}_1 \eta) + g\rho_1 \eta \underline{\nabla} \cdot (H_1 \underline{u}_1) \tag{6.39}$$

where $K_1 = \rho_1 H_1 |\underline{u}_1|^2/2$. Then substituting for $\underline{\nabla} \cdot (H_1 \underline{u}_1) = -\partial/\partial t(\eta - h)$ from (6.38b), we find

$$\frac{\partial}{\partial t}(K_1 + P_1) + \underline{\nabla} \cdot \underline{J_1} - g\rho_1 \eta \frac{\partial h}{\partial t} = 0. \tag{6.40}$$

Here the potential energy and energy flux per unit area are given by $P_1 = \frac{1}{2} g\rho_1 \eta^2$ and $\underline{J_1} = g\rho_1 H_1 \underline{u}_1 \eta$ respectively. Note we have an extra term in (6.40) when compared with (6.15). This does not come as a surprise, as the product of $\eta \partial h/\partial t$ suggests an exchange of energy between the upper and lower layers at the interface. What we do not know is if one layer receives more energy than the other layer.

The lower layer now receives equal attention. However, this derivation is made more complicated by the additional term $-g\underline{\nabla}\eta$ in (6.38c), which implies the upper layer contributes to the horizontal velocities in the lower layer.

We begin by calculating the rate of change of the kinetic energy for the lower layer, $K_2 = \rho_2 H_2 |\underline{u}_2|^2/2$

$$\frac{\partial K_2}{\partial t} = -g\rho_1 H_2 (\underline{u}_2 \cdot \underline{\nabla}\eta) - g' \rho_2 H_2 (\underline{u}_2 \cdot \underline{\nabla} h). \tag{6.41}$$

To the first term on the right hand side we add $-g\rho_1 \eta[\underline{\nabla} \cdot (H_2 \underline{u}_2) - \underline{\nabla} \cdot (H_2 \underline{u}_2)]$ so

$$-g\rho_1 H_2 (\underline{u}_2 \cdot \underline{\nabla}\eta) = -g\rho_1 [\underline{\nabla} \cdot (H_2 \underline{u}_2 \eta) - \eta \underline{\nabla} \cdot (H_2 \underline{u}_2)]. \tag{6.42}$$

By (6.38d), $\underline{\nabla} \cdot (H_2 \underline{u}_2) = -\partial h/\partial t$, and substituting this into (6.42) we have

$$-g\rho_1 H_2 (\underline{u}_2 \cdot \underline{\nabla}\eta) = -\underline{\nabla} \cdot (g\rho_1 H_2 \underline{u}_2 \eta) - g\rho_1 \eta \frac{\partial h}{\partial t}. \tag{6.43}$$

To the second term of (6.41) we add $-g'\rho_2 h[\underline{\nabla}\cdot(H_2\underline{u}_2) - \underline{\nabla}\cdot(H_2\underline{u}_2)]$ , and using (6.38d) and writing $h(\partial h/\partial t) = 1/2\,(\partial h^2/\partial t)$ we have

$$-g'\rho_2 H_2(\underline{u}_2\cdot\underline{\nabla}h) = -\underline{\nabla}(g'\rho_2 H_2\underline{u}_2 h) - \frac{1}{2}g'\rho_2\frac{\partial h^2}{\partial t}. \tag{6.44}$$

Combining (6.41), (6.43) and (6.44) we find

$$\frac{\partial}{\partial t}(K_2+P_2) + \underline{\nabla}\cdot\underline{J}_2 + g\rho_1\eta\frac{\partial h}{\partial t} = 0. \tag{6.45}$$

Here the potential energy per unit area is given by $P_2 = g'\rho_2 h^2/2$, and the energy flux is $\underline{J}_2 = g\rho_1 H_2\underline{u}_2\eta + g'\rho_2 H_2\underline{u}_2 h$.

We now clearly see that the last terms of (6.40) and (6.45) are equal and opposite. Therefore, our question of whether one layer receives more energy than the other layer at the interface is answered: there is simply an exchange of energy between the two layers.

The total energy per unit area and energy flux for the two-layer model is given by summing (6.40) and (6.45):

$$\frac{\partial}{\partial t}\left(K_1+K_2+P_1+P_2\right) + \underline{\nabla}\cdot[\underline{J}_1+\underline{J}_2] = 0, \tag{6.46}$$

where

$$K_1+K_2 = 1/2\left[\rho_1 H_1|\underline{u}_1|^2 + \rho_2 H_2|\underline{u}_2|^2\right], \tag{6.47a}$$

$$P_1+P_2 = \frac{1}{2}(g\rho_1\eta^2 + g'\rho_2 h^2), \tag{6.47b}$$

$$\underline{J}_1+\underline{J}_2 = g\rho_1\left(H_1\underline{u}_1 + H_2\underline{u}_2\right)\eta + g'\rho_2 H_2\underline{u}_2 h. \tag{6.47c}$$

Thus, (6.46) is of the form

$$\frac{\partial E}{\partial t} + \underline{\nabla}\cdot\underline{J} = 0 \tag{6.47d}$$

As in section (6.2.1), consideration of the time averaged energy flux will be essential to understand the generation of (internal) waves at the step.

### 6.3.3 Dispersion relation for surface and internal gravity waves

Having derived the general set of equations governing a two-layer fluid (6.38a-d), and the energy relations (6.46), we now proceed to determine the structure of the barotropic

and internal gravity wave modes. Differentiating (6.38d) with respect to $t$ gives

$$\frac{\partial^2 h}{\partial t^2} + H_2 \underline{\nabla} \cdot \frac{\partial \underline{u}_2}{\partial t} = 0,$$

and substituting for $\partial \underline{u}_2 / \partial t$ from (6.38c) gives

$$\left( \frac{\partial^2}{\partial t^2} - g' H_2 \underline{\nabla}^2 \right) h = g H_2 \underline{\nabla}^2 \eta. \tag{6.48}$$

Similarly we differentiate (6.38b) with respect to $t$ giving

$$\frac{\partial^2}{\partial t^2}(\eta - h) + H_1 \underline{\nabla} \cdot \frac{\partial \underline{u}_1}{\partial t} = 0, \tag{6.49}$$

and then eliminate $\partial \underline{u}_1 / \partial t$ using (6.38a), to obtain

$$\frac{\partial^2 \eta}{\partial t^2} - \frac{\partial^2 h}{\partial t^2} - g H_1 \underline{\nabla}^2 \eta = 0. \tag{6.50}$$

We substitute (6.48) into this to obtain

$$\frac{\partial^2 \eta}{\partial t^2} - g H_2 \underline{\nabla}^2 \eta - g' H_2 \underline{\nabla}^2 h - g H_1 \underline{\nabla}^2 \eta = 0. \tag{6.51}$$

Differentiating (6.48) twice with respect to $t$, and combining this with the expression for $\partial^2 h / \partial t^2$ from (6.50) we arrive at a quartic in $\eta$

$$\frac{\partial^4 \eta}{\partial t^4} - g H \nabla^2 \frac{\partial^2 \eta}{\partial t^2} + g g' H_1 H_2 \nabla^2 \nabla^2 \eta = 0 \tag{6.52}$$

where $H = H_1 + H_2$. We write in modal form $\eta = Re\left[\hat{\eta} e^{i(kx - \omega t)}\right]$, substituting this into (6.52) gives

$$\omega^2 = \frac{1}{2} g H k^2 \left[ 1 \pm \sqrt{1 - \frac{4 g' H_1 H_2}{g H^2}} \right]. \tag{6.53}$$

Since $g'/g \ll 1$ for oceanic flows, and $H_1/H < 1$, the square root may be approximated by the first two terms of a Taylor Series. Then writing $c = \omega / k$ we find two solutions which describe the barotropic (subscript $s$) and internal gravity wave (subscript $i$) modes respectively

$$c_s^2 = g H \left( 1 - \frac{g' H_1 H_2}{g H^2} + \cdots \right), \tag{6.54a}$$

$$c_i^2 = \frac{g' H_1 H_2}{H} \left( 1 + \frac{g' H_1 H_2}{g H^2} + \cdots \right). \tag{6.54b}$$

If $\rho_1 \to \rho_2$ in (6.54a), then $g'/g \to 0$ (i.e. the fluid has uniform density). Then $c_i \to 0$ (i.e, the internal wave vanishes ), and $c_s = \pm\sqrt{gH}$ which is the speed for a barotropic wave.

To leading order the wave speeds given by (6.54a) and (6.54b) reduce to

$$c_s \approx \pm\sqrt{gH} \quad \text{and} \quad c_i \approx \pm\sqrt{\frac{g'H_1H_2}{H}}. \tag{6.55}$$

Since $g' \ll g$, we see that internal gravity waves travel much slower than barotropic waves. If we consider waves forced by a semi-diurnal tide which has frequency $\omega \approx 1.45 \times 10^{-4}$ s$^{-1}$, then it follows that the wavenumber of the internal gravity waves is larger than that of the barotropic waves. Thus the former not only travels slower but also have shorter wavelengths than the latter.

A simple example serves to illustrate these differences between the barotropic and internal gravity waves. We take $H_1$=100m, $H_2$=3900m, and $g' = 0.03$m/s$^2$, and consider a semidiurnal tide which has frequency of approximately $1.45 \times 10^{-4}$ s$^{-1}$. Then the barotropic wave has $c_s \approx \pm 200$m/s , $k \approx 7.25 \times 10^{-7}$ m$^{-1}$ and $\lambda_s \approx 8700$km, and the internal gravity wave has $c_i \approx \pm 1.71$m/s, $k \approx 8.48 \times 10^{-5}$ m$^{-1}$ and $\lambda_i \approx 74$km.

We shall assume that $h = \mu n$ where $\mu$ takes a different value for the barotropic and internal gravity wave modes. Disregarding whether we are to the left or right of the shelf-break we substitute (6.55) into (6.61c), and (6.55) into (6.61c) to obtain the barotropic and internal modes

$$|h| \approx \frac{H_2}{H}\,|\eta| \qquad \text{and} \qquad |h| \approx -\frac{gH}{g'H_2}\,|\eta| \tag{6.56}$$

respectively, where $H = H_1 + H_2$. From the above analysis we can make some clear statements about internal gravity waves. We know $g' \ll g$ so by (6.56) it follows for the internal mode $|\eta| \ll |h|$, i.e., the amplitude of the internal waves is much greater than that of the surface waves.

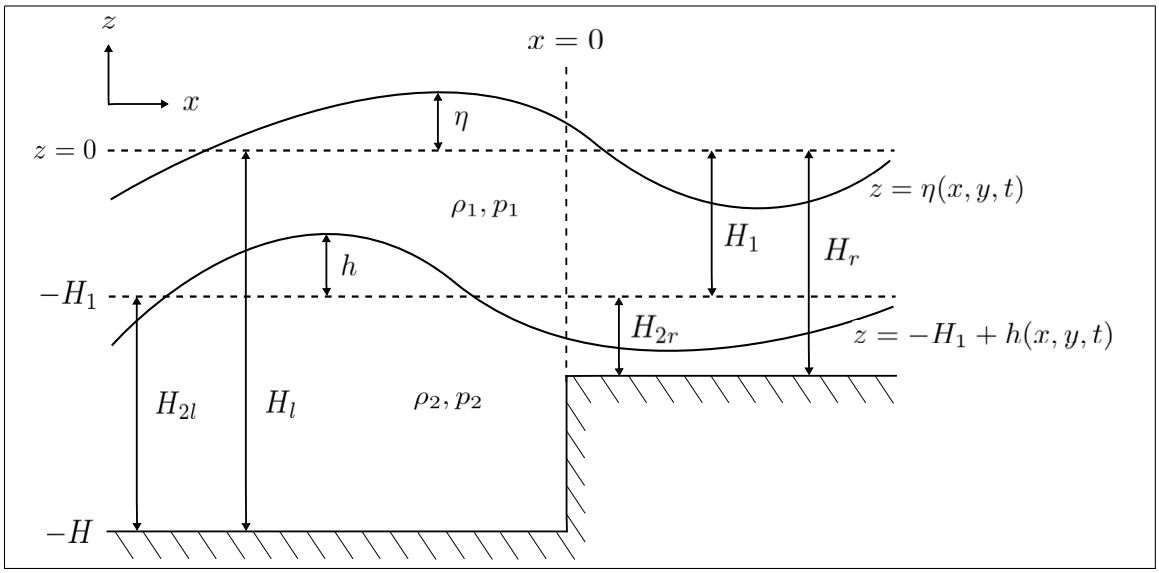


**Figure 6.4:** Two-layer model with a step

## 6.4 Reflection, transmission and generation of waves in a two-layer model

The simplest model for generation of internal gravity waves by a barotropic flow is to introduce a step as shown in Figure 6.4 to the two-layer model. Although this step is not a smooth continuous slope, it does resemble certain real life features, for example, one side of a mid-ocean ridge, or a steep continental slope (**?**).

As in section 6.2 for the single layer model, we impose an incoming barotropic wave travelling in the cross-shore direction from the deep ocean towards the step. We expect there to be a reflected and transmitted wave in each layer and we wish to find the amplitude of these waves in terms of the incident surface wave. We introduce subscripts to describe our waves:

$$i = \text{internal}, \quad s = \text{surface}, \quad I = \text{incident}, \quad R = \text{reflected}, \quad T = \text{transmitted}, \tag{6.57}$$

$$l = \text{left}\ (x < 0), \quad r = \text{right}\ (x > 0), \quad 1 = \text{upper layer}, \quad 2 = \text{lower layer}. \tag{6.58}$$

To the left of the step edge, $x < 0$, we are interested in the following primary variables: $\eta_{Is}$ (surface incident wave), $\eta_{Rs}$ (surface reflected wave), and $h_{li}$ (internal gravity wave

to the left of the step - a signature of $\eta_{li}$). To the right of the step edge, $x > 0$, we use primary variables: $\eta_{Ts}$ (surface transmitted wave) and $h_{ri}$ (internal gravity wave which is to the right of the step - a signature of $\eta_{ri}$). Here we assume the shelf is always below the depth of the upper layer, $H_1 < H_r$.

Using (6.38a), (6.38c) and (6.50) we define the relationships between $\eta, h$ and $u_1$ for the barotropic waves. By (6.38a) we have

$$u_1 = \frac{gk}{\omega}\eta, \tag{6.59}$$

By (6.38b) we have

$$\eta = \left(\frac{c^2}{c^2 - gH_1}\right) h, \tag{6.60}$$

and by (6.38c)

$$u_2 = \frac{gk}{\omega}\left(\eta + \frac{g'}{g}h\right), \tag{6.61}$$

where $c^2$ is $c_s^2$ or $c_i^2$, depending on which wave you are interested in. One can eliminate $h$ or $\eta$ using (6.60) from the final relationship, giving

$$u_2 \approx \frac{gk}{\omega}\left(\frac{c^2 - g'H_1}{c^2}\right)\eta \qquad \text{or} \qquad u_2 \approx \frac{gk}{\omega}\left(\frac{c^2 - g'H_1}{c^2 - gH_1}\right)h. \tag{6.62}$$

With the subscripts (6.58) and the assumption $g' \ll g$ we redefine the wave speeds for the surface and internal waves. To leading order the barotropic case (6.54a) reduces to

$$c_{ls} = \frac{\omega}{k_{ls}} \approx \sqrt{gH_l} \quad (x < 0), \qquad c_{rs} = \frac{\omega}{k_{rs}} \approx \sqrt{gH_r} \quad (x > 0), \tag{6.63}$$

and for the internal gravity wave to leading order (6.54b) reduces to

$$c_{li} = \frac{\omega}{k_{li}} \approx \sqrt{\frac{g'H_1H_2}{H_l}} \quad (x < 0), \qquad c_{ri} = \frac{\omega}{k_{ri}} \approx \sqrt{\frac{g'H_1H_2}{H_r}} \quad (x > 0). \tag{6.64}$$

### 6.4.1 The barotropic and internal gravity waves (IGW) modes

Using the relations given by (6.59) and (6.61) we describe the waves on either side of the step-edge as shown in Figure 6.4. For $x < 0$:

$$\begin{aligned}
\eta_l &= \eta_{Is}e^{i(k_{ls}x-\omega t)} + \eta_{Rs}e^{i(-k_{ls}x-\omega t)} + A_1 h_{li}e^{i(-k_{li}x-\omega t)},\\
u_{1l} &= \frac{g}{c_{ls}}\eta_{Is}e^{i(k_{ls}x-\omega t)} - \frac{g}{c_{ls}}\eta_{Rs}e^{i(-k_{ls}x-\omega t)} - \frac{g}{c_{li}}A_1 h_{li}e^{i(-k_{li}x-\omega t)},\\
h_l &= A_2\eta_{Is}e^{i(k_{ls}x-\omega t)} + A_2\eta_{Rs}e^{i(-k_{ls}x-\omega t)} + h_{li}e^{i(-k_{li}x-\omega t)},\\
u_{2l} &= \frac{g}{c_{ls}}A_3\eta_{Is}e^{i(k_{ls}x-\omega t)} - \frac{g}{c_{ls}}A_3\eta_{Rs}e^{i(-k_{ls}x-\omega t)} - \frac{g}{c_{li}}A_4 h_{li}e^{i(-k_{li}x-\omega t)},
\end{aligned}$$

where

$$A_1 = \left(\frac{c_{li}^2}{c_{li}^2 - gH_{1l}}\right), \quad A_2 = \left(\frac{c_{ls}^2 - gH_{1l}}{c_{ls}^2}\right), \quad A_3 = \left(\frac{c_{ls}^2 - g'H_{1l}}{c_{ls}^2}\right), \quad A_4 = \left(\frac{c_{li}^2 - g'H_{1l}}{c_{li}^2 - gH_{1l}}\right). \tag{6.66}$$

As already noted, here we express everything in terms of $\eta_{Is}$ and $\eta_{Rs}$ (surface displacements for the barotropic wave) and $h_{li}$ (interfacial displacement for the internal wave). For $x > 0$:

$$\begin{aligned}
\eta_r &= \eta_{Ts}e^{i(k_{rs}x-\omega t)} + B_1 h_{ri}e^{i(k_{ri}x-\omega t)},\\
u_{1r} &= \frac{g}{c_{rs}}\eta_{Ts}e^{i(k_{rs}x-\omega t)} + \frac{g}{c_{ri}}B_1 h_{ri}e^{i(k_{ri}x-\omega t)},\\
h_r &= B_2\eta_{Ts}e^{i(k_{rs}x-\omega t)} + h_{ri}e^{i(k_{ri}x-\omega t)},\\
u_{2r} &= \frac{g}{c_{rs}}B_3\eta_{Ts}e^{i(k_{rs}x-\omega t)} + \frac{g}{c_{ri}}B_4 h_{ri}e^{i(k_{ri}x-\omega t)},
\end{aligned}$$

where

$$B_1 = \left(\frac{c_{ri}^2}{c_{ri}^2 - gH_{1r}}\right), \quad B_2 = \left(\frac{c_{rs}^2 - gH_{1r}}{c_{rs}^2}\right), \quad B_3 = \left(\frac{c_{rs}^2 - g'H_{1r}}{c_{rs}^2}\right), \quad B_4 = \left(\frac{c_{ri}^2 - g'H_1}{c_{ri}^2 - gH_1}\right). \tag{6.68}$$

Here we express everything in terms of $\eta_{Ts}$ (surface displacements for barotropic waves) and $h_{ri}$ (interfacial displacement for internal wave).

**4×4 system**

These two solutions for $x > 0$ and $x < 0$ are matched at $x = 0$ using the conditions discussed in section 2.1.3: the continuity of pressure (2.29) and the continuity of mass (2.30), although these are appropriately modified for two layers. By (2.29) we have $\eta_l = \eta_r$ and $h_l = h_r$ at $x = 0$. In addition, by (2.30) we have $H_1 u_{1l} = H_1 u_{1r}$ at $x = 0$ for the upper layer, and $H_{2l} u_{2l} = H_{2r} u_{2r}$ at $x = 0$ for the lower layer. Here we present these conditions in matrix form, making $\eta_{Is}$ the subject in each expression

$$\eta_{Is} \begin{bmatrix} 1 \\ 1 \\ 1 \\ 1 \end{bmatrix} = \begin{bmatrix} -1 & 1 & -A_1 & B_1 \\ 1 & c_{ls}/c_{rs} & c_{ls}/c_{li}\, A_1 & c_{ls}/c_{ri}\, B_1 \\ -1 & B_2/A_2 & -1/A_2 & 1/A_2 \\ 1 & \frac{H_{2r}}{H_{2l}} \frac{c_{ls}}{c_{rs}} B_3/A_3 & \frac{c_{ls}}{c_{li}} A_4/A_3 & \frac{H_{2r}}{H_{2l}} \frac{c_{ls}}{c_{ri}} B_4/A_3 \end{bmatrix} \begin{bmatrix} \eta_{Rs} \\ \eta_{Ts} \\ h_{li} \\ h_{ri} \end{bmatrix}. \tag{6.69}$$

In this, the coefficients $A$ and $B$ are given by (6.66) and (6.68). Here the first two rows $(R_1, R_2)$ of (6.69) represent the continuity of $\eta$, and the continuity of mass of the upper layer. The third and fourth rows $(R_3, R_4)$ represent the continuity of $h$ and the continuity of mass of the lower layer. Calculated solutions of this system are delayed until section 6.4.4 so that they may be compared with analytical solutions derived from a simplified version of this system.

### 6.4.2 An approximate solution

So that we able to verify the results for the 4×4 system (6.69), we want a simplified solution to recover the 2×2 matrix for the barotropic system and a 2×2 internal gravity wave system. We achieve this by applying $g' \ll g$ to the coefficients (6.66) and (6.68) of the 4×4 system (6.69). Combining this with the approximate wave speeds of the barotropic and

internal gravity wave modes (6.63) and (6.64), we reduce (6.69) to (6.70).

$$\eta_{Is}\begin{bmatrix}1\\1\\1\\1\end{bmatrix}=\begin{bmatrix}-1 & 1 & \frac{g'H_{2l}}{gH_l} & -\frac{g'H_{2r}}{gH_r}\\ 1 & \sqrt{\frac{H_l}{H_r}} & -\sqrt{\frac{g'H_{2l}}{gH_1}} & -\sqrt{\frac{g'H_{2r}}{gH_1}}\sqrt{\frac{H_l}{H_r}}\\ -1 & \frac{H_{2r}}{H_{2l}}\frac{H_l}{H_r} & -\frac{H_l}{H_{2l}} & \frac{H_l}{H_{2l}}\\ 1 & \frac{H_{2r}}{H_{2l}}\sqrt{\frac{H_l}{H_r}} & \sqrt{\frac{g'H_1}{gH_{2l}}} & \frac{H_{2r}}{H_{2l}}\sqrt{\frac{g'H_1}{gH_{2r}}}\sqrt{\frac{H_l}{H_r}}\end{bmatrix}\begin{bmatrix}\eta_{Rs}\\ \eta_{Ts}\\ h_{li}\\ h_{ri}\end{bmatrix}. \tag{6.70}$$

If we write $g'/g=\epsilon^2$, then it follows that the matrix (6.70) contains a mixture of $O(1), O(\epsilon)$ and $O(\epsilon^2)$ terms. We use this observation so that we may decouple the barotropic and internal gravity wave modes. First we multiply $R_2$ by $H_1/H_{2l}$, then add $R_4$ to the new $R_2$ to give

$$\eta_{Is}\begin{bmatrix}1\\ \frac{H_1+H_{2l}}{H_{2l}}\\ 1\\ 1\end{bmatrix}=\begin{bmatrix}-1 & 1 & \frac{g'H_{2l}}{gH_l} & -\frac{g'H_{2r}}{gH_r}\\ \frac{H_1+H_{2l}}{H_{2l}} & \frac{H_r}{H_{2l}}\sqrt{\frac{H_l}{H_r}} & 0 & 0\\ -1 & \frac{H_{2r}}{H_{2l}}\frac{H_l}{H_r} & -\frac{H_l}{H_{2l}} & \frac{H_l}{H_{2l}}\\ 1 & \frac{H_{2r}}{H_{2l}}\sqrt{\frac{H_l}{H_r}} & \sqrt{\frac{g'H_1}{gH_{2l}}} & \frac{H_{2r}}{H_{2l}}\sqrt{\frac{g'H_1}{gH_{2r}}}\sqrt{\frac{H_l}{H_r}}\end{bmatrix}\begin{bmatrix}\eta_{Rs}\\ \eta_{Ts}\\ h_{li}\\ h_{ri}\end{bmatrix}. \tag{6.71}$$

Neglecting $O(\epsilon)$ terms, $R_1$ and $R_2$ yields

$$\eta_{Is}\begin{bmatrix}1\\1\end{bmatrix}=\begin{bmatrix}-1 & 1\\ 1 & c_{rs}/c_{ls}\end{bmatrix}\begin{bmatrix}\eta_{Rs}\\ \eta_{Ts}\end{bmatrix}. \tag{6.72}$$

This is equivalent to the formulation for the barotropic mode in the single-layer step problem (6.8) as before

$$\begin{bmatrix}\eta_{Rs}\\ \eta_{Ts}\end{bmatrix}=\frac{1}{1+c_{rs}/c_{ls}}\begin{bmatrix}-c_{rs}/c_{ls} & 1\\ 1 & 1\end{bmatrix}\begin{bmatrix}\eta_{Is}\\ \eta_{Is}\end{bmatrix}. \tag{6.73}$$

Thus to leading order, the solution for the barotropic mode is not influenced by the generation of internal waves.

To extract the solution for the internal gravity waves, we use $R_3$ and $R_4$ which represent the lower layer. Using (6.71) and (6.72) we have

$$\begin{bmatrix} h_{li} \\ h_{ri} \end{bmatrix} = \begin{bmatrix} -\frac{H_l}{H_{2l}} & \frac{H_l}{H_{2l}} \\ -\frac{c_{li}}{H_{2l}}\sqrt{\frac{H_l}{g}} & \frac{c_{ri}}{H_{2l}}\sqrt{\frac{H_l}{g}} \end{bmatrix}^{-1} \begin{bmatrix} 0 & \frac{H_{2l}H_r - H_{2r}H_l}{H_{2l}H_r} \\ 0 & \frac{c_{rs}^2 H_{2l} - c_{ls}^2 H_{2r}}{c_{rs}c_{ls}H_{2l}} \end{bmatrix} \begin{bmatrix} \eta_{Rs} \\ \eta_{Ts} \end{bmatrix} \tag{6.74}$$

To eliminate $(\eta_{Rs}\, \eta_{Ts})$ we substitute (6.73) into (6.74), so

$$\begin{bmatrix} h_{li} \\ h_{ri} \end{bmatrix} = \frac{2H_{2l}c_{ls}}{(c_{ri}+c_{li})(c_{ls}+c_{rs})} \begin{bmatrix} -c_{ri}H_l\frac{H_{2l}H_r - H_{2l}H_l}{H_{2l}H_r} + \sqrt{\frac{g}{H_l}}\frac{c_{rs}^2 H_{2l} - c_{ls}^2 H_{2r}}{H_{2l}c_{rs}c_{ls}} \\ c_{li}H_l\frac{H_{2l}H_r - H_{2l}H_l}{H_{2l}H_r} + \sqrt{\frac{g}{H_l}}\frac{c_{rs}^2 H_{2l} - c_{ls}^2 H_{2r}}{H_{2l}c_{rs}c_{ls}} \end{bmatrix} \begin{bmatrix} \eta_{Is} \\ \eta_{Is} \end{bmatrix} \tag{6.75}$$

Since $g' \ll g$ we can neglect the first terms in our results for $h_{li}$ and $h_{ri}$ and simplifying this expression using our leading order expressions (6.63) and (6.64) for the wave speeds we have for the amplitude of the internal waves

$$h_{li} = h_{ri} = \frac{2\Delta_H}{(\sqrt{H_r}+\sqrt{H_l})(\sqrt{H_l H_{2r}}+\sqrt{H_r H_{2l}})}\sqrt{\frac{gH_1}{g'}}\,\eta_{Is}, \tag{6.76}$$

where $\Delta_H = H_l - H_r$ is the size of the step. This is quite an important result as it shows that the amplitude of the internal wave on either side of the step (x=0) is the same, and scales as $\Delta_H$. We note that **?** concludes the step size is important but does not give a specific scaling between wave height and step size.

### 6.4.3 Time averaged energy flux in terms of step size $\Delta_H$

Although we have determined the amplitude of the interfacial displacements associated with the internal waves, the corresponding energy fluxes have greater physical significance. We use the results of section 6.3.2 to determine the time averaged energy flux for the internal gravity wave on either side of the step. In (6.46) we give the total energy flux $\underline{J}$ for a two-layer fluid as

$$\underline{J} = g\rho_1\left(H_1\underline{u}_1 + H_2\underline{u}_2\right)\eta + g'\rho_2 H_2\underline{u}_2 h. \tag{6.77}$$

For our one dimensional flow, this reduces to a scalar energy flux.

$$J = g\rho_1 \left(H_1 u_1 + H_2 u_2\right) \eta + g' \rho_2 H_2 u_2 h. \tag{6.78}$$

The first term (independent of $g'$) is equivalent to that of the energy flux in a single layer of fluid, (6.18). The second term (involving $g'$) can thus be identified as the energy flux due to internal waves. We write this as $J_i = g'\rho_2 H_2 u_2 h$ to calculate the time averaged energy flux $\langle J \rangle_i$. Here we state the results for the internal wave where we have written the results in terms of the step size $\Delta_H$, and the incident barotropic wave $\eta_{Is}$

$$\langle J \rangle_{2il} \approx -2g\rho_2 H_1 \Delta_H^2 \, c_{li} \left[ \frac{1}{(\sqrt{H_r} + \sqrt{Hl})(\sqrt{H_l H_{2r}} + \sqrt{H_r H_{2l}})} \right]^2 |\eta_{Is}|^2, \tag{6.79a}$$

$$\langle J \rangle_{2ir} \approx 2g\rho_2 H_1 \Delta_H^2 \, c_{ri} \left[ \frac{1}{(\sqrt{H_r} + \sqrt{Hl})(\sqrt{H_l H_{2r}} + \sqrt{H_r H_{2l}})} \right]^2 |\eta_{Is}|^2, \tag{6.79b}$$

note we have used approximate values for $h_{li}$ and $h_{ri}$ (6.76). Recall $c_{li} = \sqrt{g' H_1 H_{2l}/H_l}$ and $c_{ri} = \sqrt{g' H_1 H_{2r}/H_r}$ are the speeds of the baroclinic waves (6.64), and $\Delta_H = H_l - H_r$ is the step size.

These are the desired results: explicit expressions for the internal gravity wave energy fluxes (per unit length along the step) in terms of the amplitude of the incident surface wave. However, these were obtained using a simplified version of the full system (6.69). We now return to this, to assess the accuracy of (6.79a,b).

### 6.4.4 Evaluation of the 4×4 system, barotropic and internal gravity wave (IGW) modes

In this section we shall make comparisons of the time averaged energy fluxes of the internal gravity wave mode, $\langle \underline{J} \rangle_{2il}$ and $\langle \underline{J} \rangle_{2ir}$ which are calculated from the 4×4 system (6.69) with (6.47a-c). In addition, we compare these calculations with the time averaged energy fluxes derived using the internal gravity wave mode (6.75) extracted from the simplified 4×4 system (6.70). Here we calculate these time averaged energy fluxes by substituting (6.75) into $g'\rho_2 H_2 u_2 h$ of (6.47c) where a further simplification of $u_2 h$ has been been made

by applying $g' \ll g$. Note we also include the perturbed sea surface heights of the single layer step model (6.8) and the two-layer step model (6.72).

The depth of the ocean varies substantially, from shallow depths to 11,030m, the southern end of Mariana Trench in the Pacific Ocean. We calculate the average depth of the ocean to be approximately 4km, based on an average density $\rho = 1028\text{kg/m}^3$, area of ocean= $3.61 \times 10^{14}\text{m}^2$ and a mass of $1.4 \times 10^{21}$kg (**?**). The upper layer usually occupies a depth of 50-150m or so but this can be deeper in winter. Therefore, we assume in our simple model that this upper layer has an approximate depth of $H_1 = 250$m, and the depth of the ocean is 4km.

Table 6.1 summarises the three models which we compare. To have an idea of the amplitude of the perturbed surfaces and the time averaged energy fluxes, we show numerical values for the three models for three different step sizes. Tables 6.2, 6.3, 6.4 summarise the data for each different step size: a relatively small step, a medium sized step and a large step, i.e., $H_2$ =3000m, 2000m and 500m respectively.

Here the amplitude of the perturbed sea surface, $\eta$ and interfacial surface, $h$ are given in metres (m), and the time averaged energy flux per unit area $\langle \underline{J} \rangle$, as Watts per metre (W/m). We are specifically analysing the energy flux away from the step edge in both directions.

We begin by comparing $\eta$ and $h$ for models 1, 2 and 3, i.e., Tables 6.2, 6.3, 6.4 respectively. The incoming incident wave $\eta_{Is}$, has amplitude 1m. As the size of the step increases the amplitude of the reflected surface wave $\eta_{Rs}$, increases from 0.071831m (Table 6.2), to 0.17176m (Table 6.3) to 0.48108m (Table 6.4) in Model 1. The difference in the reflected perturbed sea surface amplitude $\eta_{Rs}$, between Models 1 and 2 is a few millimetres and not of any significance in this linear model. As the step size increases the amplitude of the transmitted surface wave $\eta_{Ts}$ also increases from 1.0718m (Table 6.2) to 1.17176m (Table 6.3) to 1.4695m (Table 6.4) in Model 1. Again, there is only a difference of at most of 1cm between the amplitude of the transmitted surface wave $\eta_{Ts}$, in Models 1 and 2.

| System type | Description |
|---|---|
| Model 1 | Energy flux per unit area calculated by evaluating (6.47a-c) with precise solutions of 4×4 system (6.69). |
| Model 2 | Barotropic (6.72) and IGW system (6.75) extracted from simplified 4×4 system (6.70) where $g' \ll g$ applied to (6.69). Calculations for energy flux per m$^2$ found by substituting (6.75) into (6.47a-c). |
| Model 3 | Extracted IGW system (6.75) substituted into simplified version of energy flux equation for IGW (6.47c) where $g' \ll g$ applied . |

Table 6.1: Description of models determined using 4×4 system (6.69) and simplified 4×4 system (6.70).

The amplitude of the internal gravity wave to the left of the step $h_{li}$, increases from 0.73073m (Table 6.2) to 1.9732m (Table 6.3) to 9.7520m (Table 6.4) in Model 1. To the right of the step we see an increase in $h_{ri}$ from 0.75306m (Table 6.2) to 2.0467m (Table 6.3) to 10.406m (Table 6.4) in Model 1. Again the differences between Models 1 and 2 are less than 1cm and thus negligible. With a 250% increase in the step size, i.e., from 1000m to 3500m we see an increase in $h_{li}$ of approximately 1240% and an increase in $h_{ri}$ of approximately 1290%. This is consistent with the $\Delta_H$ scaling in (6.76). Furthermore, there is a sharp contrast in the percentage changes in the height of the surface wave, for the reflected component $\eta_{Rs}$ this is approximately 590%, and for the transmitted component $\eta_{Ts}$ we still see an increase, however, it is much smaller at approximately 37%.

What happens to the time averaged energy flux as we increase the step size from 1000m to 2000m to 3500m? Here we compare the results shown in columns 6 to 8 of Tables 6.2, 6.3, 6.4. The order of magnitude of $\langle \underline{J} \rangle_{2il}$ and $\langle \underline{J} \rangle_{2ir}$ are the same, it therefore seems reasonable, for now, to confine our comparisons of the time averaged energy flux in Tables 6.2, 6.3, 6.4 to Model 1. At $H_r$=3000m $|\langle \underline{J} \rangle_{2il}| \approx 21$ W/m, $|\langle \underline{J} \rangle_{2ir}| \approx 22$ W/m and $|\langle \underline{J} \rangle_{l\,total}| \approx 1 \times 10^6$ W/m. As $\Delta_H$ increases from 1000m to 2000m we observe $|\langle \underline{J} \rangle_{2il}| \approx$153 W/m, $|\langle \underline{J} \rangle_{2ir}| \approx$159 W/m and $|\langle \underline{J} \rangle_{l\,total}| \approx 1 \times 10^6$ W/m. With the largest

| | $\lvert\eta_{Rs}\rvert$ | $\lvert\eta_{Ts}\rvert$ | $\lvert h_{li}\rvert$ | $\lvert h_{ri}\rvert$ | $\langle \underline{J} \rangle_{2il}$ | $\langle \underline{J} \rangle_{2ir}$ | $\langle \underline{J} \rangle_{l\,total}$ | $\langle \underline{J} \rangle_{r\,total}$ |
|---|---|---|---|---|---|---|---|---|
| M1 | 0.071831 | 1.0718 | 0.73073 | 0.75306 | -21.003 | 22.055 | 1.0222 $\times 10^6$ | $1.0222 \times 10^6$ |
| M2 | 0.071797 | 1.0718 | 0.73067 | 0.75300 | -21.000 | 22.052 | 1.0222 $\times 10^6$ | 1.0222 $\times 10^6$ |
| M3 | | | | | -21.691 | 21.449 | | |

Table 6.2: M1= model 1, M2=model 2, M3=model 3 as described in Table 6.1. Heights of waves in metres (m), and time averaged energy flux in Watts per metre (W/m). $H_r$ = 3000m $\Delta_H$=1000m, $|\eta_{Is}| = 1$.

| | $\lvert\eta_{Rs}\rvert$ | $\lvert\eta_{Ts}\rvert$ | $\lvert h_{li}\rvert$ | $\lvert h_{ri}\rvert$ | $\langle \underline{J} \rangle_{2il}$ | $\langle \underline{J} \rangle_{2ir}$ | $\langle \underline{J} \rangle_{l\,total}$ | $\langle \underline{J} \rangle_{r\,total}$ |
|---|---|---|---|---|---|---|---|---|
| M1 | 0.17176 | 1.1716 | 1.9732 | 2.0467 | -153.15 | 159.13 | $9.9708 \times 10^5$ | $9.9708 \times 10^5$ |
| M2 | 0.17157 | 1.1716 | 1.9734 | 2.0466 | -153.18 | 159.13 | $9.9708 \times 10^5$ | $9.9708 \times 10^5$ |
| M3 | | | | | -153.74 | 159.12 | | |

Table 6.3: M1= model 1, M2=model 2, M3=model 3 as described in Table 6.1. Heights of waves in metres (m), and time averaged energy flux in Watts per metre (W/m). $H_r$=2000m $\Delta_H$=2000m, $|\eta_{Is}| = 1$.

| | $\lvert\eta_{Rs}\rvert$ | $\lvert\eta_{Ts}\rvert$ | $\lvert h_{li}\rvert$ | $\lvert h_{ri}\rvert$ | $\langle \underline{J} \rangle_{2il}$ | $\langle \underline{J} \rangle_{2ir}$ | $\langle \underline{J} \rangle_{l\,total}$ | $\langle \underline{J} \rangle_{r\,total}$ |
|---|---|---|---|---|---|---|---|---|
| M1 | 0.48108 | 1.4695 | 9.7520 | 10.406 | -3740.7 | 3105.8 | $7.8599 \times 10^5$ | $7.8599 \times 10^5$ |
| M2 | 0.47759 | 1.4776 | 9.8178 | 10.464 | -3791.3 | 3140.6 | $7.8594 \times 10^5$ | $7.8602 \times 10^5$ |
| M3 | | | | | -4003.2 | 2924.3 | | |

Table 6.4: M1= model 1, M2=model 2, M3=model 3 as described in Table 6.1. Heights of waves in metres (m), and time averaged energy flux in Watts per metre (W/m). $H_r$ = 500m, $\Delta_H$=3500m, $|\eta_{Is}| = 1$.

step, i.e., $\Delta_H$=3500m, we find $|\langle \underline{J} \rangle_{2il}| \approx 3800$ W/m, $\langle \underline{J} \rangle_{2ir} \approx 3100$ W/m and $|\langle \underline{J} \rangle_{l\,total}| \approx 8 \times 10^6$ W/m.

A comparison of columns 4 or 5 $\langle \underline{J} \rangle_{2il}/\langle \underline{J} \rangle_{2ir}$ with columns 7 or 8 $|\langle \underline{J} \rangle_{l\,total}|/|\langle \underline{J} \rangle_{r\,total}|$ demonstrates that the total time averaged energy fluxes are dominated by the barotropic terms. However, we observe as the step size $\Delta H$ increases that there is a decrease in $|\langle \underline{J} \rangle_{l\,total}|$ but there is an increase in the time averaged energy fluxes of the internal gravity waves. So it follows that the internal gravity waves are drawing energy from the barotropic waves as the step size increases. This is in agreement with the increased heights of the internal gravity waves, and the energy these waves carry.

Figure 6.5 compares the time averaged energy fluxes for model 1 and 3. Note the colourbar is logarithmic and ranges from 0 to 10 kW/m. With a very small upper layer and a very small step, the time averaged internal energy for both sides of the step is zero, so a very small topography does lead to internal wave generation. As the value of $H_r$ is decreased from 3900m and we increase $H_1$, we see that the value of $\langle \underline{J} \rangle_{2ileft}$ and $\langle \underline{J} \rangle_{2iright}$ both increase, eventually to order $10^4$ W/m. As we shall show these values are consistent with moorings, satellite data and current research.

We can see that there is little difference between Figures 6.5a and 6.5c for $x < 0$, and Figures 6.5b and 6.5d for $x > 0$. However, the time averaged energy fluxes derived from the approximations are slightly higher due to the error arising from approximating several parameters used to obtain simplified expressions.

Figure 6.6 clearly shows that the absolute errors between Figures 6.5a and 6.5c, and Figures 6.5b and 6.5d are negligible.

## 6.5 Comparison of results to observations

We conclude this chapter by making a comparison of our theoretical results to observations of internal tides and related processes in the ocean.

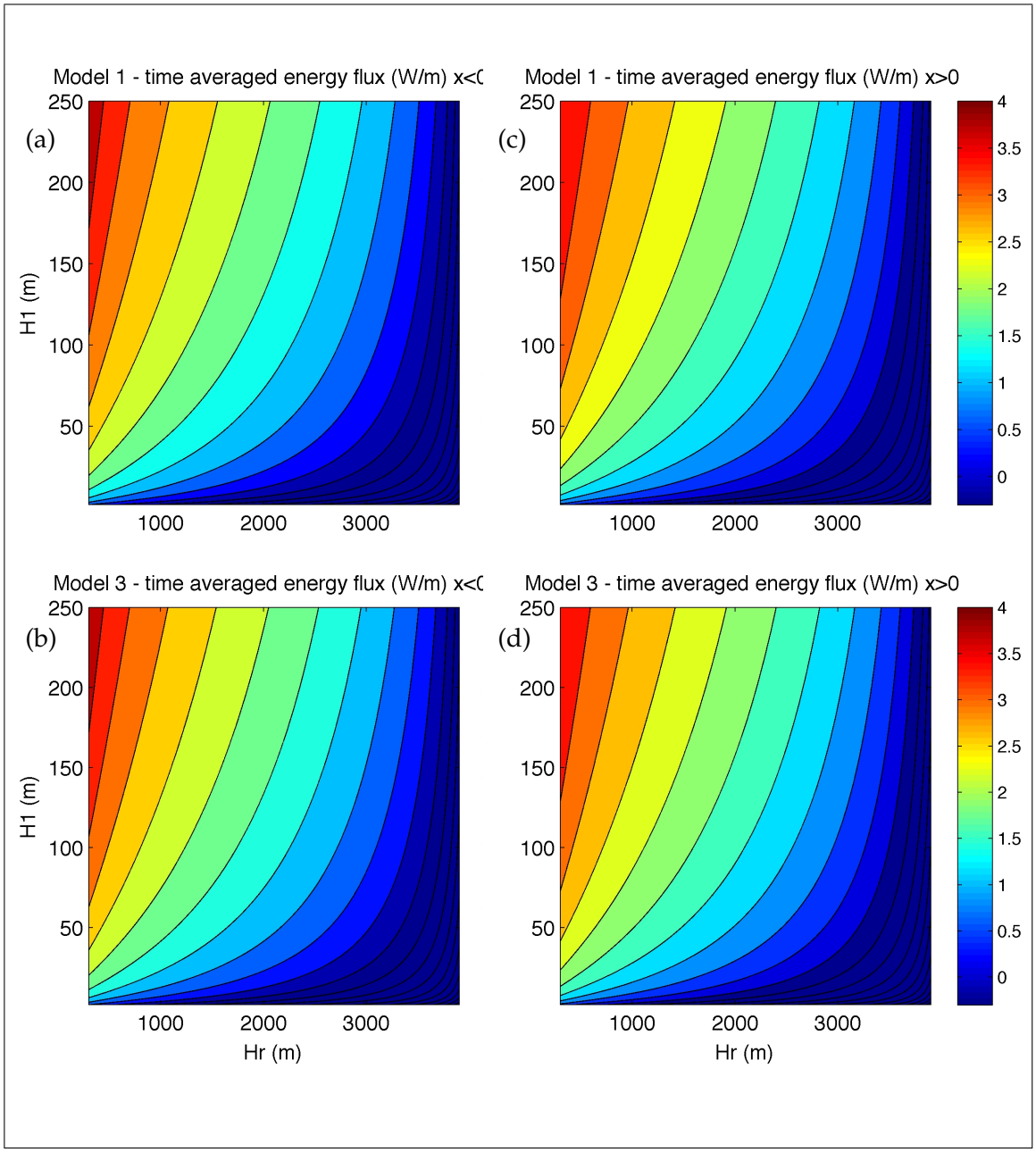


**Figure 6.5:** Time averaged energy fluxes $\langle J \rangle_{2il}$ and $\langle J \rangle_{2ir}$ for models 1 and 3 where $x < 0$ (a,b), and $x > 0$ (c,d). Here $0 < H_1 < 250$m, $300 < H_r < 3900$m and $H_l = 4000$m. For small $H_r$ and $H_1$ the time averaged energy flux in models 1 and 3 are greater for $x > 0$ than $x < 0$. The $\log_{10}$ colourbar scale ranges from 0 to 4 W/m.

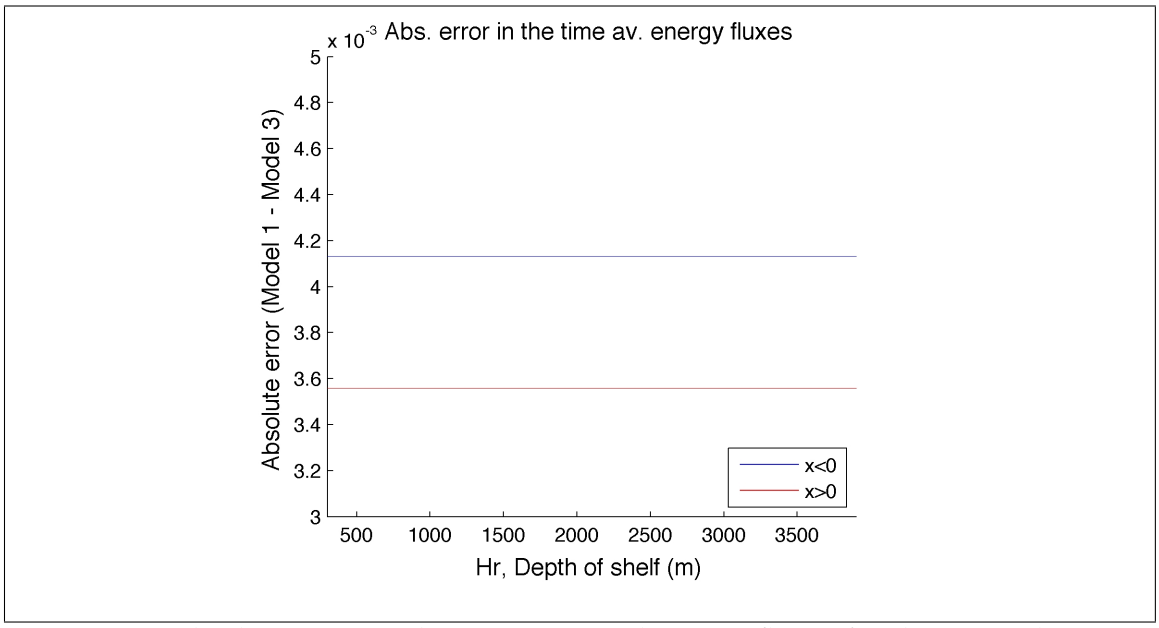


**Figure 6.6:** Absolute error in the time averaged energy fluxes for the internal gravity wave. Here we calculate the absolute errors for $|\langle J\rangle_{2il}$ (M1) - $\langle J\rangle_{2il}$ (M3)| shown in blue, and $|\langle J\rangle_{2ir}$ (M1) -$\langle J\rangle_{2ir}$ (M3)| shown in red.

**?** investigated the conversion of barotropic to baroclinic tides at steep topography with a focus on the Hawaiian Ridge which stretches for 2500km with a topography that varies from islands that protrude above the water to wide 4000m deep channels. Surpisingly, the ridge rises from deeper than 4000m to near the surface in less than 20km (**?**). The Hawaii Ocean Mixing Experiment (HOME) was motivated by the dominant $M_2$ tide, which propagates perpendicular to the topography. In particular, Carter *et al* considered a subregion of the Hawaiian Ridge that excluded Big Island and only contained one of the three main internal tide generation sites along the Hawaiian Ridge. **?** calculated that the $M_2$ tide loses 2.7 GW of energy over the study region of which 2.3GW is converted into internal tides.

The calculated baroclinic energy flux due to the $M_2$ tide is 1.7 GW integrated over the subdomain (**?**). If my parameters are $H_l = 4$ km, $H_r = 2$ km and $H_1$ =250 m then my model, using a step of length 1000km gives an approximate result of $1.0 \times 10^6$ W/m $\times 1 \times 10^6$m = 1 GW. So although I have used a very simple model, the results are of the

same order of magnitude.

**?** presents computations of horizontal internal wave propagation from 60 historical moorings and relates them to sources of internal waves computed from satellite altimeter data. In particular, the internal tide mean flux for Hawaii to the northeast is $\sim$ 1000 W/m (**?**), although my parameter values are subjective in this linear model, i.e. the value of $H_2$ we choose, we see that the order of $\langle \underline{J} \rangle_{2ileft}$ and $\langle \underline{J} \rangle_{2iright}$ are consistent with these findings. **?** estimate the energy flux for a knife ridge which models the Hawaiian Ridge is 3000 W/m here they have assumed a reference value for the stratification up to 1000m in depth where the critical internal tide generation occurs. My calculations are not in close agreement and this may be due to the different stratification regimes that we have. They conclude that much of the energy flux at a knife-ridge model of moderate height is in mode 1. Model 1 for $H_1 = 250$m, $H_r = 1000$m, $H_l$=4000m gives $|\langle J \rangle_{2ileft}|$ and $|\langle J \rangle_{2iright}|$ $\approx$1000 W/m which is more in agreement with **?**.

We have made several calculations for the energy flux when a barotropic wave meets a step in a two-layer model. The simple model described in this chapter has similarities with that developed by **?**. They explored the details of a an incident oblique barotropic Poincaré wave propagating towards the shelf-break. Here we are more interested in the assumptions of their two-layer model and its relevance to the Malin shelf.

**?** make five main assumptions in their model. Firstly, they assume they have a step-like geometry, this is a good approximation for the bathymetry of the Malin Shelf as shown in Figure 6.7. The Malin shelf has a depth of 150m, the slope extends over approximately 60km sharply dropping to a depth of approximately 1600m. The depth was measured by CTD (conductivity-temperature-depth) casts across the slope, and in Figure 6.7 we also see see potential density measurements observed at different depths.

Secondly, Guizien *et al* (1999) construct a two-layer model, although this is far from a perfect representation of the sea surrounding the Malin Shelf, it is a sufficient assumption to model this region. To demonstrate this we show the density and temperature profiles in Figure 6.8a,b respectively of two separate measurements taken as part of the

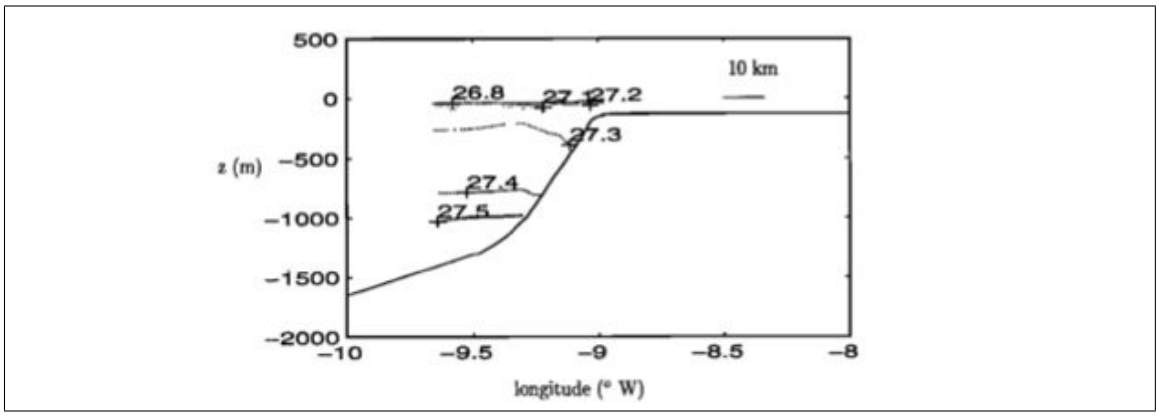


**Figure 6.7:** Bathymetry of the Malin Shelf, North of Ireland, UK. Equilibrium sea level at $z = 0$. The Malin shelf has a depth of 150m, the slope extends over approximately 60km, and drops to a depth of approximately 1600m. The densities measured at different depths are also indicated. (**?**)

SES program using ADCP (acoustic Doppler current profilers) moorings 5km from the Malin shelf-break. Figure 6.8a shows the measurement taken at 1249 on 14th July 1996 (solid line), here we clearly see a sharp pycnocline beneath a well-mixed upper layer, this approximates the sea around the Malin Shelf as a two-layer problem and we clearly see the density difference is 0.4 kg/m$^3$. A second measurement taken at 1317 on 23rd July 1996 (dashed line) shows linear stratification in the upper layer, this is a consequence of strong solar heating. Figure 6.8b shows the difference between the potential temperature profiles of the first (solid line) and second (dashed line) measurements. Although the linear stratification profile (dashed line Figure 6.8b ) is the one most consistently observed, Guizien *et al* (1999) are able to make some favourable comparisons of their model with data from the Malin Shelf project.

Guizien *et al* (1999) assume that there are no internal gravity waves entering from the deep ocean, and in particular there is no mention of this being observed in the SES project. It was found that the slope is mostly supercritical between depths ranging from 200 to 1000m, thus if energy was propagating along internal ray paths, then it could not propagate onto the shelf. Thus their assumption to force their model with a barotropic tide seems plausible. Finally, we note that **?** assumes he has reflection at the coast, however

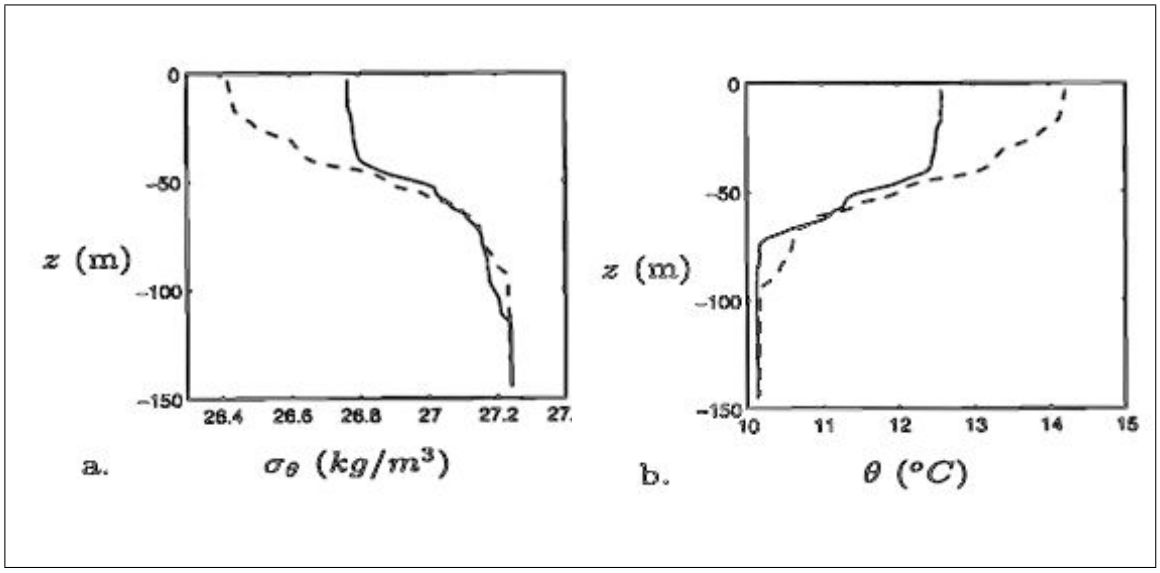


**Figure 6.8:** Density and temperature profiles (**?**). Typical diurnal profiles measured in July 1996 off the Malin Shelf. Potential density (a) and potential temperature (b) profiles observed 5km from shelf-break. Taken at 1249 on 14th July 1996 shown by a solid line we see a sharp pycnocline beneath a well-mixed upper layer. At 1317 on 23rd July 1996 shown by a dashed line we observe linear stratification in the upper layer. This is a consequence of strong solar heating thus leading to an increase in potential temperature (b).

Guizien *et al* (1999) replace this with a radiative boundary condition. Thus they eliminate the standing waves found by Rattray (1960). This assumption is based on the fact that the Scottish coastline and Hebridean Islands are strongly indented with fjords, lochs and channels and likely to absorb incoming waves.

To conclude Guizien *et al* (1999) assert that they were more focussed on validating the physical ingredients necessary for internal tide generation on a continental margin. They show that the angle of incidence of the barotropic wave is of importance, and they find good agreement with the measurements taken on the Malin Shelf for internal tide amplitudes, and the total energy of the internal tide in the vicinity of the shelf-break. This validates that their step-like topography is indeed a good approximation for the Malin Shelf. Furthermore, they are able to match their total energy calculations for the internal gravity wave mode with that observed on the Malin Shelf in the period for which there was a two-layer approximation, this was not the case when there was linear stratification. In particular, they conclude their model underpredicts the mean total energy (as with Baines' (1982)) when there exists linear stratification on the Malin Shelf .

The aim of this chapter was to recover solutions for the forcing of interfacial internal gravity waves in a two-layer fluid by a prescribed surface tide flowing over isolated two-dimensional topography. This has been achieved by developing a two-layer model with a step and showing that the size of the step $\Delta_H$ is an important factor which affects the perturbed height of the internal gravity wave. Given the renewed interest in the environment and the curiosity of tidal dissipation, I have tried to make the link between this simple, theoretical approach and real-life data by comparing the time averaged energy fluxes for the internal gravity wave. These values are consistent with practical observations and other numerical simulations as referred to previously, thus although this model is quite basic in several ways it has strong similarities with the model developed by **?**, and it has provided valid results.

# Chapter 7

# Conclusions

In this work we have considered waves that are trapped at the coast. These waves are excited by tidal forcing at particular frequencies. The overall aim is to evaluate the tidal dissipation that can arise through the excitation of internal gravity waves, that is waves which owe their existence to the stable stratification in the thermocline. To do this we first considered the structure of the barotropic modes which are forced by the tides. When these waves interact with a bottom topography they give rise to motions which can excite the internal waves.

We found that these coastally trapped barotropic waves have quite a complex nature when topography is introduced. Therefore in chapters 4 and 5 we have considered the types of barotropic waves which can occur with variable topography. We found that the waves are essentially of three different types, Kelvin waves, edge waves and topographic Rossby waves, though in practice the edge waves and Kelvin waves merge into each other. In chapter 3 we focussed on the topographic Rossby wave, following the treatment of **?** who considered step topography and **?** who considered continuously varying topography. We have extended the Longuet-Higgins analysis to include the effects of the coast (see also **?**), and we also simplified the Saint-Guily analysis, and discussed the effect of the coast on the topographic Rossby wave. An interesting feature of this work

was the existence of multiple topographic Rossby waves (only a single solution exists for step topography), and we obtained a dispersion relation based on a shallow topography assumption that gave remarkable agreement with numerical solutions even for moderate topography.

The numerical calculations of the topographic Rossby waves with a coastline included were found to relate reasonably well to the unbounded problem, except close to the coast itself. The analytical unbounded solution therefore provides a useful overview of the behaviour even when a coast is included. The step topography only gives one topographic Rossby wave whereas the continuous problem leads to a whole spectrum of waves, nevertheless the fundamental mode $n = 0$ of the continuous case has solutions which closely resemble that from the step topography solution.

Although the topographic waves are of interest, their frequency is generally rather low compared to the dominant tidal forcing frequencies. So from the point of view of tidal dissipation, it is the Kelvin waves that are of most interest. Kelvin waves are affected by topography near the coast, and we systematically investigated the dependence on parameters such as the width and depth of the continental shelf, and the wavelength parallel to the shore. Kelvin waves are strongly affected by rotation, but there also exist trapped edge waves which can exist even in a non-rotating system. Kelvin waves are trapped by rotation but edge waves are trapped by the topography, that is the steep drop at the edge of the continental shelf where total internal reflection can occur. Nevertheless, as the parameters are varied, the two types of wave merge to give a complex range of solutions. One curious feature we have identified is the anti-Kelvin wave, which requires both topography and rotation. The anti-Kelvin wave travels at a similar frequency to the Kelvin wave, but in the opposite direction. The velocity structure of the anti-Kelvin wave is remarkably similar to that of the Kelvin wave, but with the cross-shore velocity inverted.

Although the topographic Rossby wave and the Kelvin wave have quite different physical origins, somewhat surprisingly under certain conditions one type of wave can turn

into the other as parameters are continuously varied.

One concern with the work of chapters 3 and 4 was the use of step topography. How realistic is it? As we have mentioned, the $n = 0$ topographic Rossby wave under continuous topography can be well approximated by step topography in a certain limit. But then can the same be said about the Kelvin waves and edge waves? We therefore considered in chapter 5 numerical solutions of the problem with continuous topography using a hyperbolic tangent profile. The main findings have been that the step topography does a surprisingly good job in elucidating the nature of these waves. The topology of the solutions as found by the numerics in our hyperbolic tangent profile model relates closely to that found in chapter 4 using the step model.

Finally in chapter 6 we have considered the mechanism by which internal gravity waves are excited by tidal forcing. Comparing the cross-shore structure of the internal and surface waves it transpires it is the cross-topography velocity which is crucial for exciting internal waves. So it is those barotropic waves that give rise to cross-topography flows that are the most important for tidal dissipation. Thus for example, a Kelvin wave with no topography does not excite internal waves, but the waves studied in chapters 4 and 5 do have significant cross-topography velocities. This has enabled us to give simple estimates of the tidal dissipation arising from the waves considered in this study.

# Appendix A

# Integration of $\operatorname{sech} \hat{y}$ function

Let

$$I_n = \int_{-\infty}^{\infty} \operatorname{sech}^n \hat{y} \, \mathrm{d}\hat{y} = 2 \int_0^{\infty} \operatorname{sech}^n \hat{y} \, \mathrm{d}\hat{y} \tag{A.1}$$

where $-\infty < \hat{y} < \infty$. Let $x = \operatorname{sech}(\hat{y})$, thus $-dx/x\sqrt{1-x^2} = \mathrm{d}\hat{y}$ where $0 < x < 1$. Hence we have

$$I_n = 2 \int_0^1 \frac{x^{n-1}}{\sqrt{1-x^2}} \, \mathrm{dx} \tag{A.2}$$

Now let $x = \sin\, \theta$, therefore $0 < \theta < \frac{\pi}{2}$

$$I_n = 2 \int_0^{\pi/2} \sin^{n-1} \theta \, \mathrm{d}\theta.$$

Using an identity for the Beta function we have

$$2 \sin^{n-1} \theta = 2^{n-1} B\left(\frac{n}{2}, \frac{n}{2}\right). \tag{A.3}$$

Now $B\left(\frac{n}{2}, \frac{n}{2}\right) = \frac{[\Gamma\left(\frac{n}{2}\right)]^2}{\Gamma(n)}$, thus

$$I_n = 2^{n-1} \frac{[\Gamma(n/2)]^2}{\Gamma(n)}$$

# Appendix B

# Transformation to the hypergeometric function

With an aim to working towards transforming (3.51) into the hypergeometric form we return to (3.61), and use a third transformation

$$\mu = \frac{1+z}{2}.$$

Given that $z \in (-1, 1)$ when $y \in \mathbb{R}$, it follows that $\mu \in (0, 1)$. We now have

$$1 - z^2 = 4\mu(\mu - 1), \quad \gamma_z = \frac{1}{2}\gamma_\mu \quad \text{and} \quad \gamma_{zz} = \frac{1}{4}\gamma_{\mu\mu},$$

so that (3.61) becomes

$$\frac{4^2}{a^2}\mu^2(\mu-1)^2\gamma_{\mu\mu} - \frac{4(2\alpha+1)}{a^2}\mu(\mu-1)(2\mu-1)\gamma_\mu + 4\left(E + \nu - \frac{2\alpha}{a^2}\right)\mu(\mu-1)\gamma = 0.$$

Multiplying through by $a^2/4^2\mu(\mu-1)$ leads to

$$\mu(\mu-1)\gamma_{\mu\mu} - \frac{1}{4}(2\alpha+1)(2\mu-1)\gamma_\mu + \frac{1}{4}a^2\left(E + \nu - \frac{2\alpha}{a^2}\right)\gamma = 0. \tag{B.1}$$

This has the form of the hypergeometric differential equation

$$z(1-z)u_{zz} + \Big[\delta - (\tilde{\alpha} + \beta + 1)z\Big]u_z - \tilde{\alpha}\beta u = 0. \tag{B.2}$$